



The  
University  
Of  
Sheffield.

# Manipulation of the inflammatory response *in vivo* using synthetic tanshinone analogues

By:

**Matthew James Foulkes**

A thesis submitted in partial fulfilment of the requirements for the degree of  
Doctor of Philosophy

The University Of Sheffield  
Faculty of Medicine, Dentistry and Health  
Department of Infection, Immunity & Cardiovascular Disease

March 2018



## Acknowledgements

Firstly, I would like to thank my supervisors, Professor Stephen Renshaw and Professor Simon Jones, for allowing me to work on a very interesting area of research, and for all their continued supervision, mentoring, and guidance over the last few years. I would particularly like to thank Dr. Katherine Henry, and Jenna and Charlie, as well as Joseph, Rosie, Alec, Sally, Rheanna, Dan C, Debs, Shannon, Sam and Esther, plus Anne, Cat, Noémie, Dave, Nik, Hannah, Kyle, Samir, Josie, Jo, Andrew, Becca, Ashlie, Dan J, Al, Bryony, Jonny and Ben, for their friendship outside of my PhD studies, as well as their support during my studies. I also thank the rest of D31 and the rest of the Jones group, as well as various technical members of staff, Denise, Louise and Sandra in the Department of Chemistry, the Aquarium staff, and the administrative team in the Medical School. I am grateful to The University Of Sheffield for funding my research. Finally, I would especially like to thank my family, especially Mum, Dad, Holly, Nana, and Reggie, for their eternal love and support throughout my PhD studies.

## Declaration

I declare that all the work contained herein is my own work, unless otherwise referenced.

In Chapter 6, most figures, and some of the accompanying text, have been reproduced from my corresponding paper first published in *Scientific Reports*:

Foulkes, M. J. *et al.* Expression and regulation of drug transporters in vertebrate neutrophils. *Sci. Rep.* **7**, 4967 (2017).

This is copyright-compliant, and in accordance with the Nature Publishing Group permissions policy, accessed at <https://www.nature.com/reprints/permission-requests.html>.

## Contents

<b>Acknowledgements</b> .....	3
<b>Declaration</b> .....	4
<b>Contents</b> .....	5
<b>Abbreviations and commonly-used terms</b> .....	10
<b>List of figures</b> .....	15
<b>List of schemes</b> .....	17
<b>List of tables</b> .....	19
<b>1. Abstract</b> .....	20
<b>2. Introduction</b> .....	21
2.1 Inflammation .....	21
2.1.1 Neutrophils in the inflammatory response .....	21
2.1.2 Unresolved neutrophilic inflammation in human diseases .....	23
2.1.3 Current and future treatments for unresolved inflammation .....	24
2.2 Zebrafish models of human disease.....	26
2.2.1 Advantages of the zebrafish model.....	26
2.2.2 Zebrafish models of the inflammatory response .....	27
2.2.3 Use of zebrafish models in compound screens.....	28
2.3 Tanshinones.....	30
2.3.1 Origin of tanshinones .....	30
2.3.2 Biological effects of tanshinones.....	31
2.3.3 Chemical synthesis methods for TI and analogues .....	33
2.3.4 Chemical synthesis methods for TIIA and analogues.....	41
2.4 Hypothesis and research aims.....	48
<b>3. Materials and Methods</b> .....	50
3.1 Reagents and equipment .....	50
3.2 Zebrafish husbandry .....	50
3.3 Larval tailfin transection.....	51
3.4 Larval compound treatment .....	52

3.5 Neutrophil recruitment experiments .....	52
3.6 Inflammation resolution experiments .....	53
3.7 Statistical analysis.....	53
<b>4. Synthesis and evaluation of tanshinone I analogues and isotanshinone I analogues.....</b>	<b>55</b>
4.1 Introduction.....	55
4.2 Hypothesis and aims .....	56
4.3 Initial synthesis of TI.....	56
4.3.1 Initial steps .....	56
4.3.2 Minisci-type radical decarboxylative alkylation reaction .....	58
4.3.3 Intramolecular Heck reaction.....	61
4.3.4 Demethylation reaction .....	62
4.3.5 Modified Feist-Bénary reaction.....	63
4.4 Synthesis of TI analogues .....	66
4.4.1 Radical decarboxylative alkylation.....	66
4.4.2 Use of Design of Experiments (DoE) studies in optimisation of the radical alkylation.....	66
4.4.3 Radical alkylation for analogue synthesis .....	69
4.4.4 Optimisation of the intramolecular Heck reaction .....	71
4.4.5 Final demethylation and modified Feist-Bénary reaction steps.....	75
4.4.6 Synthesis of a TI-acetal.....	77
4.5 Biological evaluation of TI, iso-TI and analogues .....	78
4.5.1 Effect of TI on neutrophil recruitment.....	78
4.5.2 Comparison of commercial and synthetic TI.....	79
4.5.3 Effects of TI analogues and isomers on neutrophil recruitment <i>in vivo</i> ...	80
4.5.4 Initial <i>in vivo</i> inflammation resolution experiments .....	84
4.5.5 Optimisation of inflammation resolution experiments and validation of new experimental timepoints using TI and TIIA .....	85
4.5.6 Effects of TI analogues and isomers on resolution of neutrophilic inflammation <i>in vivo</i> .....	89

4.5.7 Summary of effects of TI analogues and isomers on neutrophil behaviour during the inflammatory response <i>in vivo</i> .....	92
4.5.8 Aqueous solubilities and <i>in vivo</i> toxicities of TI analogues and isomers ..	95
4.6 Discussion .....	96
<b>5. Synthesis and evaluation of other tanshinone analogues and related compounds</b> .....	<b>103</b>
5.1 Introduction.....	103
5.2 Hypothesis and aims.....	107
5.3 Towards the synthesis of TIIA and analogues .....	108
5.3.1 General strategy .....	108
5.3.2 Dienophile synthesis.....	109
5.3.3 Attempted synthesis of dienes.....	115
5.3.4 Diels-Alder reactions using commercially available dienes .....	117
5.3.5 Summary.....	122
5.4 Lapachone and lapachol compounds .....	123
5.4.1 Chemical synthesis .....	123
5.4.2 Biological evaluation – recruitment experiments .....	125
5.4.3 Biological evaluation – resolution experiments .....	128
5.4.4 Biological evaluation – summary .....	130
5.5 Discussion .....	132
<b>6. How tanshinones access neutrophils – expression of drug transporter molecules in human and zebrafish neutrophils</b> .....	<b>138</b>
6.1 Introduction.....	138
6.2 Hypothesis and aims.....	139
6.3 Methods .....	140
6.3.1 Identification of relevant genes and protein sequences .....	140
6.3.2 Production of phylogenetic trees.....	141
6.3.3 Expression and regulation of human transporter proteins .....	141
6.3.4 Expression and regulation of zebrafish transporter proteins.....	142
6.4 Analysis of expression and regulation of drug transporters in human neutrophils .....	143

6.5 Expression analysis of drug transporters in zebrafish neutrophils .....	151
6.6 Comparison of drug transporter expression between human and zebrafish neutrophils .....	158
6.7 Discussion .....	159
<b>7. Discussion</b> .....	164
<b>8. Experimental</b> .....	169
8.1 General .....	169
8.2 Synthesis of TI analogues and iso-TI analogues .....	170
8.3 Towards the synthesis of other tanshinone analogues .....	187
8.4 Synthesis of structurally related compounds.....	193
<b>9. Bibliography</b> .....	196
<b>10. Appendix</b> .....	221
10.1 Previous studies in the Renshaw group found that various tanshinones accelerated resolution of neutrophilic inflammation in zebrafish .....	221
10.2 E3 medium.....	222
10.3 Tricaine solution .....	222
10.4 Phylogenetic trees with proportional branch lengths .....	223
10.4.1 Subsets of SLC transporter proteins were expressed and regulated in primary human neutrophils .....	223
10.4.2 Subsets of ABC transporter proteins were expressed and regulated in primary human neutrophils .....	225
10.5 Comparison of human drug transporter expression between distinct RNAseq datasets.....	227
10.5.1 Expression of SLC transporter proteins was largely consistent across two different datasets.....	227
10.5.2 Expression of ABC transporter proteins was largely consistent across two different datasets.....	238
10.6 Phylogenetic trees with proportional branch lengths .....	240
10.6.1 Zebrafish larval neutrophils and non-neutrophil cells expressed distinct subsets of SLC transporter proteins.....	240
10.6.2 Zebrafish larval neutrophils and non-neutrophil cells expressed distinct subsets of ABC transporter proteins.....	242

10.7 Drug transporters expressed in both human and zebrafish neutrophils.....	244
10.7.1 A subset of SLC drug transporters was expressed in both human and zebrafish neutrophils .....	244
10.7.2 A subset of ABC drug transporters was expressed in both human and zebrafish neutrophils .....	246

## Abbreviations and commonly-used terms

ABC	ATP-binding cassette
Ac	Acetyl
AD	Anno Domini
AMP	Adenosine monophosphate
ANOVA	Analysis of variance
app d	Apparent doublet
app t	Apparent triplet
aq	Aqueous
Ar	Aryl
ARDS	Acute respiratory disease syndrome
ATR	Attenuated total reflection
$\beta$ -lap	$\beta$ -Lapachone
br d	Broad doublet
br s	Broad singlet
br t	Broad triplet
Cas9	CRISPR associated protein 9
cat	Catalytic quantity
CF	Cystic fibrosis
cLogP	Calculated LogP
comm	Commercial
conc	Concentrated
COPD	Chronic obstructive pulmonary disease
CRISPR	Clustered Regularly Interspaced Short Palindromic Repeats
CRISPRi	CRISPR interference
d	Doublet
DCE	1,2-Dichloroethane
DCM	Dichloromethane
dd	Doublet of doublets
ddd	Double doublet of doublets

DDQ	2,3-Dichloro-5,6-dicyano-1,4-benzoquinone
DMAP	4-Dimethylaminopyridine
DME	1,2-Dimethoxyethane
DMF	<i>N,N</i> -Dimethylformamide
DMSO	Dimethyl sulfoxide
DNA	Deoxyribonucleic acid
DoE	Design of Experiments
dpf	Days post-fertilisation
dppf	1,1'-Bis(diphenylphosphino)ferrocene
dppp	1,3-Bis(diphenylphosphino)propane
dq	Doublet of quartets
E3	Embryo medium
EI	Electron impact
eq	Equivalentents
ESI	Electrospray ionisation
Et	Ethyl
FPKM	Fragments per kilobase of exon per million fragments mapped
FT-IR	Fourier-transform infrared spectroscopy
GEO	Gene Expression Omnibus
GFP	Green fluorescent protein
GM-CSF	Granulocyte macrophage colony-stimulating factor
h	Hours
HGNC	HUGO Gene Nomenclature Committee
HMDS	Hexamethyldisilazane
hpf	Hours post-fertilisation
hpi	Hours post-injury
HUGO	Human Genome Organisation
IC <sub>50</sub>	Half maximal inhibitory concentration

IL	Interleukin
iNOS	Inducible nitric oxide synthase
IR	Infrared
iTOL	Interactive Tree of Life
<i>J</i>	NMR coupling constant
Lap	Lapachol
LC <sub>50</sub>	Half maximal lethal concentration
lit	Literature
LPS	Lipopolysaccharide
m	Multiplet
max	Maximum
Me	Methyl
μw	Microwave
mol	Moles
mp	Melting point
MPO	Myeloperoxidase (human)
mpx	Myeloid-specific peroxidase (zebrafish)
mRNA	Messenger RNA
Ms	Methanesulfonyl (mesyl)
<i>m/z</i>	Mass divided by charge number
<i>n</i>	Number of individual subjects
<i>n</i> -	Normal
NAD	Nicotinamide adenine dinucleotide
<sup>n</sup> Bu	Normal butyl
NCBI	National Center for Biotechnology Information
NET	Neutrophil extracellular trap
NMR	Nuclear magnetic resonance
NQO1	NAD(P)H quinone oxidoreductase 1
Nor-β-lap	Nor-β-lapachone

ns	Not significant
ORDA	Online Research Data
<i>P</i>	Calculated probability value
PBIN	Phospholipid bilayer diffusion is negligible
Ph	Phenyl
pK <sub>a</sub>	-log <sub>10</sub> (acid dissociation constant)
PPA	Polyphosphoric acid
ppm	Parts per million
py	Pyridine
q	Quartet
qd	Quartet of doublets
quant	Quantitative yield
<i>r</i>	Pearson correlation coefficient
RNA	Ribonucleic acid
RNAseq	RNA-sequencing
ROS	Reactive Oxygen Species
rt	Room temperature
s	Singlet
SD	Standard deviation
SEM	Standard error of the mean
SGK1	Serum- and glucocorticoid-regulated kinase 1
SLC	Solute carrier
SP	SP600125
synth	Synthetic
t	Triplet
TBAF	Tetra- <i>n</i> -butylammonium fluoride
TBAI	Tetra- <i>n</i> -butylammonium iodide
TBDMS	<i>tert</i> -Butyldimethylsilyl
<sup>t</sup> Bu	Tertiary butyl

td	Triplet of doublets
temp	Temperature
Tf	Trifluoromethanesulfonate (triflate)
TFEA	2,2,2-Trifluoroethyl trifluoroacetate
Tg	Transgenic
THF	Tetrahydrofuran
TI	Tanshinone I
TIIA	Tanshinone IIA
TIIB	Tanshinone IIB
TIPS	Triisopropylsilyl
TLC	Thin layer chromatography
TNF $\alpha$	Tumour necrosis factor alpha
Ts	Toluenesulfonyl (tosyl)
vol	Volume
WHO	World Health Organisation
ZFIN	Zebrafish Information Network

## List of figures

<b>Figure 1.</b> A simplified schematic outlining the role played by neutrophils during the inflammatory response. ....	21
<b>Figure 2.</b> A transgenic larva, <i>Tg(mpx:GFP)<sup>j114</sup></i> , age 3 days post fertilisation (3 dpf), as viewed under the normal brightfield (top) and GFP (bottom) channels of a fluorescence microscope. ....	28
<b>Figure 3.</b> Exemplar tanshinones. ....	30
<b>Figure 4.</b> Published syntheses of various TI analogues (modified parts shown in red). ....	41
<b>Figure 5.</b> Published syntheses of various TIIA analogues (modified parts shown in red). ....	48
<b>Figure 6.</b> The larval tailfin was transected with a micro-scalpel blade at the position indicated by the red line, as viewed under the normal brightfield (top) and GFP (bottom) channels of a fluorescence microscope, thereby initiating an inflammatory response. ....	52
<b>Figure 7.</b> All neutrophils in the blue box shown were included in counting. Larva shown as observed under the normal brightfield (top) and GFP (bottom) channels of a fluorescence microscope. ....	53
<b>Figure 8.</b> Structures of the previously synthesised TI <b>1</b> and its 6-hydro derivative <b>31</b> ....	57
<b>Figure 9.</b> Structures of iso-TI <b>1</b> , iso-TIIA <b>78</b> and iso-TIIB <b>79</b> . ....	65
<b>Figure 10.</b> Possible interaction of the heteroatom substituent with the inserted palladium. ....	74
<b>Figure 11.</b> TI <b>1</b> treatment significantly reduced neutrophil recruitment to a site of injury. ....	79
<b>Figure 12.</b> Commercial and chemically synthesised TI <b>1</b> both reduced neutrophil recruitment, and there was no difference between the two batches of TI <b>1</b> . ....	80
<b>Figure 13.</b> TI <b>1</b> and iso-TI <b>13</b> resulted in decreased neutrophil recruitment to a site of injury, yet 6-hydro-TI <b>31</b> did not. ....	81
<b>Figure 14.</b> Neither 6-trifluoromethyl-TI <b>100</b> , 6-fluoro-TI <b>102</b> , 6-methoxy-TI <b>104</b> , nor 4-hydro-iso-TI <b>99</b> significantly affected neutrophil recruitment. ....	82
<b>Figure 15.</b> Trifluoromethyl- <b>101</b> and fluoro- <b>103</b> substituted isotanshinones resulted in decreased neutrophil recruitment, whilst neither 4-methoxy-iso-TI <b>105</b> nor the TI acetal <b>109</b> had any effect. ....	83

<b>Figure 16.</b> Neither TIIA <b>2</b> , TI <b>1</b> , iso-TI <b>13</b> , nor 6-hydro-TI <b>31</b> had any effect on inflammation resolution at 12 hpi. ....	85
<b>Figure 17.</b> The number of neutrophils at the site of injury reached a maximum at around 4 hpi, then resolved to pre-injury neutrophil numbers by 24 hpi. ....	86
<b>Figure 18.</b> TIIA <b>2</b> significantly accelerated inflammation resolution at 8 hpi. ....	87
<b>Figure 19.</b> Both TI <b>1</b> and TIIA <b>2</b> accelerated inflammation resolution. ....	88
<b>Figure 20.</b> TI <b>1</b> resulted in decreased neutrophil recruitment, yet TIIA <b>2</b> did not. ....	89
<b>Figure 21.</b> Iso-TI <b>13</b> significantly accelerated inflammation resolution, whilst TI <b>1</b> and 6-hydro-TI <b>31</b> did not. ....	90
<b>Figure 22.</b> 6-Methoxy-TI <b>104</b> significantly accelerated inflammation resolution, yet 6-trifluoromethyl-TI <b>100</b> , 6-fluoro-TI <b>102</b> , and 4-hydro-iso-TI <b>99</b> did not. ....	91
<b>Figure 23.</b> The TI acetal <b>109</b> significantly accelerated resolution of neutrophilic inflammation, yet the isotanshinones 4-trifluoromethyl-iso-TI <b>101</b> , 4-fluoro-iso-TI <b>103</b> , and 4-methoxy-iso-TI <b>105</b> all did not. ....	92
<b>Figure 24.</b> Structures of related compounds $\beta$ -lapachone <b>112</b> and nor- $\beta$ -lapachone <b>113</b> , and their structural similarity, shown in red, with TI <b>1</b> and TIIA <b>2</b> . ....	105
<b>Figure 25.</b> Structures of related compounds lapachol <b>114</b> and norlapachol <b>115</b> . ..	106
<b>Figure 26.</b> Disconnection of the general TIIA structure to the phenol <b>58</b> and various dienes. ....	108
<b>Figure 27.</b> The dimethyl diene <b>53</b> and the simplified diene <b>123</b> would give TIIA <b>2</b> and a tanshinone analogue <b>124</b> , respectively. ....	115
<b>Figure 28.</b> Norlapachol <b>115</b> significantly reduced neutrophil recruitment to a site of injury at 0.1 and 10 $\mu$ M concentrations, but not at a 1 $\mu$ M concentration. ....	126
<b>Figure 29.</b> $\beta$ -Lapachone <b>112</b> significantly reduced neutrophil recruitment at a concentration of 1 $\mu$ M, whilst at the same concentration, neither TI <b>1</b> , lapachol <b>114</b> , nor nor- $\beta$ -lapachone <b>113</b> significantly affected neutrophil recruitment. ....	128
<b>Figure 30.</b> Norlapachol <b>115</b> significantly accelerated resolution of neutrophilic inflammation at 10 and 25 $\mu$ M concentrations, but not at 0.1 or 1 $\mu$ M concentrations. ....	129
<b>Figure 31.</b> Neither lapachol <b>114</b> , $\beta$ -lapachone <b>112</b> , nor nor- $\beta$ -lapachone <b>113</b> significantly enhanced resolution of neutrophilic inflammation at a concentration of 1 $\mu$ M. ....	130
<b>Figure 32.</b> Possible routes to tanshinone analogues using an intramolecular Heck reaction (top) or C(sp <sup>3</sup> )-H activation chemistry (bottom). ....	134

<b>Figure 33.</b> Structure of the pancreatic cancer drug gemcitabine <b>141</b> . .....	139
<b>Figure 34.</b> Subsets of SLC transporter proteins were expressed and regulated in resting primary human neutrophils. ....	146
<b>Figure 35.</b> Subsets of ABC transporter proteins were expressed and regulated in resting primary human neutrophils. ....	148
<b>Figure 36.</b> Expression levels of human SLC and ABC transporter proteins across two different datasets showed highly significant positive correlation.....	150
<b>Figure 37.</b> Structure of the SGK1 inhibitor GSK650394 <b>142</b> . ....	151
<b>Figure 38.</b> Zebrafish larval neutrophils and non-neutrophil cells expressed distinct subsets of SLC transporter proteins.....	155
<b>Figure 39.</b> Zebrafish larval neutrophils and non-neutrophil cells expressed distinct subsets of ABC transporter proteins.....	157

## List of schemes

<b>Scheme 1.</b> Synthesis of TI <b>1</b> from podocarpic acid <b>6</b> .....	34
<b>Scheme 2.</b> Use of a Diels-Alder reaction to synthesise TI <b>1</b> in six steps .....	35
<b>Scheme 3.</b> A photochemical cyclisation strategy for synthesis of TI <b>1</b> .....	36
<b>Scheme 4.</b> Use of a photochemical aromatic annulation strategy to give TI <b>1</b> in nine steps .....	37
<b>Scheme 5.</b> Synthesis of TI <b>1</b> from 5-bromovanillin <b>27</b> .....	38
<b>Scheme 6.</b> Synthesis of TI <b>1</b> in three steps using Diels-Alder, epoxidation, and Feist-Bénary reactions .....	39
<b>Scheme 7.</b> Large scale synthesis of TI <b>1</b> in three steps using a Diels-Alder strategy .	40
<b>Scheme 8.</b> Synthesis of TIIA <b>2</b> from 7-methoxy-1-tetralone <b>37</b> .....	42
<b>Scheme 9.</b> Synthesis of TIIA <b>2</b> in seventeen steps from 1,2,4-trimethoxybenzene <b>43</b> .....	43
<b>Scheme 10.</b> TIIA <b>2</b> synthesis using a Diels-Alder reaction.....	44
<b>Scheme 11.</b> Use of ultrasound to improve the outcome of the Diels-Alder reaction in the synthesis of TIIA <b>2</b> .....	45
<b>Scheme 12.</b> Use of a photochemical aromatic annulation strategy to synthesise TIIA <b>2</b> .....	46
<b>Scheme 13.</b> A SmI <sub>2</sub> -promoted radical cyclisation approach to TIIA <b>2</b> .....	47

<b>Scheme 14.</b> Baeyer-Villiger oxidation of 5-bromovanillin <b>27</b> . .....	58
<b>Scheme 15.</b> Oxidation of the 1,4-hydroquinone <b>28</b> to the 1,4-benzoquinone <b>29</b> . ...	58
<b>Scheme 16.</b> Reaction of the 1,4-benzoquinone <b>29</b> with 3-(2-methylphenyl)propionic acid <b>75</b> . .....	59
<b>Scheme 17.</b> Radical alkylation using optimised conditions. ....	60
<b>Scheme 18.</b> Palladium-catalysed intramolecular Heck reaction. ....	61
<b>Scheme 19.</b> Complete aromatisation using palladium on carbon. ....	62
<b>Scheme 20.</b> Attempted <i>O</i> -demethylation using boron trichloride. ....	62
<b>Scheme 21.</b> Attempted modified Feist-Bénary reaction. ....	64
<b>Scheme 22.</b> Synthesis of TI <b>1</b> and its isomer iso-TI <b>13</b> . ....	65
<b>Scheme 23.</b> Radical alkylation of the benzoquinone <b>29</b> with 3-phenylpropionic acid <b>80</b> . .....	66
<b>Scheme 24.</b> General radical alkylation reaction for optimisation studies using DoE. ....	67
<b>Scheme 25.</b> Radical alkylation reaction using various substituted carboxylic acids..	71
<b>Scheme 26.</b> General scheme for the intramolecular Heck reaction using the unsubstituted substrate <b>81</b> . .....	72
<b>Scheme 27.</b> Optimised intramolecular Heck reaction conditions. ....	73
<b>Scheme 28.</b> Intramolecular Heck reaction using various substituted analogues. ....	74
<b>Scheme 29.</b> Aqueous hydroxide-mediated ether demethylation for various analogues. ....	75
<b>Scheme 30.</b> Reaction of various alcohols <b>9, 30, 96-98</b> with chloroacetone to produce tanshinones <b>1, 31, 100, 102, 104</b> and isotanshinones <b>13, 99, 101, 103, 105</b> . .....	76
<b>Scheme 31.</b> Attempted microwave reactions with sources of chloroacetaldehyde.	77
<b>Scheme 32.</b> Synthesis of a dimethyl acetal <b>109</b> from TI <b>1</b> . ....	77
<b>Scheme 33.</b> Use of a Diels-Alder reaction to synthesise various tanshinone analogues. ....	104
<b>Scheme 34.</b> Enamine formation from propanal <b>57</b> and piperidine <b>116</b> . ....	109
<b>Scheme 35.</b> Attempted reaction of the enamine <b>117</b> with <i>para</i> -benzoquinone <b>32</b> . ....	110
<b>Scheme 36.</b> Attempted benzofuranol <b>58</b> formation from propanal <b>57</b> and <i>para</i> -benzoquinone <b>32</b> in the presence of L-proline. ....	111

<b>Scheme 37.</b> Enamine <b>120</b> formation using morpholine <b>119</b> followed by reaction with <i>para</i> -benzoquinone <b>32</b> and chromatographic purification. ....	112
<b>Scheme 38.</b> Acid-mediated elimination to give 3-methyl-5-benzofuranol <b>58</b> .....	113
<b>Scheme 39.</b> Synthesis of 3-methyl-5-benzofuranol <b>58</b> in three steps from propanal <b>57</b> .....	113
<b>Scheme 40.</b> Selective oxidation of 3-methyl-5-benzofuranol <b>58</b> using Fremy's salt to form the <i>ortho</i> -quinone <b>59</b> . ....	114
<b>Scheme 41.</b> The diene <b>123</b> could be synthesised from cyclohexanone <b>126</b> in two steps, comprising a Grignard reaction followed by dehydration. ....	116
<b>Scheme 42.</b> Formation of the <i>ortho</i> -quinone dienophile <b>59</b> and subsequent Diels-Alder reaction with cyclopentadiene <b>127</b> .....	118
<b>Scheme 43.</b> Formation of the <i>ortho</i> -quinone dienophile <b>59</b> and attempted Diels-Alder reaction with cyclohexadiene <b>128</b> . ....	119
<b>Scheme 44.</b> Use of an ultrasound-promoted Diels-Alder reaction to synthesise a mixture of tanshinone analogues <b>133</b> and <b>134</b> . ....	120
<b>Scheme 45.</b> Formation of the <i>ortho</i> -quinone dienophile <b>59</b> and subsequent Diels-Alder reaction with Danishefsky's diene <b>130</b> .....	121
<b>Scheme 46.</b> Synthesis of $\beta$ -lapachone <b>112</b> from lapachol <b>114</b> . ....	123
<b>Scheme 47.</b> Synthesis and proposed mechanism for the formation of norlapachol <b>115</b> from lapachol <b>114</b> by a Hooker oxidation.....	124
<b>Scheme 48.</b> Synthesis of nor- $\beta$ -lapachone <b>113</b> from norlapachol <b>115</b> .....	125

## List of tables

<b>Table 1.</b> Optimisation of conditions for the radical alkylation reaction. ....	60
<b>Table 2.</b> Reagents investigated for <i>O</i> -demethylation. ....	63
<b>Table 3.</b> The ten radical alkylation experiments carried out, as determined by the JMP DoE software. ....	68
<b>Table 4.</b> Summary of the effects of various tanshinones and isotanshinones on neutrophil recruitment and resolution of neutrophilic inflammation <i>in vivo</i> . ....	95
<b>Table 5.</b> Summary of the effects of norlapachol <b>115</b> , lapachol <b>114</b> , $\beta$ -lapachone <b>112</b> , and nor- $\beta$ -lapachone <b>113</b> on neutrophil recruitment and resolution of inflammation <i>in vivo</i> . ....	132

## 1. Abstract

During inflammation, retention of persistent neutrophils at the inflammatory site, either due to excessive neutrophil recruitment or failed spontaneous resolution of inflammation, can play a major role in many chronic inflammatory diseases, such as chronic obstructive pulmonary disease. Current treatments for dysregulated inflammation are generally ineffective, non-specific, and can exhibit undesired side effects, thus there remains a need to identify new effective clinical treatments. Tanshinones have shown promising anti-inflammatory effects by targeting neutrophils *in vivo*, yet are still an underexplored class of compounds in this regard. In this work, an optimised six step synthetic route was used to synthesise a series of substituted tanshinone analogues and isomeric isotanshinones. A radical decarboxylative alkylation and an intramolecular Heck reaction were key steps in this route, and optimisation of these processes was explored considerably, including the use of Design of Experiments software. Synthesis of additional tanshinones using a Diels-Alder reaction was investigated, whilst some further compounds with broad structural similarity to tanshinones were also produced. All synthesised compounds were evaluated *in vivo* using a zebrafish model of inflammation. Some of the compounds reduced initial neutrophil recruitment, whilst others accelerated resolution of neutrophilic inflammation, which allowed for the construction of broad structure-activity relationships and identification of compounds with promising *in vivo* anti-inflammatory effects. Notable differences in toxicity profiles between compound classes were also observed. In addition, to seek a greater understanding of how molecules such as tanshinones access their molecular target *in vivo*, analysis of the expression of drug transporter proteins in human and zebrafish neutrophils was carried out. Annotated phylogenetic trees were produced which are envisaged to provide a generally useful resource to the field in future studies.

## 2. Introduction

### 2.1 Inflammation

#### 2.1.1 Neutrophils in the inflammatory response

Inflammation is the body's natural protective response initiated either when tissue is injured, or when infection is detected within the body, due to exposure to an external pathogen or toxin. Upon initiation, the inflammatory response is induced, an essential part of host defence which comprises a highly controlled sequence of events and consists of two components: the innate (non-adaptive) immune response, and the adaptive immune response.<sup>1</sup> The innate response occurs immediately, and entails recognition of the pathogen, toxin or injury, followed by response from innate immune cells including neutrophils, macrophages, and eosinophils, and the involvement of various modulatory molecules including cytokines and lipid mediators, amongst other processes. The adaptive immune response, which only occurs in vertebrates, is considered the second line of defence, providing specificity towards any invading pathogen. Lymphocytes, comprising B cells, T cells, and natural killer cells, are primarily involved in this response.

Neutrophils are one of the largest circulating populations of white blood cell found in humans as well as most other vertebrate and non-vertebrate organisms.<sup>2</sup> They comprise around 50% of the human body's white blood cells and are amongst the most important cell types involved in the inflammatory response, as one of the first responders to injury or pathogen invasion.<sup>3</sup> Neutrophils thereby play a vital role in the mediation of all stages of the inflammatory response (Figure 1). This can be generally divided up into initial neutrophil recruitment, peak neutrophilic inflammation, and resolution of neutrophilic inflammation.<sup>4</sup>

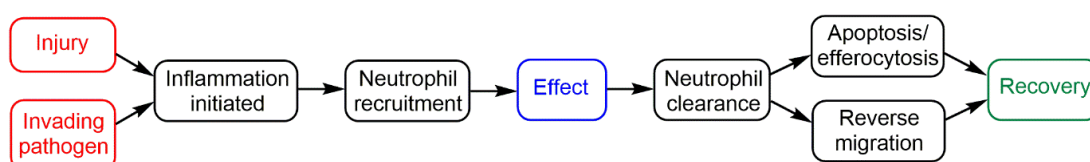


**Figure 1.** A simplified schematic outlining the role played by neutrophils during the inflammatory response.

Upon injury or pathogen invasion, neutrophils become activated and are subsequently recruited to the site of injury or infection in the affected organ(s), usually within 6 hours of initiation.<sup>5</sup> This occurs in response to chemical pro-inflammatory stimuli, which include soluble cytokines such as interleukin-8 (IL-8), and reactive oxygen species (ROS).<sup>6,7</sup>

At the site of injury or infection, recruited neutrophils act to defend and protect the body, eliminating any invading pathogens by phagocytosis, degranulation, release of neutrophil extracellular traps (NETs) and proteases, and production of ROS.<sup>6,8-11</sup> It is essential that neutrophil function is strictly regulated: whilst these processes are required for effective host defence and response, they also need to be limited to avoid persistent inflammation.<sup>12</sup>

Following this, timely removal of recruited neutrophils from the site of injury or infection, a key part of resolution of neutrophilic inflammation, is necessary.<sup>5,13,14</sup> In healthy individuals, this is a tightly controlled process which ultimately leads to recovery, as the number of neutrophils at the inflammatory site returns to pre-inflammation levels, restoring homeostasis and mediating tissue repair.<sup>5,14,15</sup> One way in which resolution is achieved is through neutrophil apoptosis, the programmed cell death of neutrophils, and subsequent engulfment of apoptotic cells by macrophages (another type of white blood cell), termed efferocytosis. The process of apoptosis has been recognised for over forty years,<sup>16</sup> and is a well-documented process for the clearance of neutrophils in the resolution stage.<sup>11,17-22</sup> Neutrophils may also be cleared by removal from the inflammatory site into inflammatory exudates.<sup>23</sup>

An additional, more recently reported mechanism for the clearance of neutrophils is reverse migration of neutrophils from the inflammatory site to other parts of the body.<sup>24</sup> As early as 1997, movement of neutrophils away from an inflammatory site was reported for intravascular neutrophils in kidneys in a rat model, and was suggested to be a previously unreported mechanism which predominated over neutrophil apoptosis.<sup>25</sup> An analogous retrograde mechanism was later identified for human neutrophils,<sup>26</sup> including in microfluidic devices,<sup>27</sup> as well as in mice.<sup>28</sup> In zebrafish, this process was originally reported to be analogous to retrograde chemotaxis,<sup>29</sup> and was

often termed as fugetaxis or chemorepulsion, meaning that the neutrophils were actively moving away from a chemokinetic agent: this suggested that neutrophil movement away from the wound was a persistent and directional phenomenon.<sup>30,31</sup> Later studies, also in zebrafish, also identified a bidirectional movement of neutrophils consistent with directional reverse migration.<sup>32-34</sup> However, analysis of the patterns of neutrophil migration observed up to this point was relatively limited. Detailed characterisation of the neutrophil reverse migration dynamics later undertaken found that neutrophils were actually randomly dispersed from the wound in a redistribution process,<sup>35</sup> and that their movement away from the wound was not directional or a form of fugetaxis as previously suggested. Recent work in zebrafish was found to be in agreement with this characterisation of reverse migration.<sup>36</sup> A later study suggested that neutrophils which had reverse migrated showed no long-term phenotypic differences compared to neutrophils which had not been involved in the inflammatory response.<sup>37</sup> The relative contributions of apoptosis and reverse migration to neutrophil clearance processes are currently unclear, but have been much discussed in the literature, with both processes thought to occur, but to varying extents in differing studies.<sup>29,36,38,39</sup>

### 2.1.2 Unresolved neutrophilic inflammation in human diseases

Excess neutrophil recruitment or dysregulation of the mechanisms of inflammation resolution can result in persistent neutrophils remaining at the inflammatory site. This can have very damaging, often irreversible effects on the surrounding tissue, due to the release of toxic granule proteins, resulting in pathogenesis of chronic inflammation.<sup>11,40,41</sup> Thus, failed resolution of neutrophilic inflammation is known to play a key role in various chronic inflammatory diseases. One of the main diseases which failed inflammation resolution can contribute to is chronic obstructive pulmonary disease (COPD),<sup>42,43</sup> and the related acute respiratory disease syndrome (ARDS).<sup>44</sup> COPD is the fourth highest cause of global mortality, claiming over three million lives annually, which corresponds to 5% of all global deaths, and this figure is projected to increase further in future years.<sup>45</sup>

Prominent neutrophilic inflammation has also been identified from analysis of the sputum of some asthmatic patients, in which neutrophils were the major inflammatory cell present.<sup>46</sup> Further studies identified that higher neutrophil numbers were associated with severe asthma, suggesting that a lack of neutrophil clearance and unresolved inflammation made a major contribution to this chronic disease.<sup>47–49</sup> A reduction in human neutrophil apoptosis in patients with chronic severe asthma was later identified.<sup>50</sup>

In addition to COPD and asthma, failed efferocytosis and chronic neutrophilic inflammation have been associated with various other chronic inflammatory lung diseases. These include cystic fibrosis (CF), non-CF bronchiectasis, and other infiltrative pulmonary diseases.<sup>51,52</sup> Furthermore, dysregulation of inflammation resolution is thought to contribute significantly to neurodegenerative disease, multiple sclerosis and rheumatoid arthritis,<sup>53–55</sup> whilst harmful inflammation is also implicated in atherosclerosis,<sup>56</sup> as well as obesity.<sup>54,57</sup>

### 2.1.3 Current and future treatments for unresolved inflammation

Chronic diseases characterised by unresolved neutrophilic inflammation largely respond poorly to current treatments, which include inhaled bronchodilators and glucocorticoids, a group of steroids which are used as anti-inflammatory agents for treating various diseases including asthma and rheumatoid arthritis.<sup>58–60</sup> However, these compounds are non-specific, poorly effective, and can exhibit many undesired side effects.<sup>61,62</sup> Long term usage of such treatments can lead to harmful effects such as increased susceptibility to infection.<sup>60</sup>

Aside from these treatments, some of the most promising therapeutic approaches for promoting inflammation resolution involve replication of endogenous pro-resolution lipid mediators such as lipoxins, protectins, resolvins and maresins.<sup>63–68</sup> Resolvins are a group of mediators produced *in vivo* during the inflammatory response, which themselves exhibit anti-inflammatory properties by promoting resolution of inflammation, exhibiting their maximal effect during the spontaneous resolution phase.<sup>64,65,69,70</sup> Maresins (**macrophage mediators in resolving inflammation**) are a group

of powerful anti-inflammatory, pro-resolution mediators, which promote inflammation resolution by regulating the entry of neutrophils, and stimulating phagocytosis by macrophages.<sup>66,71,72</sup>

Apart from lipid mediators, other classes of compounds have been found to accelerate inflammation resolution, a process which can be achieved by increased induction of neutrophil apoptosis.<sup>73,74</sup> For example, cyclin-dependent kinase inhibitors such as *R*-roscovitine have been found to promote inflammation resolution by increasing apoptosis of neutrophils.<sup>22,75</sup> Serum- and glucocorticoid-regulated kinase 1 (SGK1) is also a kinase which can be targeted to enhance resolution of neutrophilic inflammation.<sup>76</sup>

However, in general, there are currently very few treatments which are effective in promoting the resolution of neutrophilic inflammation without exhibiting unwanted side effects. This may in part be due to a lack of *in vivo* drug screening approaches, as well as limitations in understanding how drugs penetrate and access cells such as neutrophils. Whilst some treatments are showing promise, these are somewhat limited by a lack of understanding of their mechanism of action at a molecular level. Some of these also do not exhibit selectivity, for example in targeting the particular cell type of interest. There are currently no clinical treatments in use for treating unresolved inflammation which specifically target the neutrophil. Therefore, there remains a need to identify new safe and effective anti-inflammatory compounds which target neutrophils, either by modulating initial neutrophil recruitment to, and accumulation at, the site of inflammation, or by accelerating the clearance of neutrophils from the inflammatory site following peak inflammation (pro-resolution compounds), including by promoting reverse migration.<sup>13</sup> Ideal compounds would exclusively accelerate resolution of neutrophilic inflammation, as this would promote tissue healing without compromising host defence. It is clearly not desirable to reduce neutrophil recruitment to such an extent that susceptibility to infection is compromised; however, pharmacological reduction of neutrophil recruitment could still be helpful in modulating inflammation in certain patients. In particular, such treatments could be beneficial for patients who are unable to clear neutrophils following initial recruitment, and/or those

who recruit a disproportionately large number of neutrophils and later experience difficulty in clearing all of these. Indeed, ongoing research in the pharmaceutical industry has involved the identification of several possible anti-inflammatory drugs which target the neutrophil recruitment stage of the inflammatory response.<sup>77–81</sup>

## 2.2 Zebrafish models of human disease

### 2.2.1 Advantages of the zebrafish model

The zebrafish (*Danio rerio*) is an outstanding model system for studying biological processes, as a vertebrate with high gene homology to humans, particularly for the heart and blood.<sup>82</sup> This provides important translational relevance, especially for modelling various human diseases.<sup>83,84</sup> The genetic tractability of zebrafish means that genetic modifications, and therefore generation of transgenic lines, can be readily carried out.<sup>29,85,86</sup> Mutations can be efficiently induced, whilst eggs can be fertilised *in vitro* and sperm can be frozen.<sup>87</sup> Tailfin regeneration can occur not only in adults, but also in younger zebrafish,<sup>88</sup> with a mechanism similar to that in adults, both at a cellular and molecular level. Zebrafish hearts can also regenerate,<sup>89</sup> overcoming the scarring which typically occurs in humans. As a vertebrate *in vivo* model, use of the zebrafish allows for exploration of complex cellular processes in their native biological context, rather than in isolation as for *in vitro* approaches. Other advantages include the fast growth rate and cost-effectiveness of zebrafish.<sup>83,90</sup>

In addition, use of *in vivo* models such as zebrafish provides an excellent phenotypic screening approach for evaluating numerous compounds in various disease models. In particular, any possible issues with drug efficacy and toxicity can be identified early in the drug discovery and development process, as well as off-target effects.<sup>90–94</sup> This represents a great advantage compared to the more traditional drug discovery approach generally used by large pharmaceutical companies, in which *in vivo* studies are typically carried out much later on in the process. Indeed, this latter approach bears an incredibly high attrition rate, with drug toxicity and lack of efficacy representing two of the most common causes of a drug failing to reach the clinic.<sup>95–98</sup>

In the laboratory, the zebrafish provides further practical advantages. Due to the high fertility of adult zebrafish, a single mating can give rise to hundreds of larvae. Larvae and young zebrafish are transparent, meaning that individual cells can be easily tracked *in vivo*. Embryos can be visualised under a standard biological microscope, and their small size facilitates convenient handling in the laboratory, as they can be easily transferred into Petri dishes and 6-, 24- or 96- well plates, enabling efficient screening of large numbers of compounds.

### 2.2.2 Zebrafish models of the inflammatory response

Humans and zebrafish share highly conserved immune systems, meaning that zebrafish can be used as an effective model for the inflammatory response.<sup>84,99,100</sup> The adaptive immune system of zebrafish does not fully develop and become completely functional until approximately four weeks after fertilisation, meaning that the innate immune response can be studied independently during the first few weeks of development.<sup>100–102</sup> Similarities between the innate immune systems of the two organisms include the presence of conserved molecular components such as pro-inflammatory cytokines,<sup>84,100</sup> similar inflammatory response kinetics,<sup>5,86</sup> and the presence of neutrophils, allowing for effective study of neutrophil behaviour.<sup>103</sup>

Zebrafish neutrophils are functionally developed as early as 48 hours post-fertilisation and have been found to resemble those of humans,<sup>104</sup> containing segmented nuclei, cytoplasmic granules, and myeloid-specific peroxidase (Mpx), a protein which is a zebrafish equivalent of the human myeloperoxidase protein (MPO), and is specifically expressed in neutrophils.<sup>103–105</sup> Like human neutrophils, zebrafish neutrophils are also able to phagocytose and kill pathogens,<sup>106</sup> and produce NETs.<sup>107</sup> Myeloid precursors develop similarly in the zebrafish kidney and in the bone marrow of humans.<sup>105</sup>

The genetic tractability of zebrafish means that various cell types of interest can be labelled and monitored, including innate immune cells such as neutrophils.<sup>100</sup> This allows for *in vivo* manipulation and study of inflammation, including mechanisms governing different phases of the inflammatory response such as recruitment and

resolution,<sup>33,86,108</sup> as well as dissection of different clearance mechanisms for resolution of neutrophilic inflammation, namely apoptosis and reverse migration.

The first transgenic zebrafish models for analysis of the inflammatory response which used fluorescently labelled neutrophils were established in 2006, in which the neutrophil-specific *mpx* promoter controls expression of green fluorescent protein (GFP) (Figure 2).<sup>86</sup> Tissue injury was induced by injuring the tailfin with a sterile scalpel blade, initiating a reliable inflammatory response. Neutrophils were identified by their fluorescence and counted at various time points, whilst live microscopy could be used to track cells.<sup>39</sup> Later work showed that neutrophils and macrophages could be imaged simultaneously using a closely related transgenic zebrafish model,<sup>109</sup> and other macrophage-specific markers have also been identified,<sup>110,111</sup> enabling macrophage behaviour to be studied both exclusively and in conjunction with neutrophils. Furthermore, the inflammatory response could be modulated using various pharmacological agents.<sup>38</sup> Other methods apart from tailfin injury are known for inducing an inflammatory response in zebrafish, including the use of lipopolysaccharide (LPS),<sup>112</sup> other chemicals such as copper sulfate,<sup>113</sup> and manipulation of the swim bladder.<sup>114</sup>

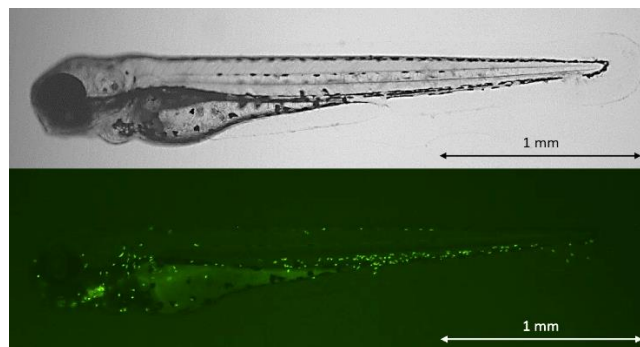


**Figure 2.** A transgenic larva, *Tg(mpx:GFP)i114*, age 3 days post fertilisation (3 dpf), as viewed under the normal brightfield (top) and GFP (bottom) channels of a fluorescence microscope.

### 2.2.3 Use of zebrafish models in compound screens

Since 2000, zebrafish have been used for undertaking large-scale compound screens, working towards identification of compounds that affect vertebrate development and

function.<sup>115</sup> The small size and large numbers of larvae available enables utilisation of high throughput drug screens, which have been employed successfully in numerous cases.<sup>36,112,113,116–119</sup>

Zebrafish have since been used for high throughput assays to identify potential anti-inflammatory compounds. For example, a chemically-induced inflammation assay has been used as a method of quickly screening thousands of compounds, to identify new leads for potential therapeutic treatments for inflammation.<sup>113</sup> More recently, a LPS-induced inflammation assay was used to screen for anti-inflammatory compounds *in vivo*,<sup>112</sup> whilst a zebrafish model was also used in the screening of a library of natural products to identify compounds which inhibited neutrophil recruitment.<sup>119</sup> In an independent study, a larger compound screen using an *in vivo* zebrafish model was used in the identification of compounds which accelerated resolution of inflammation, and found that a natural product molecule called tanshinone IIA was highly active.<sup>36</sup> This compound exhibited its effect by enhancing reverse migration of neutrophils, as well as resulting in a small increase in neutrophil apoptosis, yet without any significant effect on the number of neutrophils recruited to the site of injury. A related molecule called tanshinone I is also thought to exhibit an anti-inflammatory effect, although this has been only scarcely studied (Dr. Anne Robertson, The University Of Sheffield, Appendix 10.1).

As these tanshinones appear to display anti-inflammatory effects in zebrafish, effects of closely related structural analogues of these molecules in this model are also of interest. Little work has been done in this area (Appendix 10.1), and investigation of the effects of such molecules on neutrophil behaviour in a zebrafish model of inflammation is vastly underexplored. Many close derivatives have never been synthesised before, whilst others have not been investigated for anti-inflammatory activity, in particular, in relation to neutrophil-specific effects or in a zebrafish model. Therefore, synthesis of tanshinones, and their analogues, is of interest here.

## 2.3 Tanshinones

### 2.3.1 Origin of tanshinones

Tanshinones are a group of natural products found in *Salvia miltiorrhiza* (also known as *danshen*, *tanshen* or Chinese red sage), a plant traditionally used as a remedy in Chinese herbal medicine since as early as the first century AD.<sup>120</sup> First isolated from the plant in 1934,<sup>121</sup> these molecules are often referred to as abietane diterpenoids, and generally consist of four fused rings. Two of these rings form a naphthalene or tetrahydronaphthalene moiety, the third is usually an *ortho*- or *para*-quinone (or lactone), and the fourth ring is a furan or dihydrofuran. Particular tanshinones are differentiated by their different substituents, number of aromatic rings present in the molecule, or their stereochemical configuration: specific examples include tanshinone I (TI) **1**, tanshinone IIA (TIIA) **2**, tanshinone IIB (TIIB) **3**, dihydrotanshinone I **4** and cryptotanshinone **5** (Figure 3). In particular, TI **1** and TIIA **2** are amongst the most widely investigated tanshinones.

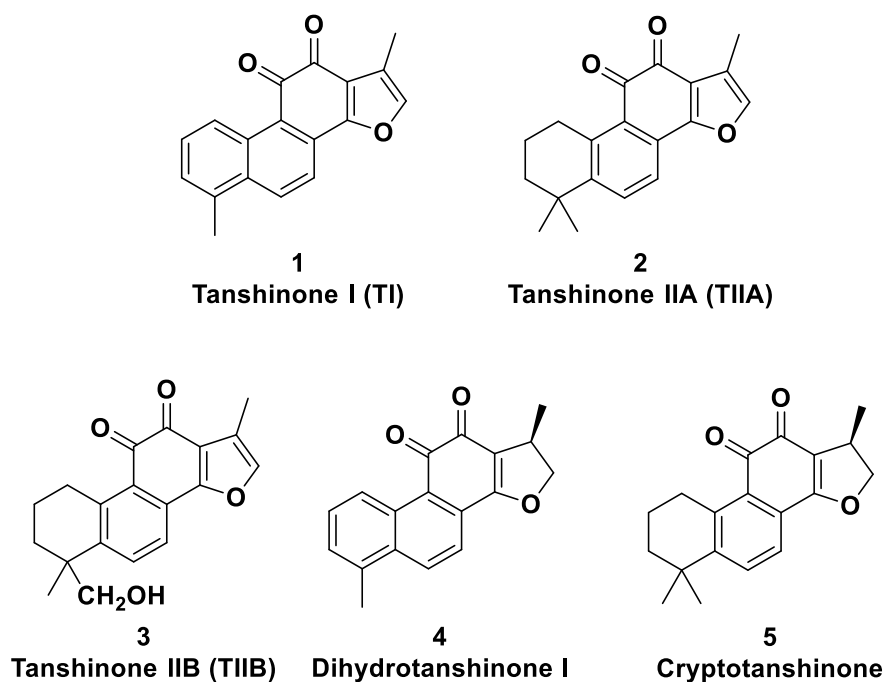


**Figure 3.** Exemplar tanshinones.

Isolation of specific tanshinones directly from *Salvia miltiorrhiza* usually requires a series of extractions starting from the dried roots immersed in alcoholic solution,<sup>122–125</sup>

followed by chromatographic separation. Whilst this is sufficient for attaining milligram quantities of a particular compound for biological testing, the specificity and low-yielding nature of this approach means that for obtaining practically useful quantities of various analogues, a synthetic organic chemistry approach is usually required, and is a necessity for the synthesis of any novel tanshinone derivatives.

### 2.3.2 Biological effects of tanshinones

*Salvia miltiorrhiza* has long been used as a remedy in traditional Chinese medicine, to treat a broad spectrum of conditions. These mainly comprise cardiovascular diseases including atherosclerosis and angina, and various inflammatory diseases such as arthritis and hepatitis, as well as other diseases including stroke, liver fibrosis, tuberculosis and leprosy, and anti-cancer activity.<sup>126–133</sup> However, recent studies have sought to isolate, identify and investigate some of the biological effects of particular tanshinones found within *Salvia miltiorrhiza*. TI **1** and TIIA **2**, as two of the more naturally abundant tanshinones in the herb, have been particularly well studied for various biological activities, especially TIIA **2**. Many analogous effects have also been reported throughout the literature for the highly structurally similar molecules dihydrotanshinone I **4** and cryptotanshinone **5**.

Numerous studies have found that TI **1** induces apoptosis in various cell types, including in activated hepatic stellate cells,<sup>134</sup> human colorectal cancer cells,<sup>135</sup> and gastric cancer cells.<sup>136</sup> Induction of apoptosis by TIIA **2** is also well-documented, in cells such as human leukaemia cells,<sup>137,138</sup> human brain tumour (glioma) cells,<sup>139</sup> cardiomyocytes,<sup>140</sup> and osteosarcoma cells.<sup>141</sup> Such effects may occur as a result of various events, including activation of caspase-3 and/or caspase-12, events which likely have important implications in other biological effects such as anti-inflammatory activity.<sup>137,142,143,144</sup> TIIA **2** is also a substrate of NAD(P)H quinone oxidoreductase 1 (NQO1), resulting in apoptotic cell death in certain lung cancer cells.<sup>145</sup>

These apoptotic effects are particularly relevant to the cytotoxic effects exhibited by tanshinones: in TI **1** this has been reported for human colon cancer cells,<sup>146,147</sup> and for different types of leukaemia cells.<sup>142</sup> Anti-cancer activity exhibited by TIIA **2** has similarly

been observed against human breast cancer cells,<sup>148</sup> as well as for various other cancer cells, and in other model organisms such as *Drosophila*.<sup>139,147,149–151</sup>

Tanshinones have been reported to exhibit antioxidant effects, possibly by reacting with lipid free radicals and preventing lipid peroxidation products from binding with DNA.<sup>152</sup> It was previously suggested that TIIA **2** did not act as an antioxidant, in contrast to other tanshinones such as TI **1**,<sup>153,154</sup> but TIIA **2** was later found to inhibit oxidation of low density lipoproteins, indicating a possible use for this molecule in preventing atherosclerosis development.<sup>155</sup>

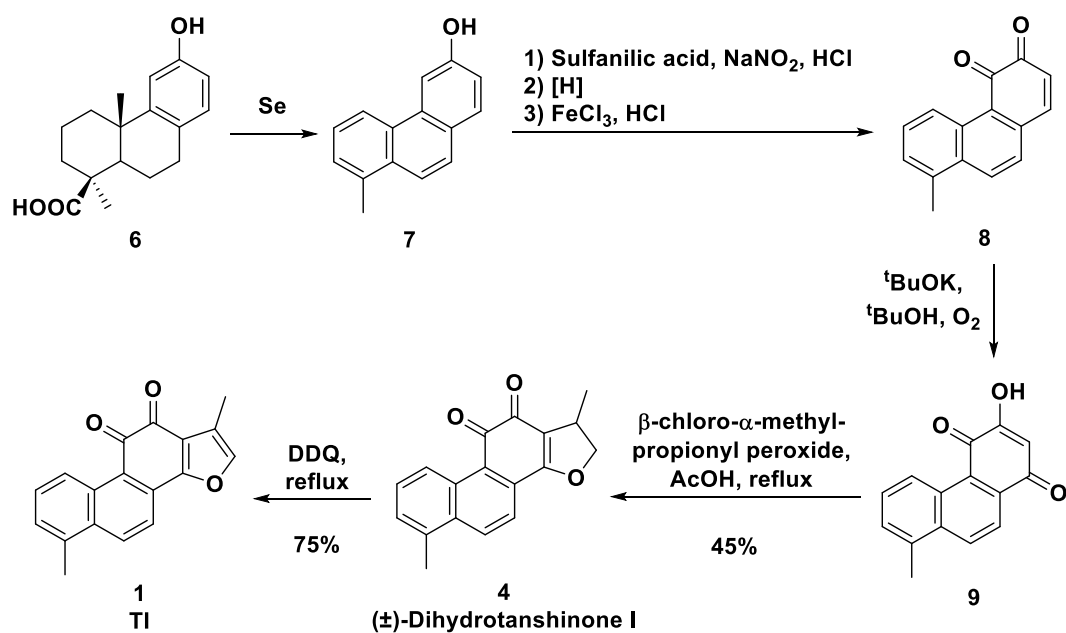
Both TI **1** and TIIA **2** have been found to demonstrate various protective effects. Beneficial cardiovascular effects have been reported for TI **1**,<sup>156</sup> as well as for TIIA **2**,<sup>157–160</sup> including anti-atherosclerotic effects.<sup>161–165</sup> TIIA **2** has shown protective effects against hepatic fibrosis and hepatotoxicity<sup>166–168</sup> and diabetes,<sup>169,170</sup> whilst TI **1** has exhibited beneficial effects for learning and memory-enhancement.<sup>171</sup> Both TI **1** and TIIA **2** have also shown antimicrobial activities, against a variety of bacterial and fungal strains.<sup>172–176</sup> Neuroprotective effects of TIIA **2** have been reported in various mouse and rat models.<sup>177–181</sup> Related effects including cardio-cerebrovascular protection are also well-documented, including protective effects against myocardial ischemia.<sup>156,182</sup> In addition, TIIA **2** has been found to reduce inflammation in brain tissue in a rat model of Alzheimer's disease,<sup>183</sup> whilst TI **1** has shown an anti-inflammatory role in neuroprotection in gerbil hippocampus.<sup>184</sup>

Various other anti-inflammatory effects have also been reported for TI **1** and TIIA **2**. TI **1** exhibited an *in vivo* anti-inflammatory effect in rats,<sup>185</sup> and it has been shown that TI **1** can inhibit production of inflammatory mediators such as IL-12 and interferon gamma,<sup>186</sup> as well as cyclooxygenase-2-mediated production of prostaglandin E2 and inducible nitric oxide synthase- (iNOS) mediated synthesis of nitric oxide.<sup>187,188</sup> TI **1** is also thought to exhibit an anti-inflammatory effect in a zebrafish model of inflammation, although this has not been fully explored (Dr. Anne Robertson, The University Of Sheffield, Appendix 10.1). Anti-inflammatory effects shown by TIIA **2** both *in vivo* and *in vitro* are relatively well documented. TIIA **2** inhibits the production of various inflammatory mediators, including the cytokines IL-1 $\beta$ , IL-6, IL-8, tumour necrosis factor

alpha (TNF $\alpha$ ), and phospholipase A2,<sup>189–192</sup> alongside other anti-inflammatory processes in other *in vitro* and *in vivo* studies,<sup>163,193–195</sup> including in relation to NQO1.<sup>196</sup> Anti-inflammatory effects exhibited by TIIA **2** *in vivo* have been shown in vertebrate models, including a rat model of renal fibrosis and inflammation,<sup>197</sup> a murine model of LPS-induced lung injury,<sup>190,197</sup> and murine models of colitis and chronic arthritis,<sup>198,199</sup> where it was shown that the effects exhibited by TIIA **2** were due to modulation of neutrophil activity, including increased apoptosis and a reduction in NET formation. It was recently shown that TIIA **2** exhibited a profound anti-inflammatory effect in a zebrafish model of inflammation, modulating neutrophil activity to accelerate inflammation resolution. TIIA **2** promoted increased reverse migration of neutrophils, as well as a small increase in neutrophil apoptosis, an effect which was conserved in treatment of human neutrophils with TIIA **2**.<sup>36</sup>

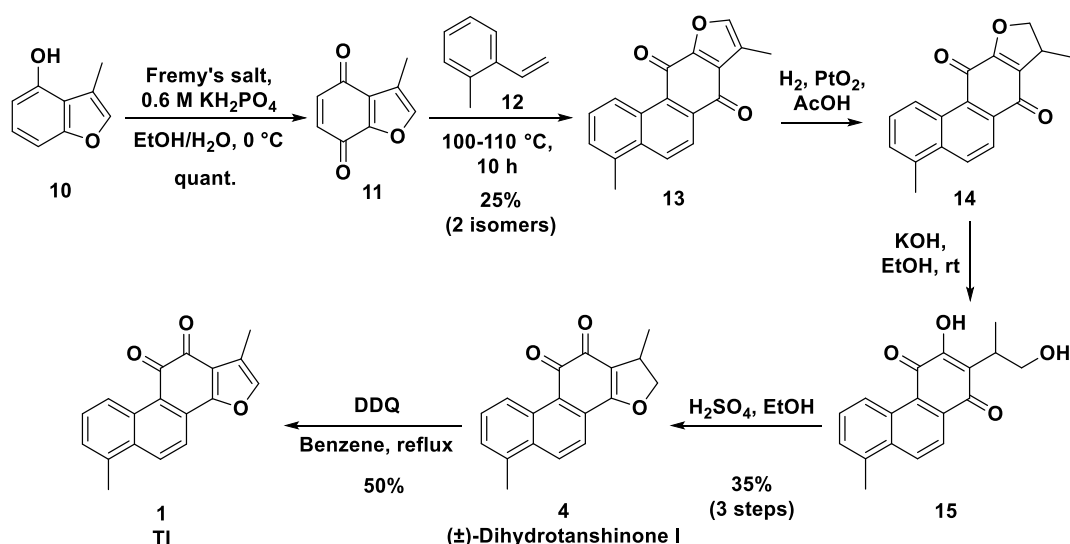
### 2.3.3 Chemical synthesis methods for TI and analogues

The first synthesis of TI **1** was achieved in a semi-synthesis starting from the natural product podocarpic acid **6** (Scheme 1).<sup>200</sup> The first step consisted of treatment with selenium, upon which dehydrogenation, demethylation and decarboxylation led to formation of 8-methyl-3-phenanthrol **7**.<sup>201</sup> This was coupled with diazotised sulfanilic acid, reduced to the amino-phenol, and converted to the corresponding 3,4-phenanthraquinone **8** using the Fieser procedure.<sup>202</sup> This was reduced to the *ortho*-quinol and underwent autoxidation in the presence of potassium *tert*-butoxide and oxygen to form the hydroxy-quinone **9**. Cyclisation with  $\beta$ -chloro- $\alpha$ -methylpropionyl peroxide gave racemic dihydrotanshinone I **4**, which was oxidised using 2,3-dichloro-5,6-dicyano-1,4-benzoquinone (DDQ) to yield TI **1** in seven steps. This was achieved in an overall yield of 34% from the 1,4-quinone **9**; a yield for the first five steps was not reported.



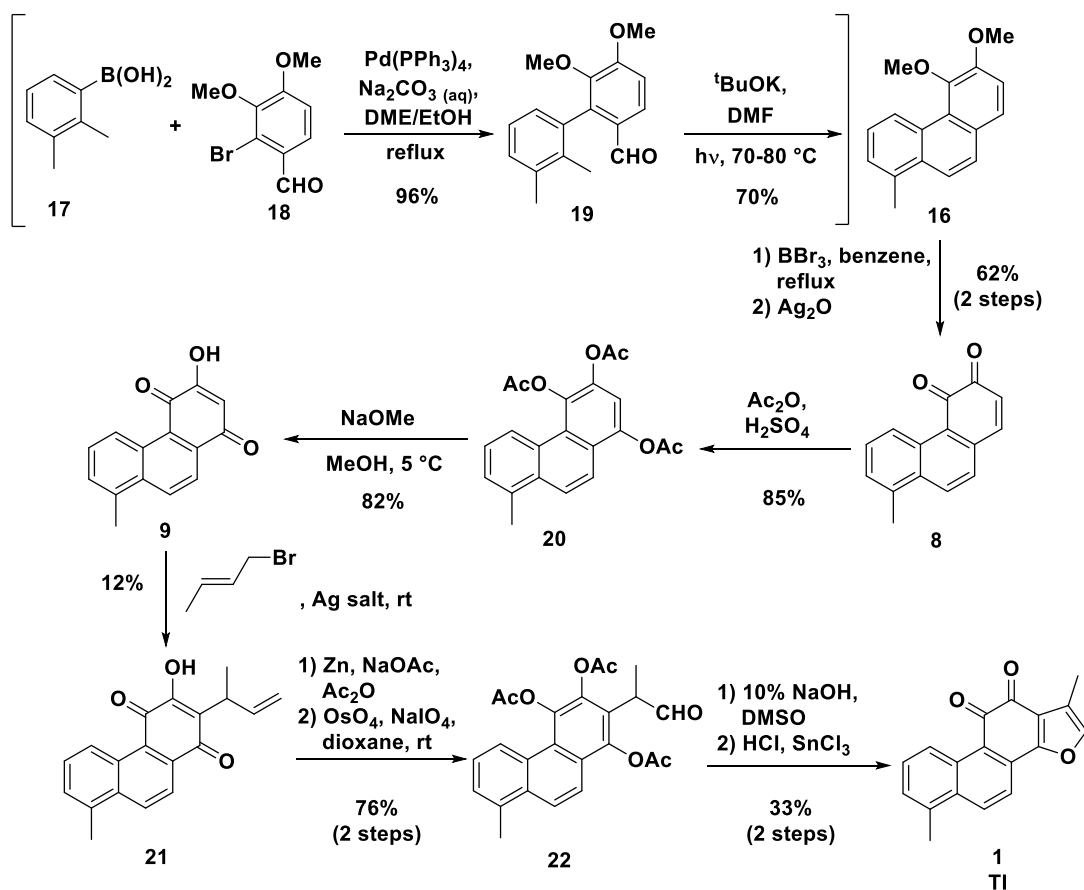
**Scheme 1.** Synthesis of TI **1** from podocarpic acid **6**.<sup>200–202</sup>

In independent synthetic efforts, a Diels-Alder reaction was used to form the main part of the tanshinone structure, a strategy applicable for accessing several different tanshinones (Scheme 2).<sup>203,204</sup> 3-Methyl-4-benzofuranol **10** was first oxidised to 3-methylbenzofuran-4,7-quinone **11** using potassium nitrosodisulfonate (Fremy's salt). The *para*-quinone **11** underwent Diels-Alder reaction with 2-methylstyrene **12** to give the aromatised Diels-Alder product **13**, albeit in low yield. This was reduced to the hydrogenated product **14** with platinum oxide, followed by hydrolysis with potassium hydroxide to give the diol **15**. Acidification with sulfuric acid gave racemic dihydrotanshinone I **4**, and final oxidation with DDQ yielded TI **1**, in an overall yield of 4% over six steps.



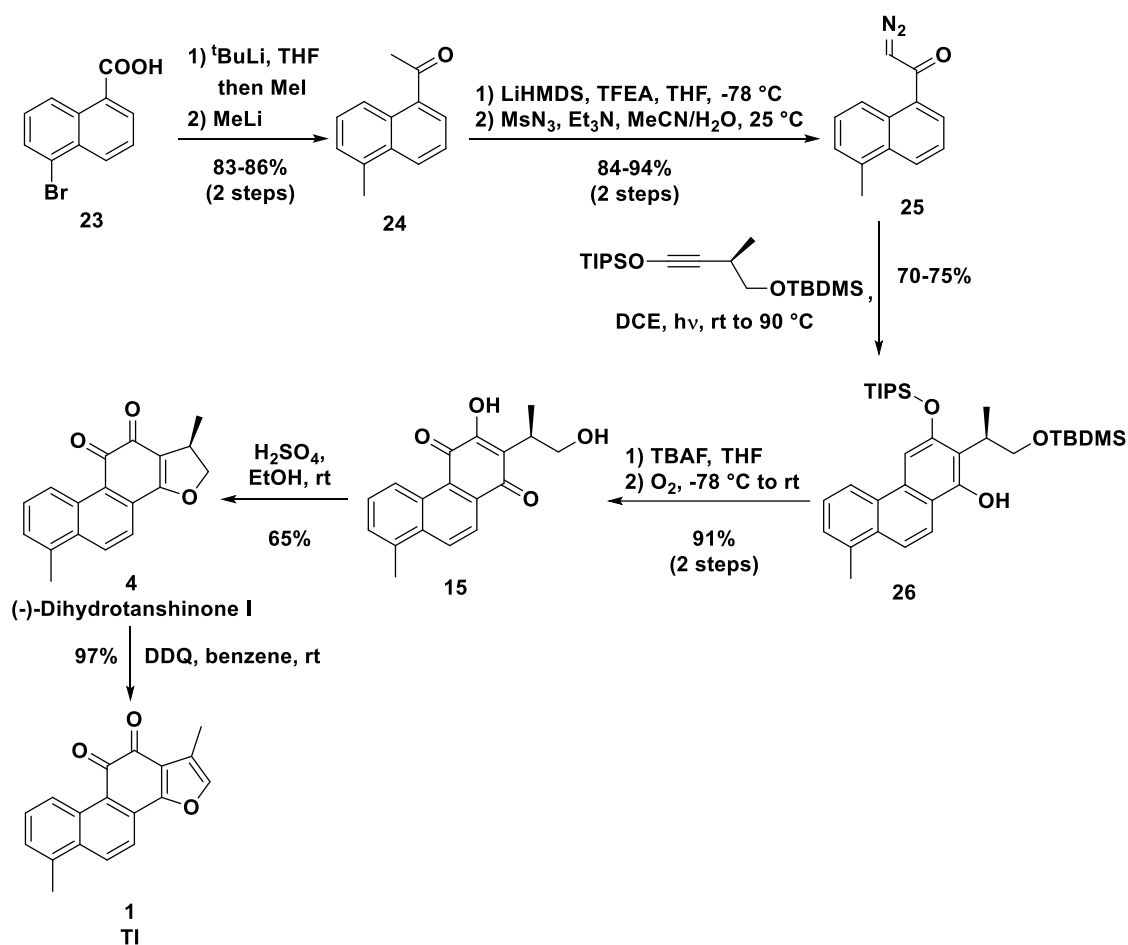
**Scheme 2.** Use of a Diels-Alder reaction to synthesise TI **1** in six steps.<sup>203,204</sup>

A photochemical cyclisation reaction induced by base was utilised as a different approach to the synthesis of TI **1**, starting with the dimethoxy-tricyclic compound **16** (Scheme 3).<sup>205</sup> A synthesis of this starting material **16** was later reported: an initial Suzuki coupling reaction between 2,3-dimethylphenylboronic acid **17** and 2-bromoveratraldehyde **18** to give the coupled product **19** was followed by reaction with potassium *tert*-butoxide under irradiation, to form the cyclised product **16**.<sup>206,207</sup> For the synthesis of TI **1**, the dimethoxy compound **16** was subjected to demethylation and oxidation to give the *ortho*-quinone **8**, followed by acetylation to provide the tri-acetate **20**. Subsequent reaction with sodium methoxide formed the hydroxy-quinone **9**, crotylation of which resulted in the alkylated product **21**. This was followed by acetylation and oxidative olefin cleavage to give the aldehyde **22**, and final hydrolysis and acid-promoted cyclisation to produce TI **1**, in less than 1% overall yield.



**Scheme 3.** A photochemical cyclisation strategy for synthesis of TI **1**.<sup>205–207</sup>

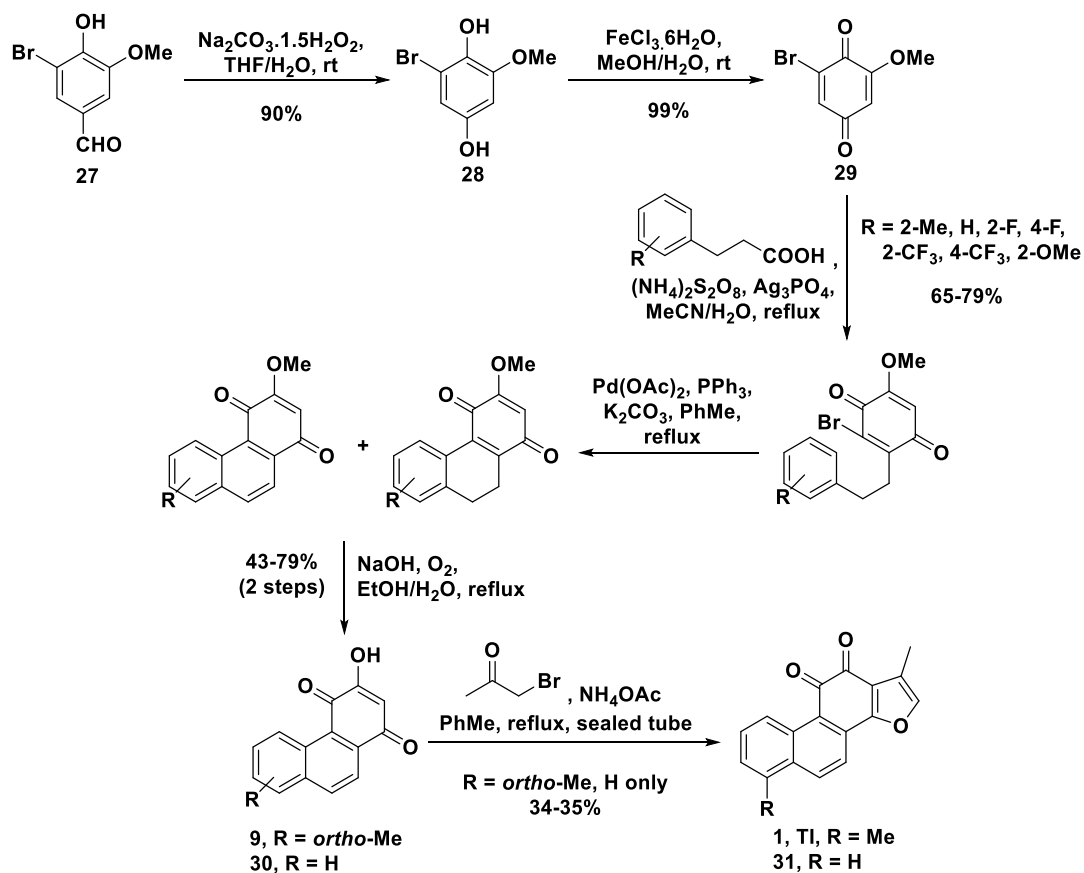
A photochemical aromatic annulation method was later developed, which enabled the synthesis of TI **1** in nine steps and 32% overall yield from bromo-1-naphthoic acid **23** (Scheme 4).<sup>208</sup> This was first converted to the ketone **24** using a previously described quenching procedure with methyllithium,<sup>209</sup> and was followed by a two-step ‘detrifluoroacetylative’ diazo transfer method to give the corresponding diazo ketone **25**.<sup>210</sup> The key aromatic annulation step between this diazo ketone **25** and a substituted alkyne gave the tricyclic product **26**. This was followed by silyl deprotection with tetra-*n*-butylammonium fluoride (TBAF) and treatment with oxygen to form the diol **15**. Subsequent reaction with sulfuric acid gave enantiopure dihydrotanshinone I **4**, and final oxidation with DDQ provided TI **1**.



**Scheme 4.** Use of a photochemical aromatic annulation strategy to give TI **1** in nine steps.<sup>208–210</sup>

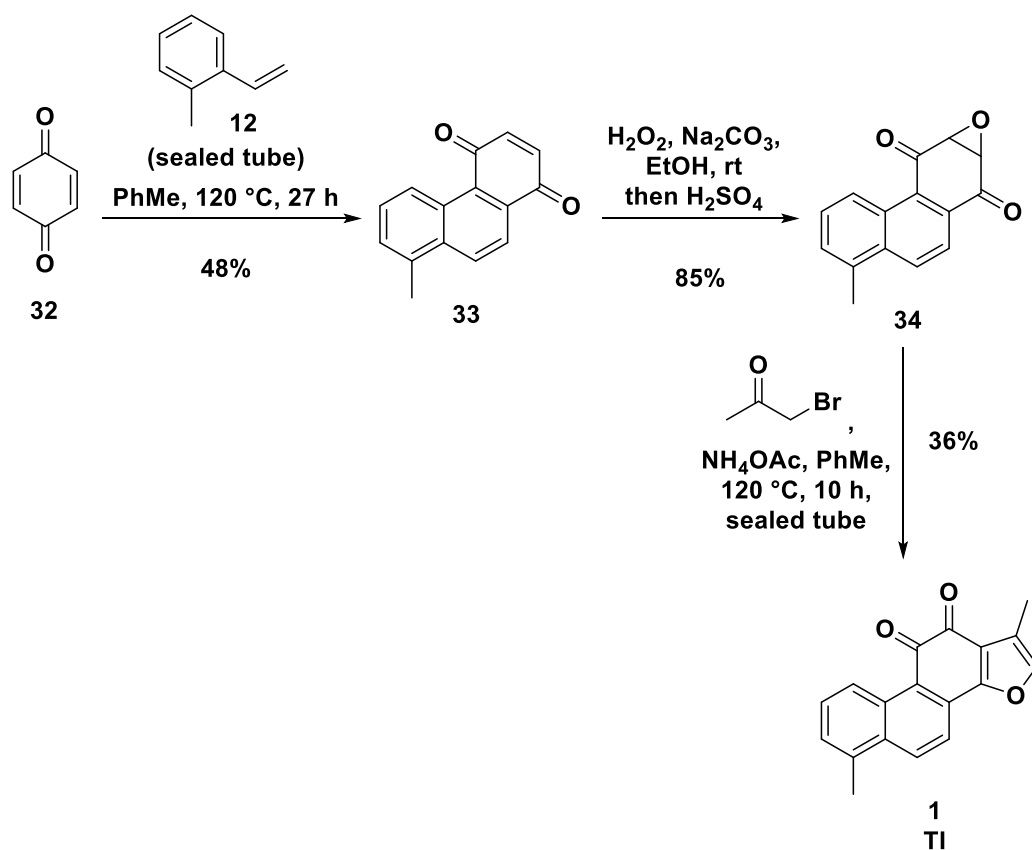
A recently reported method outlined synthesis of TI **1** and closely related analogues in six steps and up to 19% overall yield, starting from 5-bromovanillin **27** (Scheme 5).<sup>211</sup> A two-step literature procedure proceeding *via* the 1,4-hydroquinone **28** was used to form the 1,4-bromoquinone **29** in high yield.<sup>212</sup> This was coupled with a range of arylpropionic acids, with different substituents at the *ortho*- and *para*- positions of the phenyl ring, in a Minisci-type decarboxylative radical alkylation reaction. Intramolecular Heck reaction with a palladium catalyst, followed by direct treatment of the product with sodium hydroxide solution in the presence of oxygen, provided solely the fully aromatised, *O*-demethylated products. Finally, treatment of the alcohols **9** and **30** with bromo-2-propanone and ammonium acetate in a sealed tube gave the corresponding tanshinones **1** and **31**. Unlike the methods previously discussed, this strategy was more

practical for synthesising analogues of TI **1**, and did not appear to suffer from particularly low reaction yields or limited availabilities of starting material.



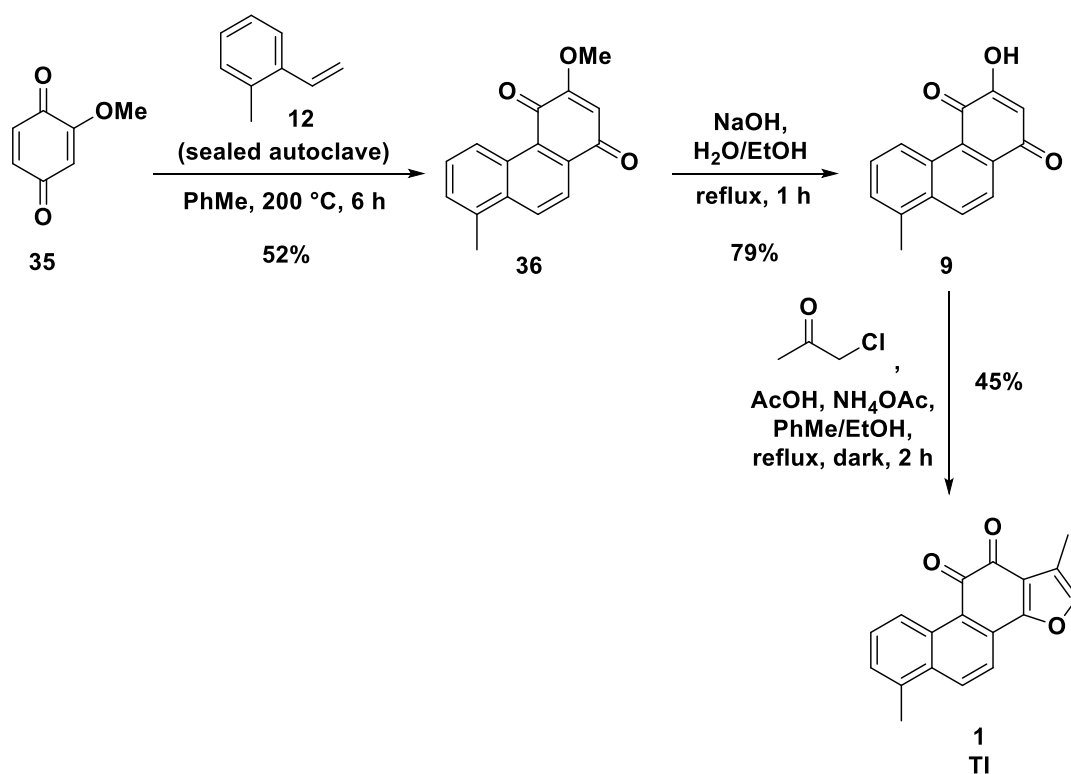
**Scheme 5.** Synthesis of TI **1** from 5-bromovanillin **27**.<sup>211,212</sup>

Another route using a Diels-Alder reaction strategy led to synthesis of TI **1** in just three steps (Scheme 6).<sup>213</sup> Diels-Alder reaction between *para*-benzoquinone **32** and 2-methylstyrene **12** gave the tricyclic adduct **33** in moderate yield. Weitz-Scheffer epoxidation gave the epoxide **34**, which was subjected to Feist-Bénary reaction conditions to form TI **1**, in an overall yield of 15%.



**Scheme 6.** Synthesis of TI **1** in three steps using Diels-Alder, epoxidation, and Feist-Bénary reactions.<sup>213</sup>

In 2017, a three step multi-gram synthesis of TI **1** was reported (Scheme 7).<sup>214</sup> A Diels-Alder reaction between 2-methoxy-1,4-benzoquinone **35** and 2-methylstyrene **12** to give the tricyclic methyl ether **36** was followed by demethylation using ethanolic hydroxide solution to give the alcohol **9**. Finally, a modified Feist-Bénary reaction using chloroacetone gave the desired TI **1** in 45% yield, and an overall yield of approximately 18% across the three steps.



**Scheme 7.** Large scale synthesis of TI **1** in three steps using a Diels-Alder strategy.<sup>214</sup>

In addition to syntheses of TI **1**, there have been various reports detailing the preparation of different analogues of TI **1**, often starting with the natural product itself (Figure 4). These have entailed exploration of various parts of the TI **1** structure, including modification of the *ortho*-quinone functionality,<sup>215–219</sup> alteration of the furan ring to different heterocycles,<sup>220</sup> addition of various substituents to the furan ring,<sup>175,221–227</sup> adjustment of the tanshinone core skeleton,<sup>227</sup> modification of the phenyl ring,<sup>228–232</sup> and the addition of different phenyl ring substituents.<sup>211</sup>

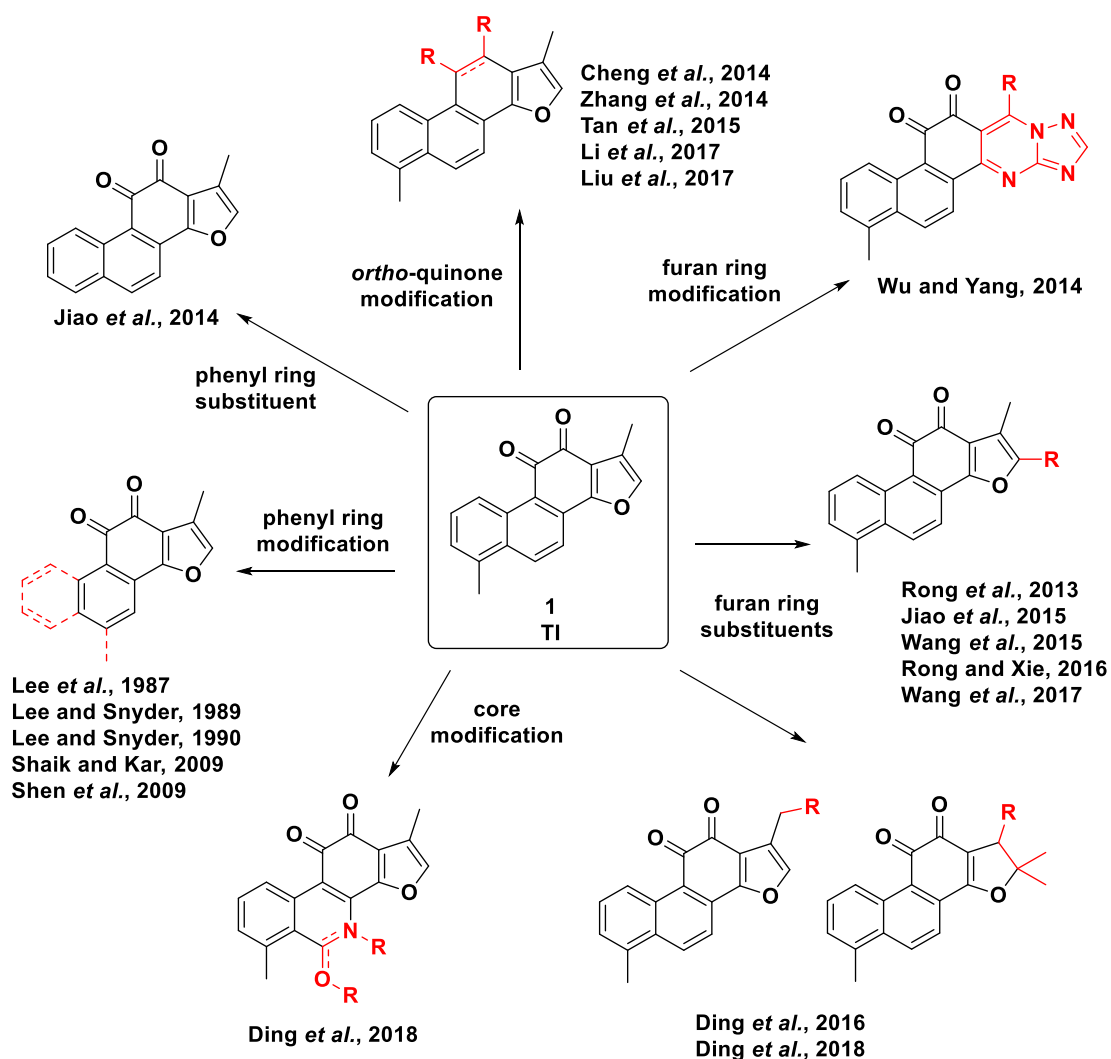
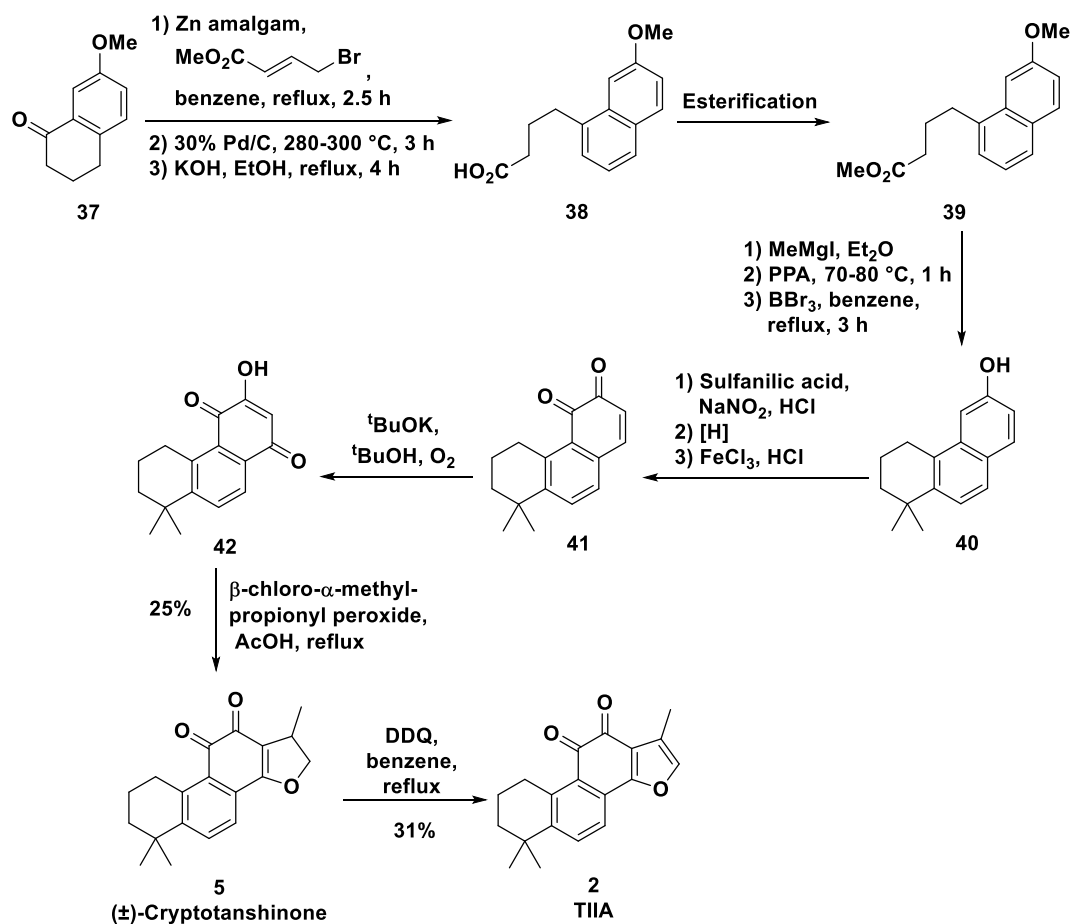


**Figure 4.** Published syntheses of various TI analogues (modified parts shown in red).

### 2.3.4 Chemical synthesis methods for TIIA and analogues

TIIA **2** was first synthesised totally using a similar method to that of the first synthesis of TI **1** in the later steps (Scheme 8).<sup>200</sup> 7-Methoxy-1-tetralone **37** underwent a Reformatsky reaction with methyl  $\gamma$ -bromocrotonate, the product of which was oxidised over palladium on carbon, and hydrolysed to the carboxylic acid **38** for purification purposes. The acid **38** was converted to the methyl ester **39**, which underwent Grignard reaction with methylmagnesium iodide, followed by cyclodehydration and demethylation to give the tricyclic phenol **40**. This was converted to the 3,4-phenanthraquinone **41** and then the hydroxy-quinone **42** using the same steps as in the

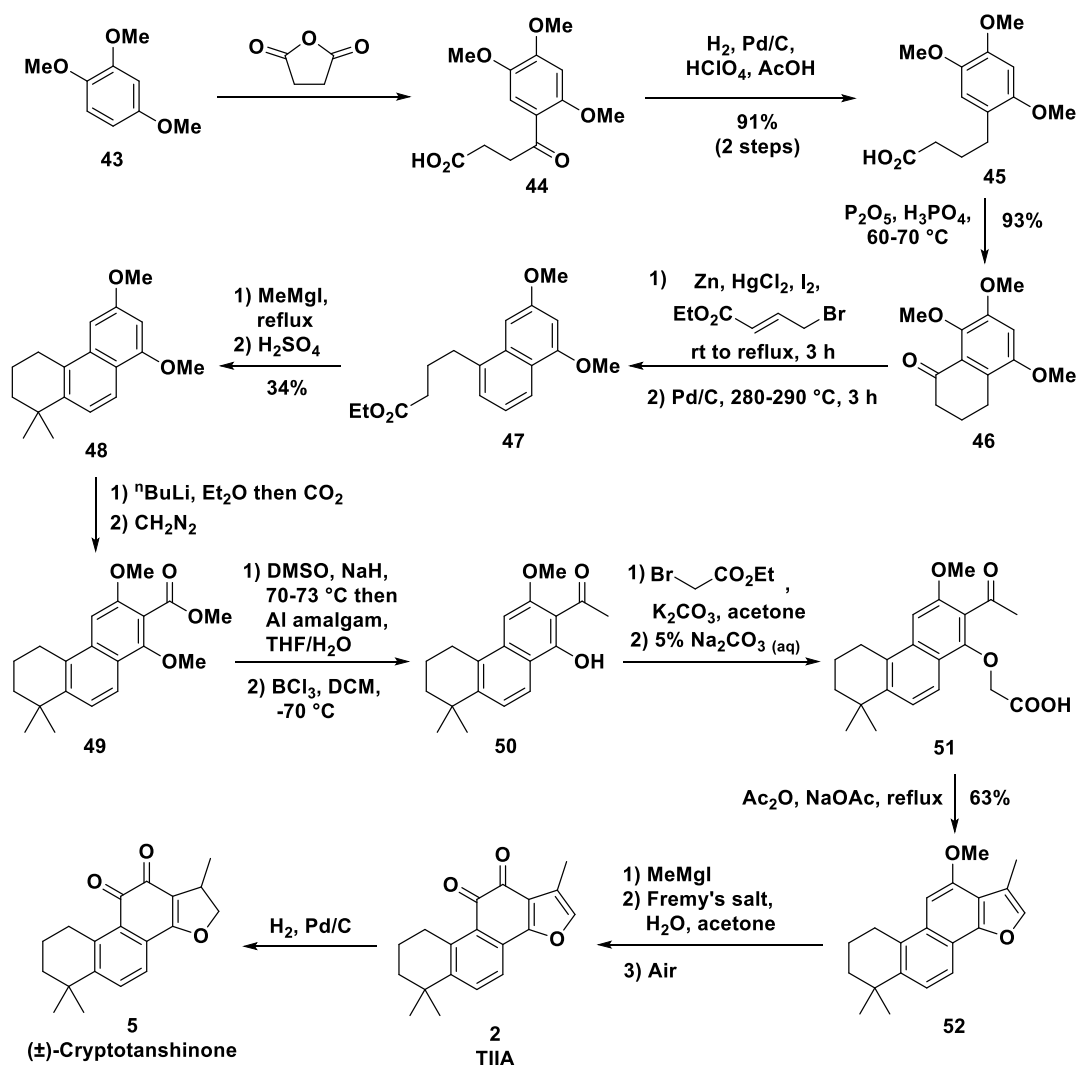
synthesis of TI **1**. Treatment with  $\beta$ -chloro- $\alpha$ -methylpropionyl peroxide formed racemic cryptotanshinone **5**, which was aromatised with DDQ to give TIIA **2** in a total of 13 steps.



**Scheme 8.** Synthesis of TIIA **2** from 7-methoxy-1-tetralone **37**.<sup>200</sup>

In the same year, a stepwise cyclisation strategy was used to synthesise TIIA **2** in seventeen steps from 1,2,4-trimethoxybenzene **43** (Scheme 9).<sup>233,234</sup> This underwent Friedel-Crafts acylation to give the aryl ketone **44**, followed by catalytic hydrogenation to give the alkane **45**, and further intramolecular Friedel-Crafts acylation to form the bicyclic product **46**. Reformatsky reaction with ethyl  $\gamma$ -bromocrotonate and removal of a methoxy group, followed by concomitant dehydration, aromatisation, and alkene hydrogenation, produced the naphthylbutyric ester **47**. Subsequent Grignard reaction and cyclodehydration using sulfuric acid formed the tricyclic product **48**. A carboxylic acid moiety was then introduced, and used to form the corresponding methyl ester **49**. This was converted to the methyl ketone **50** via a sulfoxide intermediate, and selective

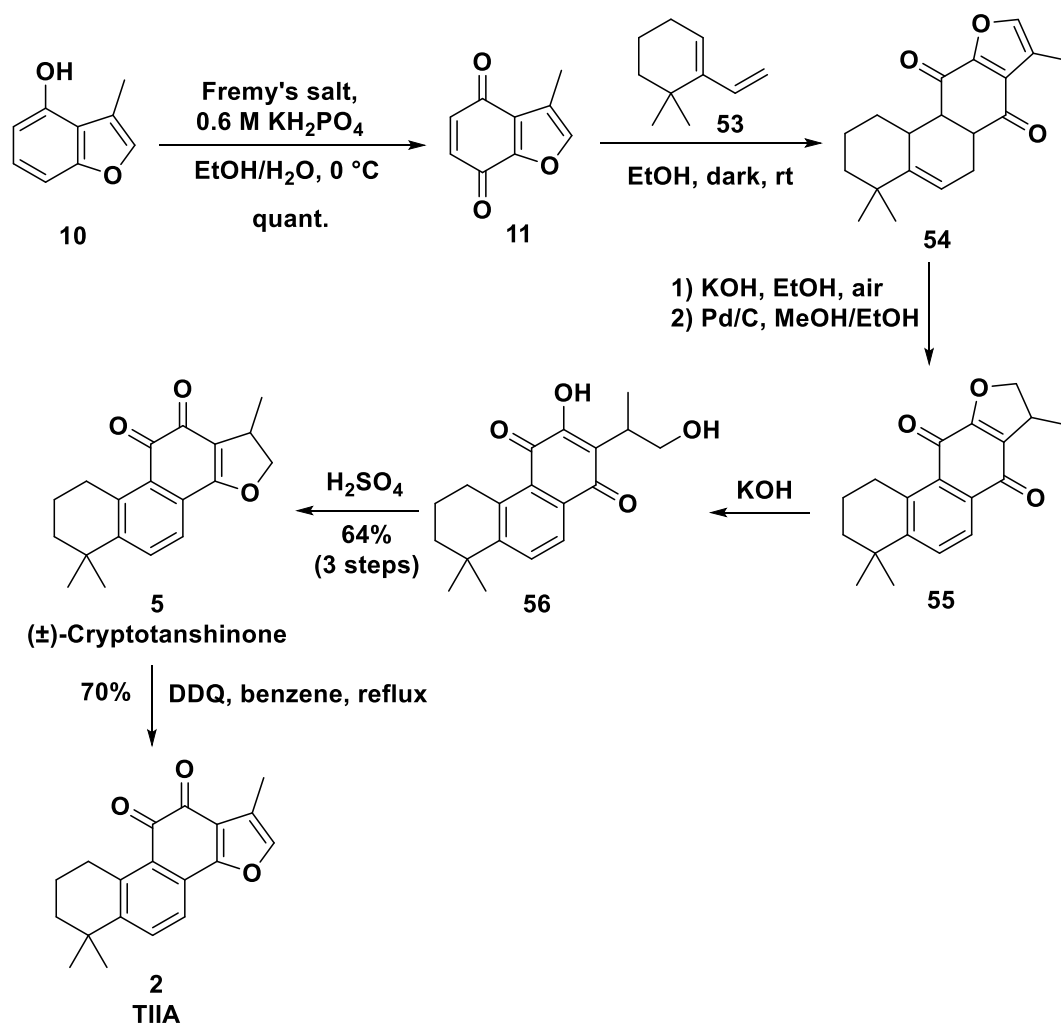
demethylation. Further reaction steps consisted of reaction with ethyl bromoacetate and saponification to give the carboxylic acid **51**, followed by an intramolecular Perkin reaction to construct the fourth ring, forming the furan **52**. Finally, reaction with methylmagnesium iodide, attempted oxidation and subsequent autoxidation produced the desired TIIA **2**. Catalytic hydrogenation was also used to convert this to racemic cryptotanshinone **5**.



**Scheme 9.** Synthesis of TIIA **2** in seventeen steps from 1,2,4-trimethoxybenzene **43**.<sup>233,234</sup>

The Diels-Alder reaction sequence previously used to synthesise TI **1** was also employed by the authors to make TIIA **2** (Scheme 10).<sup>203,204</sup> The *para*-quinone dienophile **11** was again formed from Fremy's salt-mediated oxidation of the benzofuranol **10**. The

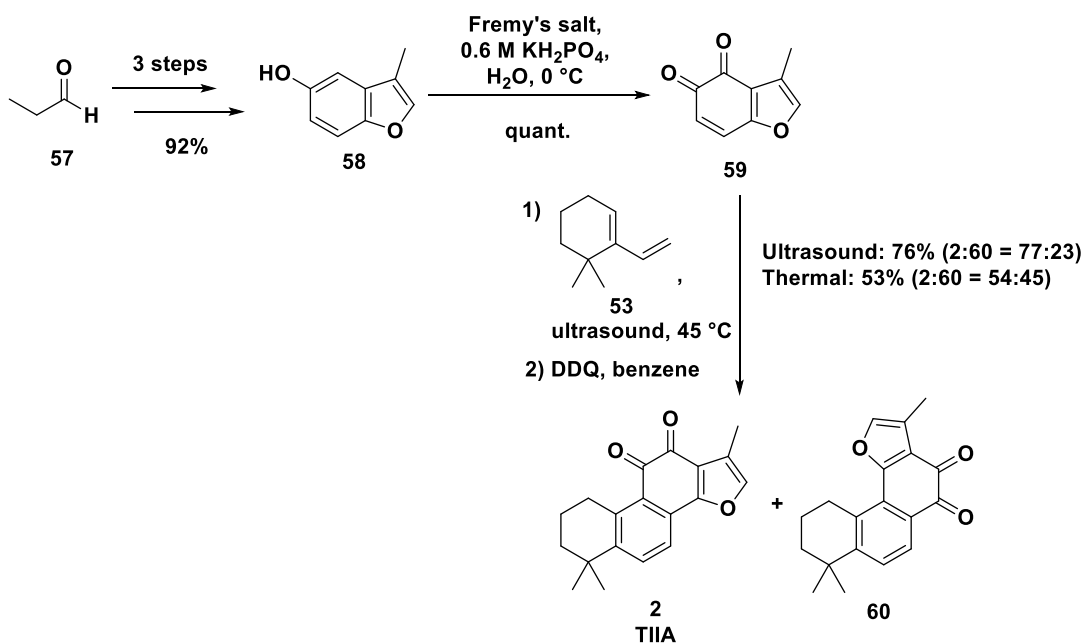
dienophile **11** underwent Diels-Alder reaction with 6,6-dimethyl-1-vinylcyclohexene **53** to form the adduct **54**, which was first aromatised in air, and then hydrogenated with palladium on carbon to give the unsaturated furan **55**. Ring opening with potassium hydroxide to form the diol **56** was followed by acid-mediated cyclisation to form racemic cryptotanshinone **5**, which was aromatised with DDQ to give TIIA **2** in a moderate overall yield.



**Scheme 10.** TIIA **2** synthesis using a Diels-Alder reaction.<sup>203,204</sup>

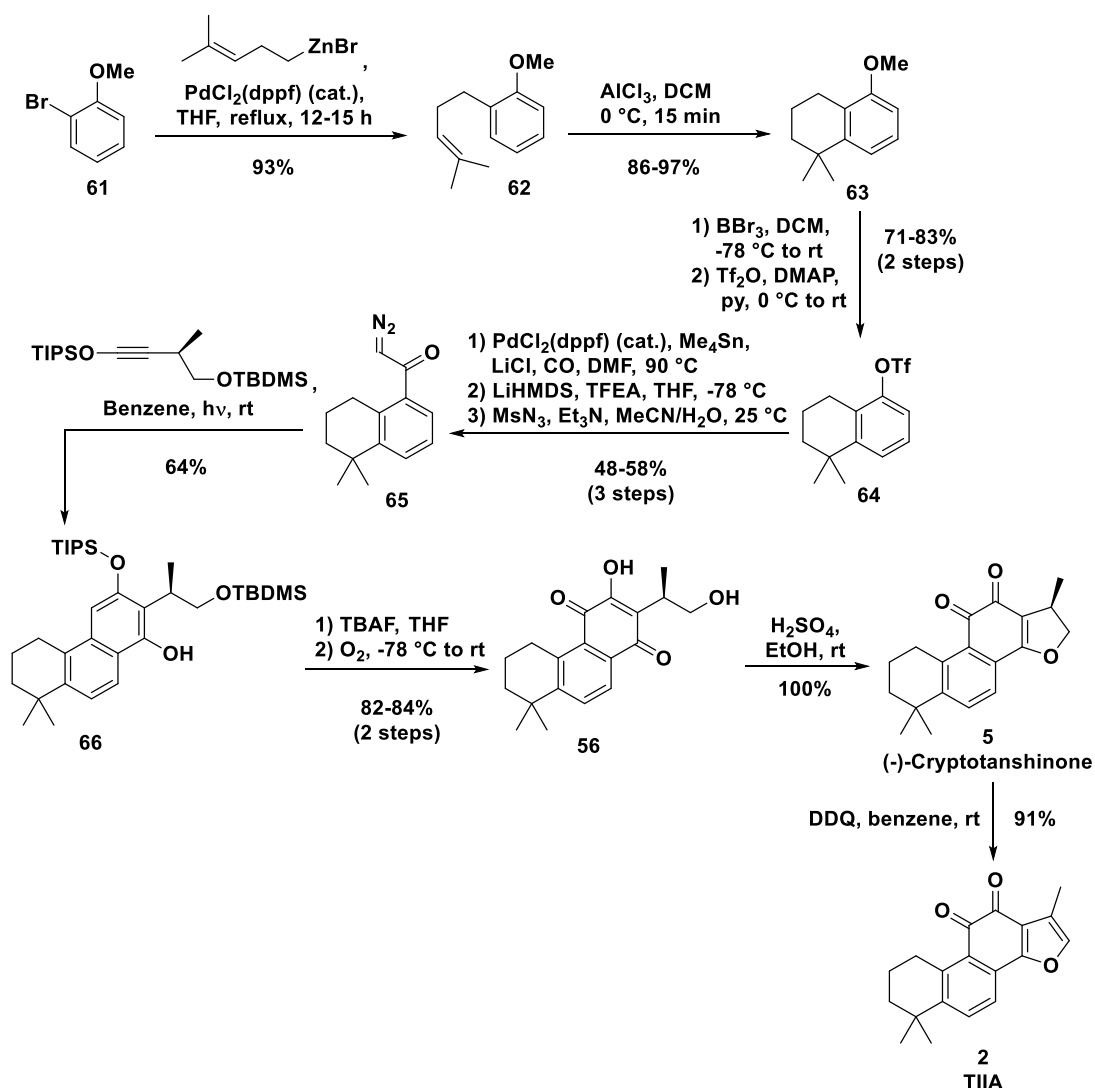
Later, it was found that a similar Diels-Alder reaction could be performed using a slightly different dienophile, and this could be promoted using ultrasound to increase both the yield and the proportion of desired product.<sup>229,230</sup> This enabled the simplified construction of tanshinones in high yields (Scheme 11). Starting with propanal **57**, 3-

methylbenzofuranol **58** was synthesised in three steps, and was converted into 3-methyl-4,5-benzofurandione **59** by Fremy's salt-mediated oxidation.<sup>228</sup> This underwent Diels-Alder reaction with 6,6-dimethyl-1-vinylcyclohexene **53** and subsequent aromatisation to give TIIA **2** and its isomer **60**.



**Scheme 11.** Use of ultrasound to improve the outcome of the Diels-Alder reaction in the synthesis of TIIA **2**.<sup>228–230</sup>

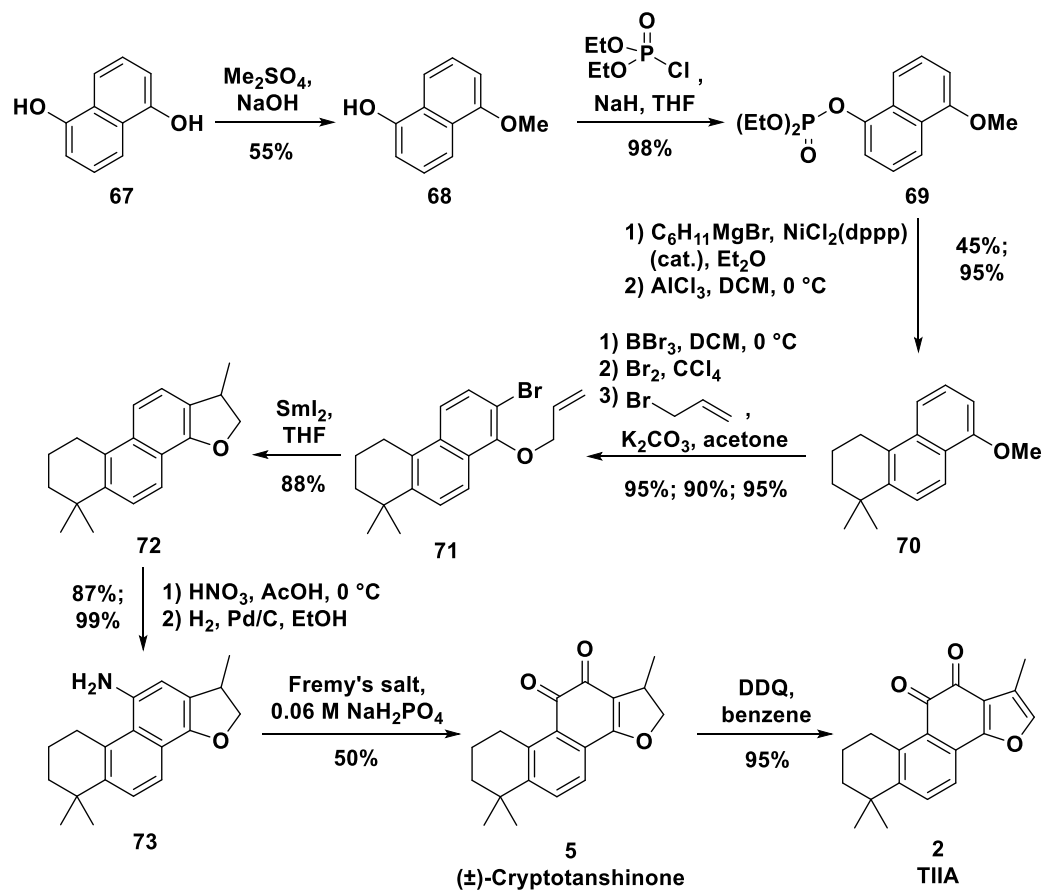
The photochemical aromatic annulation strategy previously used in the synthesis of TI **1** was also applied to the synthesis of TIIA **2** (Scheme 12).<sup>235</sup> Palladium-catalysed coupling of 2-bromoanisole **61** with a homoallylic organozinc compound gave the *ortho*-substituted aryl ether **62**, which upon treatment with aluminium trichloride underwent cyclisation to give the bicyclic compound **63**. This was demethylated, and the phenol converted to the triflate **64**. This underwent a carbonylative Stille reaction to give a ketone which was subjected to the diazo transfer conditions used previously in the synthesis of TI **1**, to give the diazo compound **65**. Photochemical aromatic annulation gave the phenol **66**, which underwent silyl deprotection followed by reaction with oxygen to give the diol **56**. Acid-mediated cyclisation produced (-)-cryptotanshinone **5**, which was aromatised with DDQ to produce TIIA **2**.



**Scheme 12.** Use of a photochemical aromatic annulation strategy to synthesise TIIA **2**.<sup>235</sup>

A different route to TIIA **2** was later reported, starting from 1,5-naphthalenediol **67** (Scheme 13).<sup>236</sup> Single methylation gave the mono-phenol **68**, and was followed by formation of the diethyl phosphate **69**, which underwent a nickel-catalysed coupling reaction, followed by aluminium trichloride-mediated cyclisation to give the tricyclic product **70**. Demethylation, aromatic bromination, and reaction with allyl bromide gave the *O*-allyl tricycle **71**. A key  $\text{SmI}_2$ -promoted intramolecular cyclisation was used to form the fourth ring, yielding the cyclised product **72** in high yield. Nitration followed by reduction gave the amine **73**, which upon treatment with Fremy's salt, gave racemic

cryptotanshinone **5**. Finally, reaction with DDQ provided TIIA **2**, in an overall yield of approximately 7%.



**Scheme 13.** A  $\text{Sml}_2$ -promoted radical cyclisation approach to TIIA **2**.<sup>236</sup>

There have also been many reports detailing the synthesis of TIIA **2** derivatives (Figure 5). These have included modification of the *ortho*-quinone functionality,<sup>217–219,237</sup> addition of furan ring substituents,<sup>147,175,238–249</sup> addition of various cyclohexyl ring substituents,<sup>150,246,250–252</sup> and alteration of the cyclohexyl ring itself.<sup>228–232</sup>

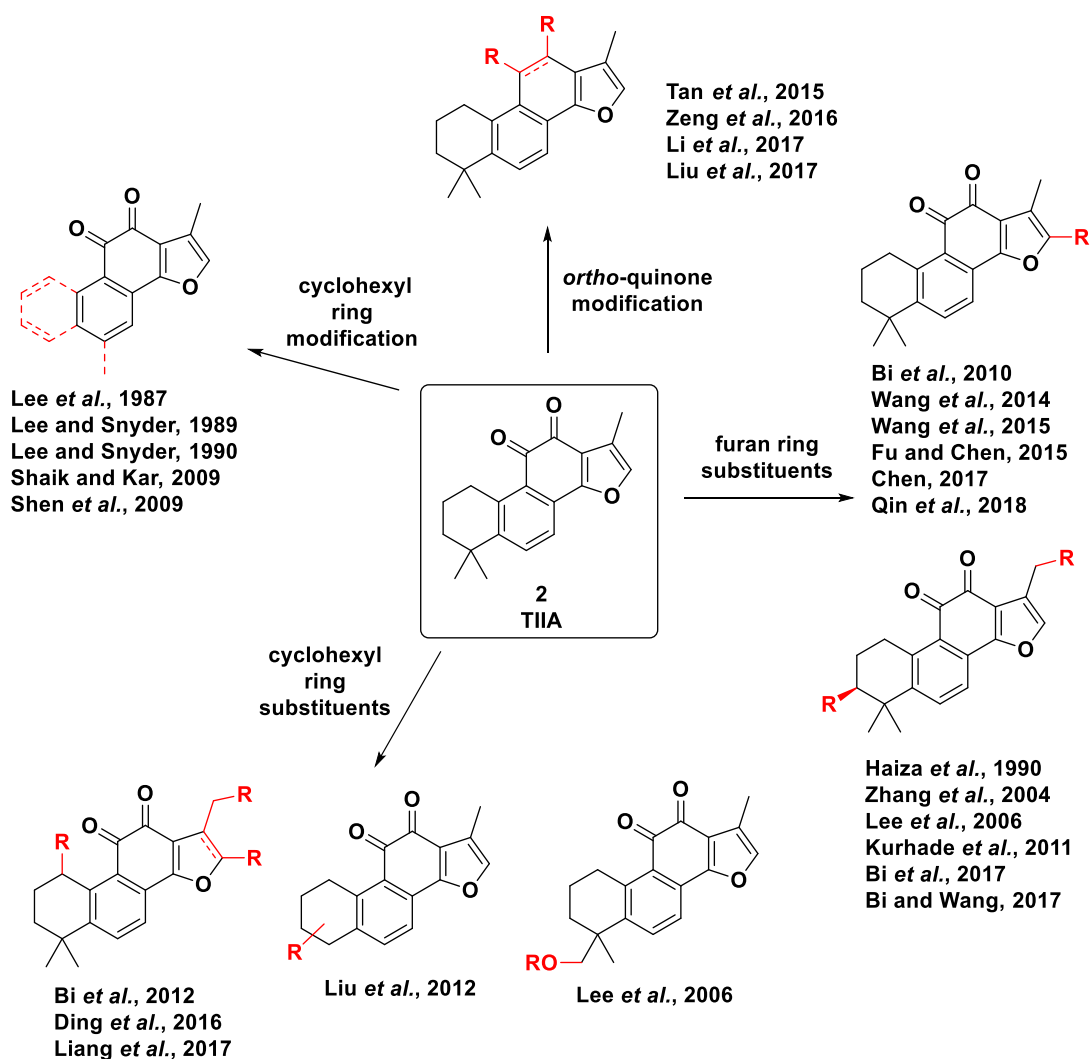


**Figure 5.** Published syntheses of various TIIA analogues (modified parts shown in red).

## 2.4 Hypothesis and research aims

It was hypothesised that various synthetic tanshinone analogues exhibit differing anti-inflammatory activities *in vivo*. Thus, such compounds could be used to manipulate and further explore the neutrophilic inflammatory response *in vivo*.

The initial aim of this research was to synthesise various analogues of both TI **1** and TIIA **2**, including previously unreported compounds. This would involve implementing previously reported synthetic routes for the syntheses of TI **1** and TIIA **2** as well as any structurally related compounds, optimising these routes where appropriate. The synthesised compounds would be used as probes to explore manipulation of the

inflammatory response, and to investigate any structure-activity relationships between the tanshinone structures and any anti-inflammatory effects. This would be done by testing the compounds in a zebrafish model of inflammation, to monitor the recruitment and resolution stages of inflammation, and analysing the number of neutrophils at various time points. Compound toxicity could also be evaluated using this model. Furthermore, a greater understanding of how molecules such as tanshinones reach their molecular target(s) *in vivo* was also sought, particularly in relation to neutrophil-specific effects. The long-term goal of this work was to work towards delivery of a safe and effective treatment for promoting resolution of inflammation, which might eventually be used in the clinic.

### 3. Materials and Methods

#### 3.1 Reagents and equipment

All reagents were obtained from Sigma Aldrich/Merck (Darmstadt, Germany) unless stated otherwise. TIIA **2** was obtained from Generon (Slough, UK) and the c-Jun N-terminal kinase inhibitor SP600125 (SP) **74** was obtained from StressMarq Biosciences (Victoria, Canada). All synthetic compounds were produced using chemistry as outlined in the Experimental section (Chapter 8). All compounds were dissolved in dimethyl sulfoxide (DMSO) for stock solutions prior to use in experiments.

Zebrafish (*Danio rerio*) larvae were injured using a straight micro-scalpel blade (stab knife) with a 15 ° blade of 5.0 mm depth, obtained from MSP Surgical Specialties Corporation (Reading, PA, USA). Embryo selection and larval injury was performed using a Leica S6D Greenough stereo microscope and a Leica L2 light source (Milton Keynes, UK). Neutrophil counting was performed on a Leica MZ10F modular stereo microscope with fluorescent light source.

#### 3.2 Zebrafish husbandry

Transgenic zebrafish which express GFP specifically in neutrophils, *Tg(mpx:GFP)*j114**,<sup>86</sup> were used for all biological experiments. Zebrafish were raised and maintained in Home Office-approved aquaria at the Bateson Centre at The University Of Sheffield, in accordance with standard protocols and procedures. Zebrafish were kept in a continuously recirculating closed system at 28 °C, and exposed to a cycle of 14 hours of light and 10 hours in the dark per day.

Zebrafish embryos were obtained through either pair matings or 'in-tank' breeding. For pair matings, male and female adult zebrafish were placed in separate parts of small, covered plastic containers fitted with a plastic divider, and were kept separate overnight. The following morning, the dividers separating the pairs of fish were removed and mating was allowed to occur. After a few hours, the fish were returned to their original tank, and embryos were obtained by pouring the water from the mating containers through a small plastic tea strainer and then rinsing with aquarium water. For

'in-tank' breedings, in the evening, a plastic container holding a layer of marbles above a wire mesh sieve was placed into a tank containing up to 40 fish. Zebrafish mated when the lights came on the following morning, and embryos were obtained by pouring the water from the marble tank through a small plastic tea strainer and rinsing with aquarium water.

Healthy, fertilised embryos were identified under a microscope and, using a plastic Pasteur pipette, sorted into Petri dishes containing approximately 40 mL embryo medium (E3) solution (Appendix 10.2), with approximately 60 embryos per dish. All dishes of embryos were incubated at 28 °C.

After the completion of all biological experiments, and prior to 5.2 dpf, larvae were sacrificed by anaesthesia with the addition of approximately 1.5 mL 0.017% tricaine solution per Petri dish (Appendix 10.3), followed by immersion in bleach solution. All procedures performed were in accordance with United Kingdom Home Office legislation, and were carried out under Project Licence Number PPL 70\_8178, *Using Zebrafish to understand inflammation resolution*.

### 3.3 Larval tailfin transection

Larvae at age 3 dpf were used for all experiments. Zebrafish larvae were anaesthetised by the addition of approximately 1.0-1.5 mL 0.017% tricaine solution to the Petri dish. Larvae were then transferred, using a plastic Pasteur pipette, onto a strip of masking tape adhered to the inside of a Petri dish lid, which had been pre-washed with deionised water to remove any tape residues. Excess liquid was removed prior to transection, to minimise movement of larvae. Larvae were then viewed under a standard biological microscope. A micro-scalpel blade was used to completely remove the caudal fin, initiating an inflammatory response. To ensure consistency, transection was performed as posterior as possible in the region where the pigment pattern was disrupted, as indicated by the red line (Figure 6). Injured larvae were transferred to a Petri dish containing approximately 40 mL fresh E3 solution which did not contain methylene blue, and incubated at 28 °C.

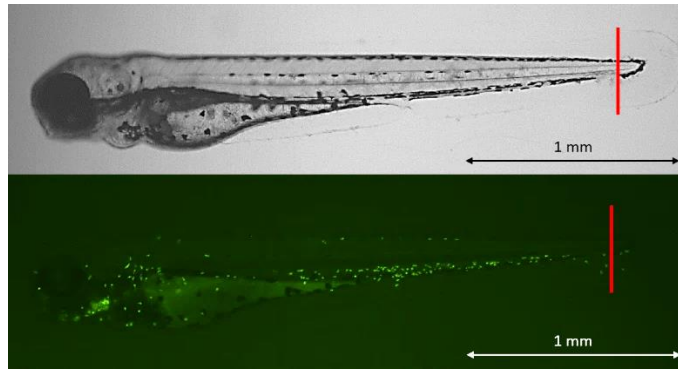


**Figure 6.** The larval tailfin was transected with a micro-scalpel blade at the position indicated by the red line, as viewed under the normal brightfield (top) and GFP (bottom) channels of a fluorescence microscope, thereby initiating an inflammatory response.

### 3.4 Larval compound treatment

Zebrafish larvae were immersed in aqueous compound solutions in 24-well plates. Larvae in E3 solution (which did not contain methylene blue) were added to compound solutions in such a way as to obtain the final experimental concentration indicated. Compounds were tested alongside a 0.5-1.0% DMSO solution which was used as a negative (vehicle) control in all experiments. In recruitment experiments, SP **74** (30  $\mu$ M) or TI **1** (25  $\mu$ M) was used as a positive control. For resolution experiments, TIIA **2** (25  $\mu$ M) was used as a positive control. Well plates were incubated with the lid on at 28 °C. In each experiment, 6-8 zebrafish larvae per treatment group were used, and each experiment was performed independently 3-4 times (unless otherwise stated), on different days. Results from each biological repeat were combined to give pooled datasets which were used for statistical analysis. All experiments were performed blind to treatment conditions for the duration of the experiment.

### 3.5 Neutrophil recruitment experiments

Zebrafish larvae were injured as previously described (Chapter 3.3). Injured larvae were treated immediately by immersion with the compound diluted in E3 solution (which did not contain methylene blue) at the concentration indicated, and incubated at 28 °C. At 4-6 hours post-injury (hpi), larvae were anaesthetised with one drop of tricaine solution per well, and for each larva, the number of neutrophils at the site of

injury was counted under a fluorescence microscope. The site of injury for neutrophil counting was defined as any neutrophils residing within the area of each larva containing disrupted pigment, as indicated by the blue box (Figure 7). Both compound treatment and neutrophil counting were performed blind to experimental conditions.

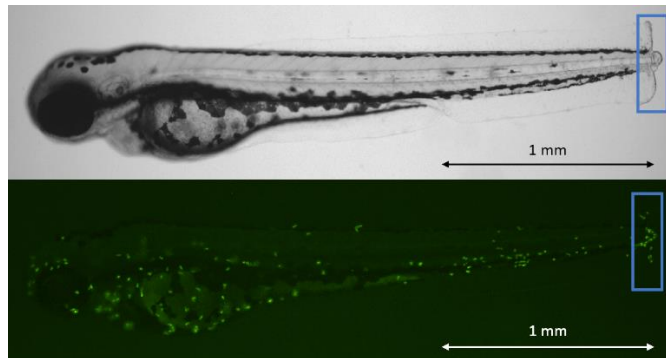


**Figure 7.** All neutrophils in the blue box shown were included in counting. Larva shown as observed under the normal brightfield (top) and GFP (bottom) channels of a fluorescence microscope.

### 3.6 Inflammation resolution experiments

Larvae were injured as previously described (Chapter 3.3). At 3.5 hpi, larvae were anaesthetised with tricaine solution, and larvae that had mounted a good inflammatory response (around 20-25 neutrophils at the site of injury; termed 'good responders') were selected prior to any experimental procedures. At 4 hpi, selected larvae were subjected to compound treatment by immersion at the concentration indicated, and incubated at 28 °C. At 8 hpi, larvae were anaesthetised with tricaine solution and for each larva, the number of neutrophils at the site of injury was counted as previously described (Chapter 3.5). Both compound treatment and neutrophil counting were performed blind to experimental conditions.

### 3.7 Statistical analysis

All statistical analysis was carried out using Prism 7.0 (GraphPad, San Diego, USA), version 7.00. For all experiments, at least three biological repeats were performed (unless otherwise stated), from which data were pooled and then analysed. Statistical

significance was assessed at various levels: \*  $P \leq 0.05$ , \*\*  $P \leq 0.01$ , \*\*\*  $P \leq 0.001$ , \*\*\*\*  $P \leq 0.0001$ , ns not significant ( $P > 0.05$ ).

In resolution experiments where data comprised two experimental groups, an unpaired  $t$ -test was used to analyse data and determine statistical significance. For data from recruitment and resolution experiments comprising three or more experimental groups, analysis was performed using a one-way analysis of variance (ANOVA) test with Dunnett's multiple comparison post-test for comparing treatment neutrophil numbers to those of the DMSO negative control. For timecourse dynamics data, analysis was performed using a one-way ANOVA test with Tukey's multiple comparison post-test for comparing neutrophil numbers for each timepoint to those of every other timepoint. For the linear regression analysis performed in Chapter 6.4, the Spearman correlation test was used to determine  $r$  values and statistical significance.

## 4. Synthesis and evaluation of tanshinone I analogues and isotanshinone I analogues

### 4.1 Introduction

In previous studies, TIIA **2** exhibited a highly significant effect in accelerating resolution in a zebrafish model of neutrophilic inflammation, an effect which was also conserved in human neutrophils.<sup>36</sup> TIIA **2** did not significantly affect initial recruitment of neutrophils to the site of injury, although there was a trend towards lower numbers of neutrophils recruited at the higher concentrations tested, up to a concentration of 25  $\mu\text{M}$ .<sup>36</sup>

TI **1** also had an effect in promoting inflammation resolution, although not to the same extent as TIIA **2** (Dr. Anne Robertson, The University Of Sheffield, Appendix 10.1). The effects of TI **1** on neutrophil recruitment have not previously been explored, and so were of interest in this work. In addition, the commercially available tanshinones cryptotanshinone **5** and dihydrotanshinone I **4**, which are structurally very similar to TIIA **2** and TI **1** respectively, were investigated for their effects on resolution of neutrophilic inflammation in the same model. Both cryptotanshinone **5** and dihydrotanshinone I **4** accelerated resolution, although not with the same clear dose-response relationship observed for TIIA **2** (Dr. Anne Robertson, The University Of Sheffield, Appendix 10.1).

Aside from these four known tanshinones, no previous tanshinones (or structurally similar molecules) have been investigated for their anti-inflammatory effects in this model. Furthermore, although these four tanshinones demonstrated observable anti-inflammatory effects *in vivo*, their molecular mechanism of action is not currently understood. The target protein(s) of these molecules remains unknown, and may even comprise more than one target. Structure-activity relationships for these molecules have also not been constructed. Such relationships could aid in identification and an improved understanding of the molecular mechanism of action of tanshinones, and lead to an optimised potential drug molecule, working towards development of new clinical treatments for inflammatory diseases.

Therefore, the synthesis of analogues for both TI **1** and TIIA **2** was of interest. Synthesised molecules could then be evaluated in the zebrafish model of inflammation, and the results of such studies used to elucidate structure-activity relationships and guide future efforts. Several routes are reported in the literature for the synthesis of TI **1** and TIIA **2**, and at the start of this work (October 2014), all previously published methods for the synthesis of TI **1** and analogues were first reviewed, as this compound class was less explored. However, many of these were not suited for the cost-effective synthesis of a set of tanshinone analogues. The route adapted from the literature was one of the few published studies at the time which was amenable to synthesis of a range of TI analogues.<sup>211</sup>

## 4.2 Hypothesis and aims

It was hypothesised that analogues of tanshinones, in particular TI **1**, would exhibit differing anti-inflammatory effects *in vivo*, depending on their structures. The first aim of this work was to prepare analogues of TI **1**. The synthesised TI analogues could then be tested *in vivo* using a zebrafish model of inflammation, to identify which (if any) of the compounds affected neutrophil recruitment and/or resolution of neutrophilic inflammation. By analysing all of these data together, this could enable determination of structure-activity relationships and a greater understanding of which parts of the TI **1** molecule were important for biological activity. This would help work towards identification of exactly how these compounds could be working at a molecular level.

## 4.3 Initial synthesis of TI

### 4.3.1 Initial steps

A synthetic route previously employed in the literature for synthesising TI **1** and a closely related analogue **31** was initially used in this work,<sup>211</sup> as it appeared to be the most amenable for the synthesis of a variety of functionalised TI analogues. The route was mainly dependent on the commercial availability of various substituted carboxylic acids in the third step of the synthesis, and their compatibility with the rest of the synthesis, which did not appear to be a major issue. It also comprised fewer steps than

most other syntheses, and was previously used in the synthesis of TI **1** and an additional tanshinone analogue **31** lacking the 6-methyl group, replaced with a hydrogen atom (Figure 8). However, besides these two tanshinones, no other tanshinones had previously been synthesised using this route. Use of this route would allow for the synthesis of tanshinone analogues with changes made to the structure which were situated away from the *ortho*-quinone moiety. This was important as it was hypothesised that this functionality was important for *in vivo* biological activity, as one of the few notable functional groups in the core tanshinone structure.

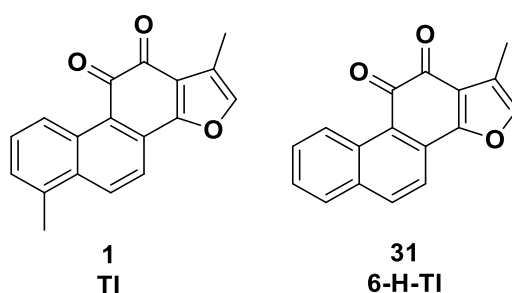
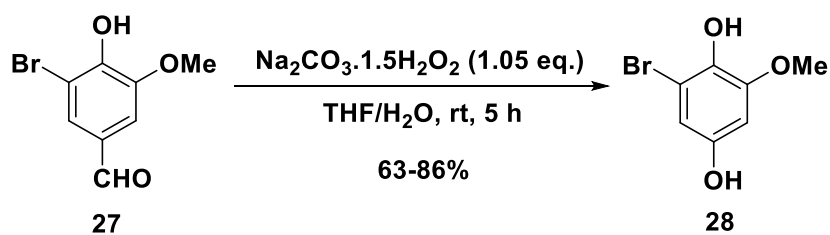


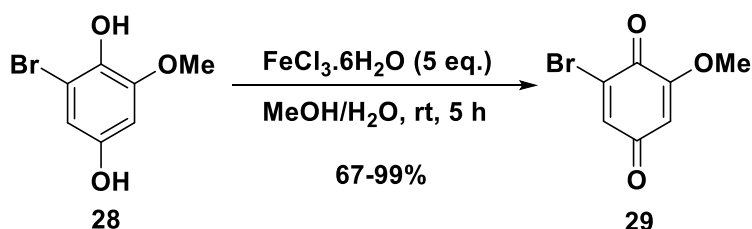
**Figure 8.** Structures of the previously synthesised TI **1** and its 6-hydro derivative **31**.<sup>211</sup>

Firstly, commercial 5-bromovanillin **27** was oxidised to the corresponding 1,4-hydroquinone **28** using sodium percarbonate in a Baeyer-Villiger oxidation and subsequent ester hydrolysis (Scheme 14), modified according to Dakin and Kabalka.<sup>253,254</sup> The percentage yield initially obtained (63%; 6 g scale) was lower than those obtained elsewhere for the same substrate,<sup>211,212</sup> although this was without any further attempts at optimising the conditions used. The slightly modified work-up procedure used here (addition of sodium sulfite to quench any residual peroxide species, and subsequent extraction) may have had an effect on this yield. However, when this reaction was repeated on a much larger (19 g) scale, with slightly more careful extraction but otherwise using the same conditions, the yield obtained was significantly higher (82%). When the reaction was later repeated again on a 25 g scale to provide enough material for analogue synthesis, a further improved yield of 86% was obtained. This reaction also required no additional purification, making this a convenient process for larger quantities.



**Scheme 14.** Baeyer-Villiger oxidation of 5-bromovanillin **27**.

This oxidation was followed by a second oxidation step, in which iron(III) chloride was used to convert the 1,4-hydroquinone **28** into the corresponding 1,4-benzoquinone **29** (Scheme 15). Originally, this reaction also proceeded in slightly lower yield (67%) than those published,<sup>211,212</sup> although this was without any attempts at optimisation. As observed with the previous oxidation, when this reaction was scaled up yet with the same reaction conditions, the yield obtained (96%) was again a significant improvement, and on an even larger scale, a 99% yield was obtained. Isolation of the 1,4-benzoquinone product **29** also required no further purification. As previous syntheses have involved the use of chromatographic purification after this oxidation step,<sup>211,212</sup> this method represented a more time- and cost-effective large-scale synthesis of the desired benzoquinone **29** compared to literature methods.

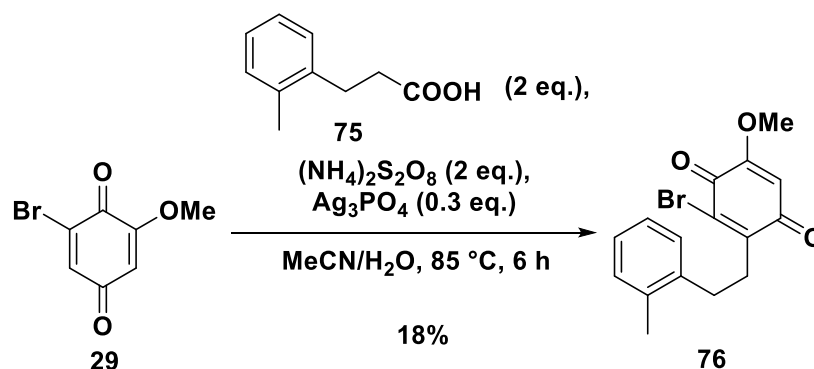


**Scheme 15.** Oxidation of the 1,4-hydroquinone **28** to the 1,4-benzoquinone **29**.

#### 4.3.2 Minisci-type radical decarboxylative alkylation reaction

The next step in the synthesis was a Minisci-type radical decarboxylative alkylation reaction between the 1,4-benzoquinone **29** and a carboxylic acid. 3-(2-Methylphenyl)propionic acid **75** was initially used as this would eventually provide TI **1**. This would be a useful compound to synthesise, as a comparison could then be made between synthetic and commercially sourced TI **1** in terms of biological activity, as a

method of validating the biological effects of synthetic compounds. Similar carboxylic acids with different phenyl substituents could later be used to give derivatives of TI **1** for further biological evaluation. The reaction was first attempted using the conditions described in the literature (Scheme 16).<sup>211</sup>



**Scheme 16.** Reaction of the 1,4-benzoquinone **29** with 3-(2-methylphenyl)propionic acid **75**.

However, this reaction only provided the desired alkylation product **76** in a disappointing 18% yield. This was especially low, given that the conditions used were those identified as being optimal in the literature, with yields of up to 65-79% previously reported.<sup>211</sup> Therefore, the reaction conditions were investigated (Table 1). The results suggested that, compared to the initial reaction conditions used (entry 1), performing the reaction in the dark led to a slight improvement in the percentage yield (entry 2), likely due to the light sensitivity of the Ag(I) salt used. Greater improvements in the reaction yield were observed when the work-up procedure was modified (entry 3), and when the ammonium persulfate oxidant was added in twice the volume of water (entry 4), corresponding to half of the original concentration of persulfate solution. A reduction in the number of equivalents of carboxylic acid **75** used (from 2 to 1.2) did not have any negative impact on the product yield (entry 5). This reduction may have minimised formation of any undesired side products such as the di-alkylated product or products from homocoupling reactions. Formation of small quantities (< 10%) of a by-product thought to be the di-alkylated product were observed throughout these reactions, so the reduction in number of equivalents of carboxylic acid **75** probably had a small

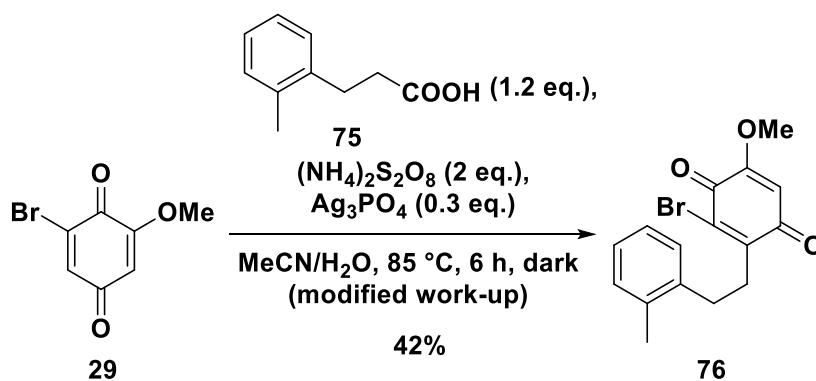
beneficial impact on reaction yield (although is not likely to have been the single main contributing factor to any noticeable increases). Interestingly, none of the alternative mono-alkylated product alkylated adjacent to the methoxide group was observed. This was consistent with previous reports,<sup>211,255</sup> and appeared to be a directing effect as a result of the bromide substituent, the exact nature of which was unclear.

**Table 1.** Optimisation of conditions for the radical alkylation reaction.

Entry	Light/ dark	Work-up	Eq. acid 75	Eq. oxidant	Volume of H <sub>2</sub> O / mL	% yield*
1	Light	1 M NaOH (10 mL)	2	2	10	18
2	Dark	1 M NaOH (10 mL)	2	2	10	25
3	Light	Ice (10 g); 1 M NaOH (3 mL)	2	2	10	33
4	Light	1 M NaOH (10 mL)	2	2	20	42
5	Light	1 M NaOH (10 mL)	1.2	2	10	35

\* Represents isolated product after chromatographic purification.

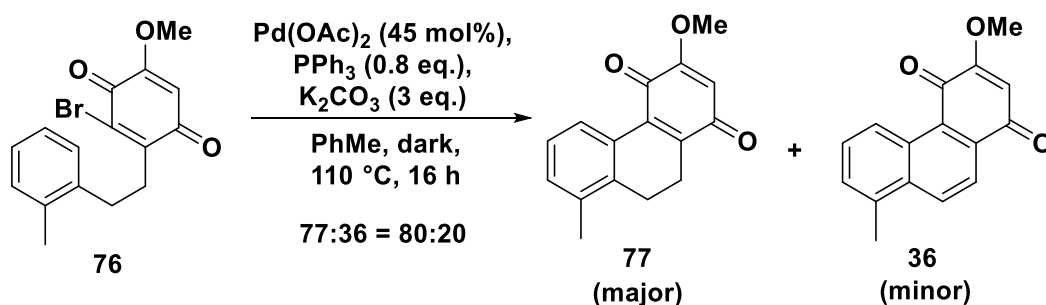
A combination of all the modified reaction conditions was then used in an additional reaction with the same substrate **29** (Scheme 17). This delivered the desired alkylation product **76** in a 42% yield, a substantial improvement on the original reaction yield. Although this was still lower than the yields obtained in the literature for the same reaction, further optimisation was not considered here, as the quantity of the alkylation product **76** provided by this reaction was sufficient for later steps, which still required investigation.



**Scheme 17.** Radical alkylation using optimised conditions.

### 4.3.3 Intramolecular Heck reaction

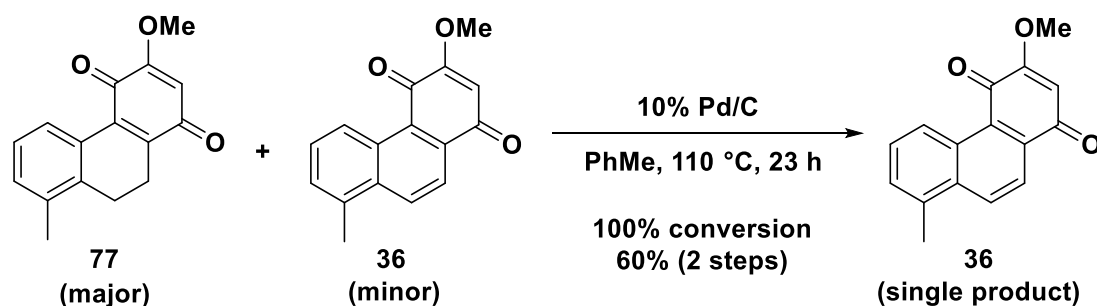
The radical alkylation product **76** was subjected to intramolecular Heck reaction conditions to form the third ring of the tanshinone skeleton, initially using palladium(II) acetate as the catalyst and conditions previously used in the literature (Scheme 18).<sup>211</sup> This yielded a mixture of ring-closed products comprising predominantly the non-aromatised product **77**, consistent with the results obtained in the literature.<sup>211</sup> This was determined by <sup>1</sup>H nuclear magnetic resonance (NMR) spectroscopy, which indicated an 80:20 ratio of non-aromatised:aromatised products **77:36**. These compounds were inseparable by column chromatography, and so the crude mixture of the two products was taken forward to a following aromatisation step without any additional purification.



**Scheme 18.** Palladium-catalysed intramolecular Heck reaction.

Previously, a one-pot dehydrogenation-demethylation strategy using an oxygen balloon was employed to achieve complete aromatisation of the intramolecular Heck reaction products.<sup>211</sup> However, aromatisation could be achieved with a safer reagent, followed by use of a conventional *O*-demethylation reagent. Thus, the aromatisation step was attempted by subjecting the crude mixture of non-aromatised **77** and aromatised **36** products to treatment with palladium on carbon (Scheme 19). Complete conversion of the mixture to solely the aromatised product **36** was successfully achieved, as indicated by <sup>1</sup>H NMR spectroscopy, with complete disappearance of the peaks corresponding to the CH<sub>2</sub> protons observed. However, when the preceding intramolecular Heck reaction was later repeated to provide more material, this surprisingly formed the aromatised product **36** as the only product, with no evidence for presence of the non-aromatised product **77** observed in the <sup>1</sup>H NMR spectrum. This

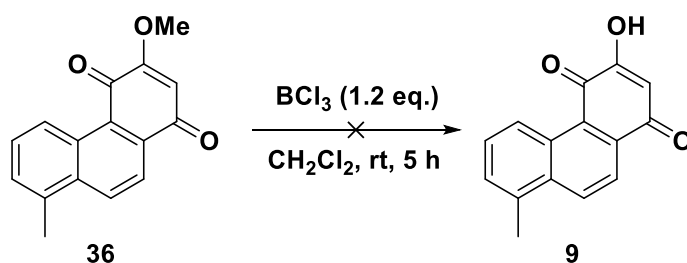
thereby eliminated the need to carry out the aromatisation reaction with palladium on carbon again. This difference may have been due to variation in the quality of the nitrogen atmosphere used for the Heck reaction, and/or the quality of the palladium source, as the presence of more 'palladium black' may have catalysed oxidation.



**Scheme 19.** Complete aromatisation using palladium on carbon.

#### 4.3.4 Demethylation reaction

Different reagents for *O*-demethylation of the ether **36** were investigated. Use of 1.2 equivalents of boron trichloride was first explored, as this was reported to be a particularly effective *O*-demethylation reagent when a carbonyl group is present in an *ortho*-position to the methoxide group (Scheme 20).<sup>256</sup>



**Scheme 20.** Attempted *O*-demethylation using boron trichloride.

However, this did not provide any of the desired demethylated product **9**, and only starting material **36** was returned. Thus, several variations on this reaction were carried out (Table 2). As observed for the use of 1.2 equivalents (entry 1), use of 3 equivalents of boron trichloride gave no desired product **9** (entry 2). A combination of boron trichloride and tetra-*n*-butylammonium iodide (TBAI) was investigated (entry 3), as this has been used successfully in the cleavage of aromatic methyl ethers,<sup>257</sup> but this also

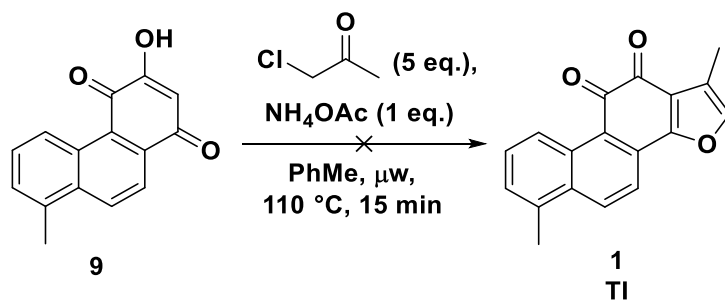
returned only starting material **36**. On the other hand, use of excess 2 M sodium hydroxide was very effective for the reaction, and enabled complete conversion of the methyl ether **36** to the desired alcohol **9**. This reagent was also used previously in the literature,<sup>211</sup> albeit under an oxygen atmosphere to achieve simultaneous aromatisation. The alcohol product **9** was isolated cleanly and meant that no further purification was required. Therefore, this was taken on to the final step of the synthetic route.

**Table 2.** Reagents investigated for *O*-demethylation.

<b>Entry</b>	<b>Reagent(s)</b>	<b>Outcome</b>
1	BCl <sub>3</sub> (1.2 eq.)	No reaction
2	BCl <sub>3</sub> (3 eq.)	No reaction
3	BCl <sub>3</sub> (3 eq.), TBAI (1.3 eq.)	No reaction
4	2 M NaOH (excess)	Complete conversion

#### 4.3.5 Modified Feist-Bénary reaction

With a successful demethylation procedure in hand, construction of the furan ring to give the final tanshinone **1** was explored. This transformation had previously been accomplished in a modest yield of 35%, with an additional 30% recovered starting material, using a modified Feist-Bénary reaction,<sup>211</sup> by heating the alcohol **9** with bromoacetone and ammonium acetate in toluene in a sealed tube. However, bromoacetone could not be easily commercially sourced, and therefore, this reaction was first attempted using five equivalents of chloroacetone, with ammonium acetate and toluene under microwave conditions (Scheme 21).



**Scheme 21.** Attempted modified Feist-Bénary reaction.

However, no reaction occurred, as predominantly starting material **9** was returned. One possible reason for this is that toluene was not an ideal solvent for this microwave reaction, due to it lacking a strong permanent dipole allowing for efficient absorption of microwaves. Therefore, the reaction was repeated using only the alcohol **9** and neat chloroacetone as both the reagent and a significantly more polar solvent. Again, only starting material **9** was returned, and this may have been due to the absence of weak base necessary for initial deprotonation of the alcohol **9** prior to reaction. Indeed, when the reaction was repeated using excess chloroacetone and a stoichiometric quantity of ammonium acetate, successful reaction occurred, and after chromatographic purification, two products were isolated. One of these was the desired TI **1** (a dark red solid), whilst the other product was identified as the isomer isotanshinone I (iso-TI) **13** (an orange solid), which was formed in an approximately equal ratio (Scheme 22), with spectroscopic data matching the literature for both TI **1**<sup>204,211,258</sup> and iso-TI **13**.<sup>203,204,259</sup> The two isomers were each isolated in approximately 20% yield, and this likely occurred either due to tautomeric intermediates, or due to the existence of the alcohol **9** as two possible tautomers under the reaction conditions. These tautomers could both react following deprotonation, with no preference for one tautomer over the other, thereby giving rise to the *ortho*- and *para*-quinone products **1** and **13** in approximately equal quantities. Although the yield of this reaction was fairly low, this provided a sufficient quantity of TI **1** for biological evaluation, as well as the additional isomer **13**, which would likely be formed for each new tanshinone analogue generated. Isotanshinones are a class of compound for which only a few examples appear to be known, such as iso-TI **13** and isotanshinone IIA (iso-TIIA) **78**,<sup>203,204,259,260</sup> isotanshinone IIB (iso-TIIB) **79**,<sup>261</sup>

and only a small number of others (Figure 9).<sup>262</sup> Related isotanshinones based on the isomeric parent compounds cryptotanshinone **5** and dihydrotanshinone I **4** are also known; these have recently been investigated as anti-cancer agents.<sup>263,264</sup> However, this class of compounds is largely underexplored, both in terms of syntheses and biological studies, and may possess interesting biological properties. It was therefore of interest to evaluate any isotanshinones synthesised here in the same way as tanshinones, to explore whether any effects exhibited by tanshinones *in vivo* were also exhibited by the relevant isotanshinones.

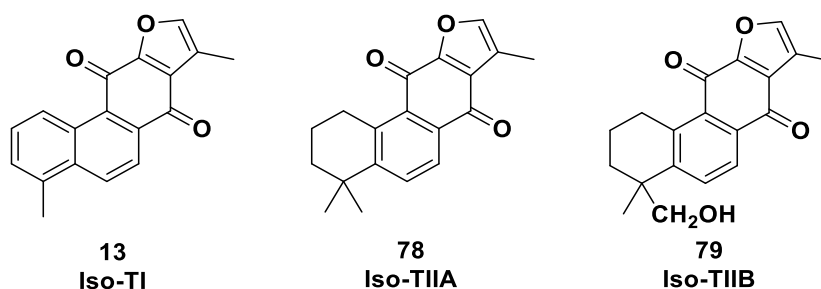
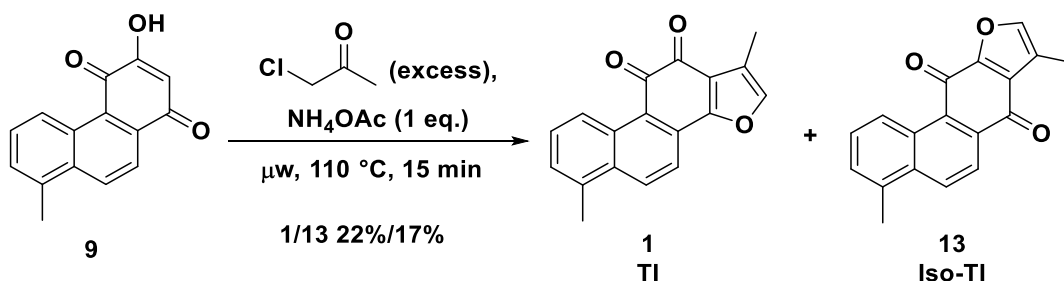


**Figure 9.** Structures of iso-TI **13**, iso-TIIA **78** and iso-TIIB **79**.



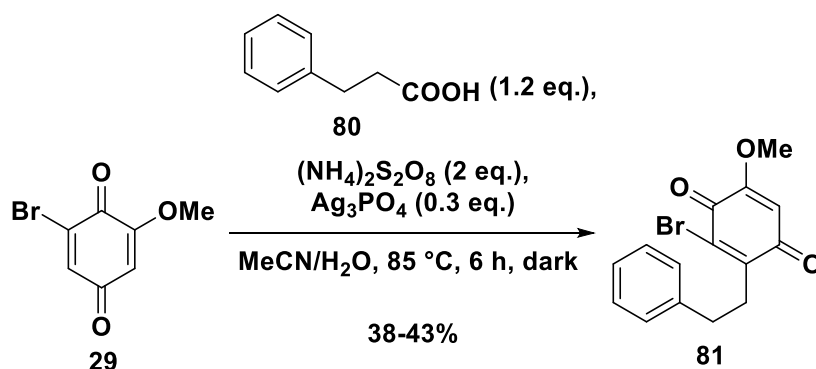
**Scheme 22.** Synthesis of TI **1** and its isomer iso-TI **13**.

This meant that the complete synthetic route to TI **1** (and its isomer **13**) was verified. Thus, synthesis of analogues of TI **1** (and their corresponding isomers) was undertaken, and further optimisation of particular reactions explored where appropriate.

## 4.4 Synthesis of TI analogues

### 4.4.1 Radical decarboxylative alkylation reaction

Firstly, reaction of the previously synthesised benzoquinone **29** with various substituted carboxylic acids in the radical decarboxylative alkylation step was to be carried out. The reaction was first performed using 3-phenylpropionic acid **80**, on both 250 and 500 mg scales, using the previously optimised reaction conditions (Scheme 23). Yields of 38% and 43% of the desired product **81** were obtained for the 250 and 500 mg scale reactions respectively. Whilst these were in line with the 42% yield obtained for the methyl-substituted product **76**, these still represented relatively modest yields, especially compared to those obtained in the literature, and so further optimisation studies for this reaction were undertaken.



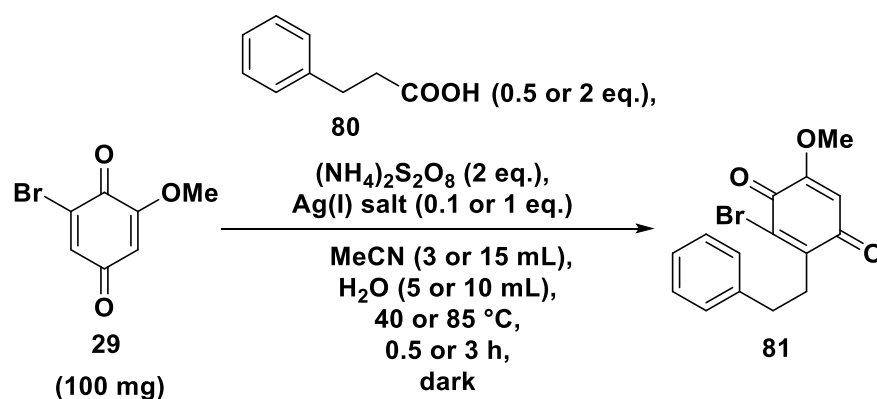
**Scheme 23.** Radical alkylation of the benzoquinone **29** with 3-phenylpropionic acid **80**.

### 4.4.2 Use of Design of Experiments (DoE) studies in optimisation of the radical alkylation

For these studies, the unsubstituted 3-phenylpropionic acid **80** was again used, in order to eliminate the possibility of an additional substituent having any electronic or steric impact on the reaction, allowing an unbiased assessment of the effect of changing various reaction conditions. Given the large number of different variables which could be investigated, a Design of Experiments (DoE) approach was utilised. DoE is a systematic method of exploring numerous parameters and their effects (and relative importance) on the reaction outcome, whilst minimising the number of individual experiments to be performed. It is an approach which has long been used in industry (especially process chemistry) and is becoming increasingly used in synthetic organic

chemistry reactions in academia.<sup>265–269</sup> Using the Custom Design function in JMP software (JMP®, Version 12. SAS Institute Inc., Cary, NC, 1989-2007), the effects of changing the following reaction variables were investigated (Scheme 24):

- Number of equivalents of carboxylic acid **80** (0.5 eq., 2 eq.)
- Number of equivalents of the silver(I) salt (0.1 eq., 1 eq.)
- Identity of the silver(I) salt ( $\text{Ag}_3\text{PO}_4$ ,  $\text{AgNO}_3$ ,  $\text{Ag}_2\text{CO}_3$ )
- Volume of acetonitrile (3 mL, 15 mL)
- Volume of water (5 mL, 10 mL)
- Reaction time (0.5 h, 3 h)
- Reaction temperature (40 °C, 85 °C)
- Method of addition of the aqueous persulfate solution to the reaction (dropping funnel, metal needle/syringe).



**Scheme 24.** General radical alkylation reaction for optimisation studies using DoE.

The indicated options for each variable were chosen for a number of reasons. Firstly, selecting two different numerical values for each quantitative variable, rather than three or more values, further reduced the number of required experiments to be performed. As each experiment required heating, work-up, and purification by column chromatography to accurately determine the reaction yield, this was highly desirable. The two values were generally chosen to represent high and low ‘extremes’ for each variable, based on previous data obtained for this reaction and evaluation of the

literature. For the reaction time, it was observed that although previous reactions carried out in this work had been performed for six hours, these reactions actually reached completion in two to three hours, and given the number of experiments to be performed, the higher value was set at three hours. Various silver(I) salts were selected based on those used previously, both in this work and in the literature. Finally, the method of addition of the aqueous persulfate solution was also chosen as an additional variable to investigate. With these input parameters, the software determined ten experiments to be performed, which were carried out within a short timeframe (Table 3).

**Table 3.** The ten radical alkylation experiments carried out, as determined by the JMP DoE software.

Entry	Eq. acid 80	Eq. Ag(I) salt	Ag(I) salt	Vol. MeCN / mL	Vol. H <sub>2</sub> O / mL	Time / h	Temp. / °C	Metal needle used?	% yield product 81*
1	0.5	1	Ag <sub>3</sub> PO <sub>4</sub>	3	5	0.5	40	No	25%
2	0.5	0.1	AgNO <sub>3</sub>	3	5	0.5	85	Yes	10%
3	0.5	0.1	Ag <sub>3</sub> PO <sub>4</sub>	15	10	0.5	85	Yes	11%
4	0.5	1	AgNO <sub>3</sub>	3	10	3	40	Yes	18%
5	0.5	1	Ag <sub>2</sub> CO <sub>3</sub>	15	5	3	85	No	26%
6	2	0.1	Ag <sub>2</sub> CO <sub>3</sub>	3	10	0.5	40	No	6%
7	2	1	Ag <sub>2</sub> CO <sub>3</sub>	15	5	0.5	40	Yes	0%
8	2	1	AgNO <sub>3</sub>	15	10	0.5	85	No	51%
9	2	0.1	AgNO <sub>3</sub>	15	5	3	40	No	18%
10	2	1	Ag <sub>3</sub> PO <sub>4</sub>	3	5	3	85	Yes	24%

\* Represents isolated product after chromatographic purification.

Following completion of these reactions, as determined by the software, changing several of these parameters appeared to have only small effects on the reaction yield. However, the single most important factor identified was the method of persulfate

addition: addition of the persulfate solution *via* glass dropping funnel gave an elevated yield compared to addition *via* metal syringe. This observation has been noted elsewhere with aqueous persulfate solutions,<sup>270</sup> and is thought to be because the metal syringe accelerates the rate of decomposition of the oxidant in solution, which is itself unstable at room temperature.<sup>271</sup> Use of silver(I) phosphate or silver(I) nitrate also gave slightly higher yields than the use of silver(I) carbonate, whilst heating at 85 °C and increasing the number of equivalents of silver(I) salt both gave a mild increase in yield, with all other changes to the system identified as having minimal or no effect.

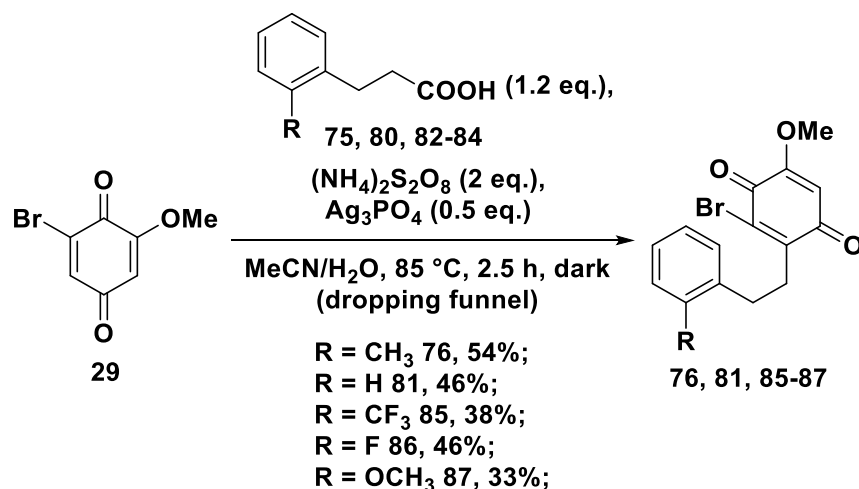
In a small set of follow up experiments, changing the silver(I) salt to silver(I) acetate, silver(I) sulfate or silver(I) tetrafluoroborate also gave no increase in product yield. From analysis of these data, there seemed to be no obvious change which would boost product yields dramatically from those obtained already. Nonetheless, the combined optimal conditions from this study were used for the radical alkylation reaction with the hydrogen-substituted carboxylic acid **80**, as well as other substituted carboxylic acids.

#### 4.4.3 Radical alkylation for analogue synthesis

In addition to the methyl-substituted **75** and hydrogen-substituted **80** carboxylic acids used already, acids with trifluoromethyl **82**, fluoro **83**, and methoxy **84** substituents in the same *ortho*-position on the phenyl ring were chosen. These were all commercially available and relatively inexpensive starting materials. These carboxylic acids and their corresponding products were all previously used in the radical alkylation, intramolecular Heck reaction, and demethylation steps of the synthesis, with no obvious compatibility issues reported,<sup>211</sup> although none of the three heteroatom-substituted analogues were converted into the corresponding final tanshinone compounds. This small set of five carboxylic acids included a mixture of electron-donating, electron-withdrawing, and neutral substituents on the phenyl ring, which would be interesting to explore in the biological evaluation of the final tanshinone compounds. Use of these acids in this route would also allow investigation of changes made some distance away from the tanshinone *ortho*-quinone moiety. In addition, comparison of the biological activities of the methyl- and hydrogen- substituted tanshinone compounds with their

trifluoromethyl- and fluoro-substituted counterparts were of interest in relation to *in vivo* metabolism. C-H bonds are often metabolised and functionalised *in vivo*,<sup>272,273</sup> and replacement of particular C-H bonds with C-F bonds is a common strategy used in drug discovery and development. This is because this change can sometimes prevent or reduce metabolism as C-F bonds are not metabolically labile, thus often improving the metabolic stability of drug molecules.<sup>274,275</sup> Other factors such as drug absorption, distribution, potency and target selectivity can also be affected, as the high electronegativity of fluorine can affect properties including pK<sub>a</sub>, conformation, hydrogen bonding and lipophilicity.<sup>274,275</sup>

In the radical alkylation reaction using the newly optimised reaction conditions (Scheme 25), products bearing methyl **76**, hydrogen **81**, and fluoro **86** substituents were all formed in consistent yields of 46-54%, whilst the trifluoromethyl variant **85** was synthesised in a slightly lower yield of 38%. In some cases, dry column chromatography was found to be successful in the purification of reactions carried out on larger scales, which improved the time- and cost-effectiveness of this step. For the methoxy substituent, some benzoquinone **29** starting material remained, which despite all efforts, could not be separated from the product **87** by either chromatographic purification or recrystallisation on a large scale. Analysis of the <sup>1</sup>H NMR spectrum of the mixture indicated a 60:40 ratio of the bromide **87** and the benzoquinone starting material **29**, corresponding to an approximate 33% overall yield of desired product **87**. These products were taken on to the intramolecular Heck reaction.

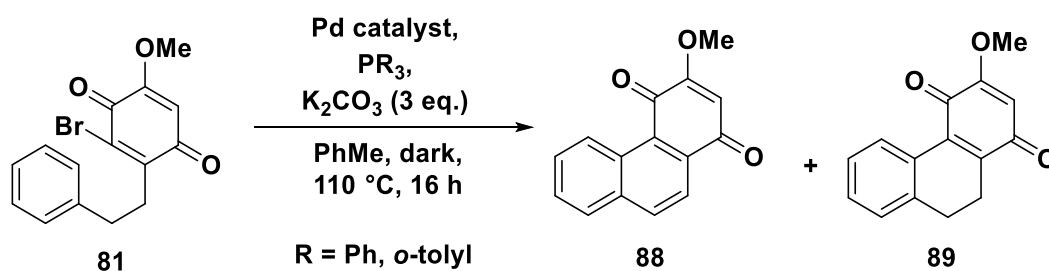


**Scheme 25.** Radical alkylation reaction using various substituted carboxylic acids.

#### 4.4.4 Optimisation of the intramolecular Heck reaction

With the alkylation products formed in reasonable yield, attention was turned to the intramolecular Heck reaction to form the tricyclic core. When the methyl-substituted alkylation product **76** was previously subjected to the Heck reaction conditions used in the literature, the desired product was formed in moderate yield following purification, as a mixture of aromatised **36** and non-aromatised **77** compounds. Given the very high quantities of palladium catalyst used (45 mol%), this was not a sufficiently high yield to justify repeating the reaction on moderate scales for multiple compounds using the same conditions. Therefore, optimisation of this reaction, with particular emphasis on efforts to considerably reduce the amount of catalyst required for the reaction, was explored.

The unsubstituted bromide **81** was used as a model system (Scheme 26), again to determine the efficiency of the reaction in the absence of any phenyl substituents which could affect the reaction.

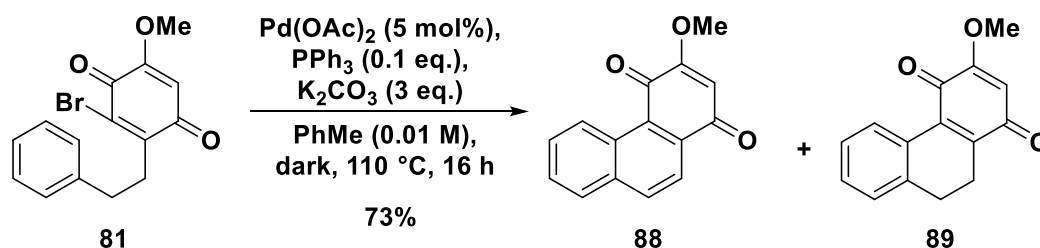


**Scheme 26.** General scheme for the intramolecular Heck reaction using the unsubstituted substrate **81**.

Reducing the amount of palladium catalyst from 45 mol% to 10 mol% gave a correspondingly low yield of 15% of the aromatised and non-aromatised products **88** and **89**, and changing the ligand from triphenylphosphine to tri(*o*-tolyl)phosphine had no obvious effect. This led to the hypothesis that the palladium catalyst might be working in a stoichiometric manner, whereby after first catalysing the intramolecular Heck reaction, it could then take part in a second reaction, aiding aromatisation of the initial product and thereby being consumed. Therefore, the reaction was repeated using 10 mol% catalyst, but with the addition of either *para*-benzoquinone **32** or palladium on carbon as a co-oxidant to the reaction. However, in each case, the yield remained low at 10-15%, suggesting that there must be another reason for the poor product yields.

The effect of concentration on this intramolecular reaction was then explored. When the reaction was performed at a three-fold lower concentration, again using 10 mol% catalyst, the combined yield of aromatised and non-aromatised products increased dramatically to 68% after purification. At a five-fold lower concentration (approximately 0.01 M), a yield of 74% was obtained, and this was conserved when the catalyst loading was reduced to 5 mol%, with a 73% yield obtained (Scheme 27). Although it was not particularly surprising that the yield of this reaction was concentration-dependant, as this reaction is an intramolecular process, it appeared that this particular transformation was especially sensitive to concentration effects. These results were especially encouraging as they now represented a vast improvement on the conditions used in the literature for this transformation, mainly a nine-fold reduction in the amount of

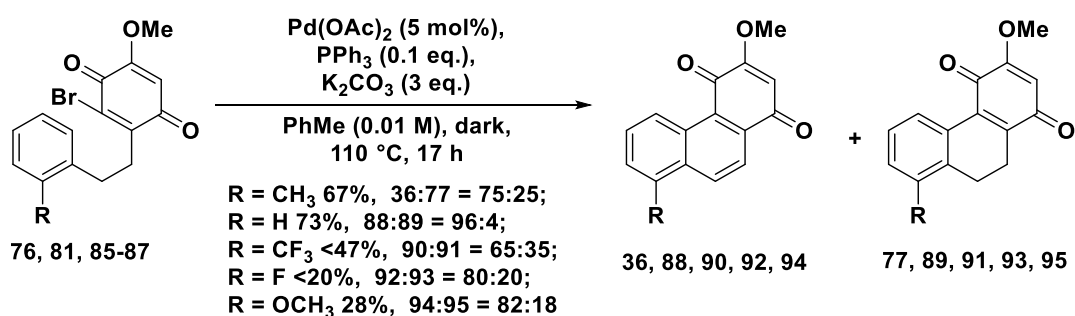
palladium catalyst required in the reaction, whilst still achieving respectable product yields in line with those obtained previously.



**Scheme 27.** Optimised intramolecular Heck reaction conditions.

The optimised Heck reaction conditions were used to synthesise the corresponding substituted analogues **36**, **77**, **90-95** (Scheme 28). Whilst a comparable yield of 67% was obtained for the methyl variants **36** and **77**, the yields were lower for the heteroatom-substituted compounds. For the trifluoromethyl analogues **90-91**, a yield below 47% was obtained, and a lower yield below 20% was attained for the fluoro analogues **92-93**; precise yield values could not be determined due to the presence of an additional inseparable, unidentified component for these two substituents. For the methoxy compounds **94-95**, the inseparable mixture of the alkylation product **87** and the benzoquinone **29** was subjected to the Heck reaction conditions but resulted in the return of mainly purified starting material **87**. This suggested that the palladium underwent faster oxidative addition with the simple benzoquinone **29** than with the alkylated compound **87**. After subjecting this recovered material to the Heck conditions for a second time, the mixture of desired aromatised and non-aromatised products **94** and **95** was isolated in a combined yield of 28%. It was hypothesised that the reduced yields for these compounds may have been because the heteroatom was participating in the reaction mechanism, by co-ordinating to the palladium catalyst (Figure 9). Thus, the closer the heteroatom lone pair to the active catalyst site, the greater the interference with the reaction and hence the lower the yield of desired product obtained. The differing electronics of the phenyl ring may have also had an effect here. Although some of the yields were low, each of the required products were obtained in adequate yields to produce sufficient quantities of the final tanshinone products after

the remaining two reactions in the route. The ratios of aromatised:non-aromatised products varied for each of the reactions undertaken, with the fully aromatised product representing the major product in each case, and it was unclear as to whether this was related to the particular analogue in question, or some other reason such as variable quality of the nitrogen atmosphere or palladium source used for each reaction. However, this was relatively unimportant, as any of the non-aromatised product could be easily converted to the desired aromatised product. This could be achieved in a separate reaction with palladium on carbon as found previously, but it was also believed that such aromatisation might occur spontaneously in later reaction steps, thereby eliminating the need for an additional synthetic step. Thus, the isolated mixtures of aromatised and non-aromatised Heck reaction products for each analogue were taken on to the demethylation step without further reaction.



**Scheme 28.** Intramolecular Heck reaction using various substituted analogues.

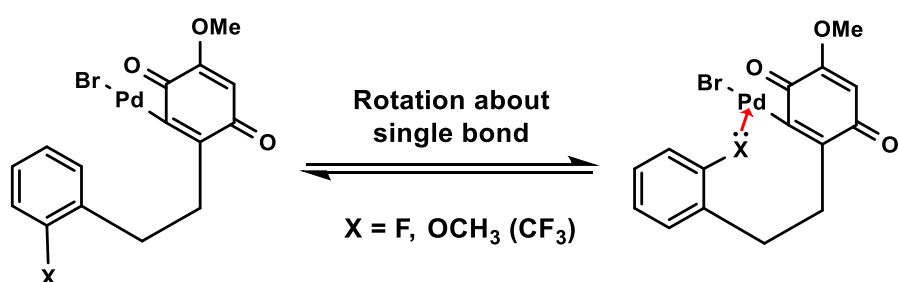
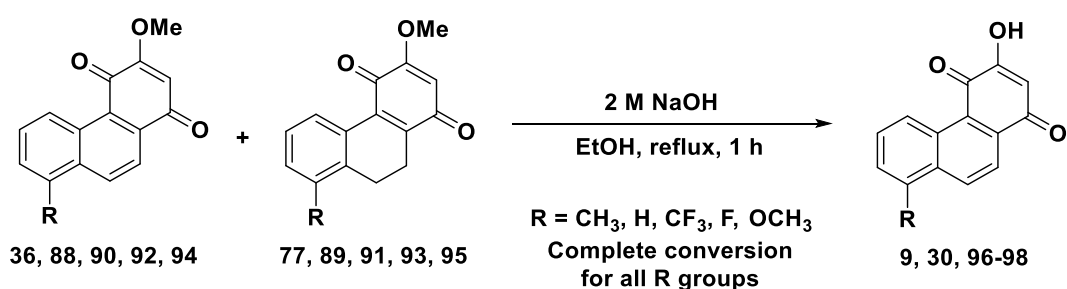


**Figure 10.** Possible interaction of the heteroatom substituent with the inserted palladium.

#### 4.4.5 Final demethylation and modified Feist-Bénary reaction steps

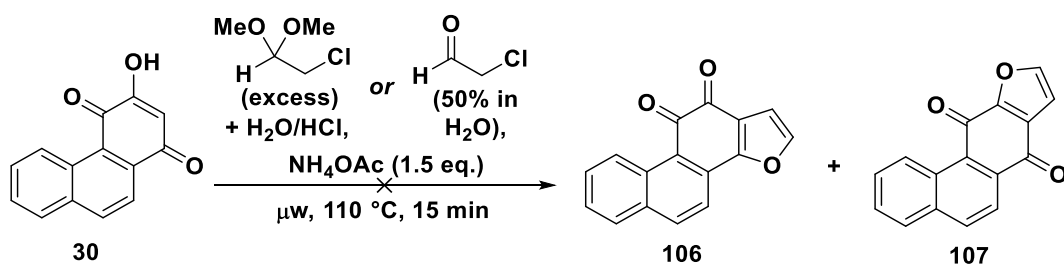
Demethylation of the hydrogen-substituted ethers **88-89** to form the corresponding alcohol **30** using ethanolic 2 M sodium hydroxide solution under reflux conditions successfully yielded the desired alcohol **30** in near-quantitative yield (Scheme 29). During this reaction, the mixture of aromatised **88** and non-aromatised **89** starting materials was converted cleanly to the fully aromatised product **30**, thereby avoiding the need for any use of palladium on carbon in a separate step. This worked well for the synthesis of all analogues **9, 30, 96-98** (Scheme 29), with complete conversion of the methyl ether products to the fully aromatised alcohol in each instance. Only the single desired demethylation was observed for the methoxy compound **98**, with the methoxy substituent on the phenyl ring remaining intact. For the methyl- **9**, hydrogen- **30** and methoxy- **98** substituted analogues, no further purification was required. However, for the trifluoromethyl- **96** and fluoro- **97** substituted compounds, the alcohol products were impure, and attempted purification by recrystallisation was unsuccessful with a variety of solvents. Efforts to purify these impure compounds by standard column chromatography were also unsuccessful, as the compounds were fairly polar, and in some cases, could only be removed from the silica using neat methanol. Therefore, in these cases, the crude alcohols **96** and **97** were taken forward to the final step without any further purification.



**Scheme 29.** Aqueous hydroxide-mediated ether demethylation for various analogues.

Finally, reaction of the various alcohols **9, 30, 96-98** with chloroacetone to give the desired tanshinones **1, 31, 100, 102, 104** and isotanshinones **13, 99, 101, 103, 105** was carried out (Scheme 30). The reaction was successful for each of the different analogues,

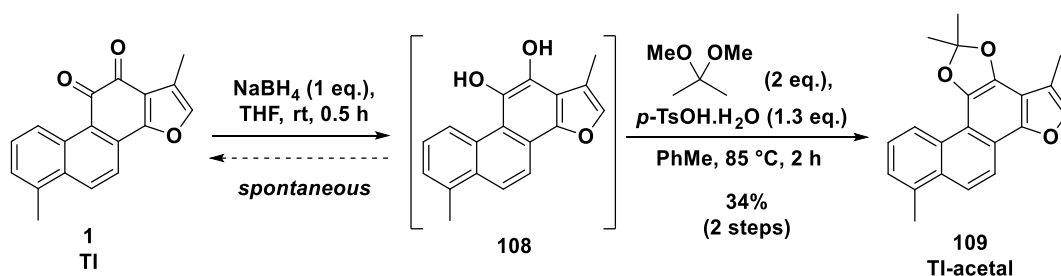




**Scheme 31.** Attempted microwave reactions with sources of chloroacetaldehyde.

#### 4.4.6 Synthesis of a TI-acetal

It was hypothesised that the *ortho*-quinone moiety of TI **1** (and other tanshinones such as TIIA **2**) was important for its biological activity, as this is a chemically interesting functional group common to most well-known tanshinones. Therefore, synthesis of a ‘masked’ analogue lacking this functionality was explored. Synthesis of a dimethyl acetal analogue of TI **1** was accomplished in a two-step procedure (Scheme 32). Facile reduction of the *ortho*-quinone with sodium borohydride generated the diol **108**. However, the diol **108** spontaneously decomposed back to TI **1** in solution and on exposure to air, matching similar observations made previously for TIIA **2** and TIIB **3**.<sup>237,244</sup> Thus, quickly treating the diol **108** with 2,2-dimethoxypropane and acid led to formation of the acetal **109**, which was stable in solution, in air, and to column chromatography. The acetal **109** was isolated in a moderate 34% yield over two steps, with some TI **1** also recovered. This acetal **109** was biologically evaluated *in vivo* in the same manner as the synthesised tanshinones and isotanshinones.



**Scheme 32.** Synthesis of a dimethyl acetal **109** from TI **1**.

## 4.5 Biological evaluation of TI, iso-TI and analogues

### 4.5.1 Effect of TI on neutrophil recruitment

Previous work carried out in the Renshaw laboratory showed that TIIA **2** promoted the resolution of neutrophilic inflammation *in vivo* but did not affect initial neutrophil recruitment.<sup>36</sup> Meanwhile, TI **1** exhibited a smaller, yet still significant effect on inflammation resolution (Dr. Anne Robertson, The University Of Sheffield, Appendix 10.1). The effect of TI **1** on recruitment of neutrophils to the site of injury was not previously investigated using this model, and was therefore of interest here.

Firstly, commercial TI **1** was evaluated at concentrations of 1, 10 and 25  $\mu\text{M}$  in neutrophil recruitment experiments, all of which were performed by myself. Zebrafish larvae at age 3 dpf were injured at the distal portion of the tailfin. The injured larvae were subjected to immediate treatment with one of the following: TI **1** (1, 10 or 25  $\mu\text{M}$  concentrations), DMSO (negative vehicle control), or SP **74** (positive control). SP **74** is a commercially available, selective, cell-permeable inhibitor of c-Jun N-terminal kinase, which prevents activation of various inflammatory genes.<sup>276,277</sup> The ability of SP **74** to significantly reduce neutrophil recruitment in both this and other zebrafish neutrophilic inflammation models has been well documented,<sup>36,114,119</sup> and so this was used as a positive control for all recruitment experiments. The three concentrations of TI **1** were chosen as these were previously used for evaluation of the effect of TI **1** on the resolution of neutrophilic inflammation in the same zebrafish model (Dr. Anne Robertson, The University Of Sheffield, Appendix 10.1). These concentrations have been commonly used in this particular model for similar dose-response incubation studies of aqueous compounds, and in particular, a concentration of 25  $\mu\text{M}$  is often used as an initial 'screening' concentration for new compounds which may be of interest. Larvae were incubated with the compounds for several hours (representing the recruitment stage of the inflammatory response), after which the number of neutrophils at the site of injury was counted.

TI **1** significantly reduced the number of neutrophils recruited to the site of injury at concentrations of both 25 and 10  $\mu\text{M}$ , compared to larvae treated with DMSO (Figure 10). There was no difference in neutrophil recruitment at a TI **1** concentration of 1  $\mu\text{M}$ .

Overall, the effect of TI **1** on neutrophil recruitment was much greater than that observed for TIIA **2**,<sup>36</sup> and may suggest the existence of different anti-inflammatory mechanisms of action for these two tanshinones. It should be noted that in these experiments, the positive control treatment SP **74** was in some instances used at a concentration of 30  $\mu\text{M}$ , and at a 60  $\mu\text{M}$  concentration in others. This was because different batches of the compound were used: the first batch was used at a 60  $\mu\text{M}$  concentration as it was found to be ineffective at 30  $\mu\text{M}$  in these experiments. It was later deduced that this batch had started to go off, having been kept for a long time. A second batch was purchased and used for later experiments, and was found to be effective at a 30  $\mu\text{M}$  concentration, consistent with most previous experiments and those of other researchers.

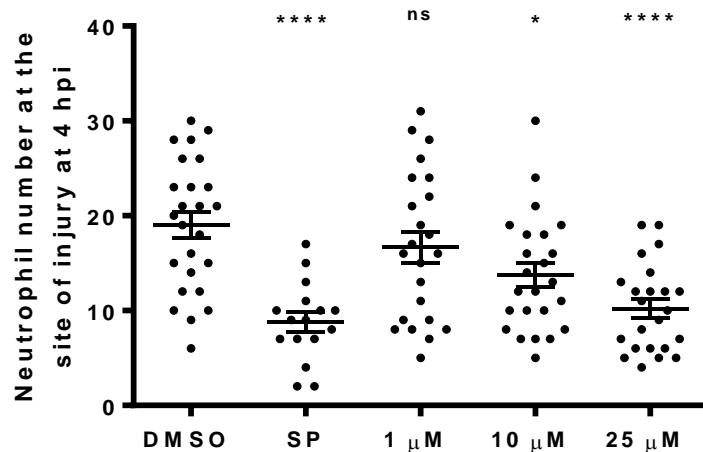


**Figure 11. TI **1** treatment significantly reduced neutrophil recruitment to a site of injury.**

DMSO used at 0.5% concentration, SP **74** used at a concentration of 30 or 60  $\mu\text{M}$ , TI **1** used at concentrations of 1, 10 and 25  $\mu\text{M}$ . Data shown as mean  $\pm$  SEM;  $n = 16$ -25 larvae from 3 independent experiments. \*  $P < 0.01$ , \*\*\*\*  $P < 0.0001$ , ns not significant, in comparison to the DMSO control (one-way ANOVA with Dunnett's multiple comparison post-test).

#### 4.5.2 Comparison of commercial and synthetic TI

Next, having found that TI **1** resulted in decreased neutrophil recruitment, commercially sourced TI **1** was compared with synthesised TI **1**, to check that these different batches of the same compound had the same effect *in vivo* (Figure 11). These

experiments, as for all biological experiments performed herein, were carried out by myself. Both batches of TI **1** resulted in decreased neutrophil recruitment to the site of injury, and there was no difference in the effects observed between commercial and chemically synthesised TI **1**. This was an encouraging result, and effectively validated the use of other chemically synthesised compounds in this model. Therefore, the entire set of synthesised tanshinone and isotanshinone analogues were evaluated in this way.

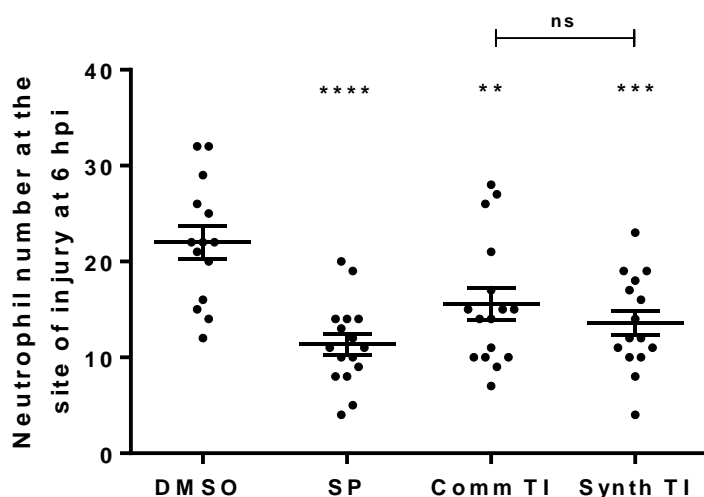


**Figure 12. Commercial and chemically synthesised TI **1** both reduced neutrophil recruitment, and there was no difference between the two batches of TI **1**.**

DMSO used at 0.5% concentration, SP **74** used at a concentration of 30  $\mu$ M, TI **1** used at a concentration of 25  $\mu$ M. Data shown as mean  $\pm$  SEM;  $n = 14-16$  larvae from 2 independent experiments. \*\*  $P < 0.01$ , \*\*\*  $P < 0.001$ , \*\*\*\*  $P < 0.0001$ , ns not significant, in comparison to the DMSO control, or between indicated groups (one-way ANOVA with Dunnett's multiple comparison post-test). Comm TI = commercial TI **1**, Synth TI = synthetic TI **1**.

#### 4.5.3 Effects of TI analogues and isomers on neutrophil recruitment *in vivo*

The series of synthesised TI analogues and isomers **1**, **13**, **31**, **99-105**, **109** were evaluated for any effects on neutrophil recruitment in the zebrafish inflammation model. Due to experimental constraints such as experiment timepoints and number of zebrafish larvae available, the whole set of 11 compounds (five tanshinones **1**, **31**, **100**, **102**, **104**, five isotanshinones **13**, **99**, **101**, **103**, **105**, and the TI acetal **109**) was split into three groups for biological evaluation. In each group, DMSO and SP **74** were used as the

negative and positive control treatments respectively, whilst TI **1** and iso-TI **13** were also included in each group for comparison.

In the first group, TI **1**, iso-TI **13**, and 6-hydro-TI **31** were evaluated (Figure 12). TI **1** again resulted in decreased neutrophil recruitment, and so too did the isomer iso-TI **13**. The effect seen with iso-TI **13** treatment was notable, as neutrophil numbers approached those observed for treatment with the positive control compound SP **74**. Replacement of the 6-methyl group of TI **1** with a hydrogen atom appeared to be detrimental to anti-inflammatory activity, as treatment with 6-hydro-TI **31** had no significant effect on neutrophil recruitment.

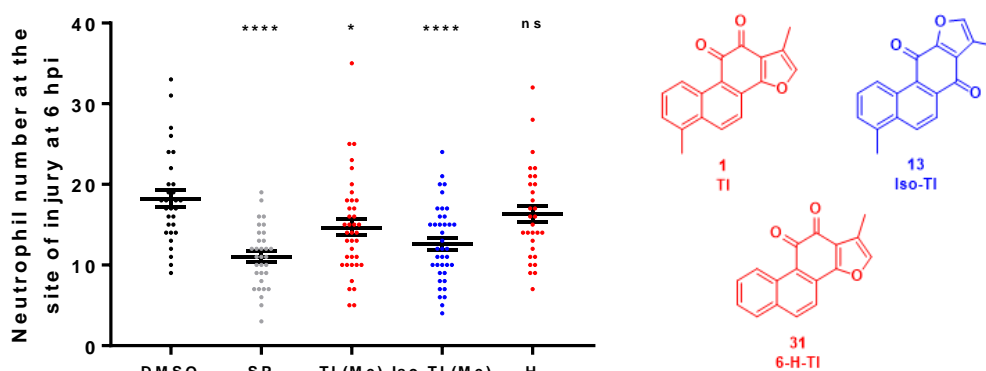


**Figure 13. TI **1** and iso-TI **13** resulted in decreased neutrophil recruitment to a site of injury, yet 6-hydro-TI **31** did not.**

DMSO used at 0.5% concentration, SP **74** used at a concentration of 30  $\mu$ M, all other compounds used at a concentration of 25  $\mu$ M. Data shown as mean  $\pm$  SEM;  $n = 31$ -39 larvae from 4 independent experiments. \*  $P < 0.05$ , \*\*\*\*  $P < 0.0001$ , ns not significant, in comparison to the DMSO control (one-way ANOVA with Dunnett's multiple comparison post-test). H = 6-hydro-TI **31**.

The second group of evaluated compounds comprised the remaining analogues based on TI **1**: 6-trifluoromethyl-TI **100**, 6-fluoro-TI **102**, and 6-methoxy-TI **104**, as well as the unsubstituted 4-hydro-iso-TI **99**, in addition to the parent compounds TI **1** and iso-TI **13** (Figure 13). TI **1** resulted in decreased neutrophil recruitment, but surprisingly, iso-TI **13** did not in this set of experiments. However, iso-TI **13** did result in a significantly reduced number of recruited neutrophils in other sets of recruitment experiments

carried out using the same conditions. The particular result in this group may have reflected an anomalous result, compound-specific variability, or may have arisen from the inherent natural variability of this experiment, given the use of living organisms, despite all efforts to control for this. Treatment with 6-trifluoromethyl-TI **100**, 6-fluoro-TI **102**, or 6-methoxy-TI **104** resulted in no significant effect on neutrophil recruitment, although there appeared to be a trend towards lower numbers of recruited neutrophils in each case. Treatment with 4-hydro-iso-TI **99** had no effect on neutrophil recruitment: the number of neutrophils at the site of injury was at least as high as those for the DMSO control treatment.

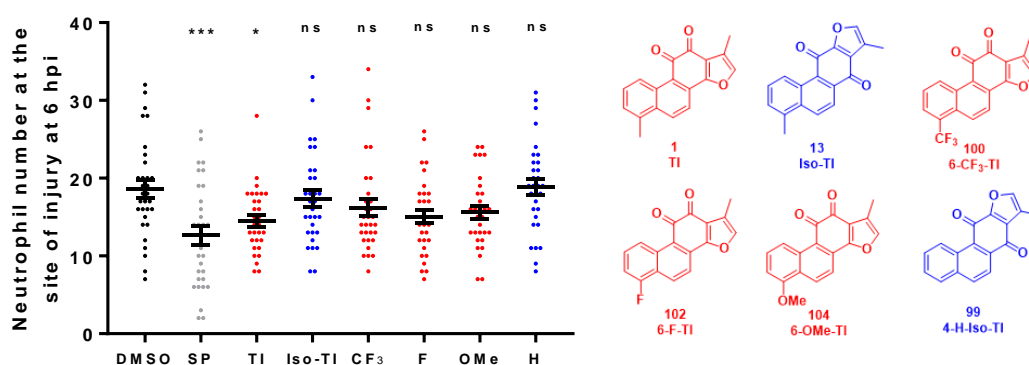


**Figure 14. Neither 6-trifluoromethyl-TI **100**, 6-fluoro-TI **102**, 6-methoxy-TI **104**, nor 4-hydro-iso-TI **99** significantly affected neutrophil recruitment.**

DMSO used at 0.5% concentration, SP **74** used at a concentration of 30  $\mu$ M, all other compounds used at a concentration of 25  $\mu$ M. Data shown as mean  $\pm$  SEM;  $n = 30$ -31 larvae from 4 independent experiments. \*  $P < 0.05$ , \*\*\*  $P < 0.001$ , ns not significant, in comparison to the DMSO control (one-way ANOVA with Dunnett's multiple comparison post-test). CF<sub>3</sub> = 6-trifluoromethyl-TI **100**, F = 6-fluoro-TI **102**, OMe = 6-methoxy-TI **104**, H = 4-hydro-iso-TI **99**.

In the third and final group of compounds, the remaining isotanshinones were evaluated: this comprised 4-trifluoromethyl-iso-TI **101**, 4-fluoro-iso-TI **103**, and 4-methoxy-iso-TI **105**, as well as the TI acetal compound **109**, and also the parent compounds TI **1** and iso-TI **13** (Figure 14). As observed previously, both TI **1** and iso-TI **13** resulted in decreased neutrophil recruitment. Treatment with either 4-trifluoromethyl-

iso-TI **101** or 4-fluoro-iso-TI **103** also led to a decrease in the number of recruited neutrophils, whilst 4-methoxy-iso-TI **105** did not result in a significant difference, although there was a trend towards lower numbers of neutrophils. Furthermore, treatment with the TI acetal **109** also resulted in no significant difference. This was consistent with the hypothesis that the *ortho*-quinone moiety was important for biological activity, yet the activity shown by the *para*-quinone isotanshinones in this work appeared to somewhat disprove this hypothesis. However, a trend towards slightly lower neutrophil numbers could be seen for the TI acetal **109**. One possible explanation for this is that the acetal **109** was hydrolysed, and then metabolised back to the parent TI **1** *in vivo*, which then exerted an effect on neutrophil recruitment. The lack of significant effect on neutrophil recruitment (compared to the clear effect shown by TI **1**) could be because hydrolysis and/or metabolism had only partially occurred by this point, or perhaps because TI **1** was only one of the products of hydrolysis and metabolism, with other products not exhibiting the same effect on neutrophil recruitment.

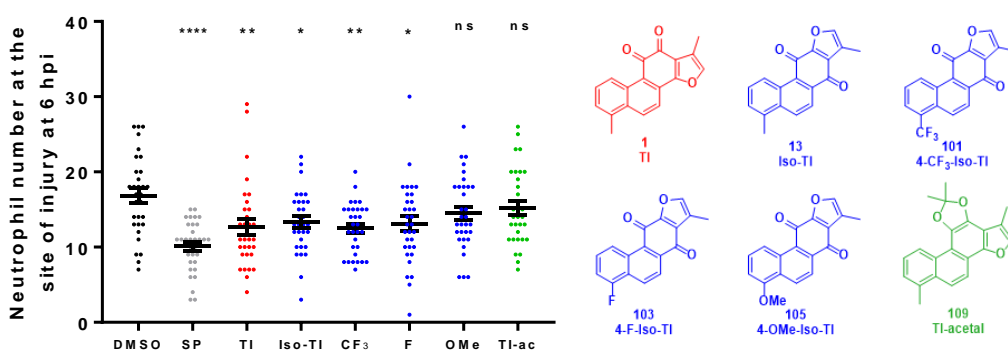


**Figure 15. Trifluoromethyl- **101** and fluoro- **103** substituted isotanshinones resulted in decreased neutrophil recruitment, whilst neither 4-methoxy-iso-TI **105** nor the TI acetal **109** had any effect.**

DMSO used at 0.5% concentration, SP **74** used at a concentration of 30  $\mu$ M, all other compounds used at a concentration of 25  $\mu$ M. Data shown as mean  $\pm$  SEM;  $n = 31$ -32 larvae from 4 independent experiments. \*  $P < 0.05$ , \*\*  $P < 0.01$ , \*\*\*\*  $P < 0.0001$ , ns not significant, in comparison to the DMSO control (one-way ANOVA with Dunnett's multiple comparison post-test). CF<sub>3</sub> = 4-trifluoromethyl-iso-TI **101**, F = 4-fluoro-iso-TI **103**, OMe = 4-methoxy-iso-TI **105**, TI-ac = TI acetal **109**.

Following completed analysis of the effects of these compounds on neutrophil recruitment, evaluation of any effects of the same compounds on resolution of neutrophilic inflammation was undertaken.

#### 4.5.4 Initial *in vivo* inflammation resolution experiments

For experiments investigating any effects of the compounds on inflammation resolution *in vivo*, the same compounds groupings were used as for the neutrophil recruitment experiments. However, TI **1** and iso-TI **13** were only evaluated in the first group, and were omitted from the second and third groups, due to experimental constraints. Furthermore, a different positive control compound was used for these experiments: instead of SP **74**, TIIA **2** was used, at a concentration of 25  $\mu$ M. TIIA **2** has previously been shown to profoundly accelerate the resolution of neutrophilic inflammation in this zebrafish model,<sup>36</sup> and use of this tanshinone as a positive control helped to link this work to previous research performed using this model.

For initial resolution experiments carried out by myself, the same procedure as reported previously was used here.<sup>36,278</sup> Zebrafish larvae at age 3 dpf were injured at the distal portion of the tailfin, then incubated in standard E3 solution for six hours. At 6 hpi, a time at which neutrophil numbers at the site of injury were typically thought to reach their peak, larvae which had mounted a good inflammatory response to the injury were identified. These typically comprised larvae with approximately 20 neutrophils at the site of injury, henceforth termed 'good responders'. Good responders were selected and treated with a 25  $\mu$ M concentration solution of the compound of interest, and incubated for a further six hours. At 12 hpi, a time at which inflammation had typically started to spontaneously resolve but had not yet completely resolved, neutrophil numbers at the injury site were recorded.

However, when the first group of compounds was evaluated in such inflammation resolution experiments, none of the compounds had any significant effect on the number of neutrophils at the site of injury, including the positive control compound TIIA **2** (Figure 15). The lack of any difference between the DMSO and TIIA **2** treatment groups

was a particular problem and suggested that there was an issue with either the compound or the experimental setup. The latter was considered more likely, especially as a relatively new batch of TIIA **2** was used for these experiments. Therefore, before proceeding any further with the evaluation of the synthesised tanshinones and isotanshinones, a series of experiments was carried out to optimise the experimental setup for inflammation resolution experiments.

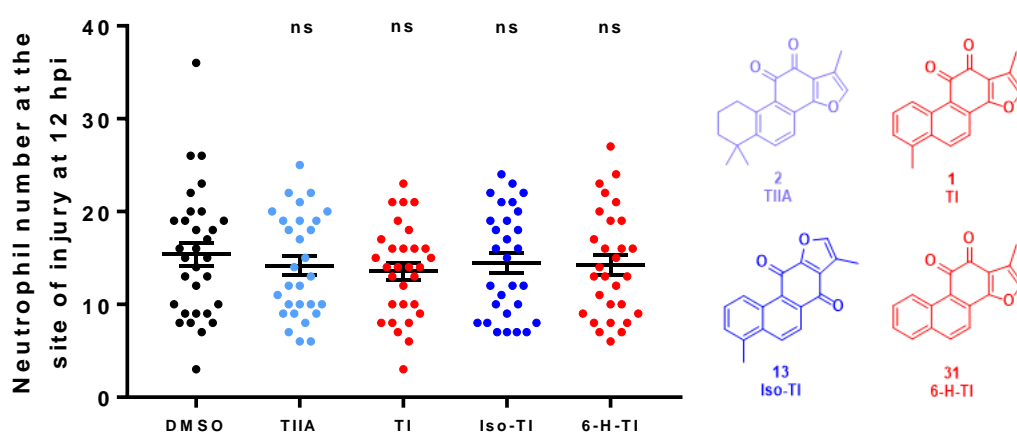


**Figure 16. Neither TIIA **2**, TI **1**, iso-TI **13**, nor 6-hydro-TI **31** had any effect on inflammation resolution at 12 hpi.**

DMSO used at 0.5% concentration, all other compounds used at a concentration of 25  $\mu$ M. Data shown as mean  $\pm$  SEM;  $n = 29$ -31 larvae from 4 independent experiments. ns Not significant, in comparison to the DMSO control (one-way ANOVA with Dunnett's multiple comparison post-test). 6-H-TI = 6-hydro-TI **31**.

#### 4.5.5 Optimisation of inflammation resolution experiments and validation of new experimental timepoints using TI and TIIA

One reason why TIIA **2** may not have worked as expected was because the timepoints for the inflammation resolution experiments were no longer the best ones to use. Therefore, to determine if this was the case (and if so, to then select new appropriate timepoints), timecourse experiments were carried out by myself on zebrafish larvae age 3 dpf (Figure 16). Larvae were injured at their tailfin, and the number of neutrophils at the site of injury was counted at various timepoints following injury. The number of neutrophils at the injury site peaked at 4 hpi, before decreasing over time from this

point. The previous resolution experiments may therefore not have worked well because by 12 hpi, inflammation of the fish in the DMSO control group had already spontaneously resolved to such an extent that it was not possible to detect further significant decreases in neutrophil numbers as a result of treatments which accelerated resolution. Thus, in light of these data, it was more appropriate to count neutrophils (and therefore, treat the larvae) at an earlier timepoint. At 8 hpi, there was a significantly greater number of neutrophils at the injury site than at 12 hpi; resolution of neutrophilic inflammation had already started to occur (as indicated by a significant decrease between 4 hpi and 8 hpi), but not to the extent of that at 12 hpi. Resolution at this time had also not yet completed, as indicated by a significant difference between 8 hpi and 24 hpi. Therefore, treatment of the good responders with compounds at 4 hpi, and counting the number of neutrophils at 8 hpi was investigated (rather than the 6 and 12 hpi timepoints used previously for these respective steps).

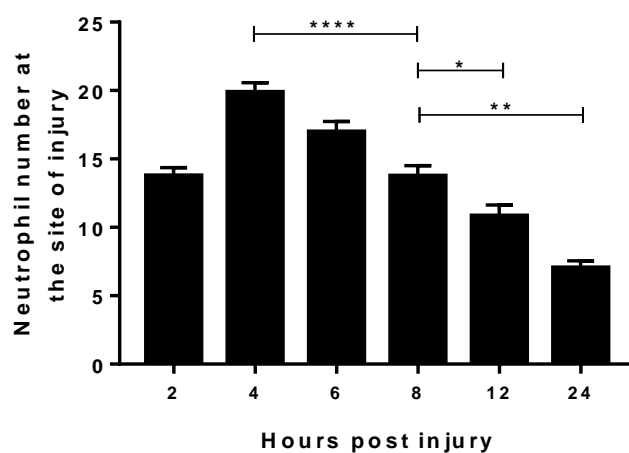


**Figure 17. The number of neutrophils at the site of injury reached a maximum at around 4 hpi, then resolved to pre-injury neutrophil numbers by 24 hpi.** Data shown as mean ± SEM;  $n = 45$  larvae from 3 independent experiments. \*  $P < 0.05$ , \*\*  $P < 0.01$ , \*\*\*\*  $P < 0.0001$  (one-way ANOVA with Tukey's multiple comparison post-test).

To explore use of the new resolution timepoints, the effects of only the negative and positive control treatments, DMSO and TIIA 2 respectively, were investigated (Figure 17). TIIA 2 significantly accelerated resolution of neutrophilic inflammation, which

indicated that the control treatments worked well using these timepoints. Compared to the lack of difference observed at 12 hpi, this appeared to confirm that the timepoints were indeed the issue previously.

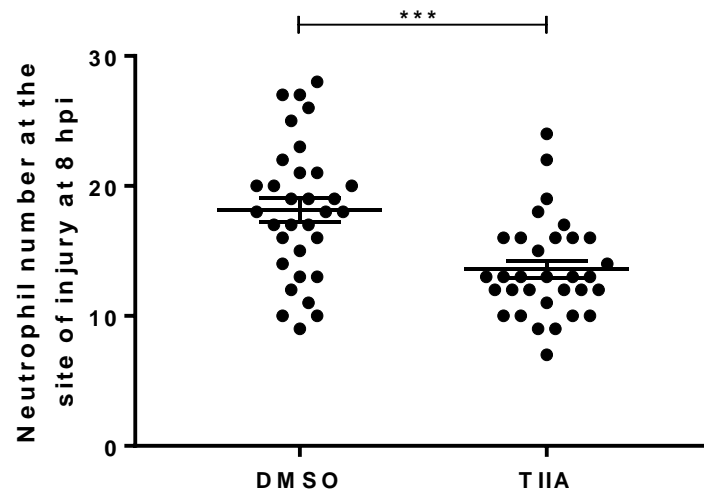


**Figure 18. TIIA 2 significantly accelerated inflammation resolution at 8 hpi.**

DMSO used at 0.5% concentration, TIIA 2 used at a concentration of 25  $\mu$ M. Data shown as mean  $\pm$  SEM;  $n = 32$  larvae from 4 independent experiments. \*\*\*  $P < 0.001$ , in comparison to the DMSO control (unpaired  $t$ -test).

To further validate the use of these new timepoints, the effects of TI 1 and TIIA 2 on resolution of neutrophilic inflammation were studied by myself in the same experiments. Neutrophil recruitment studies were also carried out by myself using the same treatment groups, again to compare the two different tanshinones within the same experiments, and ensure that previous individual findings for these two compounds could be replicated together (Dr. Anne Robertson, The University Of Sheffield, Appendix 10.1).<sup>36</sup> Thus, resolution and recruitment experiments were carried out in which TI 1 and TIIA 2 were investigated concomitantly, at concentrations of 10 and 25  $\mu$ M.

For the resolution experiments (Figure 18), TIIA 2 accelerated resolution at a concentration of 25  $\mu$ M, and also resulted in decreased neutrophil numbers at a 10  $\mu$ M concentration. These results were consistent with the dose-response effects seen for TIIA 2 previously in this model.<sup>36</sup> Interestingly, TI 1 also resulted in decreased neutrophil

numbers at 8 hpi, at both 10 and 25  $\mu\text{M}$  concentrations. Here, TI **1** worked just as well as TIIA **2** (if not better) in accelerating resolution of neutrophilic inflammation. The similar neutrophil numbers at the two different concentrations may suggest that the effect of TI **1** became 'saturated' at a concentration of 10  $\mu\text{M}$  (or even lower), whether that be due to compound solubility, pharmacokinetics, pharmacodynamics, or some other reason.

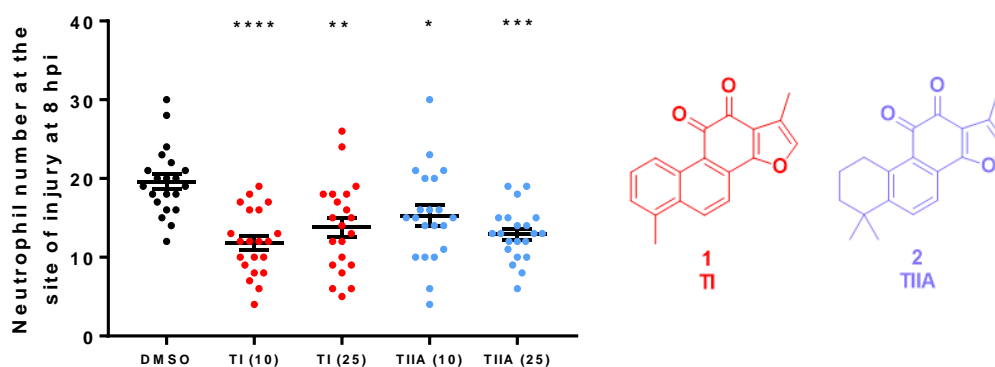


**Figure 19. Both TI **1** and TIIA **2** accelerated inflammation resolution.**

DMSO used at 0.5% concentration, TI **1** and TIIA **2** used at concentrations of 10 and 25  $\mu\text{M}$ . Data shown as mean  $\pm$  SEM;  $n = 21$  larvae from 3 independent experiments. \*  $P < 0.05$ , \*\*  $P < 0.01$ , \*\*\*  $P < 0.001$ , \*\*\*\*  $P < 0.0001$ , in comparison to the DMSO control (one-way ANOVA with Dunnett's multiple comparison post-test).

TI **1** and TIIA **2** were then investigated in neutrophil recruitment experiments, in further validation studies (Figure 19). The 6 hpi timepoint for neutrophil counting was retained here, to keep these experiments consistent with recruitment experiments performed already in this work. This was not considered to be an issue, given that the appropriate control compounds had worked well with this experimental setup. TIIA **2** did not significantly affect neutrophil recruitment at either of the two concentrations tested, although there was a trend towards a small decrease in neutrophil numbers at a 25  $\mu\text{M}$  concentration; this was consistent with previous studies of TIIA **2** in this model.<sup>36</sup> Treatment with TI **1** at a 25  $\mu\text{M}$  concentration resulted in a reduced number of neutrophils recruited to the site of injury, although this was not the case at a lower concentration of 10  $\mu\text{M}$ . This was generally consistent with previous experiments in this

work, and may suggest that TI **1** exhibited a dose response effect on neutrophil recruitment between these concentrations.

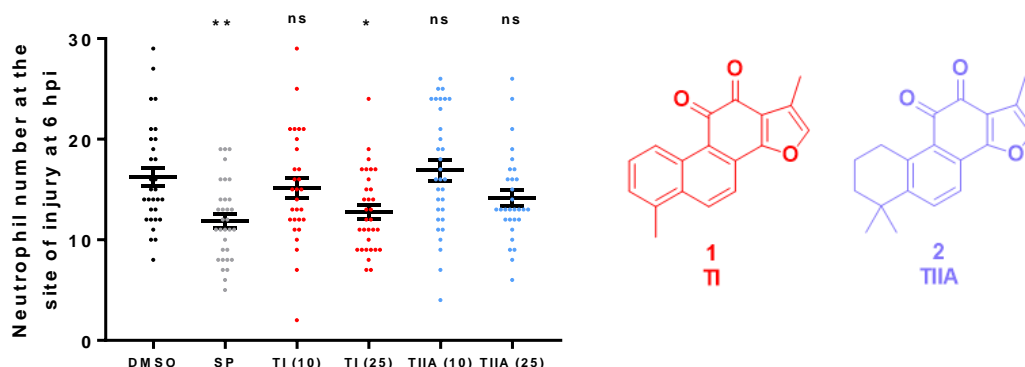


**Figure 20. TI **1** resulted in decreased neutrophil recruitment, yet TIIA **2** did not.**

DMSO used at 0.5% concentration, SP **74** used at a concentration of 30  $\mu$ M, TI **1** and TIIA **2** used at concentrations of 10 and 25  $\mu$ M. Data shown as mean  $\pm$  SEM;  $n = 29$ -32 larvae from 4 independent experiments. \*  $P < 0.05$ , \*\*  $P < 0.01$ , ns not significant, in comparison to the DMSO control (one-way ANOVA with Dunnett's multiple comparison post-test).

The results for both inflammation resolution and recruitment using these timepoints indicated that the timepoints chosen for each of the two types of experiment were appropriate, and worked well for all the control treatments. Experiments using the two tanshinones TI **1** and TIIA **2** were also successful, and were consistent with previous experiments carried out in this model. Therefore, the synthesised library of tanshinones and isotanshinones was evaluated for any effects on resolution of neutrophilic inflammation using the new timepoints.

#### 4.5.6 Effects of TI analogues and isomers on resolution of neutrophilic inflammation *in vivo*

Using the same groups of compounds and, except for the new timepoints, the same experimental conditions as previously (Chapters 4.5.3 and 4.5.4), resolution experiments were carried out for the synthesised TI analogues and isomers. The first group comprised TI **1**, iso-TI **13**, and 6-hydro-TI **31** (Figure 20). In contrast to previous

experiments (Chapter 4.5.5), TI **1** did not significantly accelerate resolution of neutrophilic inflammation, although there was a visible trend towards a lower number of neutrophils which approached significance ( $P = 0.063$ ). Treatment with iso-TI **13** resulted in a significantly lower number of neutrophils at the site of injury, and neutrophil numbers were close to those observed for the TIIA **2** positive control. As observed for neutrophil recruitment, replacement of the 6-methyl group of TI **1** with a hydrogen atom led to loss of biological activity of the compound, as 6-hydro-TI **31** had no effect on inflammation resolution.

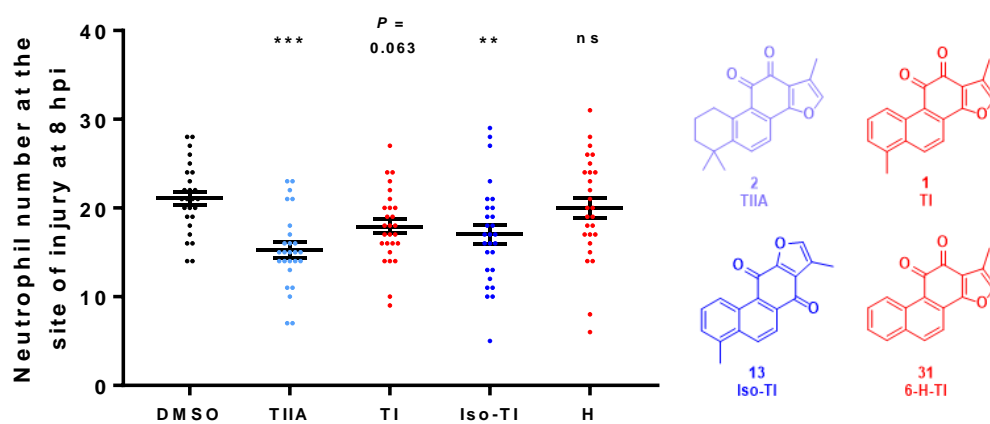


**Figure 21. Iso-TI 13 significantly accelerated inflammation resolution, whilst TI 1 and 6-hydro-TI 31 did not.**

DMSO used at 0.5% concentration, all other compounds used at a concentration of 25  $\mu$ M. Data shown as mean  $\pm$  SEM;  $n = 26$ -28 larvae from 4 independent experiments. \*\*  $P < 0.01$ , \*\*\*  $P < 0.001$ , ns not significant, in comparison to the DMSO control (one-way ANOVA with Dunnett's multiple comparison post-test). H = 6-hydro-TI **31**.

The second group of compounds comprised the remaining tanshinones 6-trifluoromethyl-TI **100**, 6-fluoro-TI **102**, and 6-methoxy-TI **104**, as well as the isotanshinone 4-hydro-iso-TI **99** (Figure 21). In this particular set of experiments, neutrophil numbers observed following treatment with the positive control compound TIIA **2** were not significantly different from those observed following DMSO treatment. However, there was a visible trend towards lower neutrophil numbers, and the results were very close to statistical significance ( $P = 0.052$ ). In all other resolution experiments

carried out using these timepoints, larvae treated with TIIA **2** had significantly lower neutrophil numbers. Therefore, the neutrophil numbers for TIIA **2** observed here were not thought to be of concern. For the remaining compounds investigated, 6-methoxy-TI **104** clearly accelerated inflammation resolution, whilst 6-trifluoromethyl-TI **100** and 6-fluoro-TI **102** did not. However, for 6-fluoro-TI **102**, there was a trend towards lower neutrophil numbers at the site of injury, whereas for 6-trifluoromethyl-TI **100**, there appeared to be a trend towards a higher number of neutrophils, compared to larvae treated with DMSO. The unsubstituted 4-hydro-iso-TI **99** had no effect on resolution, and this was consistent with the previous lack of biological activity observed, both for recruitment with the same compound, and also for resolution with the unsubstituted tanshinone 6-hydro-TI **31**.

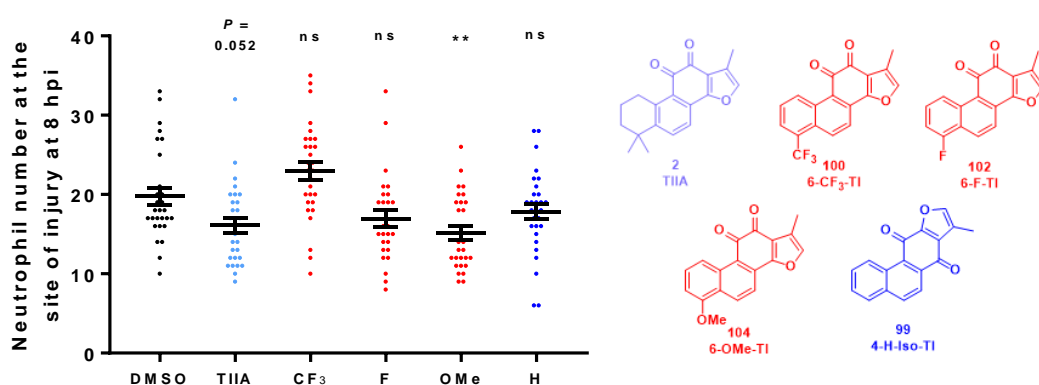


**Figure 22. 6-Methoxy-TI 104 significantly accelerated inflammation resolution, yet 6-trifluoromethyl-TI 100, 6-fluoro-TI 102, and 4-hydro-iso-TI 99 did not.**

DMSO used at 0.5% concentration, all other compounds used at a concentration of 25  $\mu$ M. Data shown as mean  $\pm$  SEM;  $n = 28-29$  larvae from 4 independent experiments. \*\*  $P < 0.01$ , ns not significant, in comparison to the DMSO control (one-way ANOVA with Dunnett's multiple comparison post-test). CF<sub>3</sub> = 6-trifluoromethyl-TI **100**, F = 6-fluoro-TI **102**, OMe = 6-methoxy-TI **104**, H = 4-hydro-iso-TI **99**.

Finally, the remaining isotanshinones – 4-trifluoromethyl-iso-TI **101**, 4-fluoro-iso-TI **103**, and 4-methoxy-iso-TI **105** - and the TI acetal **109**, were evaluated (Figure 22). None of the isotanshinones had any effect on resolution of neutrophilic inflammation, and neutrophil numbers at the site of injury were broadly comparable with the numbers for

DMSO treatment in each case. However, treatment with the TI-acetal **109** resulted in a significant reduction in neutrophil number. As suggested for the recruitment data obtained previously, one explanation for this could be that the acetal **109** was hydrolysed and then metabolised back to TI **1** *in vivo*, which then exerted a pro-resolution effect, consistent with previous results for TI **1** (Chapter 4.5.5).

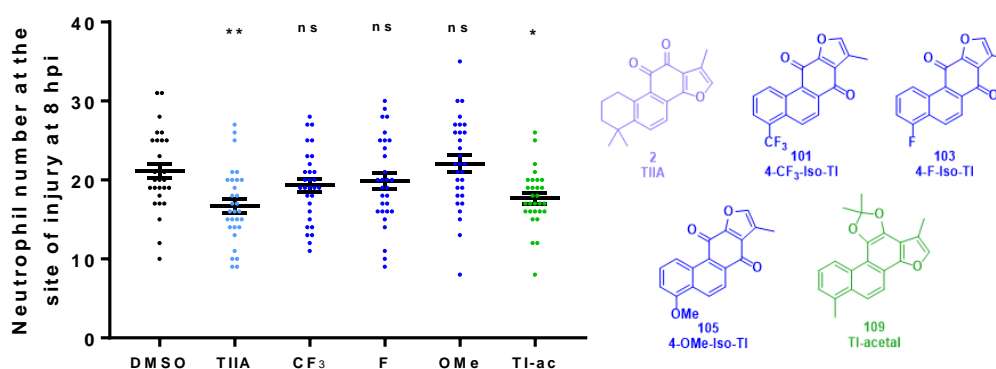


**Figure 23. The TI acetal **109** significantly accelerated resolution of neutrophilic inflammation, yet the isotanshinones 4-trifluoromethyl-iso-TI **101**, 4-fluoro-iso-TI **103**, and 4-methoxy-iso-TI **105** all did not.**

DMSO used at 0.5% concentration, all other compounds used at a concentration of 25  $\mu$ M. Data shown as mean  $\pm$  SEM;  $n = 29$ -30 larvae from 4 independent experiments. \*  $P < 0.05$ , \*\*  $P < 0.01$ , ns not significant, in comparison to the DMSO control (one-way ANOVA with Dunnett's multiple comparison post-test). CF<sub>3</sub> = 4-trifluoromethyl-iso-TI **101**, F = 4-fluoro-iso-TI **103**, OMe = 4-methoxy-iso-TI **105**, TI-ac = TI acetal **109**.

#### 4.5.7 Summary of effects of TI analogues and isomers on neutrophil behaviour during the inflammatory response *in vivo*

The effects of the compounds tested in both neutrophil recruitment and resolution of neutrophilic inflammation experiments were considered together (Table 4). For neutrophil recruitment, the patterns for compounds with each functional group broadly appeared to be consistent between tanshinones and isotanshinones. Compounds with a methyl substituent had a clear effect in reducing neutrophil recruitment, whilst analogues bearing trifluoromethyl, fluorine, or methoxy substituents exhibited some effect (although this was not always statistically significant). Removal of any

functionality at this position (by replacement with a hydrogen atom) led to a complete loss of biological effect. These results suggested that the presence of a substituent in this position was required for activity, but the nature of the substituent may not be too important. Tanshinones and isotanshinones were broadly similar in their behaviours in relation to neutrophil recruitment, and any difference between the families of compounds appeared to be fairly small.

For effects on inflammation resolution, the trends for compounds with each functional group were less clear between tanshinones and isotanshinones. The compounds bearing a methyl group generally showed some effect (either significant, or a trend towards lower neutrophil numbers), and removal of any functionality at this position resulted in loss of activity *in vivo*. Compounds substituted with a trifluoromethyl group or a fluorine atom also showed no significant effect on resolution. When the substituent was a methoxy group, the tanshinone **104** had a clear pro-resolution effect, yet the isotanshinone **105** did not. The reasons behind this were not clear, and further investigation would be required in order to fully understand this. As for recruitment, these results suggested that a substituent in this position was required for any *in vivo* effects on inflammation in this model to be observed. However, in contrast to neutrophil recruitment, the nature of the substituent seemed to be more important for pro-resolution activity.

The effects of the compounds on recruitment were further compared with the effects on resolution. Some compounds affected both recruitment and resolution, whilst some affected neither, and others had an effect on only one of these inflammatory processes. This was not particularly surprising, as molecules which had an effect on neutrophil recruitment likely interacted with a different molecular target or set of molecular targets to those which affected resolution of neutrophilic inflammation. Both of the parent compounds TI **1** and iso-TI **13** significantly decreased neutrophil recruitment and accelerated inflammation resolution, whilst both of the unsubstituted molecules 6-hydro-TI **31** and 4-hydro-iso-TI **99** had no effect on either process. The fluorine-containing tanshinones 6-trifluoromethyl-TI **100** and 6-fluoro-TI **102** also had no significant effect on either process, although both resulted in a trend towards lower

neutrophil numbers in recruitment experiments. Similarly, the isotanshinones 4-trifluoromethyl-iso-TI **101** and 4-fluoro-iso-TI **103** both resulted in decreased neutrophil recruitment, yet had no effect on resolution of neutrophilic inflammation. 6-Methoxy-TI **104** exhibited no effect on neutrophil recruitment, yet significantly promoted inflammation resolution, which was analogous to the findings observed for TIIA **2**. This suggested that this particular compound may be an interesting one to focus on, going forward in investigation of compounds which specifically target inflammation resolution processes. The same activity profile in these two types of experiment was also seen for the TI acetal **109**, although as discussed previously, this may have been due to the formation of products arising from acetal hydrolysis and metabolism, and so could perhaps be considered a lower priority. In contrast to the corresponding tanshinone, 4-methoxy-iso-TI **105** had no effect on either the recruitment or resolution stages of neutrophilic inflammation.

Comparison of the fluorine-containing compounds with their non-fluorine-containing analogues was also of interest, as this could provide insights into how *in vivo* metabolism may have affected biological activity. Whereas TI **1** had an effect on both neutrophil recruitment and resolution, 6-trifluoro-TI **100** did not significantly affect either process (although there was a trend towards fewer recruited neutrophils). Similarly, iso-TI **13** also affected both recruitment and resolution, whilst the analogous 4-trifluoromethyl-iso-TI **101** reduced neutrophil recruitment yet had no effect on resolution of neutrophilic inflammation. This could suggest that *in vivo* C-H metabolism (or some other factor relating to C-F bond substitution) was important for acceleration of inflammation resolution, but not for neutrophil recruitment. 6-Hydro-TI **31** did not affect either recruitment or resolution, and neither did 6-fluoro-TI **102**, although there were trends towards lower neutrophil numbers for both processes. Meanwhile, the unsubstituted 4-hydro-iso-TI **99** also had no effect on neutrophil numbers for either recruitment or resolution, yet treatment with 4-fluoro-iso-TI **103** resulted in decreased neutrophil recruitment, but did not affect resolution. Conversely to the results for the trifluoromethyl variants, this may suggest that replacement of a hydrogen atom with a

fluorine atom here had more effect on neutrophil recruitment than on resolution of neutrophilic inflammation.

**Table 4.** Summary of the effects of various tanshinones and isotanshinones on neutrophil recruitment and resolution of neutrophilic inflammation *in vivo*.

Entry	Compound	Effect on recruitment	Effect on resolution
1	TIIA <b>2</b>	No effect	Enhanced
2	TI <b>1</b>	Reduced	Enhanced
3	Iso-TI <b>13</b>	Reduced	Enhanced
4	6-hydro-TI <b>31</b>	No effect	No effect
5	6-trifluoromethyl-TI <b>100</b>	No effect	No effect
6	6-fluoro-TI <b>102</b>	No effect	No effect
7	6-methoxy-TI <b>104</b>	No effect	Enhanced
8	4-hydro-iso-TI <b>99</b>	No effect	No effect
9	4-trifluoromethyl-iso-TI <b>101</b>	Reduced	No effect
10	4-fluoro-iso-TI <b>103</b>	Reduced	No effect
11	4-methoxy-iso-TI <b>105</b>	No effect	No effect
12	TI-acetal <b>109</b>	No effect	Enhanced

#### 4.5.8 Aqueous solubilities and *in vivo* toxicities of TI analogues and isomers

The aqueous solubilities of the various tanshinones and isotanshinones were qualitatively examined *via* visual observations of the treatment solutions under the microscope whilst neutrophils were counted (and still blinded to identities of the various treatment groups). At a concentration of 25  $\mu$ M, precipitation was consistently observed for TI **1** in both recruitment and resolution experiments, whilst minimal precipitation was seen at a 10  $\mu$ M concentration. This indicated that the aqueous solubility of TI **1** (in E3 solution) was likely between these two values. For iso-TI **13**, there was also precipitate at a 25  $\mu$ M concentration, although this was noticeably less than for TI **1**. Considerable precipitation was observed for 6-hydro-TI **31** at the same concentration, which often appeared to be greater than that observed for TI **1**. For the remaining

tanshinones, there was minimal or no precipitation at a 25  $\mu\text{M}$  concentration. A small amount was seen for 4-hydro-iso-TI **99**, whilst slightly more was observed for both 4-trifluoromethyl-iso-TI **101** and 4-methoxy-iso-TI **105**. The TI-acetal **109** produced minimal amounts of precipitate at the same dosage, whilst none was observed for 4-fluoro-iso-TI **103**. Unsurprisingly, these observations suggested that the least water-soluble compounds were those without heteroatom substituents, whilst those with these groups tended to be more soluble. Aqueous solubility is an important consideration for any compounds taken forward for further study, and future drug development, and so was useful to gauge at a qualitative level at this stage.

Concomitantly, observations of the health of the treated zebrafish larvae were made for all experiments. At a concentration of 25  $\mu\text{M}$  (or lower), none of the evaluated tanshinones and isotanshinones exhibited any larval toxicity; larvae were generally healthy in all treatments, as determined by general body shape, tail shape, presence of circulation, and heartbeat. This was useful information to obtain, as *in vivo* toxicity is another very important consideration in drug discovery and development, and so this highlighted the utility of the zebrafish model in allowing early assessment of *in vivo* drug toxicity.

## 4.6 Discussion

In this work, synthesis of a series of analogues of TI **1**, and its isomer iso-TI **13**, was achieved in six steps from the commercially available compounds 5-bromovanillin **27** and various substituted carboxylic acids. Whilst this synthesis used the same strategy to access the final tanshinones as previous literature precedence,<sup>211</sup> a number of advantages were presented in this work. The first two oxidation steps were carried out on large (25 g) scales without the requirement for chromatographic purification. The radical decarboxylative alkylation step was also performed on moderate (1-2 g) scales, and purification was often carried out effectively using dry column chromatography as a more time- and material-efficient alternative to standard column chromatography. One of the more notable achievements of this work was the nine-fold reduction in the quantity of palladium catalyst required for the intramolecular Heck reactions. These

reactions were carried out using 5 mol% palladium(II) acetate, rather than the 45 mol% used previously in the literature, and yields of up to 74% were achieved. Complete aromatisation of the ring-closed products was observed using mild demethylation conditions, and did not require the use of an oxygen balloon, representing a safer and more convenient method. Furthermore, the modified Feist-Bénary reaction using chloroacetone and microwave conditions resulted in consistent production of both tanshinones and isotanshinones; there are generally very few reported syntheses of isotanshinones in the literature. Thus, the various optimisations carried out led to an improved synthesis of tanshinones and isotanshinones.

One particular set of optimisations involved the use of design of experiments (DoE) software. DoE has been used in industry for many years, particularly in process chemistry, but has only recently started to attract more attention in academic scenarios. In this work, although the optimised conditions as a result of the DoE study were not vastly differently from those used before the study, use of DoE allowed a range of different reaction parameters to be explored quickly using a minimal number of experiments. Significantly fewer experiments were performed than would otherwise have been required to investigate all of these factors without the use of DoE. The custom design function in the DoE software enabled identification of the most important contributing factors to overall reaction yield as well as investigation of any obvious improvements to the reaction conditions which had not previously been implemented. This particular DoE approach was relatively simplistic, in the absence of any specialist knowledge, and future studies of this type could involve the use of more complex, yet efficient, designs in the DoE software. Overall, this approach was useful for evaluating numerous reaction variables, and its use could be considered in similar situations in the future.

Throughout the synthesis, yields of isolated products obtained were often respectable, although in some cases, depended on the phenyl ring substituent. This was particularly true for the intramolecular Heck reaction, and to a lesser extent, the radical alkylation and modified Feist-Bénary reactions. The best yields were generally achieved for compounds with electron-neutral substituents, such as a methyl group **36**, **77** or

hydrogen atom **88-89**. Lower yields were obtained for heteroatom substituents, particularly where the heteroatom was directly bound to the phenyl ring, as for compounds with fluorine **92-93** and methoxide **94-95** substituents. For the Heck reaction, other than the differing electronics of the phenyl ring, this could be because in these cases, due to rotation around a single bond, the heteroatom could become closely positioned to and interact with the palladium catalyst, possibly interfering with the reaction mechanism and thereby resulting in reduced product yields. With the trifluoromethyl-substituted compounds **90-91**, the heteroatoms were perhaps further away from this active site, and so may have had less of an effect, resulting in an intermediate yield. Attempts to investigate this hypothesis were not carried out here due to time constraints, but could be further investigated using other substituents, such as by adding a bulky *tert*-Butyldimethylsilyl (TBDMS) group, and in different positions around the phenyl ring. This approach would also lead to the synthesis of other tanshinone analogues, which could be biologically evaluated to construct further structure-activity relationships.

Synthesis of further functionalised tanshinones using this synthetic route is also of interest. Such tanshinones could be used in various applications, but would be particularly useful for synthesising molecules which could be used to probe the molecular target of tanshinones *in vivo*, for example using photoaffinity labelling.<sup>279</sup> A desirable tanshinone would be the 6-hydroxy-substituted variant, as the phenol could be functionalised whilst avoiding functionalisation close to the *ortho*-quinone moiety. Various alcohol protecting groups could be explored (such as a TBDMS group), but one particular approach would be to use an allyl protecting group. This would have the advantage of likely compatibility with the various reaction conditions throughout the synthesis (although careful analysis of the Heck reaction might be required). Reaction with chloroacetone to form the corresponding tanshinone and isotanshinone would produce new analogues which could be evaluated *in vivo*. Furthermore, the key part of this strategy would be that the allyl group could then undergo ozonolysis to reveal a terminal carbonyl group, which could be functionalised in various ways to produce other derivatives. Careful consideration of the quantities and yields of each step required to

produce enough material for functionalisation would be needed, but this approach is worth considering in future studies.

Synthesis of the TI acetal **109** was undertaken to explore the hypothesis that the *ortho*-quinone moiety of tanshinones was essential for their biological activity. However, following analysis of the recruitment and resolution data for the TI acetal **109**, it was thought that hydrolysis of the acetal **109** and subsequent metabolism of hydrolysis products might have occurred *in vivo*. Therefore, the original hypothesis may not have been tested as originally hoped. Synthesis of a similar compound with greater *in vivo* stability, which 'masks' the *ortho*-quinone functionality of the tanshinone but is otherwise structurally similar, could be considered in future work. This would enable more rigorous investigation of the importance of the *ortho*-quinone moiety for biological activity.

For evaluation of the synthesised tanshinones and isotanshinones in inflammation resolution experiments, it was necessary to change the experimental timepoints, from the 6 and 12 hpi timepoints used previously, to the 4 and 8 hpi timepoints used in this work. The neutrophil timecourse data for the populations of zebrafish larvae indicated that the number of neutrophils at the site of injury peaked at around 4 hpi, rather than 6 hpi as found previously.<sup>36,86,278</sup> These data suggested that the zebrafish inflammatory response dynamics had changed, and this was likely due to zebrafish strain inter-variability, and a lack of inbred strains. The generation of adult zebrafish used to produce larvae for these experiments were changed every 18 to 24 months, so it is likely that the adult zebrafish used here were also a different age to those used previously, and that these differences explained the different experimental timepoints required for these experiments. Furthermore, it is possible that this shift in the time of readout for resolution experiments to an earlier timepoint could have consequences for recruitment assays, since neutrophil counting was still performed at 6 hpi for recruitment experiments. However, the difference in neutrophil numbers in untreated, injured larvae at 4 and 6 hpi was small (Figure 16). In addition, treatment of larvae with a 25  $\mu$ M concentration of TIIA **2** had no significant effect on neutrophil recruitment at 6 hpi (Figure 19), yet use of TIIA **2** at the same concentration consistently resulted in a

significantly lower number of neutrophils at the site of injury at 8 hpi in resolution experiments. Therefore, it is considered to be rather unlikely that the results from recruitment experiments were significantly affected by any effect of the compound on resolution of neutrophilic inflammation. As both recruitment and resolution experiments were carried out separately anyway, these results can be considered together for individual treatments.

Tanshinones, which contain an *ortho*-quinone moiety, and isotanshinones, bearing a *para*-quinone moiety, exhibited similar effects on both neutrophil recruitment and resolution of neutrophilic inflammation. However, the two classes of compounds are somewhat structurally different, thus the two types of compound may not have acted at the same binding region of the same protein target(s). For example, the slightly greater variability in neutrophil recruitment upon treatment with iso-TI **13** compared to TI **1** may be related to a difference in targets and/or polymorphisms in target genes. Furthermore, compounds which resulted in decreased neutrophil recruitment likely acted at a different protein target to those which accelerated resolution of neutrophilic inflammation, as these are different processes in the inflammatory response. Therefore, it may be that there was more than one protein target involved in the biological activities of these compounds observed here. Given the complex biological nature of the inflammatory response, it is possible that the compounds operated at more than one protein target for recruitment alone, and also at more than one target for resolution.

One alternative possibility is that compounds which significantly reduced neutrophil recruitment did not act at a particular protein target or targets, but instead exhibited an antioxidant effect, by reacting with reactive oxygen species (ROS) generated at the site of injury, such as hydrogen peroxide. Hydrogen peroxide has been found to rapidly promote the accumulation of neutrophils at a wound following injury,<sup>280</sup> thus, reaction of a compound with hydrogen peroxide could affect neutrophil recruitment. Previous work found that using the same zebrafish model of inflammation, treatment of larvae with the natural product isopimpinellin led to decreased neutrophil recruitment, yet this was highly unlikely to be due to antioxidant activity, as shown using *in vivo* and *in vitro* methods.<sup>278</sup> Thus, it is possible that the same was true for the tanshinone compounds

evaluated in this work. Future *in vivo* experiments could be carried out with the ROS dye used previously,<sup>281</sup> alongside *in vitro* methods, to determine if the tanshinones evaluated here were likely to be working in this way, although this is thought to be unlikely. This possibility is also very unlikely to be true for compounds which accelerated inflammation of resolution, as hydrogen peroxide is released very early in the process of inflammation, thus likely only affecting neutrophil recruitment. This may therefore explain the results for neutrophil recruitment effects, possibly leaving a single target responsible for the observed effects on resolution of neutrophilic inflammation. Observed differences in recruitment and resolution effects may also be due to delayed penetration of compounds into larvae, with compounds being able to penetrate the larvae quicker and more easily in recruitment experiments than in resolution experiments. Thus, one possibility is that TI **1** was able to quickly get into the larvae and act to decrease neutrophil recruitment, whereas, possibly due to structural differences, TIIA **2** was not able to access the required target quickly enough to have an effect on neutrophil recruitment, but was able to penetrate the larvae sufficiently to have an effect on resolution.

Going forward with any of these compounds which resulted in a significant decrease in the number of neutrophils at the injury site (either in the recruitment or resolution stages of inflammation), it may be wise to carry out neutrophil whole body counts for larvae which have been treated with these compounds. This would involve incubation of the larvae for the same duration as used in the previous experiments, and then counting the number of neutrophils in the whole body, to determine whether the observed decreases in neutrophil numbers at the site of injury were due to overall neutrophil number decreases in the body upon drug treatment, or not. It was previously shown that TIIA **2** accelerated resolution of neutrophilic inflammation in the zebrafish inflammation model without affecting the total number of neutrophils in the larval body;<sup>36</sup> thus it is likely that this would also be true for the structurally similar tanshinones investigated in this work, though it would be wise to evaluate this with at least some of the compounds tested here.

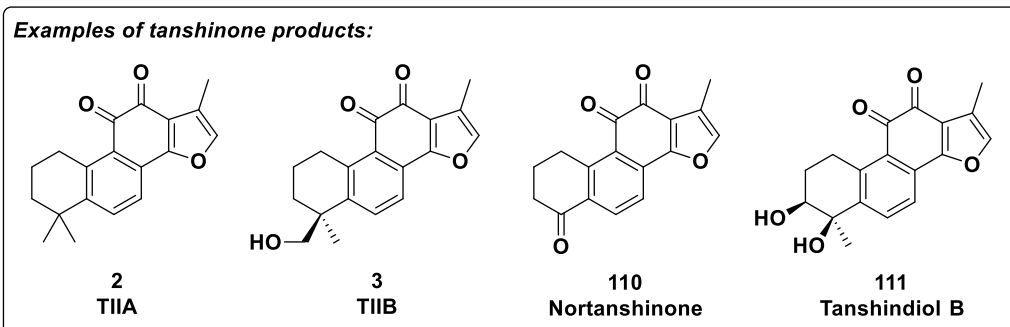
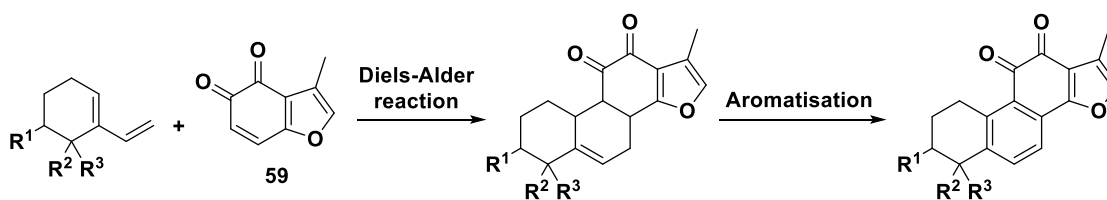
Overall, the results from this work suggested that there were some structural-activity relationships between the compounds tested and their *in vivo* biological activities, as discussed previously. However, these were not completely clearly defined, and there remained some ambiguity. In general, this phenotypic screening approach enabled identification of new compounds which demonstrated significant effects on neutrophil behaviour in the inflammatory response *in vivo*, and provided some areas for further investigation. The compounds evaluated in this work (especially the *ortho*-quinone tanshinones) were structurally very similar, with only small changes made to one particular part of the molecule. Next, evaluation of molecules which were more structurally diverse, yet still retained some similarity to tanshinones, was of interest.

## 5. Synthesis and evaluation of other tanshinone analogues and related compounds

### 5.1 Introduction

The results from the biological evaluation of the TI and iso-TI analogues indicated that there were some clear patterns, yet there appeared to be some ambiguity in structure-activity relationships between the various compounds and their effects on neutrophil behaviour during the inflammatory response *in vivo*. Although some of the compounds exhibited significant effects on neutrophil recruitment and/or resolution of neutrophilic inflammation, prediction of the precise chemical identity of these particular compounds prior to synthesis and evaluation would not have been possible. In light of these results, more broadly-related tanshinone analogues were explored, as well as other structurally related compounds. Compounds bearing some, but not all, of the structural features of tanshinones were of interest, as were compounds with a more interesting three-dimensional component, given the complete planarity of TI **1** and many of the related analogues studied.

Firstly, a general route for synthesising different broadly-related tanshinone analogues was explored. A Diels-Alder reaction strategy, followed by aromatisation, was previously used to synthesise various tanshinones and related compounds, including TIIA **2** and others such as TIIB **3**, nortanshinone **110**, and tanshindiol B **111** (Scheme 33).<sup>229,230</sup> By using different dienes, a range of analogues could be synthesised and evaluated. The particular compounds synthesised would be mainly dependent on the availability or ease of synthesis of the various dienes and the dienophile **59**, the efficiency of the Diels-Alder reaction, and the reaction selectivity, where relevant. Using the same dienophile **59** in each reaction would enable both the *ortho*-quinone moiety and the furan ring found in most tanshinones to be maintained in each synthesised compound. However, the particular Diels-Alder reaction using the dienophile **59** was previously reported to only work efficiently with reactive dienes. Less reactive dienes required more forceful conditions to generate moderate yields, although the use of ultrasound was found to improve both the yield and regioselectivity of the reaction.<sup>229,230</sup>



**Scheme 33.** Use of a Diels-Alder reaction to synthesise various tanshinone analogues.

Two interesting compounds encountered in the literature were  $\beta$ -lapachone **112** and nor- $\beta$ -lapachone **113** (Figure 23). These compounds satisfied both of the desired criteria mentioned previously, comprising three of the four rings common to most tanshinones, including the *ortho*-quinone moiety on the middle ring, an adjacent benzene ring in the same position as in all tanshinones, and an oxygen-containing five- or six- membered ring, with the oxygen atom in the same position as found in tanshinones. In particular, nor- $\beta$ -lapachone **113** contains a five-membered ring, the same ring size as the tanshinone furan ring. The dimethyl-substituted carbon atom adjacent to the oxygen atom in both compounds **112** and **113** would allow some exploration of three-dimensional space. Similarly, the different levels of saturation of the remaining one (nor- $\beta$ -lapachone **113**) or two ( $\beta$ -lapachone **112**)  $sp^3$  hybridised carbon atoms in this unsaturated ring, in comparison to the  $sp^2$  hybridised carbon atoms in the furan ring of tanshinones, were of interest. The absence of the fourth ring in these structures could also affect biological activity.

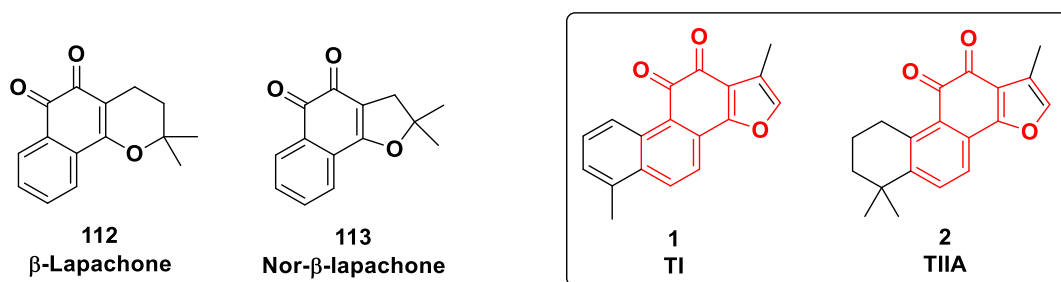


**Figure 24.** Structures of related compounds  $\beta$ -lapachone **112** and nor- $\beta$ -lapachone **113**, and their structural similarity, shown in red, with TI **1** and TIIA **2**.

$\beta$ -Lapachone **112** is a naturally-occurring *ortho*-quinone compound obtained from the bark of the lapacho tree, *Tabebuia avellanedae* in Brazil, a plant used as a traditional medicine for centuries for various treatments, including as an analgesic, as an anti-inflammatory agent, an antineoplastic agent, and as a diuretic.<sup>282,283</sup> In more recent work,  $\beta$ -lapachone **112** has been considered as a candidate drug for cancer treatment, demonstrating significant anti-cancer activity in various studies.<sup>284–288</sup> Other reported effects include anti-angiogenesis activity,<sup>289,290</sup> antimicrobial effects,<sup>291–293</sup> and wound healing properties.<sup>294</sup>

Some anti-inflammatory effects exhibited by  $\beta$ -lapachone **112** have also been reported.  $\beta$ -Lapachone **112** inhibited iNOS in the alveolar macrophages and aorta of rats,<sup>295</sup> whilst anti-inflammatory effects in LPS-stimulated microglia have been described.<sup>296</sup>  $\beta$ -Lapachone **112** is also a known substrate of NAD(P)H quinone oxidoreductase 1 (NQO1), found to modulate the metabolism of NAD and lead to an increase in cellular NAD(+).<sup>297</sup> Such inhibition led to anti-inflammatory effects in macrophages, *via* protein kinase activation.<sup>298</sup> Anti-inflammatory effects of  $\beta$ -lapachone **112** (as well as anti-arthritic activities) were also shown in rats.<sup>299</sup> In this study,  $\beta$ -lapachone **112** inhibited neutrophil migration and led to reduced concentrations of pro-inflammatory cytokines including TNF $\alpha$ , IL-6, and nitric oxide. A synthetic derivative of  $\beta$ -lapachone **112** also inhibited production of TNF $\alpha$  and nitric oxide in LPS-induced murine macrophages.<sup>300,301</sup> Furthermore, suppression of neuroinflammation by  $\beta$ -lapachone **112** was recently observed.<sup>302</sup>

In contrast to  $\beta$ -lapachone **112**, reports of previous studies involving nor- $\beta$ -lapachone **113** are scarce. Although nor- $\beta$ -lapachone **113** (and its derivatives) is considered an anti-cancer drug candidate,<sup>303,304</sup> there are no studies involving nor- $\beta$ -lapachone **113** in relation to inflammation, neutrophils, or zebrafish in the literature. This may be because  $\beta$ -lapachone **112** is a naturally occurring compound, whereas nor- $\beta$ -lapachone **113** is not.

In recent studies, both TIIA **2** and  $\beta$ -lapachone **112** were shown to act as NQO1 inhibitors.<sup>145,305</sup> The structural and pharmacological similarities of these two molecules meant that they both exhibited a synergistic anti-cancer effect when used in conjunction with the drug paclitaxel.<sup>305</sup> Although a formal connection between the lapachones and tanshinones has not been greatly established elsewhere, this recent finding may suggest that these two classes of compounds could exhibit common biological activities *in vivo*. The fact that both of these molecules have been shown to act as inhibitors of NQO1 could mean that this is considered a possible molecular target with regards to any anti-inflammatory activities of these molecules (although such investigation is outside of the scope of this work).

Both  $\beta$ -lapachone **112** and nor- $\beta$ -lapachone **113** were previously synthesised from the commercially available natural product lapachol **114**, and its one carbon homologue norlapachol **115**, respectively (Figure 24).<sup>306,307</sup>  $\beta$ -Lapachone **112** was obtained from lapachol **114** in a single step, whilst nor- $\beta$ -lapachone **113** was synthesised from lapachol **114** in two steps, *via* the intermediate nor-lapachol **115**.<sup>306,307</sup>

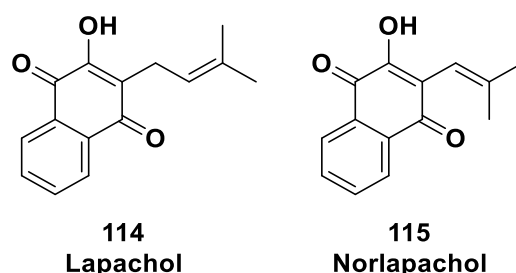


**Figure 25.** Structures of related compounds lapachol **114** and norlapachol **115**.

Lapachol **114** is a *para*-quinone compound and, like  $\beta$ -lapachone **112**, is naturally present in the lapacho tree, *Tabebuia avellaneda*.<sup>283</sup> Another similarity with  $\beta$ -lapachone

**112** is that lapachol **114** is also an inhibitor of NQO1, with an IC<sub>50</sub> value of 150 nM.<sup>308</sup> In the same study, lapachol **114** caused melanin defects in zebrafish embryos, as well as a range of other abnormalities.<sup>308</sup> Lapachol **114** has also been shown to exhibit cytotoxicity against a range of different cancer cells,<sup>309,310</sup> amongst other biological effects including anti-metastatic and antimicrobial activities.<sup>283,291,311–313</sup> Furthermore, lapachol **114** previously exhibited anti-inflammatory activity, including in a rat model of inflammation.<sup>314</sup> However, lapachol **114** has also presented significant toxicity issues, including in rat models.<sup>315–317</sup>

Analogously to  $\beta$ -lapachone **112** and nor- $\beta$ -lapachone **113**, whereas lapachol **114** has previously been investigated in numerous studies, few such investigations have been carried out on the closely related norlapachol **115**. In particular, no studies on norlapachol **115** could be found in relation to inflammation, neutrophils, or zebrafish. This may again be because lapachol **114** is a known natural product, whereas norlapachol **115** is not, instead requiring synthesis from lapachol **114**.

Overall, the relative similarities of these compounds, especially the lapachones **112** and **113**, to tanshinones, their known biological activities, and their ease of synthesis, merited investigation of these compounds in this work. This would enable wider exploration of the structure-activity relationships of tanshinones and related compounds in the zebrafish model of inflammation, compared to the more closely related compounds explored in the previous chapter.

## 5.2 Hypothesis and aims

It was hypothesised that other tanshinones, as well as compounds with some degree of structural similarity to tanshinones, such as  $\beta$ -lapachone **112** and nor- $\beta$ -lapachone **113**, would exhibit anti-inflammatory activity *in vivo*, according to structure-activity relationships. Such activity would allow for a greater understanding of the biologically active part(s) of tanshinones including TI **1** and TIIA **2**.

The first aim of this work was to synthesise various tanshinone analogues using a previously reported Diels-Alder reaction strategy. This would require use of different

dienes, which could either be synthesised or bought as required, as well as synthesis of a significant quantity of the required dienophile. Any synthesised tanshinones could be evaluated *in vivo*, utilising the zebrafish model of inflammation used previously.

The second aim of this work was to synthesise compounds more broadly related to tanshinones, namely  $\beta$ -lapachone **112** and nor- $\beta$ -lapachone **113**, using literature precedents. These compounds, alongside any intermediates, would also be tested for any anti-inflammatory activity using the zebrafish inflammation model, and the results used to explore any further structure-activity relationships more widely.

## 5.3 Towards the synthesis of TIIA and analogues

### 5.3.1 General strategy

Using the route previously documented in the literature,<sup>229,230</sup> formal disconnection of the TIIA general structure led back to the dienophile **59** and various dienes, the exact structures of which could be modified to give various tanshinone analogues (Figure 25). The dienophile **59** could be produced by selective oxidation of 3-methyl-5-benzofuranol **58** using Fremy's salt, as previously described,<sup>228,230</sup> and this phenol **58** could be synthesised in three steps from simple and cheap starting materials. This route was previously used for the synthesis of a range of TIIA derivatives,<sup>150</sup> as well as for the synthesis of other tanshinones and related compounds.<sup>318,319</sup>

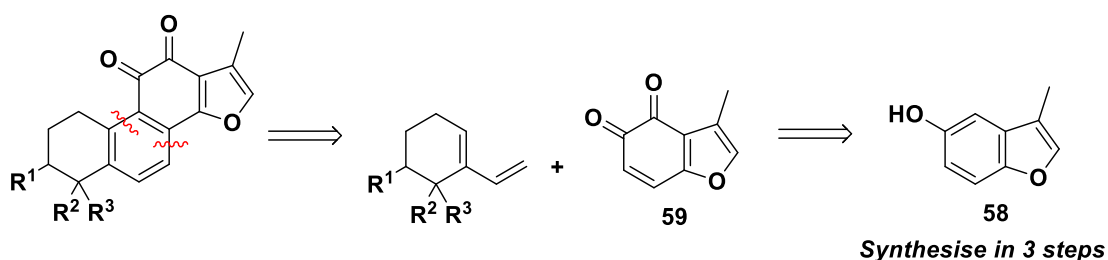
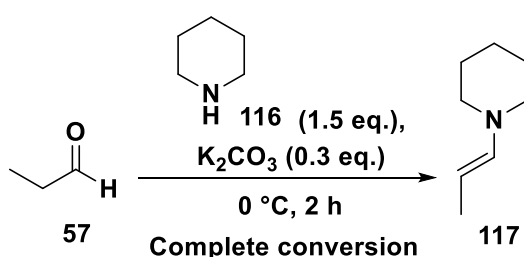


**Figure 26.** Disconnection of the general TIIA structure to the phenol **58** and various dienes.

### 5.3.2 Dienophile synthesis

The route to synthesising 3-methyl-5-benzofuranol **58** employing enamine formation, subsequent reaction with *para*-benzoquinone **32**, and acid-mediated elimination was attempted.<sup>228,230</sup> Enamine formation from propanal **57** and excess piperidine **116** (Scheme 34) initially seemed to be unsuccessful, based on analysis of the <sup>1</sup>H NMR spectrum, even with slower addition of the aldehyde **57** to piperidine **116**. However, analysis of the starting materials by <sup>1</sup>H NMR spectroscopy indicated that propanal **57** used directly from the bottle was impure. When freshly distilled propanal **57** was used immediately in the reaction, formation of the enamine **117** occurred successfully, and complete conversion of the aldehyde was observed when excess amine **116** (1.5 equivalents) was used, confirmed by <sup>1</sup>H NMR spectroscopy. The data were consistent with only the sterically expected (*E*)-isomer formation,<sup>320,321</sup> based on the coupling values of the alkene protons ( $J = 13.9$  Hz, indicating a *trans*- relationship between the two protons) as well as the absence of any additional peaks corresponding to the (*Z*)-isomer.

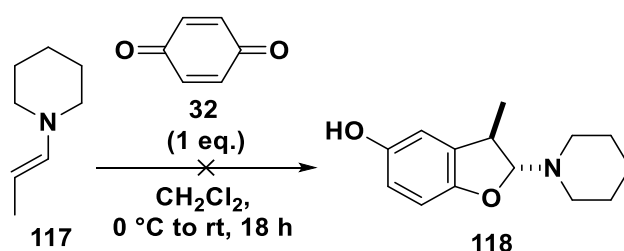


**Scheme 34.** Enamine formation from propanal **57** and piperidine **116**.

Due to the expected volatility of the enamine product **117** (relative to the residual piperidine **116**), as well as its sensitivity towards acid, purification of the enamine **117** was not trivial. Distillation under reduced pressure has previously been used for this,<sup>150,230,319</sup> and this led to an improved purity of product, although still not pure. In an attempt to circumvent this issue, the quantity of piperidine **116** used in enamine formation was varied. Both stoichiometric (1 equivalent) and sub-stoichiometric (0.8 equivalents) quantities of piperidine **116** were used, to ensure complete reaction of the piperidine **116**. However, although the enamine **117** was formed, both aldehyde **57** and

piperidine **116** remained, even with varied reaction times. Use of anhydrous ether as solvent resulted in the same outcome. Thus, following re-synthesis on a multi-gram scale using the initial reaction conditions, the crude enamine **117** was taken forward, with excess piperidine **116** as the main contaminant.

The crude enamine **117** was reacted with *para*-benzoquinone **32**, in an effort to form the piperidine-substituted benzofuranol **118** (Scheme 35). Initial formation of a wine-red solution in this reaction was observed, as reported previously.<sup>230,319</sup> The literature also reported isolation of a white solid product, simply upon removal of solvent *in vacuo*, possibly following gradual decolouration of the reaction solution over time. However, this decolouration was not observed here, and the resulting concentrated residue resembled a deep red/amber-coloured gum. The reaction was repeated both with a slower rate of addition of the crude enamine **117** and a longer reaction time, yet still gave the same result, and so too did swapping the order of addition of reagents. Analysis by <sup>1</sup>H NMR spectroscopy indicated formation of a complex mixture of products, with no desired product **118** formed.

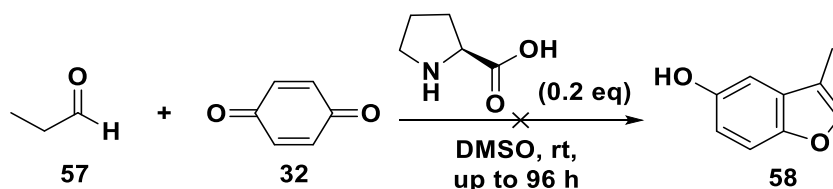


**Scheme 35.** Attempted reaction of the enamine **117** with *para*-benzoquinone **32**.

Addition of a Lewis acid to this reaction was also investigated, to promote formation of the desired product **118**. Simultaneous reactions were performed, using no additive, 0.1, and 1.0 equivalents of aluminium trichloride, respectively. However, in each instance, no significant quantities of desired product **118** were observed in the <sup>1</sup>H NMR spectra of the crude products. In addition, attempts to further purify all reagents and substrates prior to use in this reaction still did not deliver the desired product **118**.

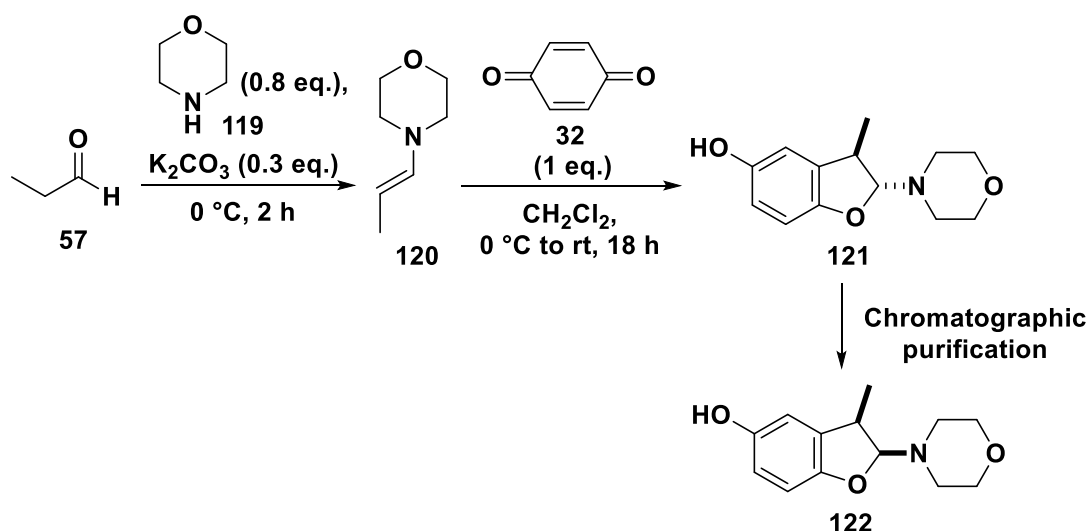
An alternative reaction was investigated, utilising distilled propanal **57** directly with *para*-benzoquinone **32** in the presence of L-proline (Scheme 36). L-Proline has previously

been found to act as an effective catalyst in a variety of (asymmetric) reactions, including the Hajos–Parrish–Eder–Sauer–Wiechert reaction, aldol reactions, Michael reactions, and Mannich reactions.<sup>322–324</sup> However, synthesis of the required benzofuranol product **58** was unsuccessful, and only propanal **57**, *para*-benzoquinone **32**, and 1,4-hydroquinone were present, even after the mixture was left to stir for several days. This particular reaction was therefore abandoned without further exploration.



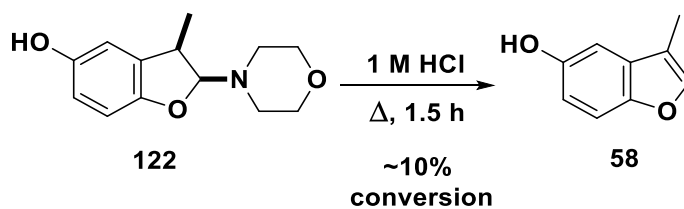
**Scheme 36.** Attempted benzofuranol **58** formation from propanal **57** and *para*-benzoquinone **32** in the presence of L-proline.

In light of these unsuccessful reactions using the piperidine-derived enamine **117**, use of morpholine **119** instead of piperidine **116** was investigated, following precedence for such reactions.<sup>228,230</sup> Enamine formation from propanal **57** and morpholine **119** proceeded successfully (Scheme 37), albeit again with residual starting materials remaining. The crude enamine **120**, again consistent with being the *E*-isomer,<sup>230,325,326</sup> was then reacted with *para*-benzoquinone **32** (Scheme 37). This produced a deep red/amber-coloured gum, as for the piperidine variant, yet analysis by <sup>1</sup>H NMR spectroscopy appeared to indicate successful formation of the desired product as the *trans*-isomer **121**, based on comparison with literature data.<sup>230,325</sup> Attempted purification by column chromatography successfully removed major impurities, but appeared to result in isolation of the epimeric *cis*-isomer **122**, as determined by the shifting of various peaks in the <sup>1</sup>H NMR spectrum of the product. Nonetheless, the isolated material was taken forward to the next step.



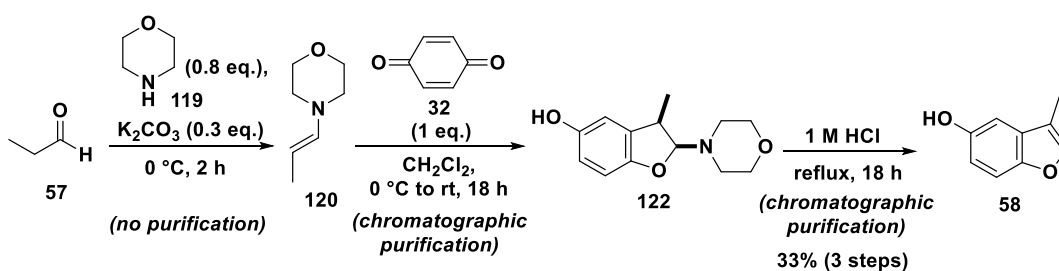
**Scheme 37.** Enamine **120** formation using morpholine **119** followed by reaction with *para*-benzoquinone **32** and chromatographic purification.

The next step comprised gentle heating with aqueous acid, to eliminate morpholine **119** and form the desired 3-methyl-5-benzofuranol product **58** (Scheme 38), as previously achieved.<sup>230,327</sup> Following work-up, analysis by both  $^1\text{H}$  NMR spectroscopy and thin layer chromatography (TLC) indicated that a mixture of products was present, and the desired product **58** appeared to be one of these. Purification by column chromatography led to the successful isolation of the desired benzofuranol **58**, albeit in small quantities. Starting material **122** was also isolated, and analysis of the respective product masses suggested that the reaction had occurred with around 10% conversion. However, this indicated that the previous reaction with *para*-benzoquinone **32** was successful. This also suggested that the morpholine-containing phenol starting material **122** was much more stable to both acid and chromatographic purification on silica than originally thought. Also, a longer reaction time and/or higher reaction temperature could be required for the complete reaction of this starting material **122** with acid. Thus, heating at reflux with aqueous 1 M hydrochloric acid for 4.5 hours provided greater conversion to the benzofuranol product **58**, although still not complete.



**Scheme 38.** Acid-mediated elimination to give 3-methyl-5-benzofuranol **58**.

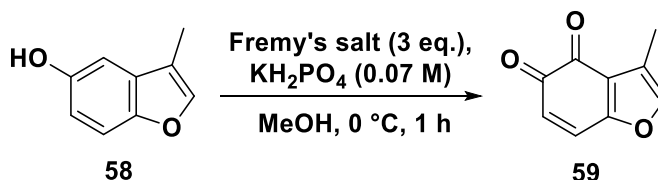
As the morpholine-containing phenol **122** appeared to be completely stable to silica, the compound was resynthesised in two steps from propanal **57** (Scheme 39). The crude product from the reaction of the enamine **120** with *para*-benzoquinone **32** was again subjected to chromatographic purification, and provided the desired phenol **122**. The purified product **122** was then heated at reflux overnight with aqueous acid (Scheme 39), and following chromatographic purification, yielded 3-methyl-5-benzofuranol **58** in a 33% yield across the three steps. Although this was a significantly lower yield than those obtained in the literature, this may be due to the lack of complete purification of the enamine **120**, with residual morpholine **119** contaminating the following reaction and lowering the yield. However, a sufficient quantity of 3-methyl-5-benzofuranol **58** was produced using these conditions, and in light of time considerations, this synthesis was not optimised any further. Overall, use of the morpholine-derived enamine **120** was much more successful than use of the piperidine-derived enamine **117**, as supported both by reaction success, and results of attempted chromatographic purifications for both variants.



**Scheme 39.** Synthesis of 3-methyl-5-benzofuranol **58** in three steps from propanal **57**.

The next step in this synthesis required the selective oxidation of 3-methyl-5-benzofuranol **58** to the *ortho*-quinone dienophile **59**. This transformation was previously

carried out using potassium nitrosodisulfonate,  $[(\text{KO}_3\text{S})_2\text{NO}]$ , commonly known as Fremy's salt.<sup>328,329</sup> Following the literature procedure,<sup>228,230</sup> oxidation of 3-methyl-5-benzofuranol **58** was first attempted on a small (100 mg) scale using three equivalents of commercial Fremy's salt (Scheme 40).



**Scheme 40.** Selective oxidation of 3-methyl-5-benzofuranol **58** using Fremy's salt to form the *ortho*-quinone **59**.

Upon addition of the Fremy's salt solution to the phenol **58**, a relatively quick change in colour from beige to deep red was observed. This suggested that the reaction had worked, as the product was known to be a dark red solid,<sup>228,230</sup> and reactions using Fremy's salt are reported to occur rapidly.<sup>328,329</sup> Following work-up, analysis of the crude product by  $^1\text{H}$  NMR spectroscopy indicated the presence of a mixture of both the desired *ortho*-quinone product **59**, and the phenol starting material **58**. This lack of complete conversion was somewhat consistent with previous reports in which instability of the *ortho*-quinone **59**, particularly in halogenated solutions, was observed.<sup>228,230</sup> Attempts to use non-halogenated solutions for spectroscopic analysis were similarly unyielding, as were longer reaction times. Characterisation of the solid product by infrared (IR) spectroscopy also indicated a mixture of the *ortho*-quinone **59** and the phenol **58**, and melting point determination further supported a product mixture. This was possibly due to the use of dichloromethane (DCM) in the work-up procedure, where decomposition of the *ortho*-quinone **59** may have already started to occur. Therefore, the crude *ortho*-quinone product **59** was taken on to the Diels-Alder reaction, without any further efforts at either characterisation or purification.

### 5.3.3 Attempted synthesis of dienes

With the synthesis of the required dienophile **59** in hand, albeit not optimal, attention then turned to synthesis of appropriate dienes. Initially, two particular dienes were considered (Figure 26). Use of the dimethyl diene **53** in the Diels-Alder reaction would lead to synthetic TIIA **2**, which could be a useful control compound to synthesise. A second, simplified diene **123** was also considered, for two reasons. Firstly, this would produce a TIIA analogue **124** without the two methyl groups, allowing for exploration of the importance of these substituents for biological activity. Secondly, synthesis of this diene **123** appeared to be easier than that of the dimethyl diene **53**, and so was explored first, to determine the feasibility of this chemistry. Should the chemistry be successful, the dienes could then be varied (within the limits of reaction tolerances and starting material availabilities) to provide various tanshinone analogues.

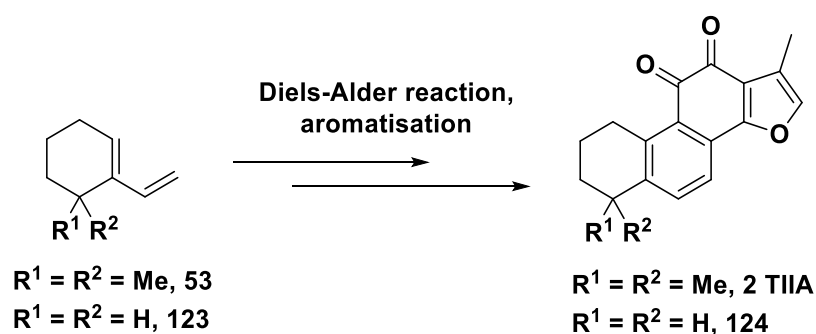
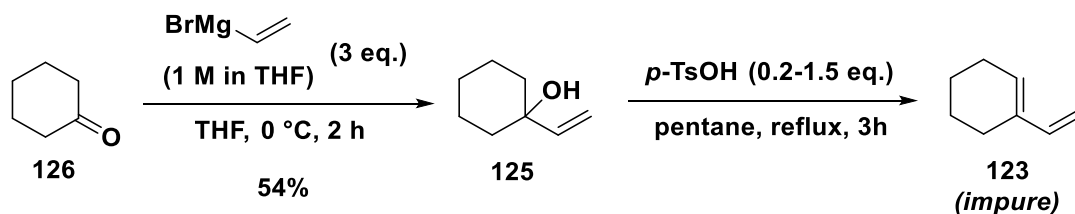


**Figure 27.** The dimethyl diene **53** and the simplified diene **123** would give TIIA **2** and a tanshinone analogue **124**, respectively.

The simplified diene **123** could be formed from dehydration of the tertiary alcohol **125**, which could be synthesised from a Grignard reaction between cyclohexanone **126** and vinylmagnesium bromide (Scheme 41). The Grignard reaction between cyclohexanone **126** and commercial vinylmagnesium bromide was carried out successfully to produce the tertiary alcohol **125**. Analysis of the <sup>1</sup>H NMR spectrum indicated that the product **125** was present yet slightly impure,<sup>330,331</sup> with small amounts of residual cyclohexanone starting material **126** still present, as well as other low-level impurities. Purification by column chromatography successfully yielded a much cleaner alcohol product **125** in 54% yield. This was considered respectable, as the product

alcohol **125** appeared to be somewhat volatile, meaning that mass returns were likely diminished with each attempted work-up and purification step. The purified product **125** was then taken on to the dehydration step.



**Scheme 41.** The diene **123** could be synthesised from cyclohexanone **126** in two steps, comprising a Grignard reaction followed by dehydration.

Dehydration of the tertiary alcohol **125** to give the desired diene **123** was first attempted by heating the alcohol **125** to reflux with aqueous hydrochloric acid (1 M) for several hours. However, this did not yield any of the desired diene **123**, and analysis of the  $^1\text{H}$  NMR spectrum indicated a mixture of compounds. Therefore, a different method of dehydration was attempted, where the alcohol **125** was heated to reflux in pentane with a catalytic amount of *para*-toluenesulfonic acid, for a shorter time of two hours (Scheme 41). Analysis of the product by  $^1\text{H}$  NMR spectroscopy indicated that the diene **123** was present,<sup>331,332</sup> but as part of a mixture with other unidentified components, and so purification by column chromatography was attempted. However, when fractions containing the least polar product were concentrated under reduced pressure, no desired compound **123** was isolated. Analysis of other eluted products indicated that these also did not correspond to the desired diene **123**. This may have resulted from decomposition of the product **123** on silica, but was probably due to the volatility of the diene **123**, which may have been lost during rotary evaporation. The reaction was therefore repeated, using an increased quantity of *para*-toluenesulfonic acid (1.5 equivalents), and again purified by column chromatography. This time, pentane was used as the eluent, and the first product-containing fractions were concentrated more carefully, to minimise loss of volatile product. This resulted in isolation of a very small quantity (11 mg) of the desired diene **123**, which was significantly cleaner than previously, but still not pure.

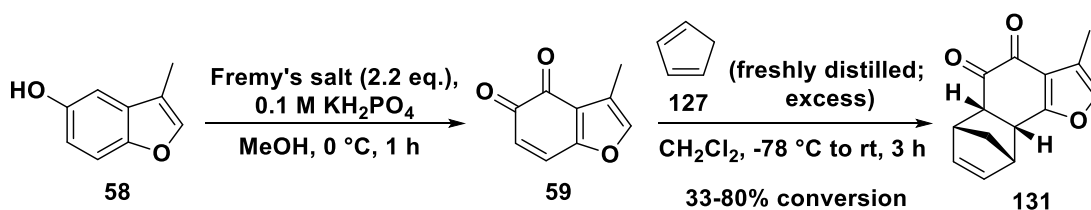
Therefore, a different method of purification was considered. The reaction was repeated using the same conditions, and purification by distillation was attempted. However, this was not successful in isolating the desired diene **123**. The reaction scale was possibly not large enough to enable effective purification by conventional distillation, and other techniques such as Kugelrohr distillation may have been more effective. However, due to time constraints associated with this work, this synthesis was not explored any further; this would be an obvious area to explore in any future studies. Instead, commercially available dienes were explored in the Diels Alder reaction with the *ortho*-quinone dienophile **59**. Any products isolated from these reactions would still exhibit significant structural similarities with tanshinones, and would therefore be worthy of biological evaluation. Given the previous results obtained from small changes made to the TI **1** structure (Chapter 4), evaluation of tanshinone analogues with more broader changes, yet still maintaining key structural features of tanshinones, was considered worthwhile.

#### 5.3.4 Diels-Alder reactions using commercially available dienes

Previous studies found that this Diels-Alder reaction worked well with reactive dienes, but was not so effective with less reactive dienes.<sup>228,230</sup> Therefore, cyclopentadiene **127** was chosen as a highly reactive diene to explore this reaction with, as this had previously been used successfully in this reaction.<sup>228,230</sup> Cyclohexadiene **128** and isoprene **129** were also considered due to some previous literature precedence,<sup>229,230</sup> leading to formation of two tanshinone analogues (or more, depending on Diels-Alder reaction selectivity) possessing common structural similarity to both TI **1** and TIIA **2**. Danishefsky's diene **130** was also used.

Selective oxidation of the benzofuranol **58** to the *ortho*-quinone dienophile **59** was performed using Fremy's salt (Scheme 42), using the same procedure as earlier in this work (Chapter 5.3.2). Again, reaction success was crudely determined by the observed colour changes which were in agreement with the literature.<sup>230</sup> The crude *ortho*-quinone dienophile **59** was reacted with an excess of freshly cracked and distilled cyclopentadiene **127**, using low temperature conditions as employed in the literature.<sup>230</sup>

Initially, this reaction was unsuccessful, as determined by  $^1\text{H}$  NMR spectroscopy. However, this was because the *ortho*-quinone starting material **59** had completely decomposed prior to use, as there was a significant amount of time between generation of the first batch of crude *ortho*-quinone **59**, which was used here, and the Diels-Alder reaction being carried out. Therefore, for all further reactions, the oxidation was carried immediately before the Diels-Alder reaction utilising the freshly synthesised *ortho*-quinone dienophile **59**. When the Diels-Alder step was repeated using freshly generated unpurified dienophile **59**, the reaction was successful. The reaction changed colour as it proceeded, from dark red to a pale yellow, consistent with literature observations and the reported yellow solid expected for the product **131**.<sup>230</sup> Analysis of the crude product by  $^1\text{H}$  NMR spectroscopy indicated successful formation of the desired product **131** as the single *endo* isomer, consistent with that reported in the literature.<sup>230</sup> Additionally, a substantial amount of 3-methyl-5-benzofuranol **58** was present, in an approximate 67:33 ratio of phenol **58**:Diels-Alder product **131**. This likely resulted from decomposition of the *ortho*-quinone dienophile **59** before it had chance to react with cyclopentadiene **127**.

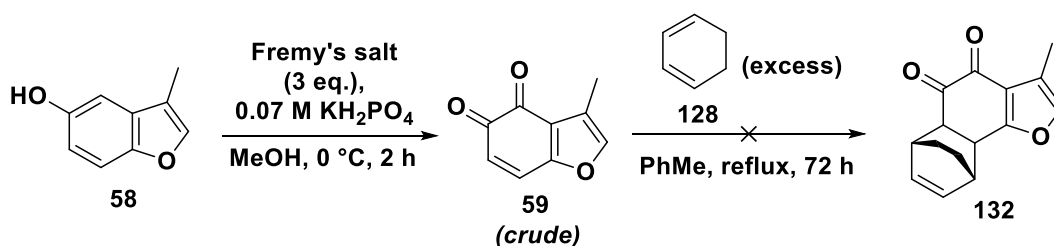


**Scheme 42.** Formation of the *ortho*-quinone dienophile **59** and subsequent Diels-Alder reaction with cyclopentadiene **127**.

Purification to remove the remaining phenol **58** was first attempted by treating the crude product with aqueous sodium hydroxide, which resulted in formation of a purple solid after work-up. The  $^1\text{H}$  NMR spectrum indicated that the desired product **131** was still present, and that the phenol was successfully removed. However, some additional peaks were present in the aromatic region of the spectrum, as well as two broad singlets further upfield. Due to a low mass return at this stage, the reaction was repeated using the same conditions, and again the desired product **131** and residual phenol **58** were

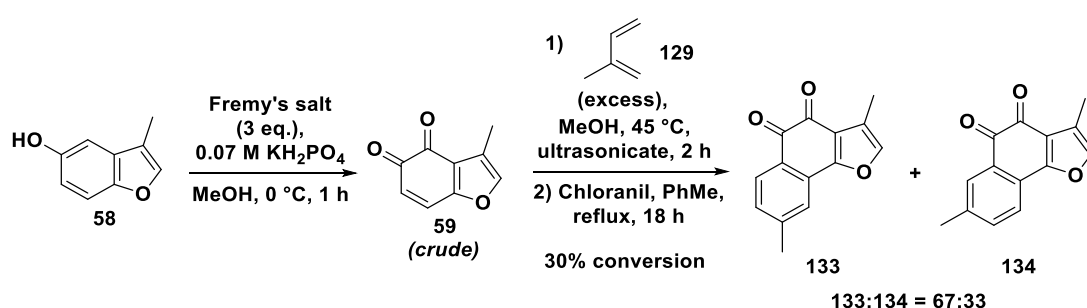
formed, although this time in a much improved ratio of 80:20 in favour of the Diels-Alder product **131**. Purification of the crude product was attempted by column chromatography. Formation of a purple solid was again observed, yet the  $^1\text{H}$  NMR spectrum of this product matched the data reported in the literature (with small levels of impurities present), even though the appearance clearly did not. Attempted purification by recrystallisation was also unsuccessful. However, this particular bicyclic product **131** was not a high priority target compound for biological evaluation, and so due to the different compound appearances as well as low mass returns, purification of this compound was not explored any further. Nonetheless, formation of this product indicated that the *ortho*-quinone dienophile **59** was successfully produced from oxidation of the phenol **58**, and that this dienophile **59** had undergone a Diels-Alder reaction with cyclopentadiene **127**. Therefore, Diels-Alder reactions using other dienes were explored.

Firstly, freshly generated *ortho*-quinone dienophile **59** was reacted with cyclohexadiene **128** (Scheme 43). Instead of employing low temperature conditions as were used with cyclopentadiene **127**, the reaction was heated at reflux for a longer period of time, due to the lower reactivity of cyclohexadiene **128** compared to cyclopentadiene **127**. However, there was no evidence of desired Diels-Alder reaction product **132** formation, based on analysis of the  $^1\text{H}$  NMR spectrum of the crude product. In the interests of time, and again as this bicyclic compound **132** was not a high priority for biological evaluation, this particular substrate was therefore abandoned.



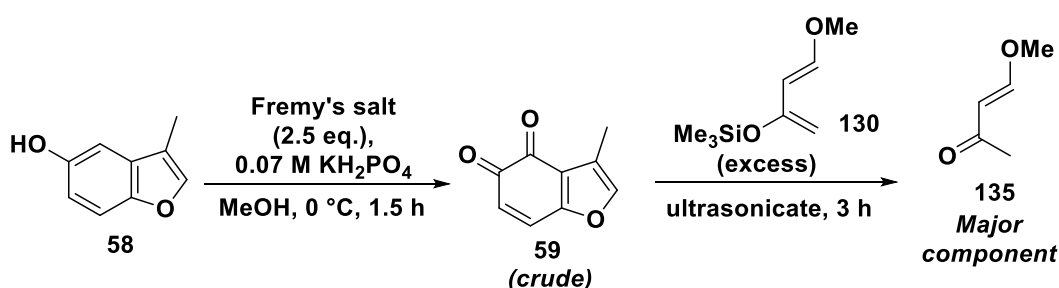
**Scheme 43.** Formation of the *ortho*-quinone dienophile **59** and attempted Diels-Alder reaction with cyclohexadiene **128**.

Next, the Diels-Alder reaction using isoprene **129** as the diene was explored (Scheme 44). Although isoprene **129** is a considerably less reactive diene than cyclopentadiene **127**, this particular transformation has been successfully carried out previously, using ultrasonication to promote the cycloaddition.<sup>229,230</sup> Therefore, this Diels-Alder reaction was carried out in an ultrasound bath, and was then heated to reflux overnight with chloranil, to achieve full aromatisation of the initial Diels-Alder reaction products. After crude purification through a silica plug, analysis by <sup>1</sup>H NMR spectroscopy indicated that the Diels-Alder reaction and subsequent aromatisation had been successful, forming the two product isomers **133** and **134** in a 67:33 ratio. The reaction was relatively low yielding, although a low yield was also reported in the literature,<sup>229,230</sup> and was not surprising given the poor reactivity of isoprene **129**. In addition, as observed with the reaction involving cyclopentadiene **127**, a significant quantity of the phenol starting material **58** was returned, corresponding to an approximate 70:30 ratio of phenol **58** to the combined product isomers **133** and **134**. Analysis of the crude product mixture by TLC indicated that although the phenol **58** could be easily removed from the mixture, separation of the two product isomers **133** and **134** was very difficult, an observation which was consistent with the purification difficulties observed in the literature.<sup>230</sup> Whereas Diels-Alder reactions of this type (with different dienes) have previously been achieved with high regioselectivity, in favour of the isomer more closely resembling natural tanshinones where relevant,<sup>229,230</sup> such regioselectivity was not achieved here with isoprene **129**. As the quantities of products involved were very small, and the separation appeared to be quite challenging, efforts to isolate pure products were not taken any further.



**Scheme 44.** Use of an ultrasound-promoted Diels-Alder reaction to synthesise a mixture of tanshinone analogues **133** and **134**.

Finally, the Diels-Alder reaction was attempted using Danishefsky's diene **130**, a diene known to possess high reactivity (Scheme 45). Ultrasonication was again used to promote both reactivity and regioselectivity. In this reaction, a colour change was observed, as the reaction mixture turned from dark red to pale yellow, in a similar manner to the successful reaction using cyclopentadiene **127** as the diene. However, analysis of the crude product mixture by  $^1\text{H}$  NMR spectroscopy indicated the presence of a single predominant compound which vastly 'swamped' the quantities of all other compounds present. This was deduced to be the unsaturated ketone **135** (Scheme 45), formed by loss of the trimethylsilyl group from the excess Danishefsky's diene **130**, followed by enol-keto tautomerisation. This ketone **135** was not volatile and so could not be removed from the reaction mixture easily, making spectroscopic determination of the quantities of other products present in the mixture difficult. In addition, analysis by TLC revealed approximately seven different spots. These likely consisted of the two Diels-Alder reaction products, the phenol starting material **58**, the ketone **135**, and possibly residual Danishefsky's diene **130**, alongside impurities which originated from the bottle of diene **130** initially obtained, as determined by  $^1\text{H}$  NMR spectroscopy, which was purchased as 94% purity. This analysis suggested that purification to provide the pure desired Diels-Alder reaction products would not be trivial, especially given the quantities involved. Quantities of reagents and crude product mixtures were generally small (less than 100 mg), mainly because these reactions all required 2.5-3 equivalents of Fremy's salt for the formation of the *ortho*-quinone dienophile **59**. This reagent was not particularly cheap, meaning that this oxidant was the limiting reagent for reaction scale.



**Scheme 45.** Formation of the *ortho*-quinone dienophile **59** and subsequent Diels-Alder reaction with Danishefsky's diene **130**.

Due to the various difficulties encountered with these Diels-Alder reactions and purification of the resultant product mixtures, alongside time constraints, this approach to synthesis of tanshinone analogues was not taken any further, although this work did leave significant scope for future work. Instead, synthesis of the lapachone compounds was explored (Chapter 5.4), since these compounds were previously synthesised easily in multiple studies in just 1-2 steps from a cheap, commercially starting material. This would allow investigation of more broadly related tanshinone analogues, whilst still retaining many of the key structural elements of tanshinones.

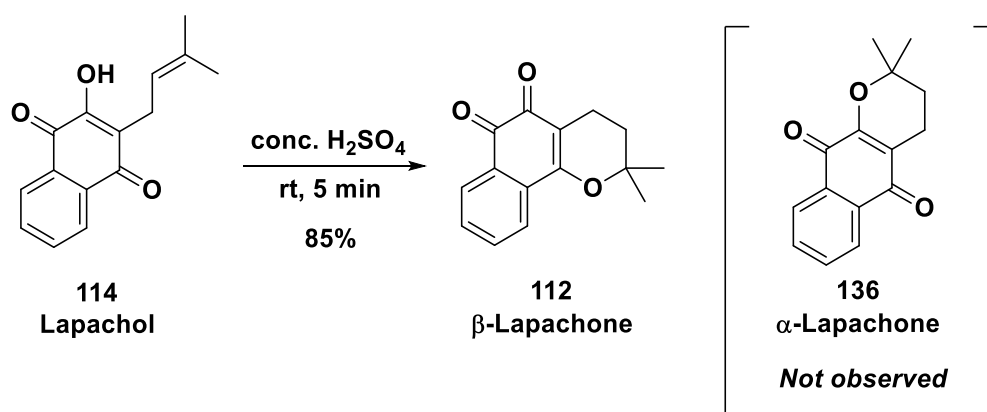
### 5.3.5 Summary

This work showed that 3-methyl-5-benzofuranol **58** could be synthesised in three steps from simple starting materials, and converted into the *ortho*-quinone **59** using Fremy's salt. This *ortho*-quinone **59** could act as a dienophile and successfully participated in Diels-Alder reactions with reactive dienes such as cyclopentadiene **127** (low temperature conditions) and Danishefsky's diene **130** (ultrasonication conditions). Ultrasonication conditions were also employed for the Diels-Alder reaction using the less reactive isoprene **129**, although this reaction gave little regioselectivity. Reaction with cyclopentadiene **127** gave a single Diels-Alder product **131**, although attempts to purify this compound were not completely successful. Purification issues were also encountered for the remaining Diels-Alder reaction product mixtures, and would require further efforts to enable isolation of tanshinone analogues suitable for biological evaluation. Synthesis of non-commercially available dienes was attempted, and appeared to be a feasible strategy using a Grignard/dehydration strategy. However, the reaction conditions may require optimisation to maximise product yields, and the purification steps for this route merit further investigation before use of this route to synthesise various related dienes. Optimisation of *ortho*-quinone dienophile **59** formation from 3-methyl-5-benzofuranol **58**, as well as of the conditions needed to ensure most efficient Diels-Alder reaction, could also be explored to address difficulties associated with cost and product purification encountered in this route.

## 5.4 Lapachone and lapachol compounds

### 5.4.1 Chemical synthesis

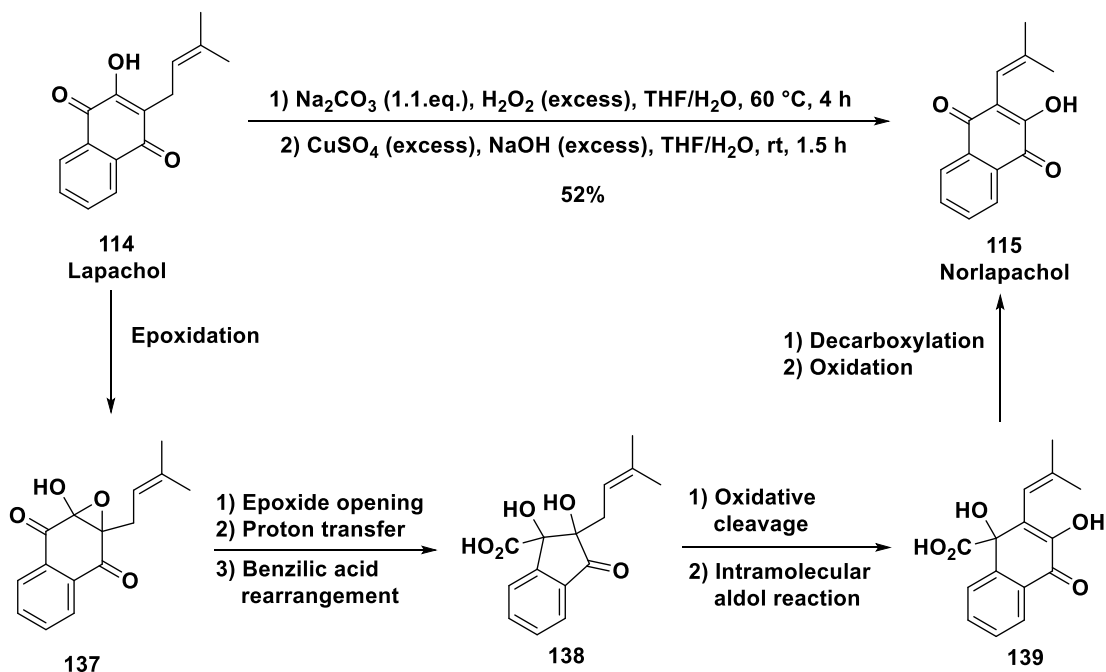
Synthesis of  $\beta$ -lapachone **112** was carried out as described in the literature (Scheme 46).<sup>306,307</sup> Acid-mediated cyclisation of the commercially available lapachol **114** selectively formed the desired  $\beta$ -lapachone **112** in a good yield of 85% after chromatographic purification, and the isomer  $\alpha$ -lapachone **136** was not observed. Mechanistically, exclusive formation of  $\beta$ -lapachone **112** under these conditions likely occurred *via* an intermediate epoxide, as proposed in the literature for similar reaction conditions.<sup>333</sup> Previous studies have shown that the proportion of each isomer obtained can be varied depending on the conditions used, including the use of various Lewis acids, the reaction time, and the temperature at which the reaction is carried out.<sup>333–335</sup>



**Scheme 46.** Synthesis of  $\beta$ -lapachone **112** from lapachol **114**.

Norlapachol **115** was synthesised from lapachol **114** in an unoptimized yet moderate yield of 52% after recrystallisation by a Hooker oxidation (Scheme 47), the mechanism of which has still not been conclusively elucidated. It has been suggested that the first step involves epoxidation of the quinone alkene under basic conditions to form an intermediate epoxy-alcohol **137** (Scheme 47).<sup>336</sup> Subsequent epoxide opening and benzylic acid rearrangement steps have been proposed, to give the well-established Hooker intermediate **138**.<sup>336</sup> This vicinal diol **138** is then believed to undergo oxidative cleavage, followed by intramolecular aldol reaction to give the  $\alpha$ -hydroxy acid

intermediate **139**. Finally, decarboxylation followed by oxidation results in the production of norlapachol **115**.<sup>336–338</sup>



**Scheme 47.** Synthesis and proposed mechanism for the formation of norlapachol **115** from lapachol **114** by a Hooker oxidation.

Finally, nor- $\beta$ -lapachone **113** was synthesised from its corresponding precursor norlapachol **115**, in an analogous manner to the synthesis of  $\beta$ -lapachone **112** (Scheme 48). Sulfuric acid-promoted cyclisation again provided the desired product **113** as a single isomer in a near-quantitative yield of 95%, after simple purification by trituration with cold hexane. No formation of the nor- $\alpha$ -lapachone **140** isomer was observed, likely for the same reasons as for the selective formation of  $\beta$ -lapachone **112** discussed previously.



based on findings from the previous work (Chapter 4), to provide a synthetic control compound to compare the effects of the synthetic norlapachol **115** to.

Norlapachol **115** significantly reduced the number of neutrophils recruited to the site of injury (in comparison to the vehicle control-treated larvae), at concentrations of both 10  $\mu\text{M}$  and 0.1  $\mu\text{M}$ . Given the structural differences between norlapachol **115** and tanshinones, norlapachol **115** may have worked in a different way to tanshinones such as TI **1**, for example by acting on a different protein target. Recruitment was not significantly reduced at a concentration of 1  $\mu\text{M}$ , although there was a trend towards slightly lower neutrophil numbers. The difference between the effects observed at 1 and 0.1  $\mu\text{M}$  concentrations was slightly surprising, but may reflect the natural variability in this type of *in vivo* experiment, despite all efforts to control for this as far as reasonably practicable.

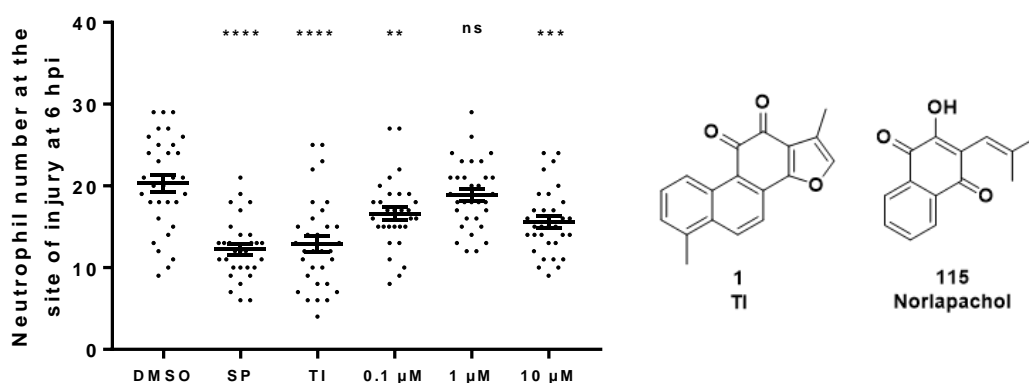


**Figure 28. Norlapachol 115 significantly reduced neutrophil recruitment to a site of injury at 0.1 and 10  $\mu\text{M}$  concentrations, but not at a 1  $\mu\text{M}$  concentration.**

DMSO used at 0.5% concentration, SP **74** used at a concentration of 30  $\mu\text{M}$ , TI **1** used at a concentration of 25  $\mu\text{M}$ . Data shown as mean  $\pm$  SEM;  $n = 30$ -32 larvae from 4 independent experiments. \*\*  $P < 0.01$ , \*\*\*  $P < 0.001$ , \*\*\*\*  $P < 0.0001$ , ns not significant, in comparison to the DMSO control (one-way ANOVA with Dunnett's multiple comparison post-test).

Next, the remaining three compounds were evaluated in the same way but at a concentration of 1  $\mu\text{M}$  (Figure 28). This time, as the synthetic TI **1** control had worked just as well as the commercial control compound SP **74** in the previous norlapachol **115**

recruitment experiments and had generally worked reliably in all recruitment experiments to date, the SP **74** control was omitted. Instead, TI **1** was used at both 25  $\mu\text{M}$  (as a known positive control) and 1  $\mu\text{M}$  concentrations, to compare the effects of this compound to the other compounds tested at the same dosage. This might reveal different 'activity ranges' for sets of compounds with differing safety profiles.

$\beta$ -Lapachone **112** led to a significant reduction in the number of neutrophils recruited to the site of injury. In addition, larvae treated with nor- $\beta$ -lapachone **113** showed a trend towards lower neutrophil numbers at the wound which approached significance ( $P = 0.08$ , in comparison to the DMSO control group). However, treatment with lapachol **114** at the same concentration did not reduce neutrophil recruitment, nor did TI **1** at this concentration, although treatment with TI **1** with the control dosage of 25  $\mu\text{M}$  led to the usual reduction in neutrophil number. No signs of toxicity or unhealthiness were observed amongst the larvae of any of the treatment groups.

These results were particularly interesting, as  $\beta$ -lapachone **112** and nor- $\beta$ -lapachone **113** are both *ortho*-quinone compounds which are structurally similar to TI **1**, and these both led to reduced neutrophil numbers (significant for  $\beta$ -lapachone **112** only, at a 1  $\mu\text{M}$  concentration), as observed with TI **1** at a 25  $\mu\text{M}$  concentration. However, TI **1** showed no significant effect when used at a concentration of 1  $\mu\text{M}$  (although did show a trend towards slightly decreased neutrophil numbers), suggesting that  $\beta$ -lapachone **112** (and possibly also nor- $\beta$ -lapachone **113**) may have been more efficacious than TI **1** *in vivo*. This would clearly require further investigation, but is of interest given the toxicity issues observed with the  $\beta$ -lapachones **112-113** yet not with TI **1** at the concentrations investigated.

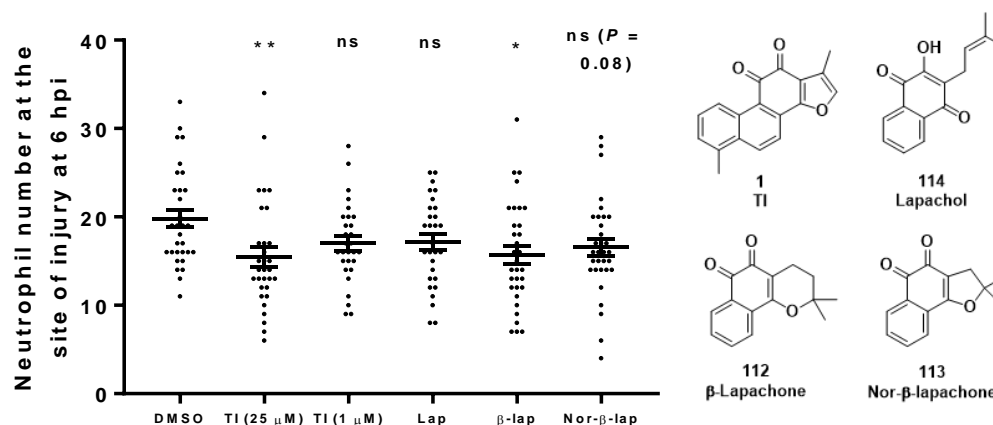


**Figure 29.  $\beta$ -Lapachone 112 significantly reduced neutrophil recruitment at a concentration of 1  $\mu$ M, whilst at the same concentration, neither TI 1, lapachol 114, nor nor- $\beta$ -lapachone 113 significantly affected neutrophil recruitment.**

DMSO used at 0.5% concentration, TI 1 used at concentrations of 25 and 1  $\mu$ M. Data shown as mean  $\pm$  SEM;  $n = 29$ -32 larvae from 4 independent experiments. \*  $P < 0.05$ , \*\*  $P < 0.01$ , ns not significant, in comparison to the DMSO control (one-way ANOVA with Dunnett's multiple comparison post-test). Lap = lapachol 114,  $\beta$ -lap =  $\beta$ -lapachone 112, nor- $\beta$ -lap = nor- $\beta$ -lapachone 113.

#### 5.4.3 Biological evaluation – resolution experiments

The same four compounds were evaluated for any effects on resolution of neutrophilic inflammation *in vivo*. As with previous resolution experiments, all carried out by myself, injured 3 dpf zebrafish larvae identified as good responders (those mounting a good inflammatory response to injury, as determined by neutrophil number at the site of injury at 4 hpi) were treated with a solution of the compound of interest, and then incubated for a further four hours. Norlapachol 115 was evaluated at a range of different concentrations from 0.1 up to 25  $\mu$ M, as the compound was not toxic to larvae at a 25  $\mu$ M concentration in these experiments. Lapachol 114,  $\beta$ -lapachone 112 and nor- $\beta$ -lapachone 113 were each tested at a concentration of 1  $\mu$ M, as higher doses were again found to be toxic.

Norlapachol 115 was first evaluated for any effects on resolution of neutrophilic inflammation at concentrations of 0.1, 1, 10 and 25  $\mu$ M (Figure 29). TIIA 2 (25  $\mu$ M concentration) was again used as a positive control, as in previous resolution experiments. Norlapachol 115 had no significant effect on the number of neutrophils at

0.1 and 1  $\mu\text{M}$  concentrations. However, a significant reduction in neutrophil number was observed at a 10  $\mu\text{M}$  concentration, and a highly significant effect was seen at a concentration of 25  $\mu\text{M}$ , although some of the larvae did show opaqueness and slow or absent circulation at this concentration.

The difference in toxicities between recruitment and resolution experiments could be attributed to the longer treatment times and less healed injury wounds associated with the recruitment experiments, perhaps allowing easier penetration of the compound into the zebrafish larvae. Overall, the resolution data for norlapachol **115** showed a good dose-response trend. It is unclear if the reduced neutrophil numbers observed at the 10  $\mu\text{M}$  concentration were a genuine effect on inflammation resolution, or whether they may have been a function of incipient drug toxicity; further experiments may need to be undertaken in the future to determine which of these explanations is most likely.

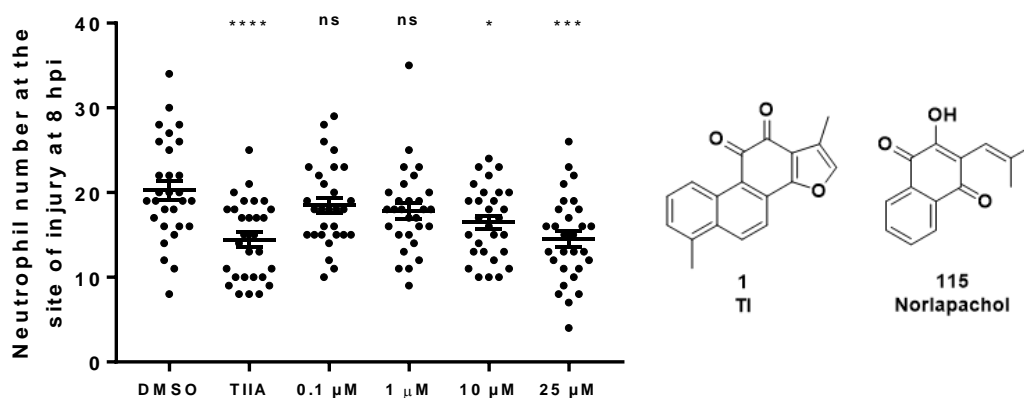


**Figure 30. Norlapachol 115 significantly accelerated resolution of neutrophilic inflammation at 10 and 25  $\mu\text{M}$  concentrations, but not at 0.1 or 1  $\mu\text{M}$  concentrations.** DMSO used at 0.5% concentration, TIIA **2** used at a concentration of 25  $\mu\text{M}$ . Data shown as mean  $\pm$  SEM;  $n = 29$  larvae from 4 independent experiments. \*  $P < 0.05$ , \*\*\*  $P < 0.001$ , \*\*\*\*  $P < 0.0001$ , ns not significant, in comparison to the DMSO control (one-way ANOVA with Dunnett's multiple comparison post-test).

Finally, the remaining compounds lapachol **114**,  $\beta$ -lapachone **112**, and nor- $\beta$ -lapachone **113** were analysed in similar resolution experiments, at a concentration of 1

$\mu\text{M}$  (Figure 30). However, none of these compounds had any significant effect on resolution of neutrophilic inflammation, as only the control treatment of TIIA **2** at a 25  $\mu\text{M}$  concentration gave a significant reduction in neutrophil number.

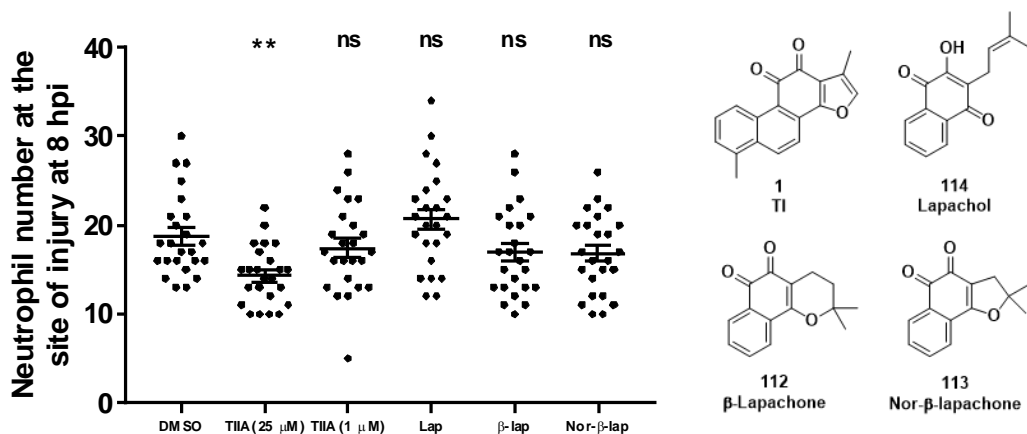


**Figure 31. Neither lapachol 114,  $\beta$ -lapachone 112, nor nor- $\beta$ -lapachone 113 significantly enhanced resolution of neutrophilic inflammation at a concentration of 1  $\mu\text{M}$ .**

DMSO used at 0.5% concentration, TIIA **2** used at 25 and 1  $\mu\text{M}$  concentrations. Data shown as mean  $\pm$  SEM;  $n = 24$  larvae from 3 independent experiments; \*\*  $P < 0.01$ , ns not significant, in comparison to the DMSO control (one-way ANOVA with Dunnett's multiple comparison post-test). Lap = lapachol **114**,  $\beta$ -lap =  $\beta$ -lapachone **112**, nor- $\beta$ -lap = nor- $\beta$ -lapachone **113**.

#### 5.4.4 Biological evaluation – summary

All biological evaluation results for norlapachol **115**, lapachol **114**,  $\beta$ -lapachone **112**, and nor- $\beta$ -lapachone **113** were considered together (Table 5). Norlapachol **115** was toxic at a concentration of 25  $\mu\text{M}$  for recruitment, yet significantly enhanced inflammation resolution at this concentration, although this may have been a result of early signs of toxicity (entry 1). At a 10  $\mu\text{M}$  concentration, norlapachol **115** both significantly reduced the number of neutrophils recruited, and enhanced inflammation resolution (entry 2). Both of these effects were lost at a lower concentration of 1  $\mu\text{M}$  (entry 3), although a reduction in the number of recruited neutrophils was also observed at the lowest concentration of 0.1  $\mu\text{M}$  (entry 4). There was no effect on resolution at this concentration, and it is unclear whether the effect on recruitment was a genuine dose-

response effect, or may have been a result of the natural biological variability of this type of experiment. Taken together, the results for norlapachol **115** treatment for both recruitment and resolution experiments suggest that this compound may warrant further investigation.

Lapachol **114** induced larval toxicity at a 10  $\mu\text{M}$  concentration, in both types of experiment (entry 5). No effect on either neutrophil recruitment or resolution of neutrophilic inflammation was observed at a 1  $\mu\text{M}$  concentration (entry 6). Like lapachol **114**,  $\beta$ -lapachone **112** also led to toxicity at a 10  $\mu\text{M}$  concentration (entry 7). However, treatment of larvae with  $\beta$ -lapachone **112** at a concentration of 1  $\mu\text{M}$  led to a significant reduction in the number of neutrophils recruited to the site of injury (entry 8). No effect on inflammation resolution was detected at the same concentration. Nor- $\beta$ -lapachone **113** produced similar results, having also led to larval toxicity at a 10  $\mu\text{M}$  concentration (entry 9). Although its effect on neutrophil recruitment at a concentration of 1  $\mu\text{M}$  was not significant, a trend towards fewer recruited neutrophils was observed, which approached statistical significance (entry 10). Again, this compound had no effect on inflammation resolution at this concentration.

**Table 5.** Summary of the effects of norlapachol **115**, lapachol **114**,  $\beta$ -lapachone **112**, and nor- $\beta$ -lapachone **113** on neutrophil recruitment and resolution of inflammation *in vivo*.

Entry	Compound	Concentration / $\mu\text{M}$	Effect on recruitment	Effect on resolution
1	Norlapachol <b>115</b>	25	<i>Toxic</i>	Enhanced (***)
2	Norlapachol <b>115</b>	10	Reduced (***)	Enhanced (*)
3	Norlapachol <b>115</b>	1	No effect	No effect
4	Norlapachol <b>115</b>	0.1	Reduced (**)	No effect
5	Lapachol <b>114</b>	10	<i>Toxic</i>	<i>Toxic</i>
6	Lapachol <b>114</b>	1	No effect	No effect
7	$\beta$ -Lapachone <b>112</b>	10	<i>Toxic</i>	<i>Toxic</i>
8	$\beta$ -Lapachone <b>112</b>	1	Reduced (*)	No effect
9	Nor- $\beta$ -Lapachone <b>113</b>	10	<i>Toxic</i>	<i>Toxic</i>
10	Nor- $\beta$ -Lapachone <b>113</b>	1	No effect ( $P = 0.08$ )	No effect

Overall, norlapachol **115** affected both neutrophil recruitment and resolution at higher concentrations, yet this could possibly be targeted towards only affecting neutrophil recruitment at a lower concentration. Lapachol **114** exhibited no observable effect on either recruitment or resolution, whilst both  $\beta$ -lapachone **112**, and nor- $\beta$ -lapachone **113** at low concentrations appear to affect only recruitment of neutrophils, and not resolution of neutrophilic inflammation.

## 5.5 Discussion

This work showed that synthesis of a variety of tanshinone analogues using a key Diels-Alder reaction to assemble the tanshinone skeleton was not trivial. Use of Fremy's salt to synthesise the required dienophile **59** from the phenol precursor **58** was successful, but was not without difficulties. Although it has previously been shown to be highly selective for the required transformation as well as similar examples,<sup>228,230,329</sup>

Fremy's salt is not a cheap reagent, and the requirement of at least 2.5-3 equivalents of this reagent to obtain a meaningful yield, as determined by mass return and  $^1\text{H}$  NMR spectroscopy, meant that this was not a particularly economical oxidation. The known instability of the dienophile **59** also meant that detailed analysis of this product was difficult. Future work could look at optimising this step further, by exploring which oxidation reagents have not previously been used for this step. Other reagents may give selectivities as good as those observed for Fremy's salt, but may be significantly cheaper.

Synthesis of required dienes for the Diels-Alder reaction was also non-trivial, mainly due to the careful purification steps required for such volatile compounds. Due to time constraints, this meant that the synthesis of various dienes could not be completed here. Studies in the future could explore synthesising particular dienes on larger gram scales, to facilitate easier purification (for example, using Kugelrohr distillation) and sufficient quantities of dienes for use in the Diels-Alder reaction.

Whilst the key Diels-Alder reaction was carried out successfully (to some extent), this reaction also merits further study. Previous work showed that this reaction worked well for reactive dienes,<sup>228,230</sup> and this was observed here, as both cyclopentadiene **127** and (seemingly) Danishefsky's diene **130** reacted with the dienophile **59**. Return of significant quantities of the phenol precursor **58** made effective purification more difficult, and ideally this reaction would be optimised to ensure that minimal quantities of this starting material were returned. Carrying out this reaction with less reactive dienes has been found to be difficult, and has required the use of heat, high pressures, and/or ultrasonication to achieve moderate yields and selectivities.<sup>228-230</sup> In this work, reaction with cyclohexadiene **128** was unsuccessful, and this could be the case for other dienes required for the synthesis of tanshinones and analogues. One possibility for future study would be to explore the use of microwave conditions for this reaction. This does not seem to have been well examined in the literature, and the use of microwave conditions may give rise to the high temperatures and pressures which appear to be required for successful reaction. Use of additives such as Lewis acids was previously found to lead to unsuccessful reaction, thought to be due to promoting decomposition of the dienophile **59**.<sup>228,230</sup> However, a more thorough solvent screen could be explored,

as solvent choice is well known to have an effect on the efficiency, selectivity and mechanism of Diels-Alder reactions.<sup>339–341</sup>

Overall, this work on the synthesis of TIIA analogues showed that this was an accessible route to tanshinone compounds, but requires further optimisation to ensure that various dienes can be used to generate required compounds effectively. The route used to synthesise various TI analogues was not used here due to difficulty in easily obtaining the required carboxylic acids, but could be explored (Figure 31). Alternatively, methods for forming the required carbon-carbon bond from the appropriate  $sp^3$  carbon atom and the bromide could be considered (Figure 31). Functionalisation reactions for forming carbon-carbon bonds from  $sp^3$  carbon atoms are becoming increasingly popular,<sup>342–345</sup> and as the desired six-membered ring formation is likely to be thermodynamically favoured compared to other possibilities in this system, there may be a method of achieving this transformation. This may work particularly for dienes where both  $R^2$  and  $R^3$  are groups other than hydrogen atoms. This would also depend on the identity of the attached R groups and commercial or synthetic availability of the required carboxylic acids for the previous radical alkylation reaction, but is a possibility which could be explored.

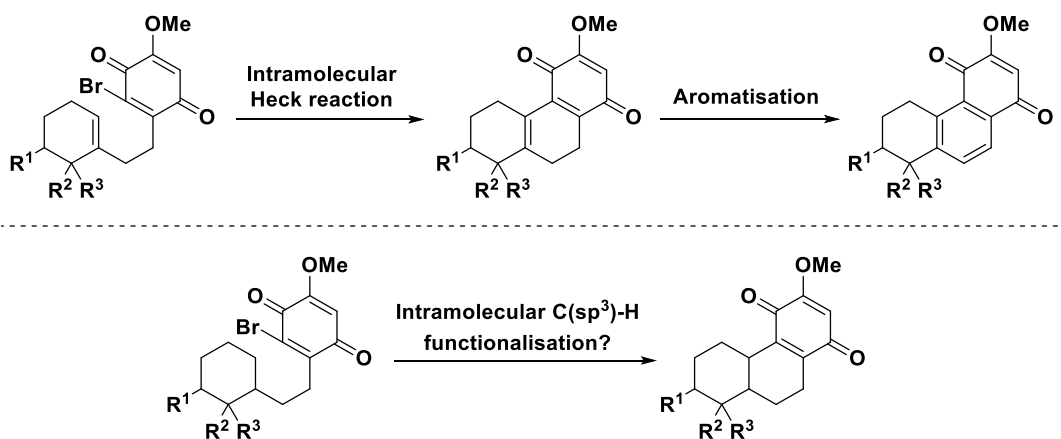


**Figure 32.** Possible routes to tanshinone analogues using an intramolecular Heck reaction (top) or C( $sp^3$ )-H activation chemistry (bottom).

The desired lapachone and lapachol compounds were synthesised much more easily, using commercially available lapachol **114** and known, good-yielding

transformations.<sup>306,307</sup> This work was the first study of the effects of both nor- $\beta$ -lapachone **113** and norlapachol **115** on zebrafish larvae. It is also the first report of the evaluation of these compounds for anti-inflammatory effects. Furthermore, although both  $\beta$ -lapachone **112** and lapachol **114** have previously been investigated for effects on zebrafish larvae and on inflammation in separate studies, these compounds have not been evaluated in a zebrafish model of inflammation.

$\beta$ -Lapachone **112**, lapachol **114**, and nor- $\beta$ -lapachone **113** all resulted in zebrafish larval toxicity at a 10  $\mu$ M concentration. For  $\beta$ -lapachone **112**, this observation was found to be broadly consistent with those of previous studies, including a zebrafish drug-repurposing screening study, in which  $\beta$ -lapachone **112**, at a screening concentration of 34  $\mu$ M, was categorised as one of 48 'toxic compounds and compounds with adverse effects'.<sup>94</sup> An earlier study also reported toxicity associated with  $\beta$ -lapachone **112**, and lethal concentration (LC<sub>50</sub>) values of approximately 1.90  $\mu$ M were reported for zebrafish larvae at both 56 and 80 hours post fertilisation (hpf).<sup>308</sup> Furthermore,  $\beta$ -lapachone **112** has been shown to induce heart defects and morphogenesis in zebrafish larvae, *via* induced apoptosis of endocardium cells and erythrocytes, possibly through an NQO1-containing pathway.<sup>346</sup> Similarly, at a 10 mM concentration, lapachol **114** has previously been found to induce abnormalities in the vast majority of zebrafish embryos at 56 hpf, leading to a mortality rate of over 50% at 80 hpf.<sup>308</sup> The LC<sub>50</sub> concentration for lapachol **114** with embryos at 80 hpf has also been reported as around 9  $\mu$ M.<sup>308</sup> However, nor- $\beta$ -lapachone **113** has never been studied before in this way. Variations in such toxicity thresholds may be due to factors such as strain of zebrafish used, method of injury, and method of compound administration. Taken together, these findings indicate the importance of determining the optimal dosage of compounds administered to living organisms, and the utility of *in vivo* models such as zebrafish in allowing quick determination of obvious compound toxicity.

At a concentration of 10  $\mu$ M, larvae treated with norlapachol **115** remained healthy, in contrast to the structurally similar compound lapachol **114**. This suggests that making a subtle change such as removing a single carbon atom from the hydrocarbon chain of the molecule can lead to a profound difference in the safety profile of the molecule *in*

*vivo*. This could be due to various reasons; for example, the change in molecular structure could lead to the molecule binding to a different target protein or receptor, or it could affect how much of the drug is able to enter and/or exit different cells *via* passage across the cell membrane (see Chapter 6).

At a concentration of 1  $\mu\text{M}$ ,  $\beta$ -lapachone **112** led to a significant reduction in the number of neutrophils recruited to the site of injury, whilst treatment with nor- $\beta$ -lapachone **113** at the same concentration showed a trend towards lower neutrophil numbers which approached significance. These reductions in neutrophil numbers mirrored similar reductions observed when larvae were treated with the structurally similar TI **1**. However, use of the latter at a concentration of 25  $\mu\text{M}$  (or 10  $\mu\text{M}$ ; see Figure 10) was required to observe a significant effect, and no significant reduction was seen at a TI **1** concentration of 1  $\mu\text{M}$ . This suggests that  $\beta$ -lapachone **112** (and perhaps also nor- $\beta$ -lapachone **113**) was more active than TI **1** in reducing neutrophil recruitment. One possible explanation is that these compounds were all acting at the same molecular target, in accordance with their high structural similarities. However, their structural differences may have affected their absorption, metabolism and/or distribution around the zebrafish larval body, meaning that there was a difference in the incubation concentrations required to observe a significant reduction in the number of neutrophils recruited to the site of injury.

A change in any one or more of these processes may also help to explain why the tanshinones were not toxic at a concentration of 25  $\mu\text{M}$ , yet the lapachones **112-113** and lapachols **114-115** were, and at even lower doses, despite their structural similarities. The extra aromatic ring of tanshinones, or the furan ring in these molecules (compared to the unsaturated oxygen-containing ring of the lapachones **112-113**, or the absence of this ring in the lapachol compounds **114-115**) may have reduced their toxicity. This could relate to target effects, such as an altered target binding efficiency or a different binding profile for other proteins (off-target effects), or transport into or out of the neutrophil or even the zebrafish larva itself. Further work could involve investigating one or more of these aspects in more detail. The differing toxicity profiles and 'activity windows' of these compounds are also of interest.  $\beta$ -Lapachone **112** and

nor- $\beta$ -lapachone **113** both led to toxicity at a concentration of 10  $\mu$ M, yet were active at a 1  $\mu$ M concentration with no obvious signs of toxicity; the 1-10  $\mu$ M concentration range could be further explored. This is in contrast to TI **1**, which has been used regularly at a concentration of 25  $\mu$ M in this type of experiment with no observable signs of toxicity.

Furthermore, it is possible, although unlikely, that any effects on neutrophil recruitment and resolution of neutrophilic inflammation observed here were due to effects on the number of neutrophils in the whole body of the larvae, and/or effects relating to generation of ROS such as hydrogen peroxide at the site of injury, as discussed in detail in Chapter 4.

## 6. How tanshinones access neutrophils – expression of drug transporter molecules in human and zebrafish neutrophils

### 6.1 Introduction

In order to fully understand how a drug exhibits its desired *in vivo* effect, it is important to consider not only the identity of the molecular target or targets, relating to pharmacodynamics, but also the journey taken by the drug through the body to access the target(s), relating to pharmacokinetics. This includes entry to cells of interest, as well as exit from these cells: timely elimination of the drug from the body after it has exhibited its effect is important in preventing undesired toxicity. Before this can be considered for specific molecules such as tanshinones, it is desirable to have a generalised understanding to enable future rational anti-inflammatory drug identification and design.

For many years, it was widely assumed that drug molecules entered cells *via* diffusion across the phospholipid bilayer of the cell membrane, and until recently, this theory remained largely unchallenged. However, within the last twenty years, it has become apparent that transporter proteins embedded in the cell membrane, which are responsible for the transfer of ions and metabolites into and out of the cell, are also utilised by drug molecules for cell entry and exit.<sup>347–352</sup> Such transporters, herein termed ‘drug transporters’, have been the subject of much recent work; in particular, several studies by Kell and co-workers have led to formation of the ‘phospholipid bilayer diffusion is negligible’ (PBIN) hypothesis, which is supported by significant evidence.<sup>353–356</sup> It is thought that most successful drugs in their active form are somewhat similar in structure to that of an endogenous metabolite, which itself is transported by one or more specific transporter proteins; thus, the drug ‘hijacks’ the same transporter(s) and uses this to cross the cell membrane.<sup>357–360</sup> It is now believed that drug transport across cell membranes is mostly comprised of this hijacking of transporter proteins rather than passive diffusion, and so drug transporters appear to be vital for absorption, distribution and excretion of drug molecules.

Drug transporters are comprised of two main families: solute carrier (SLC) and ATP-binding cassette (ABC) transporters. According to the HUGO Gene Nomenclature Committee, in humans there are 395 members of the SLC family (April 2017),<sup>361</sup> and the main physiological function of these proteins is to transport ions and metabolites into cells (influx). One of the best reported examples of drug transport *via* an SLC transporter protein is that of gemcitabine **141** (Figure 32), which is mainly transported by the SLC29A1 transporter, and is used in the treatment of pancreatic cancer,<sup>362,363</sup> whilst many other SLC transporter proteins are emerging as potential drug targets.<sup>364</sup> The ABC family is made up of 52 proteins,<sup>361</sup> and these are mainly responsible for the transport of ions and metabolites out of cells (efflux). There are some reports in the literature of drugs presenting toxicity issues in patients with particular mutations in ABC proteins, and many ABC transporters are known to be involved in active drug transport, suggesting an important role for these proteins in drug treatment.<sup>365–367</sup>

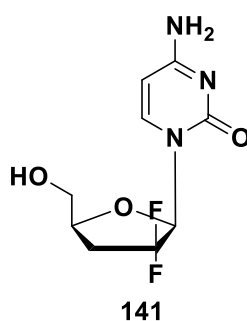


**Figure 33.** Structure of the pancreatic cancer drug gemcitabine **141**.

Although expression of SLC and ABC transporter proteins has been broadly determined both in humans and other models,<sup>368,369</sup> there is no published analysis of these transporters in neutrophils, in either humans or zebrafish.

## 6.2 Hypothesis and aims

It was hypothesised that tanshinones specifically target neutrophils to exhibit anti-inflammatory effects, and utilise SLC and ABC transporters expressed in neutrophils to get into and out of the cell. It was also hypothesised that there was a level of

conservation of SLC and ABC transporter protein expression between human and zebrafish neutrophils.

The aims of this work were to:

- Determine evolutionary relationships between different drug transporters and their sub-families within each of the SLC and ABC families in both humans and zebrafish, *via* the production of phylogenetic trees.
- Determine expression of SLC and ABC transporters in both unstimulated primary human and zebrafish neutrophils, using previously published RNA-sequencing (RNAseq) data.
- Analyse the effects, if any, of granulocyte macrophage colony-stimulating factor (GM-CSF) and tumor necrosis factor alpha (TNF $\alpha$ ) stimuli on drug transporter expression in primary human neutrophils.
- Use publically available human neutrophil proteomics datasets to determine the level of consistency between RNAseq and proteomics approaches for drug transporter expression in human neutrophils.
- Determine if there was any conservation in SLC and ABC transporter expression between primary human and zebrafish neutrophils.

## 6.3 Methods

### 6.3.1 Identification of relevant genes and protein sequences

Lists of the human SLC and ABC transporter genes were obtained from the HUGO Gene Nomenclature Committee (HGNC) database (April 2015).<sup>361</sup> The Ensembl database (human data: version GRCh38.p2, release 79; zebrafish data: version Zv9, release 79) was manually searched for each human SLC and ABC gene identifier,<sup>370</sup> and orthologous genes present in the zebrafish (*Danio rerio*) database (version Zv9, release 79) were identified. Due to some observed discrepancies in the naming of the zebrafish orthologues, such as where two different genes had identical names in the database, the unique numerical identifier (for example, *ENSDARG00000000001*) was used to search for orthologues in each case, to avoid ambiguity. Gene names as returned from Ensembl were generally retained for all further analysis. Genes with identical names

were arbitrarily given suffixes of *\_first* and *\_second* to enable distinction. Where genes were identified as being a 'novel gene' in the Ensembl database with no additional annotation, the corresponding name for the same gene was obtained from an earlier release of the same version of Ensembl (version Zv9, release 75) in accordance with the RNAseq data used [accessed *via* the NCBI Gene Expression Omnibus (GEO), under accession number GSE78954].

For both human and zebrafish datasets, the longest corresponding protein-coding sequence (highest number of amino acids) for each individual gene was obtained from the Ensembl database. Any non-protein-coding genes, regulatory genes and pseudogenes were excluded from the analysis. Files containing protein sequence data used in this work were deposited at The University Of Sheffield Research Data Catalogue and [Repository, ORDA \(\[https://figshare.com/articles/Data\\\_relating\\\_to\\\_the\\\_publication\\\_Expression\\\_and\\\_regulation\\\_of\\\_drug\\\_transporters\\\_in\\\_vertbrate\\\_neutrophils\\\_/4834217/1\]\(https://figshare.com/articles/Data\_relating\_to\_the\_publication\_Expression\_and\_regulation\_of\_drug\_transporters\_in\_vertbrate\_neutrophils\_/4834217/1\)\)](https://figshare.com/articles/Data_relating_to_the_publication_Expression_and_regulation_of_drug_transporters_in_vertbrate_neutrophils_/4834217/1).

### 6.3.2 Production of phylogenetic trees

Clustal Omega (version 1.2.3) was used for multiple sequence alignment of protein sequences.<sup>371,372</sup> The 'Phylogenetic Tree' output (.ph file) was converted to a Newick tree format using the Phylogeny.fr resource.<sup>373</sup> This was input into the Interactive Tree of Life (iTOL) programme (version 3.3) to produce phylogenetic trees displaying the evolutionary relationships in the human and zebrafish SLC and ABC families.<sup>374</sup> The phylogenetic trees were annotated with the corresponding expression and proteomics data.

### 6.3.3 Expression and regulation of human transporter proteins

Published transcriptomics datasets (GEO accession number GSE40548) were downloaded and used for analysis.<sup>375</sup> A gene was said to be expressed if it had a 'fragments per kilobase of exon per million fragments mapped' (FPKM) value greater than or equal to 1, a conservative value chosen due to its relationship to expression of the well-validated neutrophil protein myeloperoxidase (MPO), expression level 0.98

FPKM. Genes with a FPKM value less than 1 were said to be unexpressed in this analysis. Any genes with expression observed to be significantly up- or down-regulated in the presence of either of the inflammatory stimuli GM-CSF or TNF $\alpha$  in this dataset were annotated on the phylogenetic trees accordingly.

To cross-reference expression of human transporter proteins with findings from proteomics studies, human neutrophil proteomics data from eight different studies were manually searched for any SLC and ABC transporter proteins identified therein.<sup>376–383</sup> These were annotated on the relevant phylogenetic trees.

For expression validation, each SLC and ABC gene was searched for in a second published dataset, generated by Chatterjee *et al.* (GEO accession number GSE59528).<sup>384</sup> Mean FPKM values for each identified gene were plotted against the corresponding data from the initial dataset from Wright *et al.* following logarithmic transformation of both datasets.<sup>375</sup>

All human genes and proteins were referred to according to HGNC conventions throughout. Raw data files used to generate figures in this work were deposited at ORDA ([https://figshare.com/articles/Data\\_relating\\_to\\_the\\_publication\\_Expression\\_and\\_regulation\\_of\\_drug\\_transporters\\_in Vertebrate\\_neutrophils\\_/4834217/1](https://figshare.com/articles/Data_relating_to_the_publication_Expression_and_regulation_of_drug_transporters_in Vertebrate_neutrophils_/4834217/1)).

#### 6.3.4 Expression and regulation of zebrafish transporter proteins.

Previously generated zebrafish larval RNAseq data were downloaded and used for this work (GEO accession number GSE78954).<sup>385</sup> For both neutrophil and background (non-neutrophil) cell expression levels, any gene with a FPKM value greater than or equal to 1 was said to be expressed, and any with a FPKM value less than 1 was said to be unexpressed, in line with the definitions used for expression of human genes here. All zebrafish genes and proteins were referred to in accordance with the Zebrafish Information Network (ZFIN) naming conventions as far as practicably possible. Raw data files used to generate figures in this work were deposited at ORDA ([https://figshare.com/articles/Data\\_relating\\_to\\_the\\_publication\\_Expression\\_and\\_regulation\\_of\\_drug\\_transporters\\_in Vertebrate\\_neutrophils\\_/4834217/1](https://figshare.com/articles/Data_relating_to_the_publication_Expression_and_regulation_of_drug_transporters_in Vertebrate_neutrophils_/4834217/1)).

## 6.4 Analysis of expression and regulation of drug transporters in human neutrophils

To display the expression data most clearly, whilst also allowing for visualisation of the evolutionary relationships between different drug transporters and their sub-families, the transporter proteins were displayed as phylogenetic trees for each of the SLC and ABC families. Production of the trees first required the protein sequences for each individual SLC and ABC family member to be found. The longest coding protein sequence for each transporter gene was obtained from the Ensembl database,<sup>370</sup> and following alignment, was used in tree construction.<sup>371–374</sup> Any genes which did not code for functional proteins, or which were pseudogenes or regulatory genes, were removed from the dataset.

Expression analysis was carried out using a publically-available RNAseq dataset.<sup>375</sup> Here, any gene with a FPKM value greater than 1.0 was said to be expressed, with all lower values corresponding to genes not expressed. This conservative value was chosen due to its relationship to MPO expression, which is a well-validated neutrophil protein with a FPKM value of 0.98 in this human neutrophil dataset. Each branch on the tree, corresponding to a different protein, was annotated with its expression in primary human neutrophils: the presence of a black dot denoted that the gene was expressed, whilst the absence of a black dot indicated that the gene was not expressed.

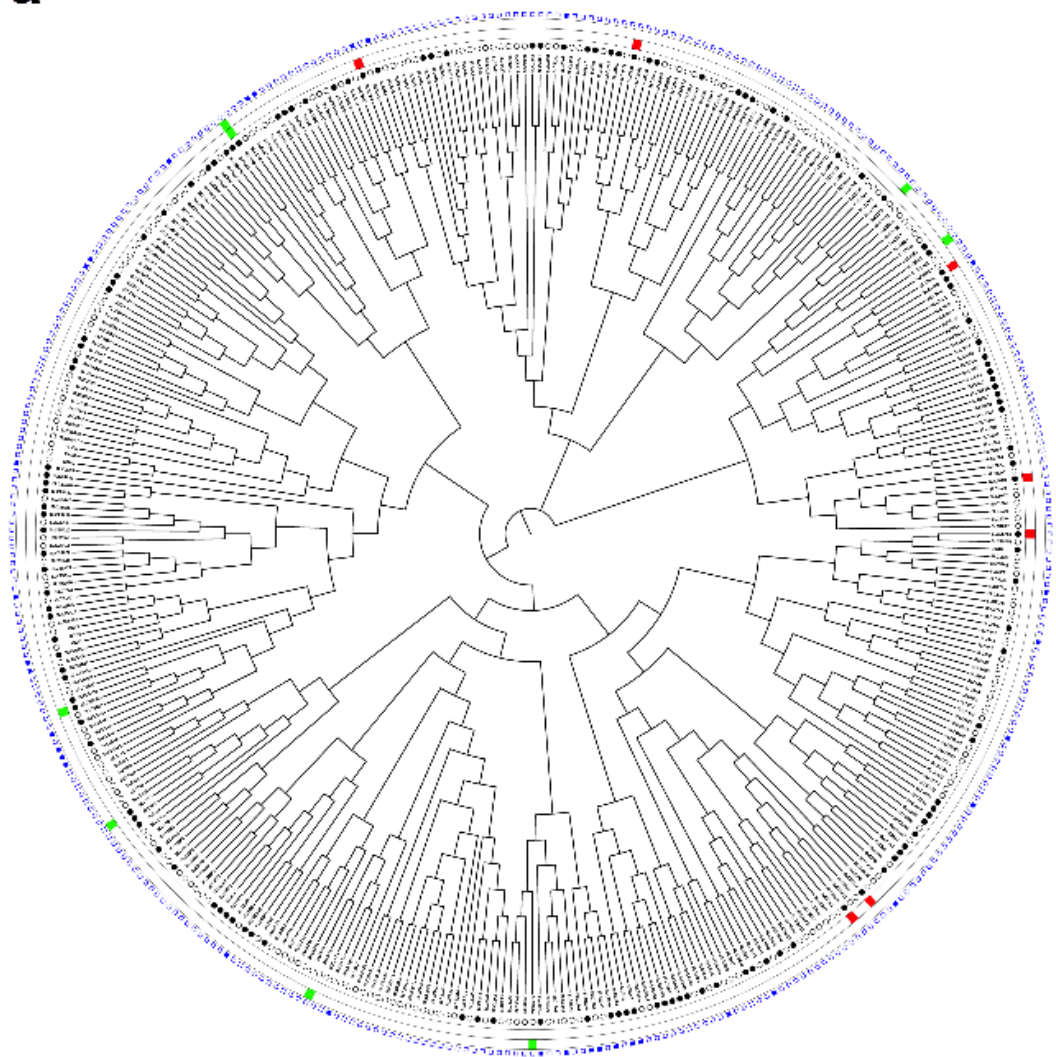
This resulted in annotated phylogenetic trees for both SLC (Figure 33) and ABC (Figure 34) transporter proteins. Two trees were displayed for each of the families, corresponding to two different display modes of the same data: the circular mode showed all the annotations in a more easily understood form, and the unrooted mode gave a more accurate indication of the individual sub-families of proteins and how they were related. For these trees, the lengths of the branches were not proportional to the genetic distances. However, trees containing branches proportional to genetic relationship were also produced for the SLC (Appendix 10.4.1) and ABC (Appendix 10.4.2) families; whilst perhaps not as clear as the non-proportional trees, these trees were important in allowing an accurate visualisation of evolutionary relationships between genes for drug transporter proteins. Furthermore, whilst labels for specific

branches in some of the larger trees are fairly small, fully scalable electronic versions of these trees were produced and made accessible.<sup>386</sup>

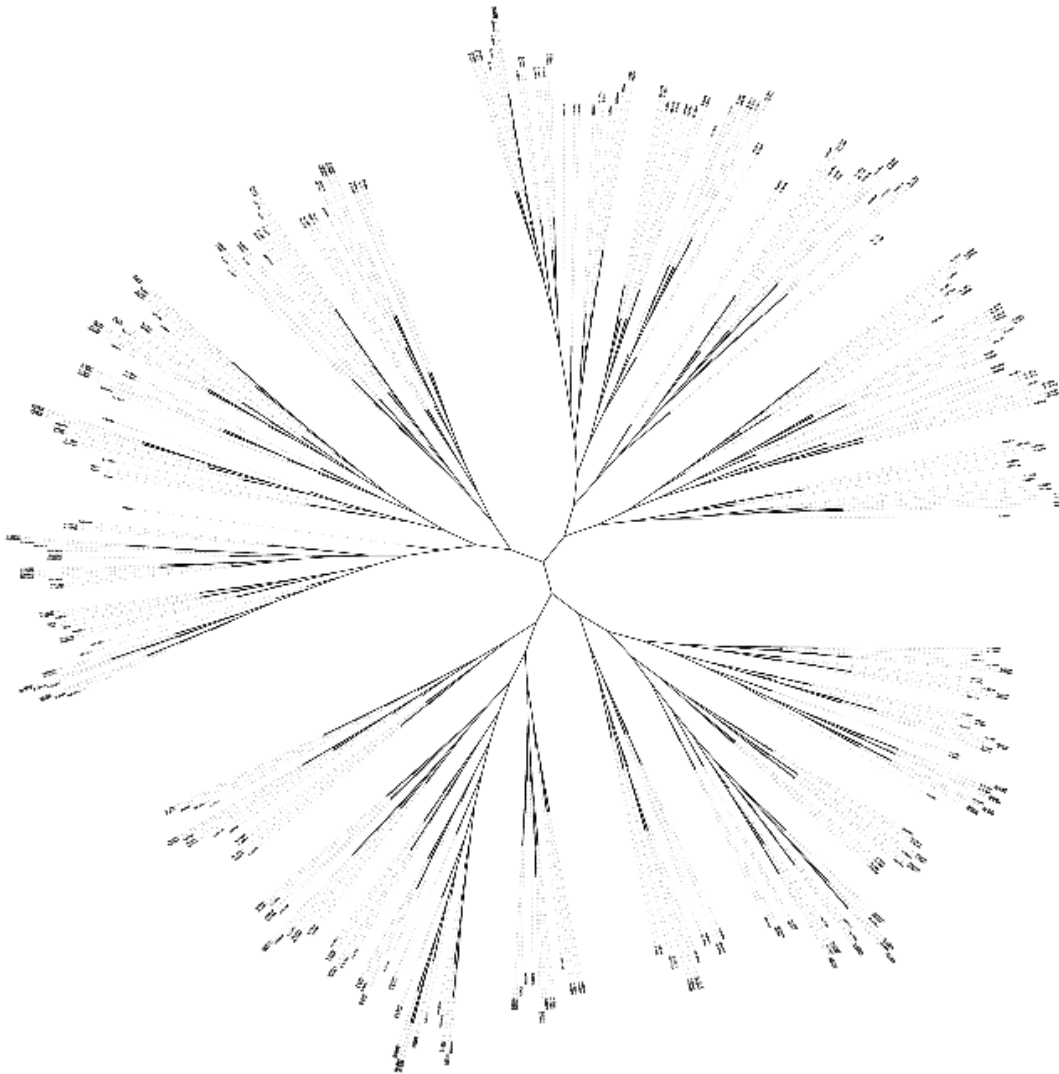
In addition to unstimulated expression data, data were also available for the expression status of the same genes in the presence of two important regulators of neutrophil function and survival: GM-CSF and TNF $\alpha$ . These data were displayed as annotations around the relevant trees, with a green box corresponding to significant up-regulation of the gene in the presence of the regulator, and a red box denoting significant down-regulation of the gene. All other genes showed no significant change in regulation in the presence of the regulator.

Furthermore, to investigate the relationship between RNAseq analysis and proteomic approaches, human neutrophil proteomics datasets from eight different publically available studies were analysed manually.<sup>376–383</sup> Any SLC or ABC transporter protein which was identified in one or more of these proteomics studies was annotated on the tree, shown by a blue box.

**a**



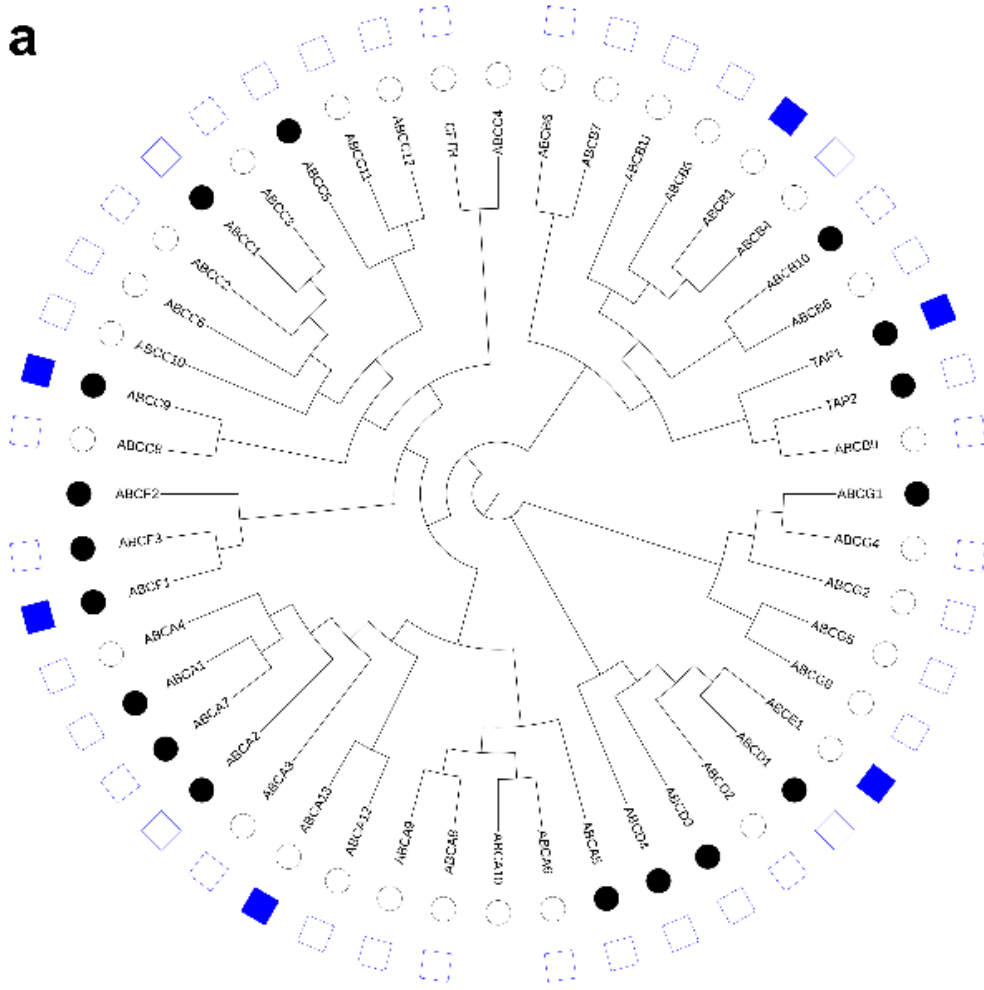
**b**



**Figure 34. Subsets of SLC transporter proteins were expressed and regulated in resting primary human neutrophils.**

Annotated phylogenetic trees in (a) circular and (b) unrooted display modes indicate evolutionary relationships between SLC transporter proteins in human neutrophils (branch lengths not proportional to genetic distance; see Appendix 10.4.1 for trees with proportional branch lengths). In (a), for resting primary human neutrophil expression data (inner circle), expressed proteins were marked with a black dot, whereas proteins not expressed were denoted with a white dot. For GM-CSF (second circle from centre) and TNF $\alpha$  (third circle from centre) regulation data, significant up-regulation of a gene was denoted with a green box, significant down-regulation was denoted by a red box, and a lack of significant change in regulation unmarked. For human neutrophil proteomics data (outer circle), any proteins identified in one or more of the analyses were denoted with a blue box, and any not identified were denoted with a white box.

**a**



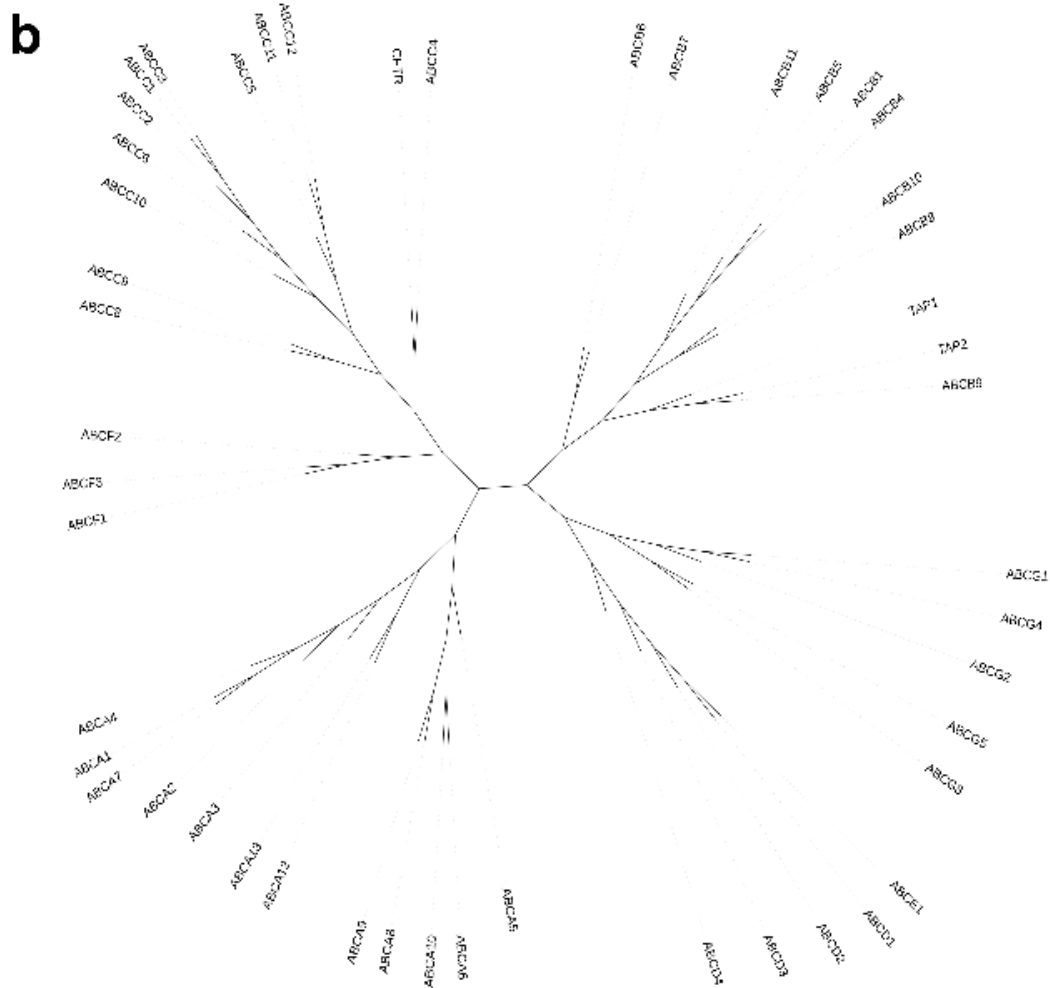


**Figure 35. Subsets of ABC transporter proteins were expressed and regulated in resting primary human neutrophils.**

Annotated phylogenetic trees in (a) circular and (b) unrooted display modes indicate evolutionary relationships between ABC transporter proteins in human neutrophils (branch lengths not proportional to genetic distance; see Appendix 10.4.2 for trees with proportional branch lengths). In (a), for resting primary human neutrophil expression data (inner circle), expressed proteins were marked with a black dot, whereas proteins not expressed were denoted with a white dot. For human neutrophil proteomics data (outer circle), any proteins identified in one or more of the analyses were denoted with a blue box, and any not identified were denoted with a white box.

As can be seen from the SLC phylogenetic trees (Figure 33), around 34% of the SLC protein-coding genes (134 of 389) were expressed above threshold values in human neutrophils. In the presence of GM-CSF, nine genes showed a significant change in regulation, all of which were expressed in human neutrophils. Of these nine genes, two were up-regulated (*SLC1A5* and *SLC25A25*) and seven were down-regulated (*SLC10A3*, *SLC15A3*, *SLC15A4*, *SLC16A14*, *SLC16A6*, *SLC19A1* and *SLC25A51*). In the presence of TNF $\alpha$ , six genes exhibited significant regulation change, of which three were expressed in human neutrophils (*SLC1A5*, *SLC35B2* and *SLC7A5*) and three were not expressed (*SLC11A2*, *SLC2A6* and *SLC30A4*). Notably, all six of these genes were up-regulated, whilst no SLC genes were found to be down-regulated in the presence of TNF $\alpha$ . Only one gene, *SLC1A5*, was common to both of these sets, showing significant up-regulation in both cases. *SLC1A5*, previously referred to as Alanine Serine Cysteine Transporter 2, is a neutral amino acid transporter, and is ubiquitously expressed. However, overexpression of this gene has been reported in various cancers,<sup>387,388</sup> and is currently being explored as a drug target in cancer treatment.<sup>389</sup> This does not by any means suggest that this transporter is used by molecules such as tanshinones; rather, this is simply a transporter of interest in relation to inflammatory processes. Across the human neutrophil proteomics datasets, only 33 SLC proteins were identified (some in a single set, others across several studies), and of these, 20 were identified as being expressed in the RNAseq data presented here.

Approximately 35% of the ABC protein-coding genes (17 of 48) were expressed above threshold values in primary human neutrophils (Figure 34). Interestingly, the proportion of drug transporters expressed in human neutrophils was approximately the same for the SLC and ABC families respectively. However, a noteworthy difference between the two families was that, in the presence of either GM-CSF or TNF $\alpha$ , none of the ABC transporters showed a significantly increased or decreased change in expression. This may reflect a particular need for the SLC transporters to transport molecules into activated neutrophils. When the various human neutrophil proteomics datasets were interrogated, a total of six ABC transporter proteins were identified, and of these, three

had been identified as being expressed in human neutrophils according to the RNAseq data.

Thus far, all of the analysis was carried out using a single RNAseq dataset.<sup>375</sup> To determine the validity of this approach and the quality of the dataset, a second more recent publically available human neutrophil RNAseq dataset was identified,<sup>384</sup> and the same analysis of SLC and ABC drug transporters expressed in unstimulated primary human neutrophils was carried out. The results from the two separate datasets were compared, and displayed in graphical form for both SLC and ABC transporters (Figure 35; tables showing raw data given in Appendices 10.5.1 and 10.5.2). The two datasets exhibited a highly significant positive correlation, both for the SLC transporters ( $r = 0.9157$ ,  $P < 0.0001$ ) and for the ABC transporters ( $r = 0.8368$ ,  $P < 0.0001$ ). This helped to validate the approach used, and provided confidence in the methodology used thus far.

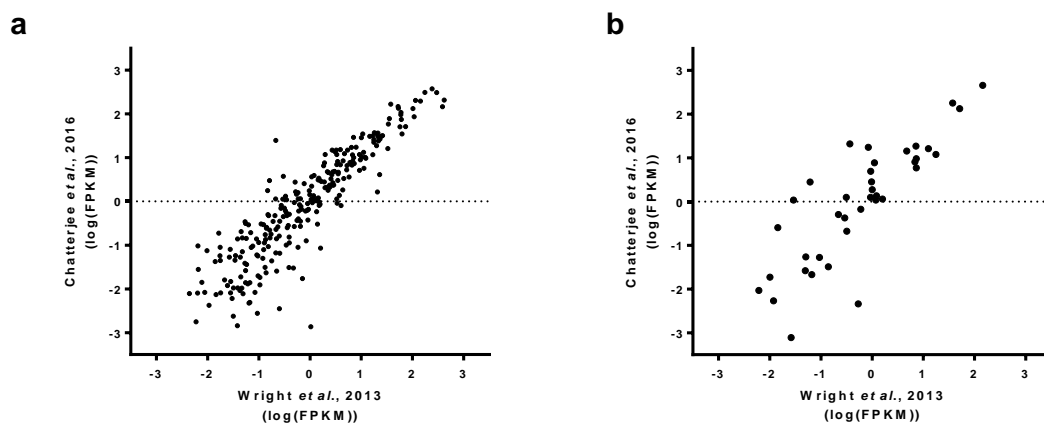


**Figure 36. Expression levels of human SLC and ABC transporter proteins across two different datasets showed highly significant positive correlation.**

Scattergraphs show comparison of expression of (a) SLC and (b) ABC transporter proteins in datasets by Wright *et al.* and Chatterjee *et al.*<sup>375,384</sup> Data points represent the mean of replicate values. Any genes in the Wright *et al.* dataset which could not be identified in the Chatterjee *et al.* dataset were not shown. For (a),  $r = 0.9157$ ,  $P < 0.0001$  (Spearman correlation,  $n = 368$  pairs). For (b),  $r = 0.8368$ ,  $P < 0.0001$  (Spearman correlation,  $n = 47$  pairs). Corresponding tables provided in Appendices 10.5.1 and 10.5.2.

## 6.5 Expression analysis of drug transporters in zebrafish neutrophils

As discussed previously, the zebrafish is an excellent *in vivo* model for anti-inflammatory drug screening, and analysis of neutrophil function.<sup>86,90,103</sup> Indeed, just one example of the practicality of this approach was shown in the identification of the SGK1 inhibitor GSK650394 **142** (Figure 36).<sup>76</sup> This compound has been shown to induce apoptosis, both in zebrafish models of inflammation *in vivo*, and in human neutrophils *in vitro*. Analysis by mass spectrometry has also provided evidence that this molecule was able to penetrate zebrafish larvae in order to induce its effect.<sup>76</sup> However, analysis of published data regarding the accumulation of drug-like compounds within zebrafish larvae showed that there was not a simple correlation between the lipophilicity of a compound (measured as cLogP, the calculated logarithm of the compound's partition coefficient between n-octanol and water) and its concentration in the larvae.<sup>386</sup> This is supportive of the hypothesis that cLogP alone is not sufficient to predict larval penetration and access into cells, consistent with much work done by Kell and others,<sup>348-350,355</sup> suggesting that transport across membranes *via* drug transporter proteins is also very important in zebrafish.

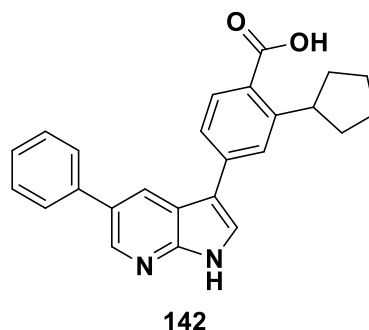


**Figure 37.** Structure of the SGK1 inhibitor GSK650394 **142**.

To begin investigation of the hypothesis that drug transporter expression in zebrafish was an important factor in larval drug penetration, and specifically, expression in zebrafish neutrophils, which was hypothesised to be particularly relevant to inflammatory disease, phylogenetic trees for both SLC and ABC transporter expression were produced. This again allowed for the visualisation of relationships between

different individual drug transporters and between sub-families, as well as clear display of expression data.

For each individual human SLC and ABC transporter gene, the Ensembl database was manually searched for orthologous genes present in the zebrafish.<sup>370</sup> Paralogues of each of these zebrafish genes were then identified in a similar manner, and any genuine SLC or ABC paralogues not already in this set were included. This was to ensure that the set of zebrafish genes used in this analysis was as comprehensive and complete as possible. In some cases, it was not clear from inspection of the gene name alone whether the paralogue was actually a 'true' paralogue or not, especially since some returned genes were clearly not 'true' paralogues and were related to different protein families, according to their name. In these ambiguous cases, the corresponding gene tree in Ensembl was examined. The gene was included in this dataset if it had a clear evolutionary relationship to one or more annotated zebrafish drug transporter genes. Any returned paralogues which could not be identified as having such a relationship were excluded from this analysis.

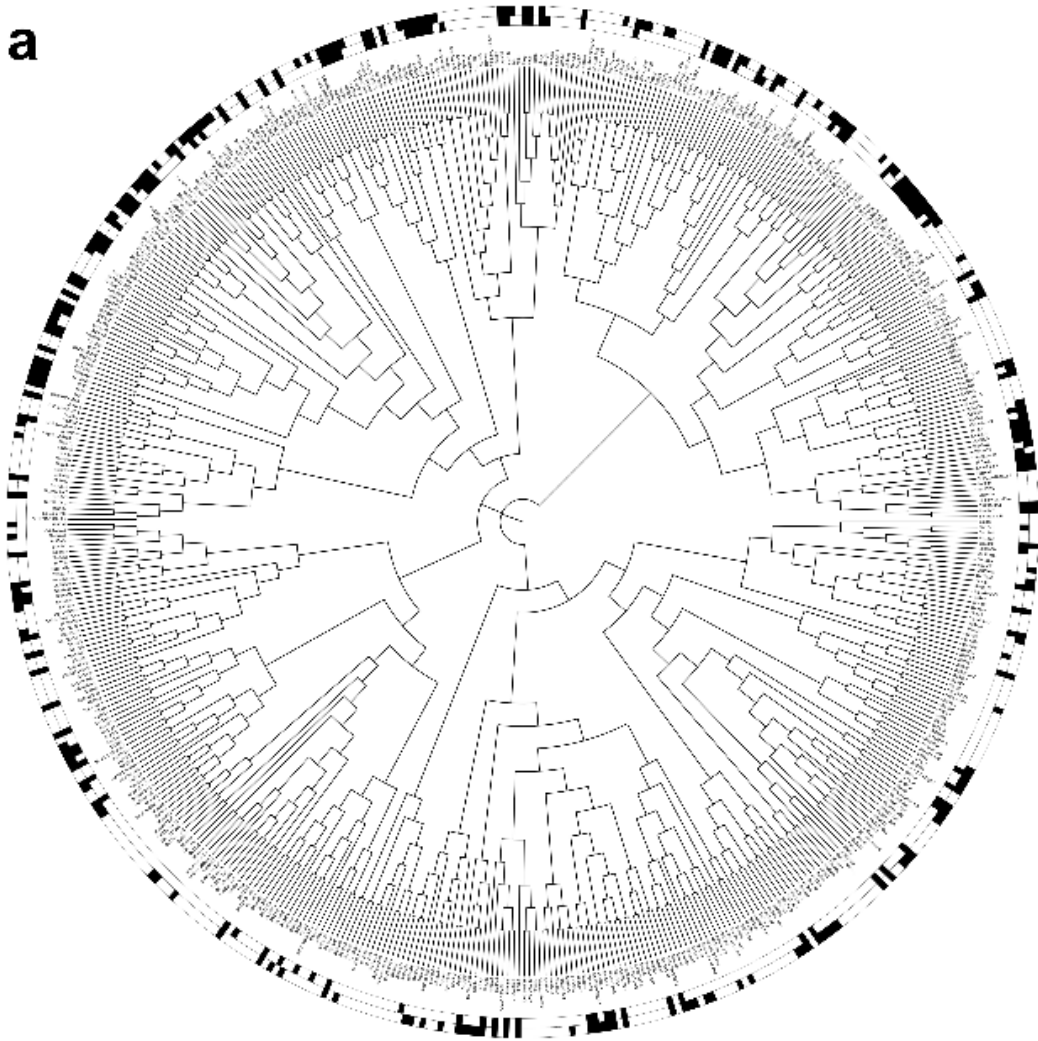
Once the two sets of zebrafish transporter genes were considered to be complete, the longest coding protein sequence for each individual gene was identified using the Ensembl database,<sup>370</sup> in the same manner as for the human genes previously. Pseudogenes, regulatory genes, and genes not coding for functional proteins were again excluded, and the remaining sequences were aligned and used in the construction of the phylogenetic trees.<sup>371-374</sup>

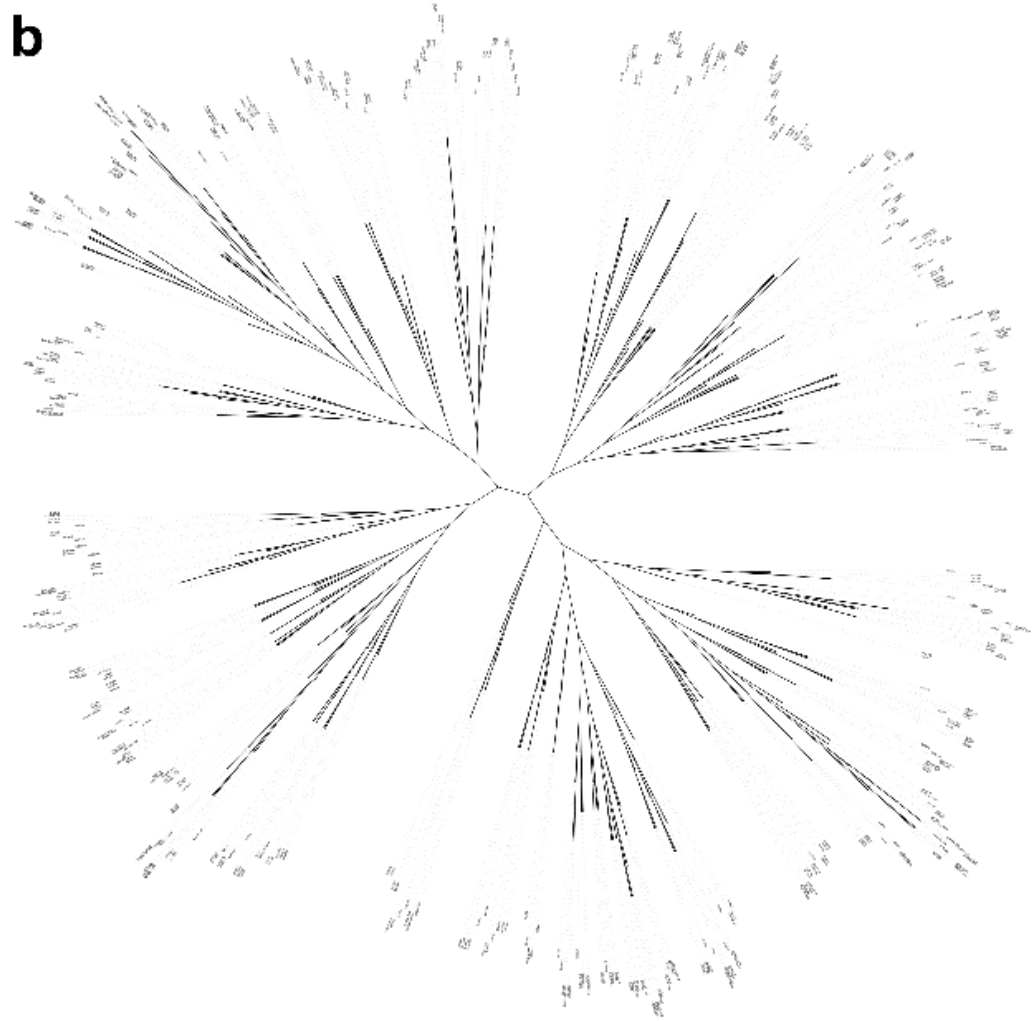
For zebrafish drug transporter analysis, expression analysis was carried out using RNAseq data from transgenic *Tg(mpx:GFP)i114* zebrafish at 5 dpf (GEO accession number GSE78954), obtained as described previously.<sup>385</sup> As this involved sorting cells into GFP-positive cells (corresponding to neutrophils only) and GFP-negative cells (all other non-neutrophil cells, termed background cells), this meant that analysis of drug transporters expression in neutrophils and in background cells could be carried out here. Again, any gene with a FPKM value greater than or equal to 1.0 was said to be expressed, and any gene with a value less than 1.0 was not considered expressed. This limit was chosen to maintain consistency with the expression definitions used in the analysis of

drug transporter expression in human neutrophils previously. As for earlier trees, each branch (protein) on the tree was annotated with its expression status in both neutrophils and background cells; in both cases, a black box meant that the gene was expressed, whilst a white box meant that the gene was not expressed.

This enabled production of annotated phylogenetic trees for SLC (Figure 37) and ABC (Figure 38) transporter proteins in zebrafish larval neutrophils, in both circular and unrooted display modes, as utilised for the human neutrophil data. Like in the human trees, the branches in the zebrafish trees did not correspond to genetic distance; trees containing proportional branch lengths were also generated for both SLC (Appendix 10.6.1) and ABC (Appendix 10.6.2) families. Scalable electronic versions of all the phylogenetic trees produced were also made available online.<sup>386</sup>

**a**

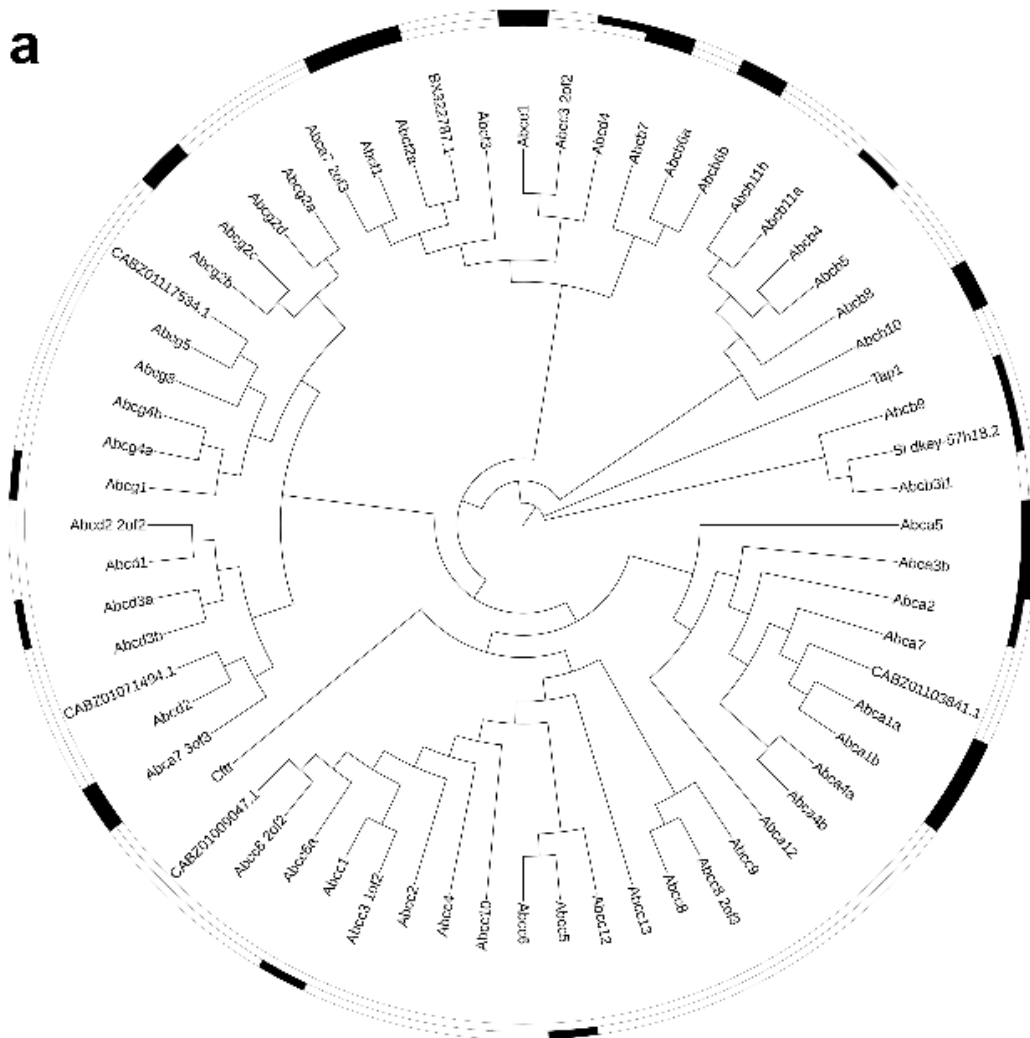




**Figure 38. Zebrafish larval neutrophils and non-neutrophil cells expressed distinct subsets of SLC transporter proteins.**

Annotated phylogenetic trees in both (a) circular and (b) unrooted display modes indicate evolutionary relationships between SLC transporter proteins in zebrafish (branch lengths not proportional to genetic distance; see Appendix 10.6.1 for trees with proportional branch lengths). In (a), for both neutrophil (inner circle) and background cell (outer circle) expression data, expressed proteins were marked with a black box, whereas proteins not expressed were unmarked.

a



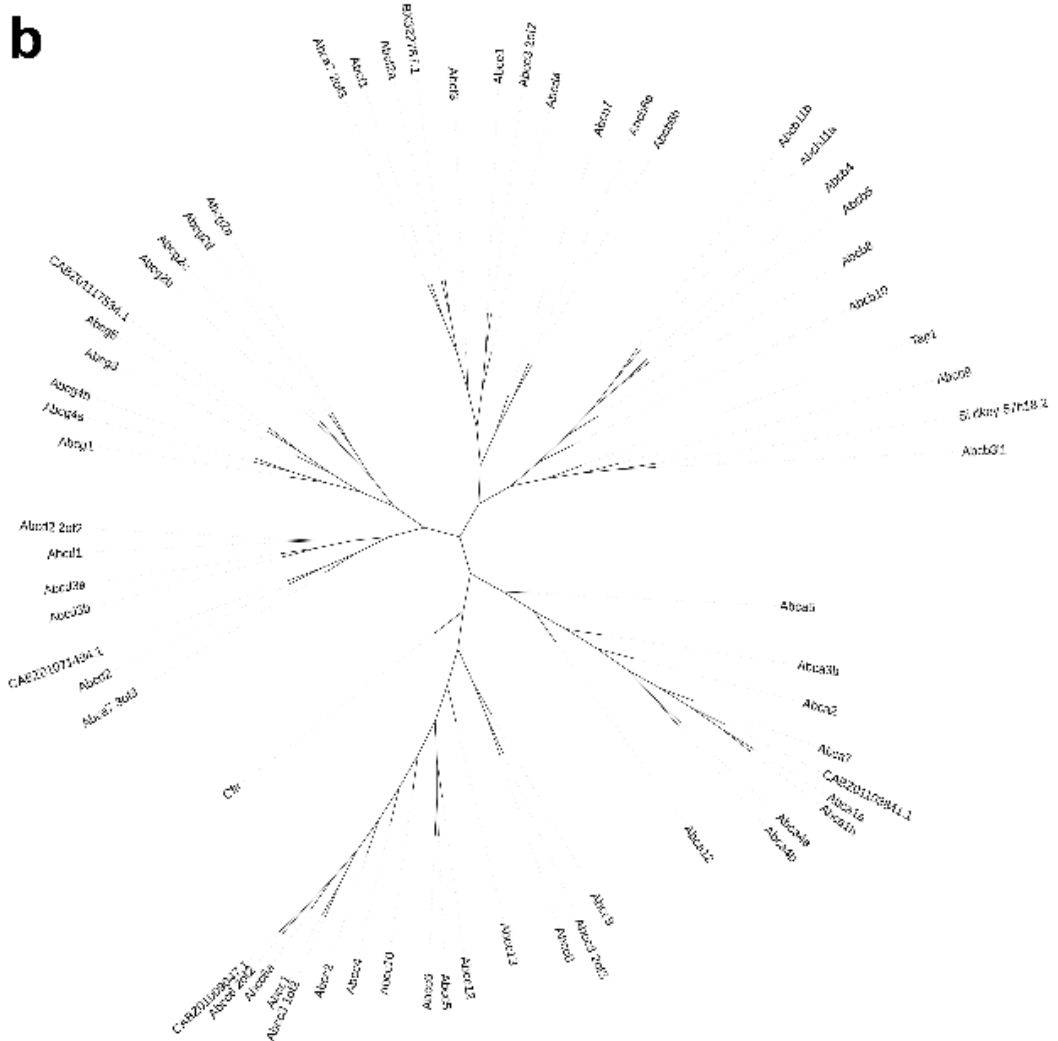


**Figure 39. Zebrafish larval neutrophil and non-neutrophil cells expressed distinct subsets of ABC transporter proteins.**

Annotated phylogenetic trees in both (a) circular and (b) unrooted display modes indicate evolutionary relationships between ABC transporter proteins in zebrafish (branch lengths not proportional to genetic distance; see Appendix 10.6.2 for trees with proportional branch lengths). In (a), for both neutrophil (inner circle) and background cell (outer circle) expression data, expressed proteins were marked with a black box, whereas proteins not expressed were unmarked.

Analysis of the SLC phylogenetic trees (Figure 37) revealed that approximately 27% of the SLC protein-coding genes (142 of 533) were expressed above threshold values in zebrafish larval neutrophils. In non-neutrophil ‘background’ cells, a slightly higher

proportion (41%, 219 of 533) were expressed. Of these, 130 were found to be expressed in both neutrophil and background cells, meaning that 89 were expressed solely in background cells and not in neutrophils. Out of the 142 genes expressed in neutrophils, 12 were only expressed in neutrophils: *slc2a3b*, *slc2a8*, *slc2a12*, *slc2a15a*, *slc3a2\_4of4*, *slc4a2b*, *slc13a1*, *slc13a5b*, *slc34a2b*, *slco3a1*, *rhcgl1*, and *CR352249.1*. This may suggest that some (or all) of these corresponding proteins have specific roles in modulating neutrophil function.

Similar consideration of the ABC phylogenetic trees (Figure 38) found that 25% of the ABC protein-coding genes (16 of 64) were expressed in zebrafish neutrophils at this developmental stage. A similar proportion, 27%, of the ABC genes (17 of 64) were expressed in background cells, and 12 of these were expressed in both neutrophils and background cells. Five genes were expressed only in background cells, and four genes were expressed solely in neutrophils: *abca2*, *abcb4*, *abcb9*, and *si:dkey-57h18.2*. Again, it is possible that the relevant proteins have more neutrophil-specific roles than other ABC transporters.

## 6.6 Comparison of drug transporter expression between human and zebrafish neutrophils

The zebrafish model for study of inflammatory diseases has many advantages, including high homology to humans. Thus, it was hypothesised that there was a level of conservation in the neutrophilic drug transporter expression of these two species. To address this hypothesis, the expression patterns of SLC and ABC transporters in primary human and zebrafish larval neutrophils were compared.

Firstly, the overall proportion of drug transporters expressed in the neutrophils of each species was determined. For the SLC family of transporters, 34% of the total human SLC genes were expressed in human neutrophils, whilst for zebrafish, 27% of the SLC genes were expressed in larval neutrophils. Similarly, for the ABC family, 35% of the ABC genes in humans were expressed in neutrophils, compared to 25% of the ABC genes expressed in zebrafish neutrophils. When the various technical differences between the

datasets were considered, the overall level of drug transporter expression in humans and zebrafish was approximately equal.

In addition, the median SLC and ABC expression values, given as FPKM values, were also compared to the median expression level of all genes identified in the relevant datasets. For the human genes, the median FPKM value for the SLC transporters was 0.22, and for the ABC transporters, this value was 0.34. These values compared with a median FPKM value of 0.26 for the entire set of genes (drug transporters and all other genes) identified across all cells. In the zebrafish dataset, the median FPKM value was 0.16 for SLC transporters and 0.12 for ABC genes, compared with a median of 0.10 for all genes in this set. Thus, within both human and zebrafish neutrophil datasets, the median FPKM values of the SLC and ABC transporter genes were similar both to each other, and to the median expression value of all genes. Comparing between human and zebrafish datasets, the median values were of the same order of magnitude and were reasonably similar, again providing some validation of the approach used here.

Finally, when the set of 134 SLC transporters identified as expressed in human neutrophils were considered, around half of these (65 out of 134, 49%) had at least one orthologous gene in zebrafish which was also expressed in zebrafish neutrophils (see Appendix 10.7.1 for a full list of these genes). Similar analysis for the set of ABC transporters expressed in human neutrophils revealed that the same proportion (8 out of 17, 47%) also had an orthologous gene expressed in zebrafish neutrophils (full list in Appendix 10.7.2). These data again suggested a level of conservation in the expression of SLC and ABC drug transporters in primary human and zebrafish larval neutrophils.

## 6.7 Discussion

Biological evaluation of synthesised TI analogues was carried out in a zebrafish model of inflammation (Chapter 4), and the results from this work indicated that some of the analogues, including TI **1** itself, led to reduced neutrophil recruitment to an injury site, and/or accelerated inflammation resolution. Other analogues appeared to have no effect, and structure-activity relationships for the whole set of data were not entirely straightforward. This was despite the fact that for the synthetic tanshinones, and also

the isotanshinones, only a single change to the parent TI **1** structure or parent isotanshinone I structure **13** was made. Similarly, treatment with lapachones **112-113**, compounds with structural similarity to tanshinones, in the same model led to reduced neutrophil recruitment (Chapter 5). However, these compounds were used at a much lower concentration than the tanshinones, due to toxicity of the lapachones **112-113** at higher concentrations.

There are several possible explanations for these differences in observed activities. Changing the structure of the tanshinones may have led to reduced target specificity, with the modified part of the molecule perhaps interacting differently (or not at all) with a particular protein residue or binding site of the protein target. Alternatively, this structural modification may have perhaps reduced the cell penetration of the compound, and resulted in the molecule no longer being able to cross the cell membrane and enter the neutrophil, or even the larva more generally. Furthermore, changing the structure of the molecule may have increased its cell permeability, which may be one possible explanation for the differing toxicity profiles observed between TI analogues and lapachones. It is now increasingly accepted that drugs mimic the structures of endogenous metabolites and hijack the relevant transporter protein(s) to cross the cell membrane.<sup>357-360</sup> Therefore, it may be that changing the tanshinone structure meant that the modified compound no longer resembled the relevant metabolite sufficiently to be able to hijack the corresponding transporter(s) and enter the neutrophil. Clearly, in order to completely optimise potential drug treatments, and design and synthesise effective compounds which are more likely to reach their target, it is important to understand not only the molecular target of the drug (pharmacodynamics), but also how the drug accesses and penetrates the cell (pharmacokinetics). Knowledge of which protein transporter(s) the drug uses to cross the cell membrane would thus be very useful: if the specific transporter(s) used by the drug was known or determined, then a drug (in this case, a tanshinone) could be designed to optimise cell penetration, thereby increasing the likelihood of a greater quantity of the drug reaching its target and exhibiting a desired effect on inflammation. For this reason, much research has recently been carried out in this area, including into

drug-metabolite likenesses, and how this information can be used more widely to inform future drug design and development.<sup>357–360</sup>

At present, the required software does not exist to be able to quickly and accurately identify the drug transporter protein(s) used by any particular molecule to cross the cell membrane. However, various approaches are being utilised to work towards this goal. In this regard, the work on drug transporters herein was carried out to provide a useful resource to the field. Prior to this work, identification of the drug transporters present in neutrophils of both humans and zebrafish larvae had not been carried out. Identification of the drug transporters in human neutrophils which were significantly up- or down-regulated in the presence of inflammatory stimuli such as TNF $\alpha$  or GM-CSF may indicate that these transporters play a particular role in the inflammatory response. Similarly, transporters enriched in zebrafish neutrophils compared to non-neutrophil (background) cells may suggest that these transporters are particularly important in coordinating neutrophil function and response. This may contribute towards explaining relative activities exhibited by different compounds on neutrophils in the zebrafish model.

One limitation of the zebrafish expression data used here is that these data corresponded to zebrafish larvae at an early stage of development (5 dpf), and such expression is likely to change as zebrafish mature. Nevertheless, these data were useful in allowing overall examination of transporter expression in zebrafish neutrophils at a stage of development commonly used in zebrafish models of disease, including the zebrafish model of inflammation already used in this work (Chapters 4 and 5).

Human neutrophil proteomic datasets were also analysed to compare identification of SLC and ABC transporter proteins to these analyses, and this found that only a small fraction of proteins were identified in the mass spectrometric studies. This represented a substantial difference between the approaches, and perhaps highlights how current proteomics datasets are somewhat incomplete. Indeed, a published comparison of some of these datasets showed the vast differences between human neutrophil protein samples:<sup>380</sup> the studies analysed detected a combined total of 1895 proteins, with overlap ranging from 4% to 40% - this is only a small subset of the total number of

proteins in neutrophils. This is possibly because proteomic analysis of neutrophils is notoriously difficult due to the large numbers of proteases within the cell, and the stochastic nature of protein mass spectrometry, including technical limits in sensitivity of protein detection. Thus, whilst mRNA expression and protein expression themselves may not always correlate, differences in datasets obtained *via* different approaches may be exacerbated due to these practical limitations. Furthermore, ongoing development of more advanced proteomics methods continues to reveal more identified proteins in cells such as neutrophils; a recent proteomics study identified over 7000 proteins in human neutrophils, including 89 SLC and 19 ABC proteins.<sup>390</sup> Future work in this area might continue analysis of these more recent datasets, alongside further development and utilisation of different proteomics methods to give further insight into the expression of drug transporter proteins in neutrophils, and indeed other cell types of interest.

A more detailed knowledge of the relative expressions of drug transporters in various organisms and cells of interests will certainly be of wider use to the field. For example, large compound screens are often carried out successfully using organisms such as zebrafish, to identify new molecules which could potentially become future drugs.<sup>36,90,115,119</sup> However, such screens can overlook particular compounds which may in fact be effective, due to the 'false negative' rates of these methods.<sup>391</sup> It is possible that such compounds are effective once they reach their intracellular target, but simply may not be able to reach this target; this may be due to differential drug transporter expression.

In addition, in both the human and zebrafish datasets, resting neutrophils (rather than inflammatory neutrophils) were studied. In the human dataset, some transporters showed regulation in the presence of an inflammatory stimulus, perhaps suggesting that transporter expression may be modified in inflammatory states. However, extracting neutrophils from inflammatory sites is technically complex, particularly in zebrafish, and may represent a limitation of this work.

Looking forward, experiments which could make use of these resources might involve identification of the SLC and ABC transporters used by particular metabolites. This

knowledge could then inform compound design to more closely mimic metabolites, where possible. *In silico* comparison of drugs and their metabolite-likenesses would help to form hypotheses of potential transporters which could be tested in the zebrafish model. One possible experimental approach would be to mutate a family of SLC transporters using CRISPR/Cas9 genome editing, or use CRISPR interference (CRISPRi), which would allow a greater number of transporters to be screened.<sup>392,393</sup> The effect of this change on drug penetration into neutrophils or zebrafish larvae could then be determined, using a well-defined phenotypic readout. There is not currently a model system for rational dissection of drug transporters and their effects on inflammation, but it is anticipated that these resources will provide the first step towards constructing such a system *in vivo*. It is hoped that this, in turn, would help towards optimising potential drug treatments, such as tanshinones, working towards identification of new, effective clinical treatments for inflammatory diseases.

## 7. Discussion

In this work, an improved synthetic route was used to synthesise TI **1**, the isomer iso-TI **13**, and a set of analogues based on both of these compounds, in six steps starting from 5-bromovanillin **27** and various phenyl-substituted carboxylic acids **75**, **80**, **82-84**. An acetal variant of TI **109** which lacked the characteristic *ortho*-quinone functionality was also synthesised from TI **1**, to explore the importance of this functional group for *in vivo* anti-inflammatory activity. Synthesis towards TIIA **2** and related analogues was attempted using a key Diels-Alder reaction to assemble the tanshinone framework, and although this reaction worked with dienes of varying reactivity, low mass returns and purification issues limited further study of reaction products. Furthermore, two lapachones **112-113**, with structural similarity to tanshinones, were synthesised from the natural product lapachol **114** and its homologue norlapachol **115**.

Biological evaluation of these compounds *in vivo* using a zebrafish model of inflammation was undertaken, to investigate the effects of these compounds on neutrophil recruitment and resolution stages of the inflammatory response. This revealed that, at an aqueous concentration of 25  $\mu$ M, the parent compounds TI **1** and iso-TI **13** both reduced initial neutrophil recruitment to a site of injury, and accelerated resolution of neutrophilic inflammation, whilst analogous compounds lacking the methyl group at the 6- or 4-position respectively had no effect on either process. Tanshinones and isotanshinones with other substituents had various effects, and structure-activity relationships arising from these results could not be completely clearly defined, although some interesting trends were observed. In particular, 6-methoxy-TI **104** accelerated resolution of neutrophilic inflammation yet did not affect initial neutrophil recruitment. This may make this compound a more attractive candidate for investigation as a pro-resolution therapeutic, since compounds which accelerate resolution without affecting recruitment are more likely to function without compromising host-defence, an important justification for the study of both neutrophil recruitment and resolution. The TI acetal **109** also exhibited some *in vivo* activity, although it was not clear whether this was as a function of the compound itself, or as a result of *in vivo* hydrolysis and metabolism. Evaluation of the lapachones **112-113** was

carried out at a concentration of 1  $\mu$ M, as larval toxicity was observed at higher doses, despite the structural similarity of these compounds to tanshinones. Lapachones **112-113** resulted in reduced numbers of recruited neutrophils to the site of injury, yet did not affect resolution. Norlapachol **115** also reduced neutrophil recruitment and accelerated inflammation resolution at higher doses, yet the homologous lapachol **114** had no effect on recruitment or resolution.

Thus, making small point changes to the tanshinone structure did not affect their toxicity, yet affected their biological activity, giving rise to non-trivial structure-activity relationships. The equivalent isotanshinones, in which two of the aromatic rings were kept the same, and the other two were oriented differently, with a *para*-quinone instead of an *ortho*-quinone, were also non-toxic and exhibited some structure-activity relationships. Evaluation of lapachones **112-113** allowed the effect of making broader changes to the tanshinone structure to be explored: the middle two rings of the tanshinone framework were kept the same, whilst the additional phenyl ring was removed completely, and the furan ring dearomatised. This had a substantial effect on the toxicity of the compounds, which were consequently evaluated at a much lower dosage than for tanshinones. The evaluated lapachones **112-113** exhibited some effects in reducing neutrophil recruitment, yet did not affect resolution of neutrophilic inflammation at this concentration. This may suggest that retention of the core *ortho*-quinone moiety of tanshinones was sufficient to retain effects on neutrophil recruitment, yet these broader changes were detrimental to pro-resolution activity.

In addition to those provided by use of zebrafish models in general, the zebrafish model for inflammatory disease presented several advantages, including the reliable and replicable modelling of acute, spontaneously resolving inflammation in living organisms. Synthesised compounds were evaluated for *in vivo* biological effects in this model at an early stage of the drug discovery and development process, which allowed efficacious compounds to be identified (and possibly prioritised for future studies). Going forward, such compounds could be tested for effects on human neutrophils, in a similar manner to that undertaken for TIIA **2** previously.<sup>36</sup> Any compounds which also exhibited observable effects on human neutrophils would be of particular interest,

having shown both *in vivo* and *in vitro* efficacy, with translatable activity. Another advantage of the zebrafish model of inflammation is that compound toxicity can be detected quickly, using various methods such as analysis of tail shape, circulation, and heartbeat. Toxicity was observed for the lapachones **112-113** and lapachols **114-115** at certain doses, in contrast to the tanshinones and isotanshinones at the same concentrations, which exhibited no observable toxicity. This raised interesting questions about why these differences in safety profiles existed, despite the respective compounds bearing many structural similarities. These data indicated that the presence of the furan ring and the additional phenyl ring likely contributed to the compounds' lack of toxicity. This may have been due to differences in pharmacokinetics (how the compounds accessed their molecular target, for example due to differences in cell membrane permeability), pharmacodynamics (differences in target interaction and/or binding), or both. Detection of both compound efficacy and toxicity at this early stage of drug development is highly advantageous, as lack of efficacy and safety concerns are two of the most common reasons for attrition in the drug discovery and development process in the pharmaceutical industry.<sup>95-98</sup>

Use of the zebrafish model was an effective phenotypic screening approach for identification of tanshinones, isotanshinones, and structurally similar compounds which exhibited anti-inflammatory effects *in vivo*. Manipulation of either the initial neutrophil recruitment or resolution of neutrophilic inflammation stages of the inflammatory response as a result of treatment with any of these synthetic tanshinone analogues was easily visualised. However, the molecular mechanism and target(s) of these tanshinone analogues in achieving these effects was not known. Furthermore, the route taken by these compounds through the zebrafish larvae to reach their cellular target was not known. An improved understanding of both of these processes would enable further drug optimisation and development to be undertaken.

To address broad gaps in knowledge regarding drug transport, and to work towards exploration of how molecules such as tanshinones reach their molecular target in neutrophils, identification and analysis of the SLC and ABC drug transporters expressed in primary human and zebrafish larval neutrophils was carried out. This resulted in

corresponding phylogenetic trees which were presented as useful resources to the wider field. The data indicated that approximately one third of all known SLC and ABC drug transporters were expressed in human neutrophils, and one quarter of identified SLC and ABC transporters were expressed in zebrafish neutrophils. Drug transporter expression profiles exhibited a good level of conservation between human and zebrafish neutrophils, consistent with the high gene homology between zebrafish and humans more generally, another important advantage of the use of zebrafish models. In addition to representing a general resource, this work identified a number of drug transporters expressed in both primary human and zebrafish larval neutrophils, some of which are likely used by tanshinones to cross the neutrophil cell membrane and reach their cellular target. Further studies in this area would ideally work towards acquiring knowledge of which particular drug transporters are used by tanshinones (and more widely, any particular drug) to access, and later be removed from, the neutrophil (or other cell types of interest). This would enable more targeted rational design in the drug discovery and development process.

The zebrafish model for inflammatory disease is not without its limitations. Firstly, automation of the *in vivo* experiments undertaken in this work would not be trivial, especially as operations such as tailfin injury need to be performed manually. Although some work in this area has been carried out previously, scaling this process up to analyse large numbers of larvae for many different compounds and concentrations would be difficult. Furthermore, zebrafish larvae were used at an early stage of development, both for *in vivo* experiments and drug transporter analysis, and this may not provide a completely accurate representation of inflammatory conditions or drug transporter expression, either in older zebrafish or in human patients. Using this model, acute and spontaneously resolving inflammation was investigated; different effects may be observed for chronic and/or non-resolving inflammation, and these types of inflammation are often more clinically relevant. In addition, some compounds which were actually active at the relevant biological target may not have been identified, due to inefficient penetration of the neutrophil, or the larva more generally, although this may mean that compounds which were identified were particularly effective. There are

also difficulties in translating some of the zebrafish experimental approaches used across into human studies. Nonetheless, the advantages of using this *in vivo* model for inflammatory disease far outweigh the limitations, and in conjunction with other approaches such as *in vitro* studies using human neutrophils, this is a powerful model for the identification and development of potential new anti-inflammatory therapeutics.

In addition to experimental approaches suggested already, future studies could include *in silico* approaches. There are a number of readily available pieces of software which allow prediction of likely protein targets of a particular compound, simply upon input of the compound structure: tanshinones could be input into such software, to compile a list of possible molecular targets. Some of these targets would likely be more relevant to inflammatory processes than others, and as such could be prioritised for further study. Although these pieces of software are unlikely to be comprehensive, or indeed entirely accurate, they may be useful to complement ongoing approaches. This could be combined with other approaches such as molecular docking, RNAseq data, and microarrays, and could also be carried out in conjunction with practical approaches including *in vitro* studies, knockdown experiments for possible targets, mass spectrometry techniques such as phosphoproteomics or thermal shift profiling, and/or methods involving further functionalised analogues, such as photoaffinity labelling. A combination of these approaches, perhaps alongside more specific zebrafish studies, would likely aid identification of a detailed molecular mechanism of action for tanshinones.

Overall, this work has provided further insight into the *in vivo* anti-inflammatory activities of tanshinones more widely, including various analogues and isomers, as well as structurally related molecules. The data and observations from these experiments, alongside the drug transporter expression data for both human and zebrafish neutrophils, have resulted in progress towards identification of effective, non-toxic compounds which might eventually be used in the clinic as anti-inflammatory compounds, and ideally for promoting the resolution of inflammation *in vivo*.

## 8. Experimental

### 8.1 General

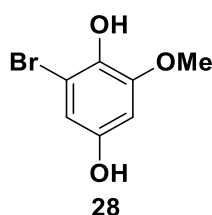
All non-aqueous reactions were carried out in flame-dried glassware and in anhydrous solvents, unless stated otherwise. Anhydrous solvents were obtained from The University Of Sheffield Department of Chemistry Grubbs solvent system. All chemicals used were purchased from commercial suppliers. Propanal **57** was distilled immediately before use. *para*-Benzoquinone **32** was triturated with DCM before use. Dicyclopentadiene **143** was freshly cracked and distilled to provide pure cyclopentadiene **127** which was used immediately. All other reagents were used as received without further purification.

Melting points were determined using a Gallenkamp melting point apparatus equipped with a thermometer. IR spectroscopy was performed on a PerkinElmer FT-IR Spectrum 65 or Spectrum 100 spectrometer, using either NaCl discs or a Universal diamond ATR. <sup>1</sup>H, <sup>13</sup>C and <sup>19</sup>F NMR experiments were run on either a Bruker Avance 400 or Bruker Avance III HD 500 spectrometer at 298 K. Chemical shifts ( $\delta$ ) are reported in parts per million (ppm) relative to the deuterated lock solvent as an internal standard, where s = singlet, d = doublet, t = triplet, q = quartet, m = multiplet, br s = broad singlet, br d = broad doublet, br t = broad triplet, app d = apparent doublet, app t = apparent triplet, dd = doublet of doublets, ddd = double doublet of doublets, td = triplet of doublets, qd = quartet of doublets, dq = doublet of quartets. All coupling constants are reported in hertz, Hz. Mass spectrometry was carried out on either an Agilent Technologies 6530 or 7200 spectrometer, using either electron impact (EI) or electrospray ionisation (ESI).

TLC was performed on Merck silica gel 60 F<sub>254</sub> aluminium-backed plates and visualised using ultraviolet light followed by staining with potassium permanganate dip. Column chromatography was carried out using silica gel obtained from VWR Chemicals, particle size 40-63  $\mu$ m. Reactions using microwave conditions were carried out on a CEM Corporation Discover S-class microwave synthesiser, at pressure  $\leq$  17 bar and power  $\leq$  200 W. Reactions using ultrasonication conditions were performed in an Ultrawave U50 ultrasonic cleaning bath, at a power of 50 W and an operating frequency of 50-60 Hz.

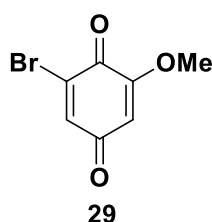
## 8.2 Synthesis of TI analogues and iso-TI analogues

### 2-Bromo-6-methoxy-1,4-hydroquinone (**28**)



Sodium percarbonate (18.71 g, 119.2 mmol) was added to a solution of 5-bromovanillin **27** (25.03 g, 108.4 mmol) in THF (300 mL) and water (120 mL) and stirred at room temperature for 5 h. The reaction was quenched with sodium sulfite (15.00 g), filtered, and concentrated *in vacuo*. The organic product was extracted with ethyl acetate (3 x 300 mL), dried (MgSO<sub>4</sub>), filtered and concentrated *in vacuo* to give the hydroquinone **28** (20.34 g, 86%) as a grey solid which was used without further purification; mp 142-146 °C (lit.<sup>212</sup> 139-141 °C);  $\delta_{\text{H}}$ [400 MHz; (CD<sub>3</sub>)<sub>2</sub>CO] 8.13 (1 H, s, OH), 7.57 (1H, s, OH), 6.59 (1 H, d, *J* 2.6, ArCH), 6.50 (1 H, d, *J* 2.6, ArCH), 3.82 (3 H, s, OCH<sub>3</sub>);  $\delta_{\text{C}}$ [100 MHz; (CD<sub>3</sub>)<sub>2</sub>CO] 150.7 (ArC), 148.7 (ArC), 137.3 (ArC), 110.0 (ArCH), 108.1 (ArC), 99.6 (ArCH), 55.6 (OCH<sub>3</sub>). All data were in agreement with the literature.<sup>212</sup>

### 2-Bromo-6-methoxy-[1,4]-benzoquinone (**29**)



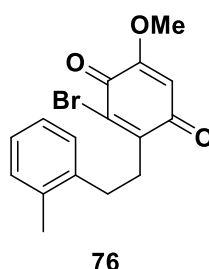
A solution of iron(III) chloride hexahydrate (125.4 g, 463.9 mmol) in water (600 mL) was added to a solution of 2-bromo-6-methoxy-1,4-hydroquinone **28** (20.32 g, 92.77 mmol) in methanol (80 mL) with stirring. The resulting mixture was stirred at room temperature for 5 h. The organic layer was separated and extracted with DCM (3 x 250 mL), combined, washed with water (500 mL) and brine (500 mL), dried (MgSO<sub>4</sub>), filtered and concentrated *in vacuo* to give the benzoquinone **29** (19.84 g, 99%) as an orange solid which was used without further purification; mp 152-156 °C (lit.<sup>212</sup> 160-162 °C);

$\delta_{\text{H}}$ (400 MHz;  $\text{CDCl}_3$ ) 7.23 (1 H, d,  $J$  2.2,  $\text{CHCO}$ ), 5.98 (1 H, d,  $J$  2.2,  $\text{CHCO}$ ), 3.88 (3 H, s,  $\text{OCH}_3$ );  $\delta_{\text{C}}$ (100 MHz;  $\text{CDCl}_3$ ) 184.7 (C), 174.6 (C), 158.3 (C), 138.5 (=CH), 134.3 (C), 107.7 (=CH), 56.9 ( $\text{OCH}_3$ ). All NMR data were in agreement with the literature.<sup>212</sup>

### General representative procedure A for radical decarboxylative alkylation reactions to form bromides **76**, **81**, **85-87**

A mixture of the quinone **29** (2.00 g, 9.26 mmol), carboxylic acid **75**, **80**, **82-84** (11.1 mmol) and silver(I) phosphate (1.94 g, 4.63 mmol) in acetonitrile (70 mL) was stirred under a nitrogen atmosphere in the dark and heated at reflux. A solution of ammonium persulfate (4.23 g, 18.5 mmol) in water (70 mL) was added slowly over 20 minutes *via* dropping funnel, and the resulting mixture was stirred at reflux for 2.5 h. The solution was cooled to room temperature and poured onto ice (50 g). Aqueous NaOH (1 M, 10 mL) and water (50 mL) were added and the organic layer was separated and extracted with DCM (3  $\times$  150 mL). The organic extracts were combined, washed with brine (400 mL), dried ( $\text{MgSO}_4$ ), filtered and concentrated *in vacuo* to give the crude product, which was purified by flash column chromatography (silica gel, DCM) to give the bromides **76**, **81**, **85-87**.

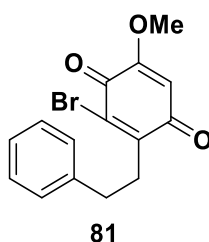
### 3-Bromo-5-methoxy-2-[2-(2-methylphenyl)ethyl]-2,5-cyclohexadiene-1,4-dione (**76**)



General procedure **A** was followed, using the carboxylic acid **75** (1.82 g), to give the bromide **76** (1.67 g, 54 %) as a yellow solid; mp 179-184 °C (lit.<sup>211</sup> mp 149-152 °C);  $\delta_{\text{H}}$ (400 MHz;  $\text{CDCl}_3$ ) 7.24-7.14 (4 H, m, 4  $\times$   $\text{ArCH}$ ), 5.99 (1 H, s,  $\text{CHCO}$ ), 3.88 (3 H, s,  $\text{OCH}_3$ ), 2.98-2.92 (2 H, m,  $\text{CH}_2$ ), 2.82-2.76 (2 H, m,  $\text{CH}_2$ ), 2.45 (3 H, s,  $\text{ArCH}_3$ );  $\delta_{\text{C}}$ (100 MHz;  $\text{CDCl}_3$ ) 183.7 (C=O), 174.8 (C=O), 158.3 (C), 149.0 (C), 138.6 (C), 136.2 (C), 133.2 (C), 130.4 ( $\text{ArCH}$ ), 129.1 ( $\text{ArCH}$ ), 126.6 ( $\text{ArCH}$ ), 126.2 ( $\text{ArCH}$ ), 107.4 ( $\text{CHCO}$ ), 56.7 ( $\text{OCH}_3$ ), 32.0 ( $\text{CH}_2$ ), 31.3

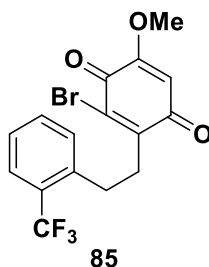
(CH<sub>2</sub>), 19.3 (CH<sub>3</sub>). All NMR data were in agreement with the literature.<sup>211</sup> Two individual measurements performed for the melting point of this compound here indicated that it was around 30 °C higher than that reported in the literature, perhaps due to the production of a more pure compound in this case.

### 3-Bromo-5-methoxy-2-(2-phenylethyl)-2,5-cyclohexadiene-1,4-dione (**81**)



General procedure **A** was followed, but on a larger scale, using the quinone **29** (3.00 g, 13.9 mmol), the carboxylic acid **80** (2.50 g, 16.7 mmol) and silver(I) phosphate (4.82 g, 11.5 mmol) in acetonitrile (150 mL), and ammonium persulfate (6.34 g, 27.8 mmol) in water (100 mL), to give the bromide **81** (2.04 g, 46%) as a yellow solid; mp 138-141 °C (lit.<sup>211</sup> 138-140 °C);  $\delta_{\text{H}}$ (400 MHz; CDCl<sub>3</sub>) 7.36-7.22 (5 H, m, 5 x ArCH), 5.98 (1 H, s, CHCO), 3.87 (3 H, s, OCH<sub>3</sub>), 3.03-2.97 (2 H, m, CH<sub>2</sub>), 2.83-2.77 (2 H, m, CH<sub>2</sub>);  $\delta_{\text{C}}$ (100 MHz; CDCl<sub>3</sub>) 183.6 (C=O), 174.8 (C=O), 158.3 (C), 149.0 (C), 140.4 (C), 133.3 (C), 128.6 (2 x ArCH), 128.53 (2 x ArCH), 126.5 (ArCH), 107.4 (=CH), 56.8 (OCH<sub>3</sub>), 33.8 (CH<sub>2</sub>), 33.2 (CH<sub>2</sub>). All data were in agreement with the literature.<sup>211</sup>

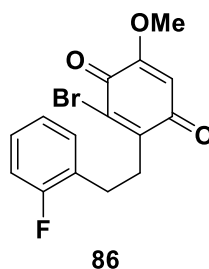
### 3-Bromo-5-methoxy-2-[2-(trifluoromethyl)phenethyl]-2,5-cyclohexadiene-1,4-dione (**85**)



General procedure **A** was followed, using the carboxylic acid **82** (2.42 g), to give the bromide **85** (1.35 g, 38%) as a yellow solid; mp 144-147 °C (lit.<sup>211</sup> 143-145 °C);  $\delta_{\text{H}}$ (400 MHz; CDCl<sub>3</sub>) 7.66 (1 H, d, *J* 7.6, ArCH), 7.52 (1 H, t, *J* 7.6, ArCH), 7.46 (1 H, d, *J* 7.6, ArCH),

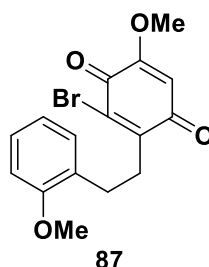
7.35 (1 H, t,  $J$  7.6, ArCH), 6.00 (1 H, s, CHCO), 3.88 (3 H, s, OCH<sub>3</sub>), 3.08-2.95 (4 H, m, 2 x CH<sub>2</sub>);  $\delta_{\text{C}}$ (100 MHz; CDCl<sub>3</sub>) 183.6 (C=O), 174.8 (C=O), 158.3 (C), 148.4 (C), 139.0 (C), 133.6 (C), 131.9 (ArCH), 131.4 (ArCH), 128.6 (q,  $J_{\text{C-F}}$  30.0, ArC), 126.6 (ArCH), 126.0 (q,  $J_{\text{C-F}}$  5.7, ArCH), 124.5 (q,  $J_{\text{C-F}}$  273.6, CF<sub>3</sub>), 107.4 (=CH), 56.7 (OCH<sub>3</sub>), 32.9 (CH<sub>2</sub>), 30.3 (CH<sub>2</sub>). All data were in agreement with the literature.<sup>211</sup>

### 3-Bromo-2-(2-fluorophenethyl)-5-methoxy-2,5-cyclohexadiene-1,4-dione (**86**)



General procedure **A** was followed, using the carboxylic acid **83** (1.87 g), to give the bromide **86** (1.44 g, 46%) as a yellow solid; mp 144-148 °C (lit.<sup>211</sup> 134-137 °C);  $\delta_{\text{H}}$ (400 MHz; CDCl<sub>3</sub>) 7.25-7.19 (2 H, m, 2 x ArCH), 7.11-6.99 (2 H, m, 2 x ArCH), 5.97 (1 H, s, CHCO), 3.87 (3 H, s, OCH<sub>3</sub>), 3.06-2.99 (2 H, m, CH<sub>2</sub>), 2.92-2.85 (2 H, m, CH<sub>2</sub>);  $\delta_{\text{C}}$ (100 MHz; CDCl<sub>3</sub>) 183.6 (C=O), 174.8 (C=O), 161.2 (d,  $J_{\text{C-F}}$  245.4, ArCF), 158.2 (C), 148.6 (C), 133.5 (C), 130.8 (d,  $J_{\text{C-F}}$  4.6, ArCH), 128.3 (d,  $J_{\text{C-F}}$  8.1, ArCH), 127.1 (d,  $J_{\text{C-F}}$  16.2, ArC), 124.1 (d,  $J_{\text{C-F}}$  3.4, ArCH), 115.3 (d,  $J_{\text{C-F}}$  22.0, ArCH), 107.4 (=CH), 56.7 (OCH<sub>3</sub>), 31.5 (CH<sub>2</sub>), 27.2 (CH<sub>2</sub>). All NMR data were in agreement with the literature.<sup>211</sup>

### 3-Bromo-5-methoxy-2-(2-methoxyphenethyl)-2,5-cyclohexadiene-1,4-dione (**87**)



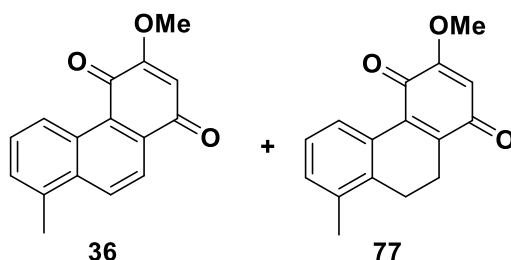
General procedure **A** was followed, using the carboxylic acid **84** (2.00 g), to give an inseparable mixture of the bromide **87** and the benzoquinone **29** (1.07 g) as a yellow solid in a 60:40 ratio which was used without further purification. Analysis of the <sup>1</sup>H NMR

spectrum of this mixture indicated a 33% yield of the bromide **87**. A sample of this mixture was further purified for analytical purposes to give the bromide **87** as a yellow solid; mp 160-163 °C (lit.<sup>211</sup> 161-163 °C);  $\delta_{\text{H}}$ (400 MHz; CDCl<sub>3</sub>) 7.22 (1 H, td, *J* 7.7, 1.6, ArCH), 7.15 (1 H, dd, *J* 7.7, 1.6, ArCH), 6.89 (1 H, td, *J* 7.7, 0.7, ArCH), 6.84 (1 H, d, *J* 7.7, ArCH), 5.96 (1 H, s, CHCO), 3.86 (3 H, s, OCH<sub>3</sub>), 3.84 (3 H, s, OCH<sub>3</sub>), 3.04-2.98 (2 H, m, CH<sub>2</sub>), 2.88-2.82 (2 H, m, CH<sub>2</sub>);  $\delta_{\text{C}}$ (100 MHz; CDCl<sub>3</sub>) 183.7 (C=O), 174.9 (C=O), 158.1 (C), 157.6 (C), 149.6 (C), 132.9 (C), 130.1 (ArCH), 128.7 (C), 127.8 (ArCH), 120.5 (ArCH), 110.2 (ArCH), 107.3 (ArCH), 56.7 (OCH<sub>3</sub>), 55.3 (OCH<sub>3</sub>), 31.4 (CH<sub>2</sub>), 28.7 (CH<sub>2</sub>). All data were in general agreement with the literature.<sup>211</sup>

### General representative procedure B for Heck reactions to form diones **36**, **77**, **88-95**

A solution of the bromide **76**, **81**, **85-87** (2.24 mmol), palladium(II) acetate (25 mg, 0.111 mmol), triphenylphosphine (59 mg, 0.225 mmol) and potassium carbonate (930 mg, 6.73 mmol) in degassed toluene (80 mL mmol<sup>-1</sup>) was heated at reflux in the dark for 17 h under a nitrogen atmosphere, with stirring. The mixture was cooled to room temperature, concentrated *in vacuo*, diluted with water (40 mL mmol<sup>-1</sup>), and extracted with DCM (3 x 40 mL mmol<sup>-1</sup>). The organic extracts were combined, washed with brine (80 mL mmol<sup>-1</sup>), dried (MgSO<sub>4</sub>), filtered and concentrated *in vacuo* to give the crude product which was separated from major impurities by flash column chromatography (silica gel, DCM) to give an inseparable mixture of the fully aromatised and non-aromatised diones **36**, **77**, **88-95**.

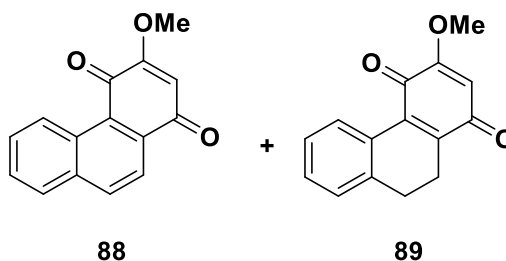
### 3-Methoxy-8-methylphenanthrene-1,4-dione (**36**) and 9,10-dihydro-3-methoxy-8-methylphenanthrene-1,4-dione (**77**)



General procedure **B** was followed, using the bromide **76** (750 mg, 2.24 mmol), to give a bright orange solid (378 mg, 67%) as an inseparable mixture of diones **36** and **77**

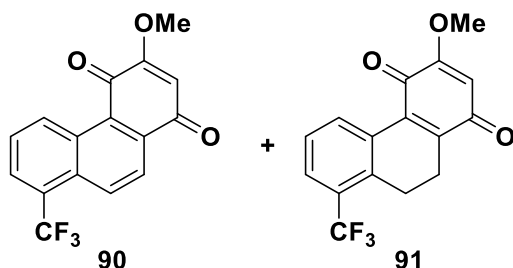
in a 75:25 ratio which was used without further purification. Selected  $^1\text{H}$  NMR data from product mixture corresponding to the dione **36**:  $\delta_{\text{H}}$ (400 MHz;  $\text{CDCl}_3$ ) 9.42 (1 H, d,  $J$  8.8, ArCH), 8.43 (1 H, br d,  $J$  8.8, ArCH), 8.25 (1 H, br d,  $J$  8.8, ArCH), 7.65 (1 H, dd,  $J$  8.8, 6.9, ArCH), 7.50 (1 H, br d,  $J$  6.9, ArCH), 6.17 (1 H, br s, CHCO), 3.97 (3 H, br s,  $\text{OCH}_3$ ), 2.77 (3 H, s,  $\text{CH}_3$ ). All data were in general agreement with the literature.<sup>214</sup> Selected  $^1\text{H}$  NMR data from product mixture corresponding to the dione **77**:  $\delta_{\text{H}}$ (400 MHz;  $\text{CDCl}_3$ ) 7.92-7.86 (1 H, app t,  $J$  4.5, ArCH), 7.23 (2 H, d,  $J$  4.5, ArCH), 5.99 (1 H, br s, CHCO), 3.88 (3 H, br s,  $\text{OCH}_3$ ), 2.79-2.74 (2 H, m,  $\text{CH}_2$ ), 2.74-2.70 (2 H, m,  $\text{CH}_2$ ), 2.36 (3 H, s,  $\text{CH}_3$ ). No data were reported in the literature for this compound.

### 3-Methoxyphenanthrene-1,4-dione (**88**) and 9,10-dihydro-3-methoxyphenanthrene-1,4-dione (**89**)



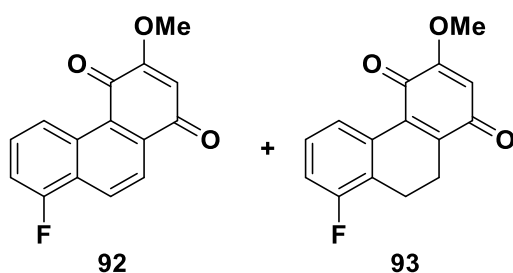
General procedure **B** was followed, using the bromide **81** (200 mg, 0.622 mmol), to give a pale red solid (109 mg, 73%) as an inseparable mixture of diones **88** and **89** in a 96:4 ratio which was used without further purification. Selected  $^1\text{H}$  NMR data from product mixture corresponding to the dione **88**:  $\delta_{\text{H}}$ (400 MHz;  $\text{CDCl}_3$ ) 9.55 (1 H, d,  $J$  8.8, ArCH), 8.20 (2 H, app d,  $J$  1.2, 2 x ArCH), 7.92 (1 H, d,  $J$  8.1, ArCH), 7.77 (1 H, ddd,  $J$  8.8, 6.8, 1.2, ArCH), 7.66 (1 H, ddd,  $J$  8.1, 6.8, 1.2, ArCH), 6.17 (1 H, s, CHCO), 3.96 (3 H, s,  $\text{OCH}_3$ ). All data were in general agreement with the literature.<sup>394,395</sup> Selected  $^1\text{H}$  NMR data from product mixture corresponding to the dione **89**:  $\delta_{\text{H}}$ (400 MHz;  $\text{CDCl}_3$ ) 5.99 (1 H, s, CHCO), 3.88 (3 H, s,  $\text{OCH}_3$ ), 2.83-2.78 (2 H, m,  $\text{CH}_2$ ), 2.76-2.72 (2 H, m,  $\text{CH}_2$ ). No data were reported in the literature for this compound.

**3-Methoxy-8-(trifluoromethyl)phenanthrene-1,4-dione (90) and 9,10-dihydro-3-methoxy-8-trifluoromethyl)phenanthrene-1,4-dione (91)**



General procedure **B** was followed, using the bromide **85** (1.35 g, 3.47 mmol), to give a dark orange solid (500 mg) as an inseparable mixture including diones **90** and **91** in a 65:35 ratio alongside an additional unidentified compound, which was used without further purification. Selected  $^1\text{H}$  NMR peaks from product mixture corresponding to the dione **90**:  $\delta_{\text{H}}$ (400 MHz;  $\text{CDCl}_3$ ) 9.81 (1 H, d,  $J$  8.9, ArCH), 8.59 (1 H, dq,  $J$  8.9, 0.9, ArCH), 8.37 (1 H, d,  $J$  8.9, ArCH), 8.06 (1 H, d,  $J$  7.2, ArCH), 7.86-7.81 (1 H, m, ArCH), 6.23 (1 H, s, CHCO), 3.99 (3 H, s,  $\text{OCH}_3$ ). Selected  $^1\text{H}$  NMR peaks from product mixture corresponding to the dione **91**:  $\delta_{\text{H}}$ (400 MHz;  $\text{CDCl}_3$ ) 5.97 (1 H, s, CHCO), 3.85 (3 H, s,  $\text{OCH}_3$ ), 3.04-2.97 (2 H, m,  $\text{CH}_2$ ), 2.80-2.74 (2 H, m,  $\text{CH}_2$ ). Selected  $^1\text{H}$  NMR peaks from product mixture corresponding to the unidentified compound:  $\delta_{\text{H}}$ (400 MHz;  $\text{CDCl}_3$ ) 6.01(1 H, s, =CH), 3.89 (3 H, s,  $\text{OCH}_3$ ). No data were reported in the literature for these compounds.

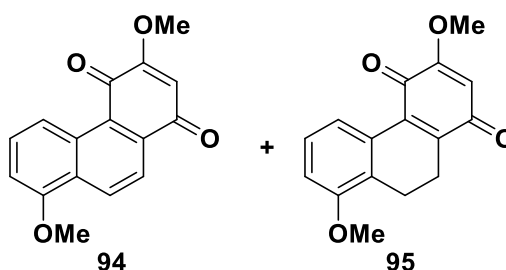
**8-Fluoro-3-methoxyphenanthrene-1,4-dione (92) and 9,10-dihydro-8-fluoro-3-methoxyphenanthrene-1,4-dione (93)**



General procedure **B** was followed, using the bromide **86** (1.34 g, 3.95 mmol), to give a dark orange solid (197 mg) as an inseparable mixture including diones **92** and **93** in an 80:20 ratio alongside an additional unidentified compound, which was used without further purification. Selected  $^1\text{H}$  NMR peaks from product mixture corresponding to the

dione **92**:  $\delta_{\text{H}}$ (400 MHz;  $\text{CDCl}_3$ ) 9.35 (1 H, d,  $J$  8.8, ArCH), 8.54 (1 H, d,  $J$  8.8, ArCH), 8.29 (1 H, d,  $J$  8.8, ArCH), 7.74-7.67 (1 H, m, ArCH), 7.37-7.32 (1 H, m, ArCH), 6.21 (1 H, s, CHCO), 3.98 (3 H, s,  $\text{OCH}_3$ ). Selected  $^1\text{H}$  NMR peaks from product mixture corresponding to the dione **93**:  $\delta_{\text{H}}$ (400 MHz;  $\text{CDCl}_3$ ) 5.95 (1 H, s, =CH), 3.84 (3 H, s,  $\text{OCH}_3$ ), 2.93-2.87 (2 H, m,  $\text{CH}_2$ ), 2.80-2.73 (2 H, m,  $\text{CH}_2$ ). Selected  $^1\text{H}$  NMR peaks from product mixture corresponding to the unidentified compound:  $\delta_{\text{H}}$ (400 MHz;  $\text{CDCl}_3$ ) 6.90 (1 H, s, ArCH), 5.99 (1 H, s, CHCO), 3.88 (3 H, s,  $\text{OCH}_3$ ). No data were reported in the literature for these compounds.

**3,8-Dimethoxyphenanthrene-1,4-dione (94) and 9,10-dihydro-3,8-dimethoxyphenanthrene-1,4-dione (95)**



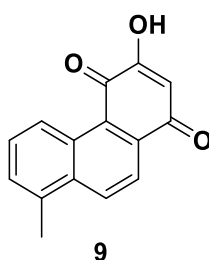
General procedure **B** was followed, using the bromide **87** (1.02 g, 2.91 mmol), to give a red solid (218 mg, 28%) as an inseparable mixture of diones **94** and **95** in an 82:18 ratio which was used without further purification. Selected  $^1\text{H}$  NMR data from product mixture corresponding to the dione **94**:  $\delta_{\text{H}}$ (400 MHz;  $\text{CDCl}_3$ ) 9.10 (1 H, d,  $J$  8.8, ArCH), 8.71 (1 H, d,  $J$  8.8, ArCH), 8.18 (1 H, d,  $J$  8.8, ArCH), 7.66 (1 H, br t,  $J$  8.4, ArCH), 6.98 (1 H, d,  $J$  7.7, ArCH), 6.15 (1 H, s, CHCO), 4.04 (3 H, s,  $\text{OCH}_3$ ), 3.95 (3 H, s,  $\text{OCH}_3$ ). All data were in agreement with the literature.<sup>395</sup> Selected  $^1\text{H}$  NMR data from product mixture corresponding to the dione **95**:  $\delta_{\text{H}}$ (400 MHz;  $\text{CDCl}_3$ ) 5.94 (1 H, s, CHCO), 3.83 (3 H, s,  $\text{OCH}_3$ ), 3.80 (3 H, s,  $\text{OCH}_3$ ), 2.88-2.82 (2 H, m,  $\text{CH}_2$ ), 2.77-2.72 (2 H, m,  $\text{CH}_2$ ). No data were reported in the literature for this compound.

**General representative procedure C for demethylation to form alcohols 9, 30, 96-98**

Aqueous NaOH (2 M, 50 mL  $\text{g}^{-1}$ , 40.0 mmol) was added to a mixture of the fully aromatised and non-aromatised ethers **36, 77, 88-95** (378 mg, 1.50 mmol) in ethanol

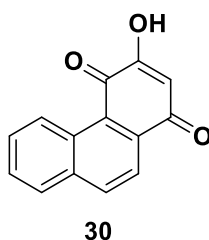
(50 mL g<sup>-1</sup>), and the resulting mixture was stirred at reflux for 1 h. The solution was cooled to room temperature, acidified with aqueous HCl (1 M, 100 mL g<sup>-1</sup>), water was added (50 mL g<sup>-1</sup>), and the solution was extracted with ethyl acetate (3 × 63 mL g<sup>-1</sup>). The organic extracts were combined, washed with brine (250 mL g<sup>-1</sup>), dried (MgSO<sub>4</sub>), filtered and concentrated *in vacuo* to give the alcohols **9**, **30**, **96-98**.

### 3-Hydroxy-8-methylphenanthrene-1,4-dione (**9**)



General procedure **C** was followed, using the mixture of diones **36** and **77** (378 mg, 1.50 mmol) to give the alcohol **9** (347 mg, 97%) as a pale red solid that did not require further purification; mp 208-214 °C (lit.<sup>211</sup> mp 209-212 °C);  $\delta_{\text{H}}$ [400 MHz; (CD<sub>3</sub>)<sub>2</sub>SO] 11.67 (1 H, br s, ArOH), 9.32 (1 H, d, *J* 8.8, ArCH), 8.51 (1 H, d, *J* 8.8, ArCH), 8.12 (1 H, d, *J* 8.8, ArCH), 7.69 (1 H, dd, *J* 8.8, 7.0, ArCH), 7.57 (1 H, d, *J* 7.0, ArCH), 6.15 (1 H, s, CHCO), 2.72 (3 H, s, ArCH<sub>3</sub>);  $\delta_{\text{C}}$ [100 MHz; (CD<sub>3</sub>)<sub>2</sub>SO] 185.5 (C=O), 184.3 (C=O), 160.6 (C), 135.6 (C), 135.1 (C), 132.6 (C), 132.1 (ArCH), 130.4 (ArCH), 130.1 (C), 129.4 (ArCH), 125.8 (C), 125.2 (ArCH), 121.7 (ArCH), 108.4 (ArCH), 19.9 (CH<sub>3</sub>). All data were in general agreement with the literature.<sup>211</sup>

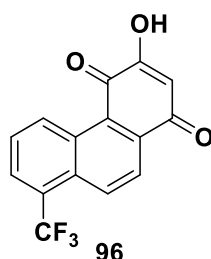
### 3-Hydroxyphenanthrene-1,4-dione (**30**)



General procedure **C** was followed, using the mixture of diones **88** and **89** (222 mg, 0.931 mmol) to give the alcohol **30** (200 mg, 97%) as a dark orange solid which was used

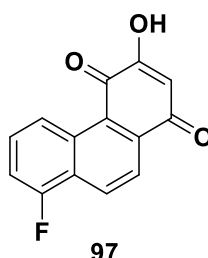
without further purification; mp 199-202 °C (lit.<sup>396</sup> 200 °C);  $\delta_{\text{H}}$ [400 MHz; (CD<sub>3</sub>)<sub>2</sub>CO] 9.83 (1 H, br s, OH), 9.58 (1 H, d, *J* 8.7, ArCH), 8.41 (1 H, d, *J* 8.7, ArCH), 8.19 (1 H, dd, *J* 8.7, 1.7, ArCH), 8.10 (1 H, d, *J* 8.2, ArCH), 7.86-7.80 (1 H, m, ArCH), 7.77-7.71 (1 H, m, ArCH), 6.25 (1 H, d, *J* 1.7, CHCO). All <sup>1</sup>H NMR data were in broad agreement with the literature,<sup>211</sup> although precise values were slightly shifted due to the different solvent used for analysis.

### 3-Hydroxy-8-(trifluoromethyl)phenanthrene-1,4-dione (96)



General procedure **C** was followed, using the mixture of diones **90** and **91** (500 mg) to give the crude alcohol **96** (447 mg) as an orange solid which could not be purified further by either flash column chromatography or recrystallisation. Selected peaks from <sup>1</sup>H NMR spectrum of crude material corresponding to the alcohol **96**:  $\delta_{\text{H}}$ [400 MHz; (CD<sub>3</sub>)<sub>2</sub>CO] 9.89 (1 H, d, *J* 9.0, ArCH), 8.64 (1 H, br d, *J* 9.0, ArCH), 8.40 (1 H, d, *J* 9.0, ArCH), 8.21 (1 H, d, *J* 7.3, ArCH), 8.00-7.94 (1 H, m, ArCH), 6.31 (1 H, s, CHCO). All <sup>1</sup>H NMR data were in broad agreement with the literature,<sup>211</sup> although precise values were slightly shifted due to the different solvent used for analysis.

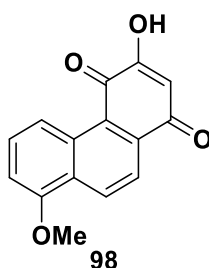
### 8-Fluoro-3-hydroxyphenanthrene-1,4-dione (97)



General procedure **C** was followed, using the mixture of diones **92** and **93** (194 mg) to give the crude alcohol **97** (170 mg) as a dark red solid which could not be purified

further by either flash column chromatography or recrystallisation. Selected peaks from  $^1\text{H}$  NMR spectrum of crude material corresponding to the alcohol **97**:  $\delta_{\text{H}}$ [400 MHz;  $(\text{CD}_3)_2\text{CO}$ ] 9.95 (1 H, br s, OH), 9.40 (1 H, d,  $J$  8.8, ArCH), 8.60 (1 H, d,  $J$  8.8, ArCH), 8.29 (1 H, d,  $J$  8.8, ArCH), 7.86-7.79 (1 H, m, ArCH), 7.51 (1 H, ddd,  $J$  10.4, 7.8, 0.7, ArCH), 6.28 (1 H, s, CHCO). All  $^1\text{H}$  NMR data were in broad agreement with the literature,<sup>211</sup> although precise values were slightly shifted due to the different solvent used for analysis.

### 3-Hydroxy-8-methoxyphenanthrene-1,4-dione (**98**)



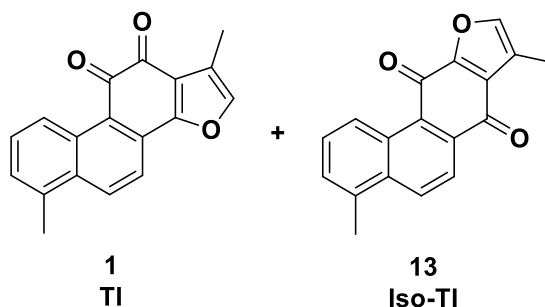
General procedure **C** was followed, using the mixture of diones **94** and **95** (218 mg, 0.813 mmol) to give the alcohol **98** (192 mg, 93%) as a dark red solid which was used without further purification; mp 204-207 °C (lit.<sup>211</sup> 185-187 °C);  $\nu_{\text{max}}$ (NaCl discs)/ $\text{cm}^{-1}$  3281 (O-H), 1657 (C=O), 1634 (C=O), 1582 (C=C);  $\delta_{\text{H}}$ [400 MHz;  $(\text{CD}_3)_2\text{SO}$ ] 11.65 (1 H, br s, OH), 8.97 (1 H, d,  $J$  8.8, ArCH), 8.59 (1 H, d,  $J$  8.8, ArCH), 8.02 (1 H, d,  $J$  8.8, ArCH), 7.70 (1 H, t,  $J$  7.8, ArCH), 7.15 (1 H, d,  $J$  7.8, ArCH), 6.13 (1 H, s, CHCO), 4.00 (3 H, s,  $\text{OCH}_3$ ). IR spectroscopy data were not reported in the literature. All other spectroscopic data were in agreement with the literature.<sup>211</sup>

### General representative procedure **D** for reactions with chloroacetone to form tanshinones **1**, **31**, **100**, **102**, **104** and isotanshinones **13**, **99**, **101**, **103**, **105**

A mixture of the alcohol **9**, **30**, **96-98** (100 mg, 0.42 mmol), ammonium acetate (32 mg, 0.42 mmol, 4 mmol  $\text{g}^{-1}$ ) and chloroacetone (10 mL  $\text{g}^{-1}$ , 12 mmol) was heated in a sealed tube at 110 °C for 15 minutes under microwave conditions. The solution was cooled to room temperature, diluted with water (400 mL  $\text{g}^{-1}$ ) and extracted with DCM (3 x 400 mL  $\text{g}^{-1}$ ). The organic extracts were combined, dried ( $\text{MgSO}_4$ ), filtered and concentrated *in vacuo* to give the crude mixture which was purified by flash column

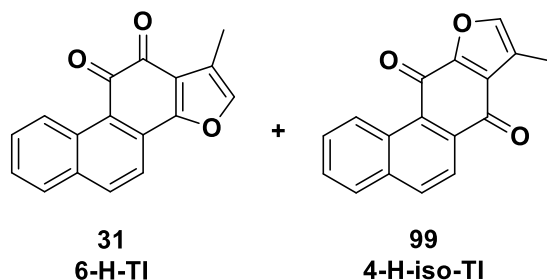
chromatography (silica gel, DCM) to give the tanshinones **1**, **31**, **100**, **102**, **104** and isotanshinones **13**, **99**, **101**, **103**, **105**.

**1,6-Dimethylphenanthro[1,2-*b*]furan-10,11-dione, TI (1) and 4,8-dimethylphenanthro[3,2-*b*]furan-7,11-dione, iso-TI (13)**



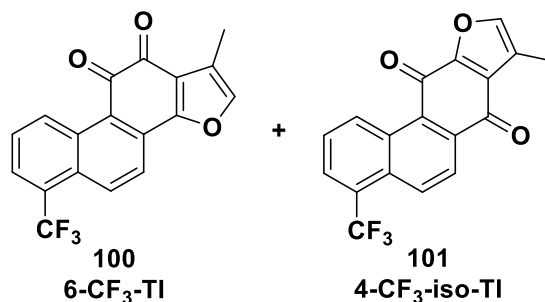
General procedure **D** was followed, using the alcohol **9** (100 mg, 0.42 mmol) to give the dione **1** (21 mg, 18%) as a dark red solid; mp 232-234 °C (lit.<sup>204</sup> 229-230 °C);  $\delta_{\text{H}}$ (400 MHz; CDCl<sub>3</sub>) 9.23 (1 H, d, *J* 8.8, ArCH), 8.27 (1 H, d, *J* 8.8, ArCH), 7.77 (1 H, d, *J* 8.8, ArCH), 7.54 (1 H, dd, *J* 8.8, 7.1, ArCH), 7.34 (1 H, d, *J* 7.1, ArCH), 7.30 (1 H, s, OCH), 2.68 (3 H, s, CH<sub>3</sub>), 2.30 (3 H, d, *J* 0.8, CH<sub>3</sub>);  $\delta_{\text{C}}$ (100 MHz; CDCl<sub>3</sub>) 183.4 (C=O), 175.6 (C=O), 161.2 (ArC), 142.0 (ArCH), 135.2 (ArC), 133.6 (ArC), 132.9 (ArCH), 132.7 (ArC), 130.7 (ArCH), 129.6 (ArC), 128.3 (ArCH), 124.8 (ArCH), 123.1 (ArC), 121.8 (ArC), 120.5 (ArC), 118.7 (ArCH), 19.9 (CH<sub>3</sub>), 8.8 (CH<sub>3</sub>); *m/z* (ESI<sup>+</sup>) 299 (10%, M+Na<sup>+</sup>), 277 (100, M+H<sup>+</sup>). All data were in general agreement with the literature.<sup>204,211,258</sup> Also obtained was the dione **13** (22 mg, 19%) as an orange solid; mp 218-220 °C (lit.<sup>203</sup> 219-220 °C);  $\nu_{\text{max}}$ (ATR)/cm<sup>-1</sup> 1655 (C=O), 1588 (C=O), 1533 (C=C);  $\delta_{\text{H}}$ (400 MHz; CDCl<sub>3</sub>) 9.66 (1 H, d, *J* 8.9, ArCH), 8.40 (1 H, dd, *J* 8.9, 0.8, ArCH), 8.32 (1 H, d, *J* 8.9, ArCH), 7.63 (1 H, dd, *J* 8.9, 7.0, ArCH), 7.54-7.52 (1 H, m, OCH), 7.48 (1 H, dt, *J* 7.0, 0.8, ArCH), 2.76 (3 H, s, ArCH<sub>3</sub>), 2.41 (3 H, d, *J* 1.2, CH<sub>3</sub>);  $\delta_{\text{C}}$ (101 MHz; CDCl<sub>3</sub>) 182.2 (C=O), 177.2 (C=O), 153.9 (ArC), 145.2 (ArCH), 136.0 (ArC), 134.7 (ArC), 133.5 (ArC), 131.2 (ArC), 131.0 (ArCH), 129.8 (ArCH), 129.3 (ArCH), 127.2 (ArC), 126.5 (ArC), 126.2 (ArCH), 122.1 (ArCH), 120.9 (ArC), 20.0 (CH<sub>3</sub>), 8.8 (CH<sub>3</sub>); *m/z* (ESI<sup>+</sup>) 299 (25%, M+Na<sup>+</sup>), 277 (100, M+H<sup>+</sup>). No <sup>13</sup>C NMR spectroscopy data were reported in the literature; all other data were in general agreement with the literature.<sup>203,204,259</sup>

**1-Methylphenanthro[1,2-*b*]furan-10,11-dione, 6-H-TI (31) and 8-methylphenanthro[3,2-*b*]furan-7,11-dione, 4-H-iso-TI (99)**



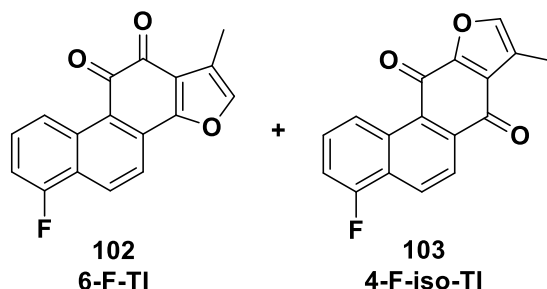
General procedure **D** was followed, using the alcohol **30** (100 mg, 0.44 mmol) to give the dione **31** (24 mg, 21%) as a dark red solid; mp 229-233 °C (lit.<sup>211</sup> 226-229 °C);  $\nu_{\max}$ (NaCl discs)/ $\text{cm}^{-1}$  2922 (C-H), 2852 (C-H), 1669 (C=O), 1593 (C=C);  $\delta_{\text{H}}$ (400 MHz;  $\text{CDCl}_3$ ) 9.42 (1 H, d,  $J$  8.7, ArCH), 8.12 (1 H, d,  $J$  8.7, ArCH), 7.83 (2 H, br d,  $J$  8.7, 2 x ArCH), 7.71 (1 H, br t,  $J$  7.7, ArCH), 7.55 (1 H, t,  $J$  7.7, ArCH), 7.33 (1 H, s, ArCH), 2.32 (3 H, s,  $\text{CH}_3$ ). No IR spectroscopy data were reported in the literature.  $^1\text{H}$  NMR data were in broad agreement with the literature,<sup>211</sup> although precise chemical shift values were slightly shifted due to the different solvent used for analysis. Also obtained was the dione **99** (28 mg, 24%) as an orange solid; mp 199-202 °C;  $\nu_{\max}$ (NaCl discs)/ $\text{cm}^{-1}$  2921 (C-H), 1766 (C=O), 1664 (C=O), 1536 (C=C);  $\delta_{\text{H}}$ (400 MHz;  $\text{CDCl}_3$ ) 9.77 (1 H, d,  $J$  8.5, ArCH), 8.28 (1 H, d,  $J$  8.5, ArCH), 8.18 (1 H, d,  $J$  8.5, ArCH), 7.90 (1 H, d,  $J$  8.5, ArCH), 7.78-7.72 (1 H, m, ArCH), 7.68-7.61 (1 H, m, ArCH), 7.53 (1 H, s, ArCH), 2.40 (3 H, s,  $\text{CH}_3$ );  $\delta_{\text{C}}$ (101 MHz;  $\text{CDCl}_3$ ) 182.2 (C=O), 177.2 (C=O), 153.7 (ArC), 145.3 (ArCH), 136.7 (ArC), 135.1 (ArCH), 134.0 (ArC), 130.9 (ArC), 130.1 (ArCH), 128.7 (ArCH), 128.5 (ArCH), 128.0 (ArCH), 127.0 (ArC), 126.5 (ArC), 122.3 (ArCH), 120.9 (ArC), 8.8 ( $\text{CH}_3$ );  $m/z$  (EI<sup>+</sup>) 262.0622 (100%,  $\text{M}^+$   $\text{C}_{17}\text{H}_{10}\text{O}_3$  requires 262.0624), 234 (42), 206 (40), 176 (36), 151 (15), 126 (8), 87 (7), 76 (8).

**1-Methyl-6-(trifluoromethyl)phenanthro[1,2-*b*]furan-10,11-dione, 6-CF<sub>3</sub>-TI (100) and 8-methyl-4-(trifluoromethyl)phenanthro[3,2-*b*]furan-7,11-dione, 4-CF<sub>3</sub>-iso-TI (101)**



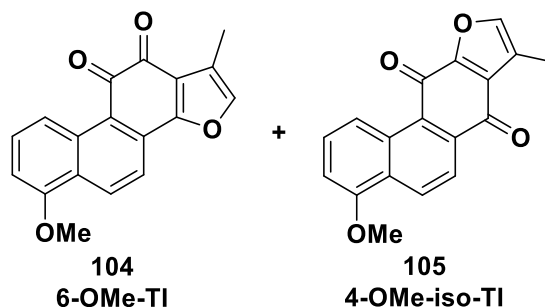
General procedure **D** was followed, using the unpurified alcohol **96** (435 mg) to give the dione **100** (6 mg, 1% over 3 steps) as a dark red solid; mp 204-208 °C;  $\nu_{\max}(\text{NaCl discs})/\text{cm}^{-1}$  1674 (C=O), 1550 (C=C);  $\delta_{\text{H}}(400 \text{ MHz; CDCl}_3)$  9.65 (1 H, d,  $J$  8.9, ArCH), 8.50 (1 H, d,  $J$  8.9, ArCH), 7.98 (1 H, d,  $J$  8.9, ArCH), 7.94 (1 H, d,  $J$  7.2 ArCH), 7.75 (1 H, br t,  $J$  8.1, ArCH), 7.39 (1 H, br d,  $J$  1.1, OCH), 2.33 (3 H, d,  $J$  1.1, CH<sub>3</sub>);  $\delta_{\text{C}}(100 \text{ MHz; CDCl}_3)$  183.3 (C=O), 175.2 (C=O), 160.2 (ArC), 142.8 (ArCH), 133.0 (ArC), 132.8 (q,  $J_{\text{C-F}}$  3.0, ArCH), 131.0 (ArCH), 130.5 (ArC), 129.8 (ArC), 129.1 (ArCH), 127.0 (q,  $J_{\text{C-F}}$  30.3, ArC), 126.0 (q,  $J_{\text{C-F}}$  5.9, ArCH), 124.2 (q,  $J_{\text{C-F}}$  273.9, CF<sub>3</sub>), 123.1 (ArC), 122.1 (ArC), 121.2 (ArC), 120.8 (ArCH), 8.8 (CH<sub>3</sub>);  $\delta_{\text{F}}(377 \text{ MHz; CDCl}_3)$  -58.8;  $m/z$  (ESI<sup>+</sup>) 353 (18%, M+Na<sup>+</sup>), 331.0580 (100, M+H<sup>+</sup> C<sub>18</sub>H<sub>10</sub>O<sub>3</sub>F<sub>3</sub> requires 331.0577). Also obtained was the dione **101** (20 mg, 2% over 3 steps) as a dark brown solid; mp 183-186 °C;  $\nu_{\max}(\text{NaCl discs})/\text{cm}^{-1}$  1661 (C=O), 1601 (C=O), 1536 (C=C);  $\delta_{\text{H}}(400 \text{ MHz; CDCl}_3)$  10.07 (1 H, d,  $J$  9.0, ArCH), 8.58 (1 H, d,  $J$  9.0, ArCH), 8.45 (1 H, d,  $J$  9.0, ArCH), 8.05 (1 H, d,  $J$  7.1 ArCH), 7.79 (1 H, dd,  $J$  9.0, 7.1, ArCH), 7.57 (1 H, q,  $J$  1.1, OCH), 2.42 (3 H, d,  $J$  1.1, CH<sub>3</sub>);  $\delta_{\text{C}}(100 \text{ MHz; CDCl}_3)$  181.4 (C=O), 176.7 (C=O), 153.5 (ArC), 145.7 (ArCH), 134.0 (ArC), 132.4 (ArCH), 132.2 (ArC), 131.6 (ArC), 130.8 (q,  $J_{\text{C-F}}$  2.7, ArCH), 128.2 (ArCH), 127.2 (ArC), 127.0 (q,  $J_{\text{C-F}}$  5.9, ArCH), 126.7 (d,  $J_{\text{C-F}}$  3.0, ArC), 126.5 (ArC), 124.3 (q,  $J_{\text{C-F}}$  274.0, CF<sub>3</sub>), 124.0 (ArCH), 121.0 (ArC), 8.7 (CH<sub>3</sub>);  $\delta_{\text{F}}(377 \text{ MHz; CDCl}_3)$  -59.0;  $m/z$  (EI<sup>+</sup>) 330.0496 (90%, M<sup>+</sup> C<sub>18</sub>H<sub>9</sub>O<sub>3</sub>F<sub>3</sub> requires 330.0498), 261 [100, (M-CF<sub>3</sub>)<sup>+</sup>].

**6-Fluoro-1-methylphenanthro[1,2-*b*]furan-10,11-dione, 6-F-TI (102) and 4-fluoro-8-methylphenanthro[3,2-*b*]furan-7,11-dione, 4-F-iso-TI (103)**



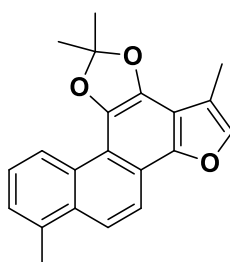
General procedure **D** was followed, using the unpurified alcohol **97** (140 mg) to give the dione **102** (18 mg, 2% over 3 steps) as a dark red solid; mp 187-191 °C;  $\nu_{\max}$ (NaCl discs)/ $\text{cm}^{-1}$  1675 (C=O), 1664 (C=O), 1594 (C=C);  $\delta_{\text{H}}$ (400 MHz;  $\text{CDCl}_3$ ) 9.20 (1 H, d,  $J$  8.8, ArCH), 8.45 (1 H, d,  $J$  8.8, ArCH), 7.89 (1 H, d,  $J$  8.8, ArCH), 7.67-7.60 (1 H, m, ArCH), 7.36 (1 H, q,  $J$  1.2, OCH), 7.22 (1 H, ddd,  $J$  10.0, 7.8, 0.7, ArCH), 2.32 (3 H, d,  $J$  1.2,  $\text{CH}_3$ );  $\delta_{\text{C}}$ (100 MHz;  $\text{CDCl}_3$ ) 183.0 (C=O), 175.0 (C=O), 160.5 (ArC), 158.8 (d,  $J_{\text{C-F}}$  253.6, ArC), 142.5 (ArCH), 133.3 (d,  $J_{\text{C-F}}$  2.5, ArC), 131.0 (d,  $J_{\text{C-F}}$  8.5, ArCH), 130.9 (ArC), 129.4 (d,  $J_{\text{C-F}}$  7.3, ArCH), 124.7 (d,  $J_{\text{C-F}}$  15.4, ArC), 122.5 (d,  $J_{\text{C-F}}$  4.7, ArCH), 122.4 (d,  $J_{\text{C-F}}$  2.3, ArC), 122.0 (ArC), 121.0 (ArC), 119.3 (d,  $J_{\text{C-F}}$  1.6, ArCH), 111.1 (d,  $J_{\text{C-F}}$  19.3, ArCH), 8.8 ( $\text{CH}_3$ );  $\delta_{\text{F}}$ (377 MHz;  $\text{CDCl}_3$ ) -120.7;  $m/z$  (ESI<sup>+</sup>) 326 (34%,  $\text{M}+2\text{Na}^+$ ), 303 (20,  $\text{M}+\text{Na}^+$ ), 281.0612 (100,  $\text{M}+\text{H}^+$   $\text{C}_{17}\text{H}_{10}\text{O}_3\text{F}$  requires 281.0608). Also obtained was the dione **103** (12 mg, 1% over 3 steps) as a pale orange solid; mp 185-189 °C;  $\nu_{\max}$ (NaCl discs)/ $\text{cm}^{-1}$  1662 (C=O), 1591 (C=O), 1535 (C=C);  $\delta_{\text{H}}$ (400 MHz;  $\text{CDCl}_3$ ) 9.56 (1 H, d,  $J$  8.9, ArCH), 8.50 (1 H, d,  $J$  8.9, ArCH), 8.34 (1 H, d,  $J$  8.9, ArCH), 7.71-7.64 (1 H, m, ArCH), 7.55 (1 H, d,  $J$  1.0, OCH), 7.32 (1 H, dd,  $J$  9.9, 7.8, ArCH), 2.41 (3 H, d,  $J$  1.0,  $\text{CH}_3$ );  $\delta_{\text{C}}$ (100 MHz;  $\text{CDCl}_3$ ) 181.8 (C=O), 176.8 (C=O), 158.4 (d,  $J_{\text{C-F}}$  253.0, ArC), 153.6 (ArC), 145.5 (ArCH), 134.5 (ArC), 131.9 (d,  $J_{\text{C-F}}$  2.8, ArC), 130.0 (d,  $J_{\text{C-F}}$  8.1, ArCH), 127.5 (d,  $J_{\text{C-F}}$  6.9, ArCH), 127.1 (d,  $J_{\text{C-F}}$  15.8, ArC), 126.8 (d,  $J_{\text{C-F}}$  2.6, ArC), 126.7 (ArC), 124.0 (d,  $J_{\text{C-F}}$  4.6, ArCH), 122.7 (d,  $J_{\text{C-F}}$  1.6, ArCH), 121.0 (ArC), 112.1 (d,  $J_{\text{C-F}}$  19.3, ArCH), 8.7 ( $\text{CH}_3$ );  $\delta_{\text{F}}$ (377 MHz;  $\text{CDCl}_3$ ) -120.9;  $m/z$  (EI<sup>+</sup>) 280.0532 (100%,  $\text{M}^+$   $\text{C}_{17}\text{H}_9\text{O}_3\text{F}$  requires 280.0530).

**6-Methoxy-1-methylphenanthro[1,2-*b*]furan-10,11-dione, 6-OMe-TI (104) and 4-methoxy-8-methylphenanthro[3,2-*b*]furan-7,11-dione, 4-OMe-iso-TI (105)**



General procedure **D** was followed, using the alcohol **98** (100 mg, 0.39 mmol) to give the dione **104** (22 mg, 19%) as a dark brown solid; mp 249-253 °C;  $\nu_{\max}(\text{NaCl discs})/\text{cm}^{-1}$  1670 (C=O), 1660 (C=O), 1587 (C=C), 1548 (C=C);  $\delta_{\text{H}}(400 \text{ MHz; CDCl}_3)$  9.00 (1 H, d,  $J$  8.9, ArCH), 8.66 (1 H, d,  $J$  8.7, ArCH), 7.82 (1 H, d,  $J$  8.7, ArCH), 7.62 (1 H, app t,  $J$  8.4, ArCH), 7.34 (1 H, s, ArCH), 6.89 (1 H, d,  $J$  7.8, ArCH), 4.04 (3 H, s, OCH<sub>3</sub>), 2.32 (3 H, s, CH<sub>3</sub>);  $\delta_{\text{C}}(126 \text{ MHz; CDCl}_3)$  183.4 (C=O), 175.7 (C=O), 161.2 (ArC), 155.7 (ArC), 142.1 (ArCH), 133.5 (ArC), 131.5 (ArCH), 131.2 (ArCH), 130.5 (ArC), 126.8 (ArC), 122.4 (ArC), 121.8 (ArC), 120.7 (ArC), 118.5 (ArCH), 118.2 (ArCH), 105.5 (ArCH), 55.7 (OCH<sub>3</sub>), 8.8 (CH<sub>3</sub>);  $m/z$  (ESI<sup>+</sup>) 315 (11%, M+Na<sup>+</sup>), 293.0813 (100, M+H<sup>+</sup> C<sub>18</sub>H<sub>13</sub>O<sub>4</sub> requires 293.0808). Also obtained was the dione **105** (21 mg, 18%) as a red solid; mp 231-234 °C;  $\nu_{\max}(\text{ATR})/\text{cm}^{-1}$  1662 (C=O), 1582 (C=O), 1535 (C=C);  $\delta_{\text{H}}(400 \text{ MHz; CDCl}_3)$  9.32 (1 H, d,  $J$  8.8, ArCH), 8.68 (1 H, d,  $J$  8.8, ArCH), 8.24 (1 H, d,  $J$  8.8, ArCH), 7.63 (1 H, dd,  $J$  8.8, 7.9, ArCH), 7.51 (1 H, d,  $J$  0.8, ArCH), 6.95 (1 H, d,  $J$  7.9, ArCH), 4.04 (3 H, s, OCH<sub>3</sub>), 2.40 (3 H, d,  $J$  0.8, CH<sub>3</sub>);  $\delta_{\text{C}}(101 \text{ MHz; CDCl}_3)$  182.3 (C=O), 177.2 (C=O), 155.3 (ArC), 153.9 (ArC), 145.1 (ArCH), 134.4 (ArC), 132.0 (ArC), 130.5 (ArCH), 129.3 (ArC), 129.2 (ArCH), 126.5 (2 x ArC), 121.6 (ArCH), 120.8 (ArC), 119.8 (ArCH), 106.2 (ArCH), 55.7 (OCH<sub>3</sub>), 8.8 (CH<sub>3</sub>);  $m/z$  (ESI<sup>+</sup>) 315 (43%, M+Na<sup>+</sup>), 293.0810 (100, M+H<sup>+</sup> C<sub>18</sub>H<sub>13</sub>O<sub>4</sub> requires 293.0808).

### 1,6-Dimethylphenanthro[1,2-*b*]furan-10,11-dimethyldioxole, TI-acetal (**109**)

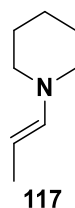


**109**  
TI-acetal

TI **1** (27 mg, 0.10 mmol) was dissolved in anhydrous THF (7 mL) and stirred under a nitrogen atmosphere at room temperature. Sodium borohydride (4.0 mg, 0.10 mmol) was added in a single portion, and the solution stirred for 30 minutes. The solution was poured onto ice/water (20 mL), acidified with aqueous HCl solution (1 M, 3 mL), and extracted with DCM (3 x 20 mL). The organic extracts were combined, dried (MgSO<sub>4</sub>), filtered and concentrated *in vacuo* to give the crude diol **108** as an olive-green solid (29 mg), which was immediately dissolved in anhydrous toluene (10 mL). 2,2-Dimethoxypropane (0.025 mL, 0.20 mmol) and *para*-toluenesulfonic acid monohydrate (25 mg, 0.13 mmol) were added, and the reaction was stirred under a nitrogen atmosphere at reflux for 2 h. The mixture was cooled to room temperature, aqueous saturated NaHCO<sub>3</sub> solution (20 mL) added, and extracted with diethyl ether (3 x 20 mL). The organic extracts were combined, dried (MgSO<sub>4</sub>), filtered and concentrated *in vacuo* to give an off-white solid (38 mg), which was purified twice by flash column chromatography (silica gel, DCM, and then silica gel, 19:1 40/60 petroleum ether/ethyl acetate) to give the acetal **109** as a beige solid (11 mg, 34%); mp 176-180 °C;  $\nu_{\max}(\text{ATR})/\text{cm}^{-1}$  2917 (C-H);  $\delta_{\text{H}}(400 \text{ MHz}; \text{CDCl}_3)$  9.13 (1 H, d, *J* 8.4, ArCH), 8.22 (1 H, d, *J* 9.2, ArCH), 7.89 (1 H, dd, *J* 9.2, 0.8, ArCH), 7.57-7.52 (2 H, m, 2 x ArCH), 7.45 (1 H, dt, *J* 7.1, 0.9, ArCH), 2.79 (3 H, s, ArCH<sub>3</sub>), 2.46 (3 H, d, *J* 1.3, ArCH<sub>3</sub>), 1.91 (6 H, s, 2 x CH<sub>3</sub>);  $\delta_{\text{C}}(126 \text{ MHz}; \text{CDCl}_3)$  148.3 (ArC), 141.5 (ArCH), 138.2 (ArC), 137.8 (ArC), 134.1 (ArC), 130.7 (ArC), 128.9 (ArC), 127.3 (ArCH), 125.6 (ArCH), 125.4 (ArCH), 120.4 (ArCH), 119.2 (ArCH), 118.5 (ArC), 114.5 (ArC), 114.3 (ArC), 113.0 (ArC), 112.7 (ArC), 26.1 (2 x CH<sub>3</sub>), 20.2 (ArCH<sub>3</sub>), 9.2 (ArCH<sub>3</sub>); *m/z* (ESI<sup>+</sup>) 319.1322 (100%, M+H<sup>+</sup> C<sub>21</sub>H<sub>19</sub>O<sub>3</sub> requires 319.1329), 383 (8), 359 (28), 261 (22).

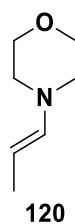
### 8.3 Towards the synthesis of other tanshinone analogues

#### (*E*)-1-(1-Propenyl)piperidine (**117**)



A mixture of piperidine **116** (9.10 mL, 91.8 mmol) and potassium carbonate (2.53 g, 18.4 mmol) was cooled to 0 °C in an ice bath under a nitrogen atmosphere. Freshly distilled propanal **57** (4.40 mL, 61.2 mmol) was added dropwise over 45 minutes, and the mixture was stirred for a further 2 h at 0 °C. The mixture was filtered and washed with diethyl ether (20 mL), and the resulting filtrate was concentrated *in vacuo* to give the crude enamine **117** (8.83 g) as a colourless oil which was used without any further purification. Selected <sup>1</sup>H NMR data from reaction mixture corresponding to the enamine **117**:  $\delta_{\text{H}}$ (400 MHz; CDCl<sub>3</sub>) 5.82 (1 H, dq, *J* 13.9, 1.4, NCH=CHCH<sub>3</sub>), 4.37 (1 H, dq, *J* 13.9, 6.5, NCH=CHCH<sub>3</sub>), 2.74-2.70 (4 H, m, 2 x CH<sub>2</sub>), 1.63 (3 H, dd, *J* 6.5, 1.4, NCH=CHCH<sub>3</sub>), 1.59-1.44 (6 H, m, 3 x CH<sub>2</sub>). All NMR data were in general agreement with the literature.<sup>320,321</sup>

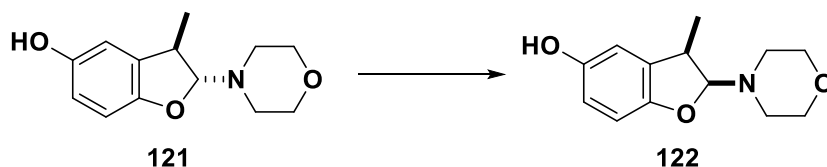
#### (*E*)-4-(1-Propenyl)morpholine (**120**)



A mixture of morpholine **119** (1.30 mL, 15.0 mmol) and potassium carbonate (780 mg, 5.64 mmol) was cooled to 0 °C in an ice bath under a nitrogen atmosphere. Propanal **57** (1.30 mL, 18.7 mmol) was added dropwise over 15 minutes, and the mixture was stirred for a further 2 h at 0 °C. The mixture was filtered and washed with diethyl ether (10 mL), and the resulting solution was concentrated *in vacuo* to give the crude enamine **120** (1.45 g) as a colourless oil which was used without any further purification. Selected <sup>1</sup>H NMR data from reaction mixture corresponding to the enamine **120**:  $\delta_{\text{H}}$ (400 MHz;

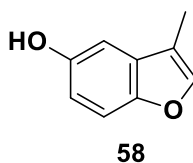
CDCl<sub>3</sub>) 5.83 (1 H, dq, *J* 13.9, 1.4, NCH=CHCH<sub>3</sub>), 4.47 (1 H, dq, *J* 13.9, 6.5, NCH=CHCH<sub>3</sub>), 3.75-3.71 (4 H, m, 2 x OCH<sub>2</sub>), 2.79-2.75 (4 H, m, 2 x NCH<sub>2</sub>), 1.65 (3 H, dd, *J* 6.5, 1.4, NCH=CHCH<sub>3</sub>). All NMR data were in general agreement with the literature.<sup>230,325,326</sup>

**(±)-*trans*-2,3-Dihydro-5-hydroxy-2-morpholino-3-methylbenzo[1,2-*b*]furan (121) and (±)-*cis*-2,3-dihydro-5-hydroxy-2-morpholino-3-methylbenzo[1,2-*b*]furan (122)**



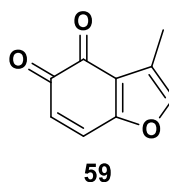
*para*-Benzoquinone **32** (638 mg, 5.90 mmol) was dissolved in anhydrous DCM (15 mL) and cooled to 0 °C under a nitrogen atmosphere in an ice bath. A solution of the unpurified enamine **120** (750 mg) in anhydrous DCM (5 mL) was added dropwise over 10 minutes, the reaction was warmed to room temperature, and stirred for 18 h. The reaction mixture was concentrated *in vacuo* to give the crude product as a dark brown gum (1.00 g), the <sup>1</sup>H NMR spectrum of which contained product peaks which were in broad agreement with those in the literature.<sup>230,325</sup> Selected <sup>1</sup>H NMR peaks from crude reaction mixture corresponding to the *trans*-phenol **121**: δ<sub>H</sub>(400 MHz; CDCl<sub>3</sub>) 6.66-6.64 (1 H, m, ArCH), 6.61-6.60 (2 H, m, 2 x ArCH), 4.97 (1 H, d, *J* 4.7, CH), 3.31-3.26 (1 H, m, CH), 2.86-2.79 (2 H, m, CH<sub>2</sub>), 2.63-2.56 (2 H, m, CH<sub>2</sub>), 1.33 (3 H, d, *J* 7.0, CH<sub>3</sub>). Removal of major impurities by flash column chromatography (silica gel, 1:1 40/60 petroleum ether/ethyl acetate) gave a different product, thought to be the other epimer **122**, as a viscous brown oil (477 mg). Selected <sup>1</sup>H NMR peaks: δ<sub>H</sub>(400 MHz; CDCl<sub>3</sub>) 6.72-6.67 (2 H, m, 2 x ArCH), 6.65-6.61 (1 H, m, ArCH), 5.60 (1 H, d, *J* 2.3, CH), 5.28 (1 H, br s, OH), 3.89-3.85 (1 H, m, CH), 3.19 (1 H, qd, *J* 7.3, 1.8, CH), 2.86-2.82 (1 H, m, CH), 1.36 (1 H, d, *J* 7.3, CH), 1.29 (3 H, d, *J* 7.3, CH<sub>3</sub>). The phenol **122** was used without further purification.

### 5-Hydroxy-3-methylbenzo[1,2-*b*]furan (58)



Aqueous HCl (1 M, 120 mL) was added to the crude benzofuranol **122** (2.43 g), and the resulting mixture was stirred at reflux for 18 h. The solution was cooled to room temperature and extracted with diethyl ether (3 × 150 mL). The organic extracts were combined, dried (MgSO<sub>4</sub>), filtered and concentrated *in vacuo* to give a viscous pale brown oil (1.42 g). The solid was purified by flash column chromatography (silica gel, 2:1, 40-60 petroleum ether/ethyl acetate) to give the benzofuranol **58** (704 mg, 33% over 3 steps) as a white solid; mp 94-96 °C (lit.<sup>230</sup> mp 93-94 °C);  $\delta_{\text{H}}$ (400 MHz; CDCl<sub>3</sub>) 7.40 (1 H, d, *J* 1.1, OCH), 7.32 (1 H, d, *J* 8.7, ArCH), 6.95 (1 H, d, *J* 2.5, ArCH), 6.82 (1 H, dd, *J* 8.7, 2.5, ArCH), 4.73 (1 H, br s, OH), 2.21 (3 H, d, *J* 1.1, CH<sub>3</sub>);  $\delta_{\text{C}}$ (100 MHz; CDCl<sub>3</sub>) 151.1 (ArC), 150.3 (ArC), 142.5 (ArCH), 129.9 (ArC), 115.5 (ArC), 112.7 (ArCH), 111.7 (ArCH), 104.6 (ArCH), 7.9 (CH<sub>3</sub>). All data were in general agreement with the literature.<sup>230,325</sup>

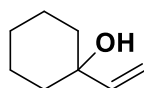
### 4,5-Dihydro-3-methylbenzo[1,2-*b*]furan-4,5-dione (59)



A solution of 3-methyl-5-benzofuranol **58** (50 mg, 0.34 mmol) in methanol (1.5 mL) was cooled to 0 °C in an ice bath. Separately, Fremy's salt (200 mg, 0.75 mmol) was dissolved in aqueous KH<sub>2</sub>PO<sub>4</sub> (0.07 M, 17 mL, adjusted to pH 7) and cooled to 0 °C in an ice bath. The Fremy's salt solution was added to the solution of the phenol **58** dropwise at 0 °C with stirring, and the reaction was stirred for a further 1 h at 0 °C. The red precipitate formed was collected by filtration, washed with cold water (5 mL) and cold 40/60 petroleum ether (5 mL), and dried under low vacuum to give the crude dione **59** (22 mg) as a red solid. The filtrate was extracted with ethyl acetate (3 × 20 mL) and the organic extracts were combined, washed with water (2 × 40 mL) and brine (40 mL), dried

(MgSO<sub>4</sub>), filtered and concentrated *in vacuo* to give further crude dione **59** (23 mg) as a red solid which was combined with the previously obtained red solid and used without further purification. Selected IR and <sup>1</sup>H NMR data from reaction mixture corresponding to the dione **59**:  $\nu_{\text{max}}(\text{ATR})/\text{cm}^{-1}$  1632 (C=O), 1614 (C=O);  $\delta_{\text{H}}(400 \text{ MHz}; \text{CDCl}_3)$  7.30 (1 H, br s, OCH), 7.28 (1 H, d, *J* 10.3, COCH), 6.17 (1 H, d, *J* 10.3, =CH), 2.27 (3 H, d, *J* 1.0, CH<sub>3</sub>). All data were in general agreement with the literature.<sup>230</sup>

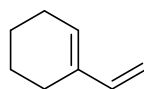
### 1-Vinylcyclohexanol (**125**)



**125**

A solution of cyclohexanone **126** (1.06 mL, 10.2 mmol) in anhydrous THF (25 mL) was cooled to 0 °C in an ice bath, under a nitrogen atmosphere. Vinylmagnesium bromide (1.0 M in THF, 31.0 mL, 31.0 mmol) was added dropwise, and the mixture was stirred at 0 °C for 2 h. The reaction was quenched by the addition of saturated ammonium chloride solution (100 mL), and the organic layer was separated and extracted with diethyl ether (3 x 75 mL). The organic extracts were combined, dried (MgSO<sub>4</sub>), filtered and concentrated *in vacuo* to give a pale yellow oil (908 mg). The crude product was purified by flash column chromatography (silica gel, 4:1 40/60 petroleum ether/ethyl acetate) to give the alcohol **125** (692 mg, 54%) as a colourless oil which was used without further purification;  $\delta_{\text{H}}(400 \text{ MHz}; \text{CDCl}_3)$  6.00 (1 H, dd, *J* 17.4, 10.8, =CH), 5.27 (1 H, dd, *J* 17.4, 1.3, =CHH), 5.06 (1 H, dd, *J* 10.4, 1.3, =CHH), 1.71-1.49 (10 H, m, 5 x CH<sub>2</sub>), 1.33 (1 H, s, OH). All data were in general agreement with the literature.<sup>330,331</sup>

### 1-Vinylcyclohexene (**123**)

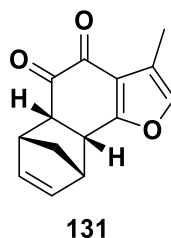


**123**

*para*-Toluenesulfonic acid monohydrate (452 mg, 2.37 mmol) was added to a solution of 1-vinylcyclohexanol **125** (200 mg, 1.58 mmol) in pentane (10 mL), and the mixture was heated at reflux for 3 h. The mixture was cooled to room temperature, water (20

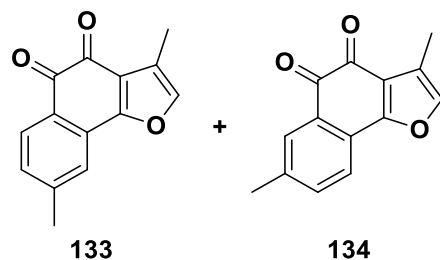
mL) was added, and the organic layer was separated and extracted with pentane (3 x 10 mL). The organic extracts were combined, dried (MgSO<sub>4</sub>), filtered and concentrated *in vacuo* to give a pale yellow oil (200 mg). Purification of the crude mixture was attempted by flash column chromatography (silica gel, pentane) to give the impure diene **123** (11 mg) as a colourless oil which was not purified any further. Selected <sup>1</sup>H NMR data from product mixture corresponding to the diene **123**: δ<sub>H</sub>(400 MHz; CDCl<sub>3</sub>) 6.37 (1 H, dd, *J* 17.5, 10.8, =CH), 5.78 (1 H, br s, =CH), 5.09 (1 H, d, *J* 17.5, =CHH), 4.91 (1 H, d, *J* 10.8, =CHH), 2.19-2.11 (4 H, m, 2 x CH<sub>2</sub>), 1.74-1.59 (4 H, m, 2 x CH<sub>2</sub>). All data were in general agreement with the literature.<sup>331,332</sup>

### 6,9-Dihydro-6,9-methano-3-methylnaphtho[1,2-*b*]furan-4,5-dione (**131**)



Freshly prepared unpurified dione **59** (20 mg) was dissolved in anhydrous DCM (4 mL) and cooled to -78 °C under a nitrogen atmosphere. Freshly cracked cyclopentadiene **127** (0.35 mL, 4.2 mmol) was added and the reaction was stirred at -78 °C for 1 h. The reaction was warmed to room temperature and stirred for a further 2 h. The mixture was concentrated *in vacuo* to give a pale brown solid (23 mg) as a mixture of the dione **131** and the phenol **58** in an 80:20 ratio which could not be purified further. Selected <sup>1</sup>H NMR data from reaction mixture corresponding to the dione **131**: δ<sub>H</sub>(400 MHz; CDCl<sub>3</sub>) 7.16 (1 H, q, *J* 1.2, OCH), 6.12 (1 H, dd, *J* 5.7, 2.9, =CH), 5.79 (1 H, dd, *J* 5.7, 2.9, =CH), 3.78 (1 H, dd, *J* 7.8, 4.0, CH), 3.59 (1 H, br s, CH), 3.48 (1 H, br s, CH), 3.32 (1 H, dd, *J* 7.8, 4.0, CH), 2.22 (3 H, d, *J* 1.2, CH<sub>3</sub>), 1.72 (1 H, dt, *J* 9.0, 1.7, CHH), 1.62 (1 H, br d, *J* 9.0, CHH). All data were in general agreement with the literature.<sup>230</sup>

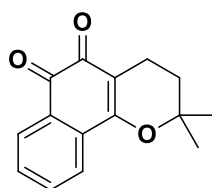
**3,8-Dimethyl-4,5-dihydronaphtho[1,2-*b*]furan-4,5-dione (133) and 3,7-dimethyl-4,5-dihydronaphtho[1,2-*b*]furan-4,5-dione (134)**



A mixture of the unpurified dione **59** (100 mg), isoprene **129** (2.0 mL, 20 mmol) and methanol (1.0 mL) in a sealed round-bottomed flask was warmed at 45 °C for 2 h in an ultrasonic cleaning bath (50-60 Hz, 50 W). The mixture was cooled to room temperature, concentrated *in vacuo*, and passed through a plug of silica (DCM). The eluted product mixture was concentrated *in vacuo*, toluene (30 mL) and chloranil (165 mg, 0.67 mmol) were added, and the mixture was heated at reflux for 18 h. The mixture was cooled to room temperature, concentrated *in vacuo*, passed through a plug of silica (DCM) and re-concentrated *in vacuo* to give a red solid (32 mg) as a mixture of the phenol **58** and the diones **133** and **134** in a 70:20:10 ratio which was not purified any further. Selected  $^1\text{H}$  NMR data from reaction mixture corresponding to the dione **133**:  $\delta_{\text{H}}$ (400 MHz;  $\text{CDCl}_3$ ) 7.98 (1 H, d,  $J$  7.9, ArCH), 7.51 (1 H, s, ArCH), 7.27-7.24 (2 H, m, 2 x ArCH), 2.48 (3 H, s,  $\text{CH}_3$ ), 2.31 (3 H, s,  $\text{CH}_3$ ). All data were in agreement with the literature.<sup>11</sup> Selected  $^1\text{H}$  NMR data from reaction mixture corresponding to the dione **134**:  $\delta_{\text{H}}$ (400 MHz;  $\text{CDCl}_3$ ) 7.90 (1 H, br s, ArCH), 7.61-7.58 (1 H, m, ArCH), 7.45-7.43 (1 H, m, ArCH), 7.26-7.24 (1 H, m, ArCH), 2.44 (3 H, s,  $\text{CH}_3$ ), 2.30 (3 H, s,  $\text{CH}_3$ ). All data were in general agreement with the literature.<sup>230</sup>

## 8.4 Synthesis of structurally related compounds

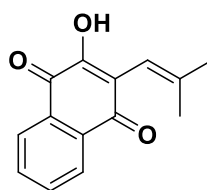
### $\beta$ -Lapachone (**112**)



**112**

Concentrated H<sub>2</sub>SO<sub>4</sub> (1.0 mL) was added slowly to lapachol **114** (25 mg, 0.10 mmol), with stirring, until the solid completely dissolved. The solution was stirred for a further 5 minutes and poured onto ice (20 g). The precipitate was filtered off by vacuum filtration and washed with cold water (5 mL) to give an orange solid. The crude product was purified by flash column chromatography (silica gel, DCM – 19:1 DCM/MeOH) to give the dione **112** (21 mg, 85%) as an orange solid; mp 151-153 °C (lit.<sup>333</sup> 152-154 °C);  $\delta_{\text{H}}$ (400 MHz; CDCl<sub>3</sub>) 8.07 (1 H, dd, *J* 7.7, 1.0, ArCH), 7.83 (1 H, d, *J* 7.7, ArCH), 7.66 (1 H, td, *J* 7.7, 1.0, ArCH), 7.52 (1 H, td, *J* 7.7, 1.0, ArCH), 2.58 (2 H, t, *J* 6.7, CH<sub>2</sub>), 1.87 (2 H, t, *J* 6.7, CH<sub>2</sub>), 1.48 (6 H, s, 2 x CH<sub>3</sub>);  $\delta_{\text{C}}$ (101 MHz; CDCl<sub>3</sub>) 179.9 (C=O), 178.6 (C=O), 162.1 (ArC), 134.8 (ArCH), 132.6 (ArC), 130.7 (ArCH), 130.1 (ArC), 128.6 (ArCH), 124.1 (ArCH), 112.7 (ArC), 79.3 [C(CH<sub>3</sub>)<sub>2</sub>], 31.6 (CH<sub>2</sub>), 26.8 (2 x CH<sub>3</sub>), 16.2 (CH<sub>2</sub>). All data were in general agreement with the literature.<sup>307,333</sup>

### Norlapachol (**115**)

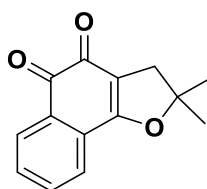


**115**

Lapachol **114** (150 mg, 0.62 mmol) was dissolved in THF (5 mL), sodium carbonate (72 mg, 0.68 mmol) in water (5 mL) was added, and the solution was heated to 60 °C. Aqueous hydrogen peroxide (30%, 1.0 mL, 13 mmol) was added and the solution was heated at 60 °C for 4 h. The reaction was cooled to rt, acidified with concentrated HCl (0.2 mL), and quenched with sodium sulfite (3.0 g). Aqueous NaOH (25%, 5 mL) and

copper(II) sulfate (625 mg, 3.9 mmol) in water (5 mL) were added and the mixture was stirred at room temperature for 1.5 h. The solution was filtered through a pad of Celite, acidified with concentrated HCl (7 mL) and extracted with diethyl ether (3 x 75 mL). The organic extracts were combined, washed with brine (200 mL), dried (MgSO<sub>4</sub>), filtered and concentrated *in vacuo* to give an orange solid. The crude product was purified by recrystallisation from *n*-hexane to give the dione **115** (73 mg, 52%) as an orange solid; mp 123-125 °C (from *n*-hexane), (lit.<sup>307</sup> 121-122 °C);  $\nu_{\max}$ (NaCl discs)/cm<sup>-1</sup> 3364 (O-H), 2928 (C-H), 2910 (C-H), 1662 (C=O), 1645 (C=O), 1627 (C=C), 1593 (C=C);  $\delta_{\text{H}}$ (400 MHz; CDCl<sub>3</sub>) 8.15 (1 H, d, *J* 7.6, ArCH), 8.11 (1 H, d, *J* 7.6, ArCH), 7.78 (1 H, td, *J* 7.6, 1.1, ArCH), 7.71 (1 H, td, *J* 7.6, 1.1, ArCH), 7.55 (1 H, br s, OH), 6.02 (1 H, br s, CH), 2.01 (3 H, s, CH<sub>3</sub>), 1.70 (3 H, s, CH<sub>3</sub>);  $\delta_{\text{C}}$ (101 MHz; CDCl<sub>3</sub>) 184.8 (C=O), 181.6 (C=O), 151.2 (C), 143.6 (C), 134.9 (ArCH), 133.0 (ArCH), 132.9 (C), 129.5 (C), 126.9 (ArCH), 126.1 (ArCH), 120.9 (C), 113.7 (CH), 26.6 (CH<sub>3</sub>), 21.8 (CH<sub>3</sub>); *m/z* (ESI<sup>+</sup>) 251 (5%, M+Na<sup>+</sup>), 229.0862 (100, M+H<sup>+</sup> C<sub>14</sub>H<sub>13</sub>O<sub>3</sub> requires 229.0859). All data were in general agreement with the literature.<sup>307,397,398</sup>

### Nor- $\beta$ -lapachone (**113**)



**113**

Concentrated H<sub>2</sub>SO<sub>4</sub> (1.5 mL) was added slowly to norlapachol **115** (30 mg, 0.13 mmol), with stirring, until the solid completely dissolved. The solution was stirred at room temperature for a further 5 minutes, poured onto ice (20 g) and rinsed with water (20 mL). The solution was extracted with DCM (3 x 40 mL), and the organic extracts were combined, washed with brine (100 mL), dried (MgSO<sub>4</sub>), filtered, and concentrated *in vacuo* to give an orange/pink solid. The crude product was purified by trituration with cold hexane (2 x 2 mL) and dried under high vacuum to give the dione **113** (29 mg, 95%) as an orange solid; mp 190-193 °C (lit.<sup>399</sup> 188-189 °C);  $\delta_{\text{H}}$ (400 MHz; CDCl<sub>3</sub>) 8.10 (1 H, d, *J* 7.6, ArCH), 7.68-7.64 (2 H, m, 2 x ArCH), 7.63-7.57 (1 H, m, ArCH), 2.97 (2 H, s, CH<sub>2</sub>), 1.63

(6 H, s, 2 x CH<sub>3</sub>);  $\delta_c$ (101 MHz; CDCl<sub>3</sub>) 181.4 (C=O), 175.7 (C=O), 168.8 (ArC), 134.5 (ArCH), 131.9 (ArCH), 130.9 (ArC), 129.3 (ArCH), 127.9 (ArC), 124.6 (ArCH), 115.0 (ArC), 93.8 [C(CH<sub>3</sub>)<sub>2</sub>], 39.3 (CH<sub>2</sub>), 28.4 (2 x CH<sub>3</sub>). All data were in general agreement with the literature.<sup>307,399</sup>

## 9. Bibliography

1. Rang, H. P., Dale, M. M., Ritter, J. M., Flower, R. J. & Henderson, G. *Pharmacology*. (Churchill Livingstone, 2012).
2. Athens, J. W. *et al.* Leukokinetic studies. IV. The total blood, circulating and marginal granulocyte pools and the granulocyte turnover rate in normal subjects. *J. Clin. Invest.* **40**, 989–95 (1961).
3. McCracken, J. M. & Allen, L.-A. H. Regulation of Human Neutrophil Apoptosis and Lifespan in Health and Disease. *J. Cell Death* **7**, 15–23 (2014).
4. Serhan, C. N. *et al.* Resolution of inflammation: state of the art, definitions and terms. *FASEB J.* **21**, 325–332 (2007).
5. Serhan, C. N. & Savill, J. Resolution of inflammation: the beginning programs the end. *Nat. Immunol.* **6**, 1191–1197 (2005).
6. Medzhitov, R. Origin and physiological roles of inflammation. *Nature* **454**, 428–435 (2008).
7. Phillipson, M. & Kubes, P. The neutrophil in vascular inflammation. *Nat. Med.* **17**, 1381–1390 (2011).
8. Dahlgren, C. & Karlsson, A. Respiratory burst in human neutrophils. *J. Immunol. Methods* **232**, 3–14 (1999).
9. Brinkmann, V. *et al.* Neutrophil extracellular traps kill bacteria. *Science (80-. )*. **303**, 1532–5 (2004).
10. Liu, H. & Pope, R. M. Phagocytes: mechanisms of inflammation and tissue destruction. *Rheum. Dis. Clin. North Am.* **30**, 19–39 (2004).
11. Fox, S., Leitch, A. E., Duffin, R., Haslett, C. & Rossi, A. G. Neutrophil apoptosis: relevance to the innate immune response and inflammatory disease. *J. Innate Immun.* **2**, 216–27 (2010).
12. Lehrer, R. I., Ganz, T., Selsted, M. E., Babior, B. M. & Curnutte, J. T. Neutrophils and Host Defense. *Ann. Intern. Med.* **109**, 127–142 (1988).
13. Lucas, C. D., Hoodless, L. J. & Rossi, A. G. Swimming against the tide: drugs drive neutrophil reverse migration. *Sci. Transl. Med.* **6**, 225fs9 (2014).
14. Headland, S. E. & Norling, L. V. The resolution of inflammation: Principles and challenges. *Semin. Immunol.* **27**, 149–160 (2015).
15. Jones, H. R., Robb, C. T., Perretti, M. & Rossi, A. G. The role of neutrophils in inflammation resolution. *Semin. Immunol.* **28**, 137–145 (2016).
16. Kerr, J. F. R., Wyllie, A. H. & Currie, A. R. Apoptosis: A Basic Biological Phenomenon with Wideranging Implications in Tissue Kinetics. *Br. J. Cancer* **26**, 239–257 (1972).
17. Savill, J. Apoptosis in resolution of inflammation. *J. Leukoc. Biol.* **61**, 375–80 (1997).
18. Savill, J. S. *et al.* Macrophage phagocytosis of aging neutrophils in inflammation. Programmed cell death in the neutrophil leads to its recognition by macrophages.

- J. Clin. Invest.* **83**, 865–75 (1989).
19. Savill, J. & Haslett, C. Granulocyte clearance by apoptosis in the resolution of inflammation. *Semin. Cell Biol.* **6**, 385–393 (1995).
  20. Haslett, C. Granulocyte Apoptosis and Its Role in the Resolution and Control of Lung Inflammation. *Am. J. Respir. Crit. Care Med.* **160**, S5–S11 (1999).
  21. Rowe, S. J., Allen, L., Ridger, V. C., Hellewell, P. G. & Whyte, M. K. B. Caspase-1-deficient mice have delayed neutrophil apoptosis and a prolonged inflammatory response to lipopolysaccharide-induced acute lung injury. *J. Immunol.* **169**, 6401–7 (2002).
  22. Rossi, A. G. *et al.* Cyclin-dependent kinase inhibitors enhance the resolution of inflammation by promoting inflammatory cell apoptosis. *Nat. Med.* **12**, 1056–1064 (2006).
  23. Uller, L., Persson, C. G. A. & Erjefält, J. S. Resolution of airway disease: removal of inflammatory cells through apoptosis, egression or both? *Trends Pharmacol. Sci.* **27**, 461–466 (2006).
  24. Nourshargh, S., Renshaw, S. A. & Imhof, B. A. Reverse Migration of Neutrophils: Where, When, How, and Why? *Trends Immunol.* **37**, 273–86 (2016).
  25. Hughes, J. *et al.* Neutrophil fate in experimental glomerular capillary injury in the rat. Emigration exceeds in situ clearance by apoptosis. *Am. J. Pathol.* **150**, 223–34 (1997).
  26. Buckley, C. D. *et al.* Identification of a phenotypically and functionally distinct population of long-lived neutrophils in a model of reverse endothelial migration. *J. Leukoc. Biol.* **79**, 303–311 (2006).
  27. Hamza, B. *et al.* Retrotaxis of human neutrophils during mechanical confinement inside microfluidic channels. *Integr. Biol.* **6**, 175–183 (2014).
  28. Woodfin, A. *et al.* The junctional adhesion molecule JAM-C regulates polarized transendothelial migration of neutrophils in vivo. *Nat. Immunol.* **12**, 761–769 (2011).
  29. Mathias, J. R. *et al.* Resolution of inflammation by retrograde chemotaxis of neutrophils in transgenic zebrafish. *J. Leukoc. Biol.* **80**, 1281–1288 (2006).
  30. Vianello, F., Olszak, I. T. & Poznansky, M. C. Fugetaxis: active movement of leukocytes away from a chemokinetic agent. *J. Mol. Med.* **83**, 752–763 (2005).
  31. Tharp, W. G. *et al.* Neutrophil chemorepulsion in defined interleukin-8 gradients in vitro and in vivo. *J. Leukoc. Biol.* **79**, 539–554 (2006).
  32. Brown, S. B. *et al.* Class III antiarrhythmic methanesulfonanilides inhibit leukocyte recruitment in zebrafish. *J. Leukoc. Biol.* **82**, 79–84 (2007).
  33. Hall, C., Flores, M. V., Storm, T., Crosier, K. & Crosier, P. The zebrafish lysozyme C promoter drives myeloid-specific expression in transgenic fish. *BMC Dev. Biol.* **7**, 42 (2007).
  34. Yoo, S. K. & Huttenlocher, A. Spatiotemporal photolabeling of neutrophil

- trafficking during inflammation in live zebrafish. *J. Leukoc. Biol.* **89**, 661–667 (2011).
35. Holmes, G. R. *et al.* Repelled from the wound, or randomly dispersed? Reverse migration behaviour of neutrophils characterized by dynamic modelling. *J. R. Soc. Interface* **9**, 3229–39 (2012).
  36. Robertson, A. L. *et al.* A zebrafish compound screen reveals modulation of neutrophil reverse migration as an anti-inflammatory mechanism. *Sci. Transl. Med.* **6**, 225ra29 (2014).
  37. Ellett, F., Elks, P. M., Robertson, A. L., Ogryzko, N. V. & Renshaw, S. A. Defining the phenotype of neutrophils following reverse migration in zebrafish. *J. Leukoc. Biol.* **98**, 975–981 (2015).
  38. Loynes, C. A. *et al.* Pivotal Advance: Pharmacological manipulation of inflammation resolution during spontaneously resolving tissue neutrophilia in the zebrafish. *J. Leukoc. Biol.* **87**, 203–12 (2010).
  39. Elks, P. M. *et al.* Activation of hypoxia-inducible factor-1 $\alpha$  (Hif-1 $\alpha$ ) delays inflammation resolution by reducing neutrophil apoptosis and reverse migration in a zebrafish inflammation model. *Blood* **118**, 712–22 (2011).
  40. Epstein, F. H. & Weiss, S. J. Tissue Destruction by Neutrophils. *N. Engl. J. Med.* **320**, 365–376 (1989).
  41. Haslett, C. Resolution of acute inflammation and the role of apoptosis in the tissue fate of granulocytes. *Clin. Sci.* **83**, 639–48 (1992).
  42. Stockley, R. A. Neutrophils and the Pathogenesis of COPD. *Chest* **121**, 151S–155S (2002).
  43. Brown, V., Elborn, J. S., Bradley, J. & Ennis, M. Dysregulated apoptosis and NF $\kappa$ B expression in COPD subjects. *Respir. Res.* **10**, 24 (2009).
  44. Matute-Bello, G. *et al.* Neutrophil apoptosis in the acute respiratory distress syndrome. *Am. J. Respir. Crit. Care Med.* **156**, 1969–77 (1997).
  45. World Health Organization. Chronic obstructive pulmonary disease (COPD). (2018). Available at: <http://www.who.int/respiratory/copd/en/>.
  46. Fahy, J. V., Kim, K. W., Liu, J. & Boushey, H. A. Prominent neutrophilic inflammation in sputum from subjects with asthma exacerbation. *J. Allergy Clin. Immunol.* **95**, 843–852 (1995).
  47. Wenzel, S. E. *et al.* Bronchoscopic evaluation of severe asthma. Persistent inflammation associated with high dose glucocorticoids. *Am. J. Respir. Crit. Care Med.* **156**, 737–43 (1997).
  48. Jatakanon, A. *et al.* Neutrophilic Inflammation in Severe Persistent Asthma. *Am. J. Respir. Crit. Care Med.* **160**, 1532–1539 (1999).
  49. Ordoñez, C. L., Shaughnessy, T. E., Matthay, M. A. & Fahy, J. V. Increased Neutrophil Numbers and IL-8 Levels in Airway Secretions in Acute Severe Asthma. *Am. J. Respir. Crit. Care Med.* **161**, 1185–1190 (2000).

50. Uddin, M. *et al.* Prosurvival activity for airway neutrophils in severe asthma. *Thorax* **65**, 684–9 (2010).
51. Vandivier, R. W., Henson, P. M. & Douglas, I. S. Burying the dead: the impact of failed apoptotic cell removal (efferocytosis) on chronic inflammatory lung disease. *Chest* **129**, 1673–82 (2006).
52. Gernez, Y., Tirouvanziam, R. & Chanez, P. Neutrophils in chronic inflammatory airway diseases: can we target them and how? *Eur. Respir. J.* **35**, 467–9 (2010).
53. Pillinger, M. H. & Abramson, S. B. The neutrophil in rheumatoid arthritis. *Rheum. Dis. Clin. North Am.* **21**, 691–714 (1995).
54. Nathan, C. & Ding, A. Nonresolving inflammation. *Cell* **140**, 871–82 (2010).
55. Wright, H. L., Moots, R. J. & Edwards, S. W. The multifactorial role of neutrophils in rheumatoid arthritis. *Nat. Rev. Rheumatol.* **10**, 593–601 (2014).
56. Libby, P. Atherosclerosis: the new view. *Sci. Am.* **286**, 46–55 (2002).
57. Wellen, K. E. & Hotamisligil, G. S. Inflammation, stress, and diabetes. *J. Clin. Invest.* **115**, 1111–9 (2005).
58. Schleimer, R. P., Claman, H. N., Oronsky, A. & Goodwin, J. S. Antiinflammatory steroid action: Basic and clinical aspects. *Arthritis Rheum.* **33**, 1448–1448 (1990).
59. Barnes, P. J. & Stockley, R. A. COPD: current therapeutic interventions and future approaches. *Eur. Respir. J.* **25**, 1084–106 (2005).
60. Patrick, G. L. *An Introduction to Medicinal Chemistry*. (Oxford University Press, Oxford, 2013).
61. Stewart, A. Mediators and receptors in the resolution of inflammation: drug targeting opportunities. *Br. J. Pharmacol.* **158**, 933–935 (2009).
62. Morjaria, J. B., Malerba, M. & Polosa, R. Biologic and pharmacologic therapies in clinical development for the inflammatory response in COPD. *Drug Discov. Today* **15**, 396–405 (2010).
63. Serhan, C. N. *et al.* Design of lipoxin A4 stable analogs that block transmigration and adhesion of human neutrophils. *Biochemistry* **34**, 14609–15 (1995).
64. Serhan, C. N. *et al.* Resolvins: a family of bioactive products of omega-3 fatty acid transformation circuits initiated by aspirin treatment that counter proinflammation signals. *J. Exp. Med.* **196**, 1025–37 (2002).
65. Schwab, J. M., Chiang, N., Arita, M. & Serhan, C. N. Resolvin E1 and protectin D1 activate inflammation-resolution programmes. *Nature* **447**, 869–74 (2007).
66. Serhan, C. N., Chiang, N. & Van Dyke, T. E. Resolving inflammation: dual anti-inflammatory and pro-resolution lipid mediators. *Nat. Rev. Immunol.* **8**, 349–361 (2008).
67. Norling, L. V. & Serhan, C. N. Profiling in resolving inflammatory exudates identifies novel anti-inflammatory and pro-resolving mediators and signals for termination. *J. Intern. Med.* **268**, 15–24 (2010).
68. Serhan, C. N. Pro-resolving lipid mediators are leads for resolution physiology.

*Nature* **510**, 92–101 (2014).

69. Serhan, C. N. *et al.* Novel Functional Sets of Lipid-Derived Mediators with Antiinflammatory Actions Generated from Omega-3 Fatty Acids via Cyclooxygenase 2-Nonsteroidal Antiinflammatory Drugs and Transcellular Processing. *J. Exp. Med.* **192**, 1197–1204 (2000).
70. Hasturk, H. *et al.* Resolvin E1 regulates inflammation at the cellular and tissue level and restores tissue homeostasis in vivo. *J. Immunol.* **179**, 7021–9 (2007).
71. Serhan, C. N. *et al.* Maresins: novel macrophage mediators with potent antiinflammatory and proresolving actions. *J. Exp. Med.* **206**, 15–23 (2009).
72. Marcon, R. *et al.* Maresin 1, a proresolving lipid mediator derived from omega-3 polyunsaturated fatty acids, exerts protective actions in murine models of colitis. *J. Immunol.* **191**, 4288–98 (2013).
73. Hallett, J. M. *et al.* Novel pharmacological strategies for driving inflammatory cell apoptosis and enhancing the resolution of inflammation. *Trends Pharmacol. Sci.* **29**, 250–257 (2008).
74. Filep, J. G. & Kebir, D. El. Neutrophil apoptosis: A target for enhancing the resolution of inflammation. *J. Cell. Biochem.* **108**, 1039–1046 (2009).
75. Leitch, A. E. *et al.* The cyclin-dependent kinase inhibitor R-roscovitine down-regulates Mcl-1 to override pro-inflammatory signalling and drive neutrophil apoptosis. *Eur. J. Immunol.* **40**, 1127–38 (2010).
76. Burgon, J. *et al.* Serum and Glucocorticoid-Regulated Kinase 1 Regulates Neutrophil Clearance during Inflammation Resolution. *J. Immunol.* **192**, 1796–1805 (2014).
77. Burch, R. M. *et al.* NPC 15669 inhibits the reversed passive Arthus reaction in rats by blocking neutrophil recruitment. *J. Pharmacol. Exp. Ther.* **263**, 933–7 (1992).
78. Chapman, R. W. *et al.* A novel, orally active CXCR1/2 receptor antagonist, Sch527123, inhibits neutrophil recruitment, mucus production, and goblet cell hyperplasia in animal models of pulmonary inflammation. *J. Pharmacol. Exp. Ther.* **322**, 486–93 (2007).
79. Lazaar, A. L. *et al.* SB-656933, a novel CXCR2 selective antagonist, inhibits ex vivo neutrophil activation and ozone-induced airway inflammation in humans. *Br. J. Clin. Pharmacol.* **72**, 282–293 (2011).
80. Virtala, R., Ekman, A.-K., Jansson, L., Westin, U. & Cardell, L. O. Airway inflammation evaluated in a human nasal lipopolysaccharide challenge model by investigating the effect of a CXCR2 inhibitor. *Clin. Exp. Allergy* **42**, 590–596 (2012).
81. De Soyza, A. *et al.* A randomised, placebo-controlled study of the CXCR2 antagonist AZD5069 in bronchiectasis. *Eur. Respir. J.* **46**, 1021–32 (2015).
82. Thisse, C. & Zon, L. I. Organogenesis--heart and blood formation from the zebrafish point of view. *Science (80-. ).* **295**, 457–62 (2002).
83. Lieschke, G. J. & Currie, P. D. Animal models of human disease: zebrafish swim into view. *Nat. Rev. Genet.* **8**, 353–367 (2007).

84. Renshaw, S. A. & Trede, N. S. A model 450 million years in the making: zebrafish and vertebrate immunity. *Dis. Model. Mech.* **5**, 38–47 (2012).
85. Amsterdam, A. *et al.* A large-scale insertional mutagenesis screen in zebrafish. *Genes Dev.* **13**, 2713–24 (1999).
86. Renshaw, S. A. *et al.* A transgenic zebrafish model of neutrophilic inflammation. *Blood* **108**, 3976–8 (2006).
87. Haffter, P. *et al.* The identification of genes with unique and essential functions in the development of the zebrafish, *Danio rerio*. *Development* **123**, 1–36 (1996).
88. Kawakami, A., Fukazawa, T. & Takeda, H. Early fin primordia of zebrafish larvae regenerate by a similar growth control mechanism with adult regeneration. *Dev. Dyn.* **231**, 693–9 (2004).
89. Poss, K. D., Wilson, L. G. & Keating, M. T. Heart regeneration in zebrafish. *Science* **298**, 2188–90 (2002).
90. MacRae, C. A. & Peterson, R. T. Zebrafish as tools for drug discovery. *Nat Rev Drug Discov* **14**, 721–731 (2015).
91. Bowman, T. V. & Zon, L. I. Swimming into the Future of Drug Discovery: *In Vivo* Chemical Screens in Zebrafish. *ACS Chem. Biol.* **5**, 159–161 (2010).
92. Strähle, U. & Grabher, C. The zebrafish embryo as a model for assessing off-target drug effects. *Dis. Model. Mech.* **3**, 689–92 (2010).
93. Sander, J. D. *et al.* Targeted gene disruption in somatic zebrafish cells using engineered TALENs. *Nat. Biotechnol.* **29**, 697–698 (2011).
94. Wittmann, C. *et al.* A Zebrafish Drug-Repurposing Screen Reveals sGC-Dependent and sGC-Independent Pro-Inflammatory Activities of Nitric Oxide. *PLoS One* **10**, e0137286 (2015).
95. Kola, I. & Landis, J. Can the pharmaceutical industry reduce attrition rates? *Nat. Rev. Drug Discov.* **3**, 711–716 (2004).
96. Cook, D. *et al.* Lessons learned from the fate of AstraZeneca’s drug pipeline: a five-dimensional framework. *Nat. Rev. Drug Discov.* **13**, 419–431 (2014).
97. Boyer, S., Brealey, C. & Davis, A. M. in *Attrition in the Pharmaceutical Industry* 5–45 (John Wiley & Sons Inc, Hoboken, 2015).
98. Waring, M. J. *et al.* An analysis of the attrition of drug candidates from four major pharmaceutical companies. *Nat. Rev. Drug Discov.* **14**, 475–486 (2015).
99. Kumar, S. & Hedges, S. B. A molecular timescale for vertebrate evolution. *Nature* **392**, 917–920 (1998).
100. Trede, N. S., Langenau, D. M., Traver, D., Look, A. T. & Zon, L. I. The Use of Zebrafish to Understand Immunity. *Immunity* **20**, 367–379 (2004).
101. Davis, J. M. *et al.* Real-Time Visualization of Mycobacterium-Macrophage Interactions Leading to Initiation of Granuloma Formation in Zebrafish Embryos. *Immunity* **17**, 693–702 (2002).
102. Lam, S. H., Chua, H. L., Gong, Z., Lam, T. J. & Sin, Y. M. Development and

maturation of the immune system in zebrafish, *Danio rerio*: a gene expression profiling, in situ hybridization and immunological study. *Dev. Comp. Immunol.* **28**, 9–28 (2004).

103. Henry, K. M., Loynes, C. A., Whyte, M. K. B. & Renshaw, S. A. Zebrafish as a model for the study of neutrophil biology. *J. Leukoc. Biol.* **94**, 633–642 (2013).
104. Lieschke, G. J., Oates, A. C., Crowhurst, M. O., Ward, A. C. & Layton, J. E. Morphologic and functional characterization of granulocytes and macrophages in embryonic and adult zebrafish. *Blood* **98**, 3087–3096 (2001).
105. Bennett, C. M. *et al.* Myelopoiesis in the zebrafish, *Danio rerio*. *Blood* **98**, 643–651 (2001).
106. Colucci-Guyon, E., Tinevez, J.-Y., Renshaw, S. A. & Herbomel, P. Strategies of professional phagocytes in vivo: unlike macrophages, neutrophils engulf only surface-associated microbes. *J. Cell Sci.* **124**, 3053–9 (2011).
107. Palić, D., Ostojić, J., Andreasen, C. B. & Roth, J. A. Fish cast NETs: Neutrophil extracellular traps are released from fish neutrophils. *Dev. Comp. Immunol.* **31**, 805–816 (2007).
108. Mathias, J. R. *et al.* Live imaging of chronic inflammation caused by mutation of zebrafish *Hai1*. *J. Cell Sci.* **120**, 3372–83 (2007).
109. Gray, C. *et al.* Simultaneous intravital imaging of macrophage and neutrophil behaviour during inflammation using a novel transgenic zebrafish. *Thromb. Haemost.* **105**, 811–9 (2011).
110. Ellett, F., Pase, L., Hayman, J. W., Andrianopoulos, A. & Lieschke, G. J. *mpeg1* promoter transgenes direct macrophage-lineage expression in zebrafish. *Blood* **117**, e49-56 (2011).
111. Walton, E. M., Cronan, M. R., Beerman, R. W. & Tobin, D. M. The Macrophage-Specific Promoter *mfap4* Allows Live, Long-Term Analysis of Macrophage Behavior during Mycobacterial Infection in Zebrafish. *PLoS One* **10**, e0138949 (2015).
112. Yang, L.-L. *et al.* Endotoxin molecule lipopolysaccharide-induced zebrafish inflammation model: a novel screening method for anti-inflammatory drugs. *Molecules* **19**, 2390–409 (2014).
113. d’Alençon, C. A. *et al.* A high-throughput chemically induced inflammation assay in zebrafish. *BMC Biol.* **8**, 151 (2010).
114. Zhang, Y. *et al.* Manipulating the air-filled zebrafish swim bladder as a neutrophilic inflammation model for acute lung injury. *Cell Death Dis.* **7**, e2470–e2470 (2016).
115. Peterson, R. T., Link, B. A., Dowling, J. E. & Schreiber, S. L. Small molecule developmental screens reveal the logic and timing of vertebrate development. *Proc. Natl. Acad. Sci. U. S. A.* **97**, 12965–9 (2000).
116. Zon, L. I. & Peterson, R. T. In vivo drug discovery in the zebrafish. *Nat. Rev. Drug Discov.* **4**, 35–44 (2005).
117. Takaki, K., Cosma, C. L., Troll, M. A. & Ramakrishnan, L. An In Vivo Platform for

- Rapid High-Throughput Antitubercular Drug Discovery. *Cell Rep.* **2**, 175–184 (2012).
118. Hall, C. J. *et al.* Repositioning drugs for inflammatory disease – fishing for new anti-inflammatory agents. *Dis. Model. Mech.* **7**, 1069–1081 (2014).
  119. Wang, X. *et al.* Inhibitors of neutrophil recruitment identified using transgenic zebrafish to screen a natural product library. *Dis. Model. Mech.* **7**, 163–9 (2014).
  120. Hoizey, D. & Hoizey, M.-J. *A History of Chinese Medicine*. (Edinburgh University Press, Edinburgh, 1993).
  121. Nakao, M. & Fukushima, T. On the Chemical Composition of *Salvia Miltiorrhiza* (Chinese drug Tan-shen). *Yakugaku Zasshi* **54**, 844–858 (1934).
  122. Chang, H. M. *et al.* Structure elucidation and total synthesis of new tanshinones isolated from *Salvia miltiorrhiza* Bunge (Danshen). *J. Org. Chem.* **55**, 3537–3543 (1990).
  123. Pan, X., Niu, G. & Liu, H. Microwave-assisted extraction of tanshinones from *Salvia miltiorrhiza bunge* with analysis by high-performance liquid chromatography. *J. Chromatogr. A* **922**, 371–375 (2001).
  124. Zeng, A. *et al.* Extraction of Tanshinone IIA and Cryptotanshinone from the Rhizome of *Salvia miltiorrhiza* Bunge: Kinetics and Modeling. *Sep. Sci. Technol.* **49**, 2330–2337 (2014).
  125. Xie, T., Ma, S., Lou, H., Zhu, R. & Sun, L. Two novel abietane norditerpenoids with anti-inflammatory properties from the roots of *Salvia miltiorrhiza* var. *alba*. *Tetrahedron Lett.* **55**, 7106–7109 (2014).
  126. Liu, J., Shen, H.-M. & Ong, C.-N. *Salvia miltiorrhiza* inhibits cell growth and induces apoptosis in human hepatoma HepG2 cells. *Cancer Lett.* **153**, 85–93 (2000).
  127. Zhou, L., Zuo, Z. & Chow, M. S. S. Danshen: An Overview of Its Chemistry, Pharmacology, Pharmacokinetics, and Clinical Use. *J. Clin. Pharmacol.* **45**, 1345–1359 (2005).
  128. Cheng, T. O. Cardiovascular effects of Danshen. *Int. J. Cardiol.* **121**, 9–22 (2007).
  129. Lin, T.-H. & Hsieh, C.-L. Pharmacological effects of *Salvia miltiorrhiza* (Danshen) on cerebral infarction. *Chin. Med.* **5**, 22 (2010).
  130. Chen, X., Guo, J., Bao, J., Lu, J. & Wang, Y. The Anticancer Properties of *Salvia Miltiorrhiza* Bunge (Danshen): A Systematic Review. *Med. Res. Rev.* **34**, 768–794 (2014).
  131. Su, C.-Y., Ming, Q.-L., Rahman, K., Han, T. & Qin, L.-P. *Salvia miltiorrhiza*: Traditional medicinal uses, chemistry, and pharmacology. *Chin. J. Nat. Med.* **13**, 163–182 (2015).
  132. Wang, L. *et al.* *Salvia miltiorrhiza*: A Potential Red Light to the Development of Cardiovascular Diseases. *Curr. Pharm. Des.* **23**, 1077–1097 (2017).
  133. Chen, W. & Chen, G. Danshen (*Salvia miltiorrhiza* Bunge): A Prospective Healing Sage for Cardiovascular Diseases. *Curr. Pharm. Des.* **23**, 5125–5135 (2018).

134. Kim, J. Y. *et al.* Induction of Apoptosis by Tanshinone I via Cytochrome c Release in Activated Hepatic Stellate Cells. *Pharmacol. Toxicol.* **92**, 195–200 (2003).
135. Lu, M., Wang, C. & Wang, J. Tanshinone I induces human colorectal cancer cell apoptosis: The potential roles of Aurora A-p53 and survivin-mediated signaling pathways. *Int. J. Oncol.* **49**, 603–610 (2016).
136. Jing, X. *et al.* Tanshinone I induces apoptosis and pro-survival autophagy in gastric cancers. *Cancer Chemother. Pharmacol.* **77**, 1171–1181 (2016).
137. Sung, H. J., Choi, S. M., Yoon, Y. & An, K. S. Tanshinone IIA, an ingredient of *Salvia miltiorrhiza* BUNGE, induces apoptosis in human leukemia cell lines through the activation of caspase-3. *Exp. Mol. Med.* **31**, 174–178 (1999).
138. Yoon, Y., Kim, Y.-O., Jeon, W.-K., Park, H.-J. & Sung, H. J. Tanshinone IIA isolated from *Salvia miltiorrhiza* BUNGE induced apoptosis in HL60 human premyelocytic leukemia cell line. *J. Ethnopharmacol.* **68**, 121–127 (1999).
139. Wang, J. *et al.* Growth inhibition and induction of apoptosis and differentiation of tanshinone IIA in human glioma cells. *J. Neurooncol.* **82**, 11–21 (2007).
140. Feng, J., Li, S. & Chen, H. Tanshinone IIA ameliorates apoptosis of cardiomyocytes induced by endoplasmic reticulum stress. *Exp. Biol. Med.* **241**, 2042–2048 (2016).
141. Huang, S.-T. *et al.* Tanshinone IIA induces intrinsic apoptosis in osteosarcoma cells both in vivo and in vitro associated with mitochondrial dysfunction. *Sci. Rep.* **7**, 40382 (2017).
142. Liu, J.-J. *et al.* Inactivation of PI3k/Akt signaling pathway and activation of caspase-3 are involved in tanshinone I-induced apoptosis in myeloid leukemia cells in vitro. *Ann. Hematol.* **89**, 1089–1097 (2010).
143. Jung, J. H. *et al.* Apoptosis Induced by Tanshinone IIA and Cryptotanshinone Is Mediated by Distinct JAK/STAT3/5 and SHP1/2 Signaling in Chronic Myeloid Leukemia K562 Cells. *Evid. Based. Complement. Alternat. Med.* **2013**, 805639 (2013).
144. Su, C.-C. Tanshinone IIA Could Inhibit Pancreatic Cancer BxPC-3 Cells through Increasing PERK, ATF6, Caspase-12 and CHOP Expression to Induce Apoptosis. *J. Biomed. Sci. Eng.* **8**, 149–159 (2015).
145. Liu, H.-Y., Li, Q.-R., Cheng, X.-F., Wang, G.-J. & Hao, H.-P. NAMPT inhibition synergizes with NQO1-targeting agents in inducing apoptotic cell death in non-small cell lung cancer cells. *Chin. J. Nat. Med.* **14**, 582–589 (2016).
146. Su, C.-C., Chen, G.-W. & Lin, J.-G. Growth inhibition and apoptosis induction by tanshinone I in human colon cancer Colo 205 cells. *Int. J. Mol. Med.* **22**, 613–8 (2008).
147. Wang, L. *et al.* Evaluation and SAR analysis of the cytotoxicity of tanshinones in colon cancer cells. *Chin. J. Nat. Med.* **12**, 167–171 (2014).
148. Wang, X. *et al.* Potential anticancer activity of tanshinone IIA against human breast cancer. *Int. J. Cancer* **116**, 799–807 (2005).
149. Yuan, S.-L., Wang, X.-J. & Wei, Y.-Q. Anticancer effect of tanshinone and its

- mechanisms. *Chin. J. Cancer* **22**, 1363–6 (2003).
150. Liu, W. *et al.* Antiandrogenic, maspin induction, and antiprostata cancer activities of tanshinone IIA and its novel derivatives with modification in ring A. *J. Med. Chem.* **55**, 971–5 (2012).
  151. Jiang, H. *et al.* Tanshinone IIA enhances bystander cell killing of cancer cells expressing *Drosophila melanogaster* deoxyribonucleoside kinase in nuclei and mitochondria. *Oncol. Rep.* **34**, 1487–1493 (2015).
  152. Cao, E.-H., Liu, X.-Q., Wang, J.-J. & Xu, N.-F. Effect of natural antioxidant tanshinone II-A on DNA damage by lipid peroxidation in liver cells. *Free Radic. Biol. Med.* **20**, 801–806 (1996).
  153. Zhang, K., Bao, Y., Wu, P. & Station, A. E. Antioxidative Components of Tanshen (*Salvia miltiorrhiza* Bung). *J Agric Food Chem* **38**, 1194–1197 (1990).
  154. Chu Weng, X. & Gordon, M. H. Antioxidant Activity of Quinones Extracted from Tanshen (*Salvia miltiorrhiza* Bunge). *J. Agric. Food Chem* **40**, 7331–1336 (1992).
  155. Niu, X.-L. *et al.* Tanshinone II-A inhibits low density lipoprotein oxidation *in vitro*. *Free Radic. Res.* **33**, 305–312 (2000).
  156. Yagi, A., Okamura, N., Tanonaka, K. & Takeo, S. Effects of Tanshinone VI Derivatives on Post-Hypoxic Contractile Dysfunction of Perfused Rat Hearts. *Planta Med.* **60**, 405–409 (1994).
  157. Fu, J. *et al.* Tanshinone IIA protects cardiac myocytes against oxidative stress-triggered damage and apoptosis. *Eur. J. Pharmacol.* **568**, 213–221 (2007).
  158. Ren, Z. H., Tong, Y. H., Xu, W., Ma, J. & Chen, Y. Tanshinone II A attenuates inflammatory responses of rats with myocardial infarction by reducing MCP-1 expression. *Phytomedicine* **17**, 212–218 (2010).
  159. Shang, Q., Xu, H. & Huang, L. Tanshinone IIA: A Promising Natural Cardioprotective Agent. *Evid. Based. Complement. Alternat. Med.* **2012**, 716459 (2012).
  160. Gao, S. *et al.* Cardiovascular actions and therapeutic potential of tanshinone IIA. *Atherosclerosis* **220**, 3–10 (2012).
  161. Xu, S. *et al.* Tanshinone II-A inhibits oxidized LDL-induced LOX-1 expression in macrophages by reducing intracellular superoxide radical generation and NF- $\kappa$ B activation. *Transl. Res.* **160**, 114–124 (2012).
  162. Chang, C.-C. *et al.* The anti-atherosclerotic effect of tanshinone IIA is associated with the inhibition of TNF- $\alpha$ -induced VCAM-1, ICAM-1 and CX3CL1 expression. *Phytomedicine* **21**, 207–216 (2014).
  163. Chen, Z. & Xu, H. Anti-Inflammatory and Immunomodulatory Mechanism of Tanshinone IIA for Atherosclerosis. *Evid. Based. Complement. Alternat. Med.* **2014**, 267976 (2014).
  164. Fang, J., Little, P. J. & Xu, S. Atheroprotective Effects and Molecular Targets of Tanshinones Derived From Herbal Medicine Danshen. *Med. Res. Rev.* **38**, 201–228 (2018).

165. Wang, B., Ge, Z., Cheng, Z. & Zhao, Z. Tanshinone IIA suppresses the progression of atherosclerosis by inhibiting the apoptosis of vascular smooth muscle cells and the proliferation and migration of macrophages induced by ox-LDL. *Biol. Open* **6**, 489–495 (2017).
166. Liu, Y., Chen, H. & Jiang, Y. Effect of tanshinone IIA on CCl<sub>4</sub>-induced liver fibrosis in rats. *J. Chinese Med. Mater.* **25**, 31–3 (2002).
167. Liu, Y., Wang, X. & Liu, Y. Protective effects of tanshinone IIA on injured primary cultured rat hepatocytes induced by CCl<sub>4</sub>. *J. Chinese Med. Mater.* **26**, 415–7 (2003).
168. Wang, W. *et al.* Tanshinone IIA protects against acetaminophen-induced hepatotoxicity via activating the Nrf2 pathway. *Phytomedicine* **23**, 589–596 (2016).
169. Hwang, S.-L. *et al.* Tanshinone IIA improves endoplasmic reticulum stress-induced insulin resistance through AMP-activated protein kinase. *Biochem. Biophys. Res. Commun.* **430**, 1246–1252 (2013).
170. Li, Y.-H. *et al.* Mechanisms of protection against diabetes-induced impairment of endothelium-dependent vasorelaxation by Tanshinone IIA. *Biochim. Biophys. Acta - Gen. Subj.* **1850**, 813–823 (2015).
171. Kim, D. H. *et al.* Tanshinone I enhances learning and memory, and ameliorates memory impairment in mice via the extracellular signal-regulated kinase signalling pathway. *Br. J. Pharmacol.* **158**, 1131–1142 (2009).
172. Zhu, J. Antibacterial study of tanshinone IIA. *Zhongguo Yaoke Daxue Xuebao* **35**, 368–370 (2004).
173. Mothana, R. A. A., Jansen, R., Gruenert, R., Bednarski, P. J. & Lindequist, U. Antimicrobial and cytotoxic abietane diterpenoids from the roots of *Meriandera benghalensis* (Roxb.) Benth. *Pharmazie* **64**, 613–5 (2009).
174. Zhao, J. *et al.* Diterpenoid Tanshinones and Phenolic Acids from Cultured Hairy Roots of *Salvia miltiorrhiza* Bunge and Their Antimicrobial Activities. *Molecules* **16**, 2259–2267 (2011).
175. Wang, D. *et al.* Unveiling the Mode of Action of Two Antibacterial Tanshinone Derivatives. *Int. J. Mol. Sci.* **16**, 17668–81 (2015).
176. Jassbi, A. R., Zare, S., Firuzi, O. & Xiao, J. Bioactive phytochemicals from shoots and roots of *Salvia* species. *Phytochem. Rev.* **15**, 829–867 (2016).
177. Lam, B. Y. H. *et al.* Neuroprotective effects of tanshinones in transient focal cerebral ischemia in mice. *Phytomedicine* **10**, 286–291 (2003).
178. Dong, K., Xu, W., Yang, J., Qiao, H. & Wu, L. Neuroprotective effects of Tanshinone IIA on permanent focal cerebral ischemia in mice. *Phyther. Res.* **23**, 608–613 (2009).
179. Liu, L. *et al.* The neuroprotective effects of Tanshinone IIA are associated with induced nuclear translocation of TORC1 and upregulated expression of TORC1, pCREB and BDNF in the acute stage of ischemic stroke. *Brain Res. Bull.* **82**, 228–

233 (2010).

180. Wang, W. *et al.* Tanshinone IIA attenuates neuronal damage and the impairment of long-term potentiation induced by hydrogen peroxide. *J. Ethnopharmacol.* **134**, 147–155 (2011).
181. Tang, Q. *et al.* Neuroprotective effects of tanshinone IIA and/or tetramethylpyrazine in cerebral ischemic injury in vivo and in vitro. *Brain Res.* **1488**, 81–91 (2012).
182. Zhang, Y. *et al.* Tanshinone IIA pretreatment protects myocardium against ischaemia/reperfusion injury through the phosphatidylinositol 3-kinase/Akt-dependent pathway in diabetic rats. *Diabetes, Obes. Metab.* **12**, 316–322 (2010).
183. Lu, B.-L., Li, J., Zhou, J., Li, W.-W. & Wu, H.-F. Tanshinone IIA decreases the levels of inflammation induced by A $\beta$ 1–42 in brain tissues of Alzheimer’s disease model rats. *Neuroreport* **27**, 883–893 (2016).
184. Park, J. H. *et al.* Anti-inflammatory Effect of Tanshinone I in Neuroprotection Against Cerebral Ischemia–Reperfusion Injury in the Gerbil Hippocampus. *Neurochem. Res.* **39**, 1300–1312 (2014).
185. Kim, S. Y. *et al.* Effects of tanshinone I isolated from *Salvia miltiorrhiza bunge* on arachidonic acid metabolism and in vivo inflammatory responses. *Phyther. Res.* **16**, 616–20 (2002).
186. Kang, B. Y., Chung, S. W., Kim, S. H., Ryu, S. Y. & Kim, T. S. Inhibition of interleukin-12 and interferon- $\gamma$  production in immune cells by tanshinones from *Salvia miltiorrhiza*. *Immunopharmacology* **49**, 355–361 (2000).
187. Choi, M.-S. *et al.* Molecular mechanisms of inhibitory activities of tanshinones on Lipopolysaccharide-Induced nitric oxide generation in RAW 264.7 cells. *Arch. Pharm. Res.* **27**, 1233–1237 (2004).
188. Jeon, S. J., Son, K. H., Kim, Y. S., Choi, Y. H. & Kim, H. P. Inhibition of prostaglandin and nitric oxide production in lipopolysaccharide-treated RAW 264.7 cells by tanshinones from the roots of *Salvia miltiorrhiza bunge*. *Arch. Pharm. Res.* **31**, 758–763 (2008).
189. Jang, S.-I. *et al.* Tanshinone IIA from *Salvia miltiorrhiza* Inhibits Inducible Nitric Oxide Synthase Expression and Production of TNF- $\alpha$ , IL-1 $\beta$  and IL-6 in Activated RAW 264.7 Cells. *Planta Med.* **69**, 1057–1059 (2003).
190. Xu, M. *et al.* Tanshinone IIA reduces lethality and acute lung injury in LPS-treated mice by inhibition of PLA2 activity. *Eur. J. Pharmacol.* **607**, 194–200 (2009).
191. Ma, S., Zhang, D., Lou, H., Sun, L. & Ji, J. Evaluation of the anti-inflammatory activities of tanshinones isolated from *Salvia miltiorrhiza* var. *alba* roots in THP-1 macrophages. *J. Ethnopharmacol.* **188**, 193–199 (2016).
192. Zhuang, S. *et al.* Tanshinone IIA Induces Heme Oxygenase 1 Expression and Inhibits Cyclic Strain-Induced Interleukin 8 Expression in Vascular Endothelial Cells. *Am. J. Chin. Med.* **44**, 377–388 (2016).
193. Shi, X., Huang, L., Xiong, S. & Zhong, X. Protective effect of tanshinone II A on

- lipopolysaccharide-induced lung injury in rats. *Chin. J. Integr. Med.* **13**, 137–140 (2007).
194. Fan, G.-W. *et al.* The anti-inflammatory activities of Tanshinone IIA, an active component of TCM, are mediated by estrogen receptor activation and inhibition of iNOS. *J. Steroid Biochem. Mol. Biol.* **113**, 275–280 (2009).
  195. Yin, X. *et al.* Tanshinone IIA attenuates the inflammatory response and apoptosis after traumatic injury of the spinal cord in adult rats. *PLoS One* **7**, e38381 (2012).
  196. Liu, F., Hao, H.-P. & Wang, G.-J. NQO1-mediated biotransformation determines the cytotoxicity of tanshinone IIA. *Chin. J. Nat. Med.* **10**, 353–357 (2012).
  197. Xu, M. *et al.* Tanshinone IIA therapeutically reduces LPS-induced acute lung injury by inhibiting inflammation and apoptosis in mice. *Acta Pharmacol. Sin.* **36**, 179–87 (2015).
  198. Liu, X. *et al.* Tanshinone IIA Protects against Dextran Sulfate Sodium- (DSS-) Induced Colitis in Mice by Modulation of Neutrophil Infiltration and Activation. *Oxid. Med. Cell. Longev.* **2016**, 7916763 (2016).
  199. Zhang, S. *et al.* Tanshinone IIA ameliorates chronic arthritis in mice by modulating neutrophil activities. *Clin. Exp. Immunol.* **190**, 29–39 (2017).
  200. Baillie, A. C. & Thomson, R. H. Naturally occurring quinones. Part XI. The tanshinones. *J. Chem. Soc. C* **0**, 48–52 (1968).
  201. Sherwood, I. R. & Short, W. F. Podocarpic Acid. Part I. *J Chem Soc* **0**, 1006–1013 (1938).
  202. Fieser, L. 1,2-Naphthoquinone. *Org. Synth.* **17**, 68 (1937).
  203. Kakisawa, H. & Inouye, Y. Total syntheses of tanshinone-I, tanshinone-II, and cryptotanshinone. *Chem. Commun.* **0**, 1327b–1328 (1968).
  204. Inouye, Y. & Kakisawa, H. Total Syntheses of Tanshinone-I, Tanshinone-II and Cryptotanshinone. *Bull. Chem. Soc. Jpn.* **42**, 3318–3323 (1969).
  205. Huot, R. & Brassard, P. Synthesis of 3-methylfuroquinones. *Can. J. Chem.* **52**, 88–94 (1974).
  206. de Koning, C. B., Michael, J. P. & Rousseau, A. L. A novel method for the synthesis of phenanthrenes and benzo[a]carbazoles. *Tetrahedron Lett.* **39**, 8725–8728 (1998).
  207. de Koning, C. B., Michael, J. P. & Rousseau, A. L. A novel method for the synthesis of substituted naphthalenes and phenanthrenes. *J. Chem. Soc. Perkin Trans. 1* **0**, 787–797 (2000).
  208. Danheiser, R. L., Casebier, D. S. & Loebach, J. L. Total synthesis of dan shen diterpenoid quinones. *Tetrahedron Lett.* **33**, 1149–1152 (1992).
  209. Rubottom, G. M. & Kim, C. Preparation of Methyl Ketones by the Sequential Treatment of Carboxylic Acids with Methylolithium and Chlorotrimethylsilane. *J. Org. Chem.* **48**, 1550–1552 (1983).
  210. Danheiser, R. L. ., Miller, R. F., Brisbois, R. G. & Park, S. Z. An Improved Method

- for the Synthesis of  $\alpha$ -Diazo Ketones. *J. Org. Chem.* **55**, 1959–1964 (1990).
211. Jiao, M., Ding, C. & Zhang, A. Facile construction of 3-hydroxyphenanthrene-1,4-diones: Key intermediates to tanshinone I and its A-ring-modified analogue. *Tetrahedron* **70**, 2976–2981 (2014).
  212. Inman, M. & Moody, C. J. Synthesis of indolequinones from bromoquinones and enamines mediated by Cu(OAc)<sub>2</sub>.H<sub>2</sub>O. *J. Org. Chem.* **75**, 6023–6 (2010).
  213. Yang, H.-R., Wang, J.-J., Shao, P.-P., Yuan, S.-Y. & Li, X.-Q. A facile three-step total synthesis of tanshinone I. *J. Asian Nat. Prod. Res.* **18**, 677–683 (2016).
  214. Wu, N., Ma, W.-C., Mao, S.-J., Wu, Y. & Jin, H. Total Synthesis of Tanshinone I. *J. Nat. Prod.* **80**, 1697–1700 (2017).
  215. Cheng, X. *et al.* Syntheses of diacyltanshinol derivatives and their suppressive effects on macrophage foam cell formation by reducing oxidized LDL uptake. *Bioorg. Chem.* **52**, 24–30 (2014).
  216. Zhang, Z.-R. *et al.* In Vivo Angiogenesis Screening and Mechanism of Action of Novel Tanshinone Derivatives Produced by One-Pot Combinatorial Modification of Natural Tanshinone Mixture from *Salvia Miltiorrhiza*. *PLoS One* **9**, e100416 (2014).
  217. Tan, Y., Sun, X., Dong, F., Tian, H. & Jiang, R. Enhancing the Structural Diversity and Bioactivity of Natural Products by Combinatorial Modification Exemplified by Total Tanshinones. *Chinese J. Chem.* **33**, 1084–1088 (2015).
  218. Li, J., Xue, Y., Fan, Z., Ding, C. & Zhang, A. Difluorination of Furonaphthoquinones. *J. Org. Chem.* **82**, 7388–7393 (2017).
  219. Liu, X.-W. *et al.* Diversity-oriented TsOH catalysis-enabled construction of tanshinone-substituted bis(indolyl/pyrrolyl)methanes and their biological evaluation for anticancer activities. *Synth. Commun.* **47**, 2378–2386 (2017).
  220. Wu, L. & Yang, X. Synthesis and cytotoxic activity of tanshinone I derivatives having azacyclo moiety. *J. Chem. Pharm. Res.* **6**, 442–445 (2014).
  221. Rong, F., Xu, R., Xie, F. & Lai, H. 2-Alkyl- or aryl-substituted tanshinone derivatives, and preparation method and application thereof. (2013).
  222. Jiao, M., Ding, C. & Zhang, A. Preparation of 2-aryl derivatives of tanshinone I through a palladium-catalyzed Csp<sup>2</sup>-H activation/arylation approach. *Tetrahedron Lett.* **56**, 2799–2802 (2015).
  223. Rong, F. & Xie, F. Tanshinone I compound modified by polymer or nano micelle thereof, and preparation method and use thereof. (2016).
  224. Ding, C. *et al.* Tanshinone I derivative, preparation method and applications thereof. (2016).
  225. Wang, D. *et al.* A tanshinone I derivative enhances the activities of antibiotics against *Staphylococcus aureus* in vitro and in vivo. *Res. Microbiol.* **168**, 46–54 (2017).
  226. Wang, D. *et al.* Synthesis, characterization and anticancer activity of tanshinone I

- grafted low molecular chitosan. *Glycoconj. J.* **34**, 3–12 (2017).
227. Ding, C. *et al.* Structural Modification of Natural Product Tanshinone I Leading to Discovery of Novel Nitrogen-Enriched Derivatives with Enhanced Anticancer Profile and Improved Drug-like Properties. *J. Med. Chem.* **61**, 760–776 (2018).
228. Lee, J., Tang, J. & Snyder, J. K. Preparation and dienophilicity of 3-methyl-4,5-benzofurandione. *Tetrahedron Lett.* **28**, 3427–3430 (1987).
229. Lee, J. & Snyder, J. K. Ultrasound-Promoted Diels-Alder Reactions: Syntheses of Tanshinone IIA, Nortanshinone, and ( $\pm$ )-Tanshindiol B. *J. Am. Chem. Soc.* **111**, 1522–1524 (1989).
230. Lee, J. & Snyder, J. K. Ultrasound-Promoted Cycloadditions in the Synthesis of *Salvia miltiorrhiza* Abietanoid o-Quinones. *J. Org. Chem.* **55**, 4995–5008 (1990).
231. Shaik, F. H. & Kar, G. K. Studies on polynuclear furoquinones. Part 1: Synthesis of tri- and tetra-cyclic furoquinones simulating BCD/ABCD ring system of furoquinone diterpenoids. *Beilstein J. Org. Chem.* **5**, 47 (2009).
232. Shen, Y.-D., Tian, Y.-X., Bu, X.-Z. & Gu, L.-Q. Natural tanshinone-like heterocyclic-fused ortho-quinones from regioselective Diels–Alder reaction: Synthesis and cytotoxicity evaluation. *Eur. J. Med. Chem.* **44**, 3915–3921 (2009).
233. Kakisawa, H., Tateishi, M. & Kusumi, T. Synthesis of tanshinone-II and cryptotanshinone. *Tetrahedron Lett.* **9**, 3783–3786 (1968).
234. Tateishi, M., Kusumi, T. & Kakisawa, H. Synthesis of tanshinones. *Tetrahedron* **27**, 237–244 (1971).
235. Danheiser, R. L., Casebier, D. S. & Firooznia, F. Aromatic Annulation Strategy for the Synthesis of Angularly-Fused Diterpenoid Quinones. Total Synthesis of (+)-Neocryptotanshinone, (-)-Cryptotanshinone, Tanshinone IIA, and ( $\pm$ )-Royleanone. *J. Org. Chem.* **60**, 8341–8350 (1995).
236. Jiang, Y.-Y., Li, Q., Lu, W. & Cai, J.-C. Facile and efficient total synthesis of ( $\pm$ )-cryptotanshinone and tanshinone IIA. *Tetrahedron Lett.* **44**, 2073–2075 (2003).
237. Zeng, L.-W. *et al.* Design, synthesis, and antimicrobial activities of new tanshinone IIA esters. *Nat. Prod. Res.* **30**, 2662–2668 (2016).
238. Bi, Y.-F. *et al.* Synthesis and vasodilative activity of tanshinone IIA derivatives. *Bioorg. Med. Chem. Lett.* **20**, 4892–4894 (2010).
239. Fu, Y. & Chen, J. Synthesis of heterocyclic sulfonic acid derivative and application of heterocyclic sulfonic acid derivative in medicament therapy. (2015).
240. Fu, Y. & Chen, J. Synthesis and application of sulfonamide compounds. (2015).
241. Chen, J. Sulfotanshinone IIA derivatives, and synthesis and applications thereof as drug. (2017).
242. Chen, J. Tanshinone IIA phosphoric acid derivative and synthesis and use thereof as medicine. (2017).
243. Qin, Y.-L. *et al.* Continuous synthesis and anti-myocardial injury of tanshinone IIA derivatives. *J. Asian Nat. Prod. Res.* **20**, 139–147 (2018).

244. Haiza, M., Lee, J. & Snyder, J. K. Asymmetric syntheses of *Salvia miltiorrhiza* abietanoid o-quinones: methyl tanshinonate, tanshinone IIB, tanshindiol B and 3-hydroxytanshinone. *J. Org. Chem.* **55**, 5008–5013 (1990).
245. Zhang, J., Duan, W. & Cai, J. Asymmetric synthesis of 3(S),17-dihydroxytanshinone. *Tetrahedron* **60**, 1665–1669 (2004).
246. Lee, J.-S. *et al.* Synthesis of novel chemical probes for the study of tanshinone binding proteins. *Bioorg. Med. Chem. Lett.* **16**, 4733–4737 (2006).
247. Kurhade, S. E., Sanchawala, A. I., Ravikumar, V., Bhuniya, D. & Reddy, D. S. Total Synthesis of Isofregenedadiol. *Org. Lett.* **13**, 3690–3693 (2011).
248. Bi, X. *et al.* Synthesis and biological evaluation of tanshinone IIA derivatives as novel endothelial protective agents. *Future Med. Chem.* **9**, 1073–1085 (2017).
249. Bu, Y. & Wang, Z. Tanshinone compound 17-esterified derivative and preparation process and application thereof. (2017).
250. Bi, Y.-F. *et al.* Design, synthesis and vasodilative activity of tanshinone IIA derivatives. *Bioorg. Med. Chem. Lett.* **22**, 5141–3 (2012).
251. Ding, C., Li, J., Jiao, M. & Zhang, A. Catalyst-Free sp<sup>3</sup> C–H Acyloxylation: Regioselective Synthesis of 1-Acyloxy Derivatives of the Natural Product Tanshinone IIA. *J. Nat. Prod.* **79**, 2514–2520 (2016).
252. Liang, B. *et al.* Site-selective Csp<sup>3</sup>-H aryloxylation of natural product Tanshinone IIA and its analogues. *Tetrahedron Lett.* **58**, 1822–1825 (2017).
253. Dakin, H. D. The oxidation of hydroxy derivatives of benzaldehyde, acetophenone and related substances. *Am. Chem. J.* **42**, 477–498 (1909).
254. Kabalka, G. W., Reddy, N. K. & Narayana, C. Sodium percarbonate: A convenient reagent for the dakin reaction. *Tetrahedron Lett.* **33**, 865–866 (1992).
255. Ding, C. *et al.* One-Pot Three-Step Synthesis of Naphtho[2,3-a]carbazole-5,13-diones using a Tandem Radical Alkylation-Cyclization-Aromatization Reaction Sequence. *Adv. Synth. Catal.* **352**, 847–853 (2010).
256. Pettit, G. R., Thornhill, A., Melody, N. & Knight, J. C. Antineoplastic agents. 578. Synthesis of stilstatins 1 and 2 and their water-soluble prodrugs. *J. Nat. Prod.* **72**, 380–8 (2009).
257. Brooks, P. R. *et al.* Boron Trichloride/Tetra-n-Butylammonium Iodide: A Mild, Selective Combination Reagent for the Cleavage of Primary Alkyl Aryl Ethers. *J. Org. Chem.* **64**, 9719–9721 (1999).
258. Senol, F. S. *et al.* Selective in vitro and in silico butyrylcholinesterase inhibitory activity of diterpenes and rosmarinic acid isolated from *Perovskia atriplicifolia* Benth. and *Salvia glutinosa* L. *Phytochemistry* **133**, 33–44 (2017).
259. Kakisawa, H., Hayashi, T. & Yamazaki, T. Structures of isotanshinones. *Tetrahedron Lett.* **10**, 301–304 (1969).
260. Hayashi, T. *et al.* Mass spectral studies on tanshinones. *Org. Mass Spectrom.* **3**, 1293–1305 (1970).

261. Lee, A.-R., Wu, W.-L., Chang, W.-L., Lin, H.-C. & King, M.-L. Isolation and bioactivity of new tanshinones. *J. Nat. Prod.* **0**, 157–160 (1987).
262. Marrero, J. G., Andrés, L. S. & Luis, J. G. Quinone Derivatives by Chemical Transformations of 16-Hydroxycarnosol from *Salvia* Species. *Chem. Pharm. Bull. (Tokyo)*. **53**, 1524–1529 (2005).
263. Guo, S. *et al.* Isocryptotanshinone, a STAT3 inhibitor, induces apoptosis and pro-death autophagy in A549 lung cancer cells. *J. Drug Target.* **24**, 934–942 (2016).
264. Wu, C.-Y. *et al.* Anti-cancer effect of danshen and dihydroisotanshinone I on prostate cancer: targeting the crosstalk between macrophages and cancer cells via inhibition of the STAT3/CCL2 signaling pathway. *Oncotarget* **8**, 40246–40263 (2017).
265. Aggarwal, V. K., Staubitz, A. C. & Owen, M. Optimization of the Mizoroki–Heck Reaction Using Design of Experiment (DoE). *Org. Process Res. Dev.* **10**, 64–69 (2006).
266. Mateos, C., Mendiola, J., Carpintero, M. & Mínguez, J. M. Regioselective Palladium-Catalyzed Arylation of 4-Chloropyrazoles. *Org. Lett.* **12**, 4924–4927 (2010).
267. Renzi, P. *et al.* Kinetic Resolution of Oxazinones: Rational Exploration of Chemical Space through the Design of Experiments. *Chem. Eur. J.* **20**, 11768–11775 (2014).
268. Stone, S. *et al.* Application of design of experiments (DoE) optimization to the one-pot synthesis of 4,6-dihydropteridinones. *Org. Biomol. Chem.* **13**, 10471–10476 (2015).
269. Murray, P. M. *et al.* The application of design of experiments (DoE) reaction optimisation and solvent selection in the development of new synthetic chemistry. *Org. Biomol. Chem.* **14**, 2373–2384 (2016).
270. Cowden, C. J. Use of N-Protected Amino Acids in the Minisci Radical Alkylation. *Org. Lett.* **5**, 4497–4499 (2003).
271. Behrman, E. J.; Edwards, J. O. The thermal decomposition of peroxodisulfate ions. *Rev. Inorg. Chem.* **2**, 179–206 (1980).
272. Guengerich, F. P. Common and Uncommon Cytochrome P450 Reactions Related to Metabolism and Chemical Toxicity. *Chem. Res. Toxicol.* **14**, 611–650 (2001).
273. Lewis, J. C., Coelho, P. S. & Arnold, F. H. Enzymatic functionalization of carbon-hydrogen bonds. *Chem. Soc. Rev.* **40**, 2003–21 (2011).
274. Park, B. K., Kitteringham, N. R. & O’Neill, P. M. Metabolism of fluorine-containing drugs. *Annu. Rev. Pharmacol. Toxicol.* **41**, 443–470 (2001).
275. Gillis, E. P., Eastman, K. J., Hill, M. D., Donnelly, D. J. & Meanwell, N. A. Applications of Fluorine in Medicinal Chemistry. *J. Med. Chem.* **58**, 8315–8359 (2015).
276. Bennett, B. L. *et al.* SP600125, an anthrapyrazolone inhibitor of Jun N-terminal kinase. *Proc. Natl. Acad. Sci. U. S. A.* **98**, 13681–6 (2001).
277. Han, Z. *et al.* c-Jun N-terminal kinase is required for metalloproteinase expression

- and joint destruction in inflammatory arthritis. *J. Clin. Invest.* **108**, 73–81 (2001).
278. Robertson, A. L. *et al.* Identification of benzopyrone as a common structural feature in compounds with anti-inflammatory activity in a zebrafish phenotypic screen. *Dis. Model. Mech.* **9**, 621–632 (2016).
279. Smith, E. & Collins, I. Photoaffinity labeling in target- and binding-site identification. *Future Med. Chem.* **7**, 159–183 (2015).
280. Niethammer, P., Grabher, C., Look, A. T. & Mitchison, T. J. A tissue-scale gradient of hydrogen peroxide mediates rapid wound detection in zebrafish. *Nature* **459**, 996–999 (2009).
281. Rieger, S. & Sagasti, A. Hydrogen Peroxide Promotes Injury-Induced Peripheral Sensory Axon Regeneration in the Zebrafish Skin. *PLoS Biol.* **9**, e1000621 (2011).
282. Miranda, F. G. G. de, Vilar, J. C., Alves, I. A. N., Cavalcanti, S. C. de H. & Antonioli, Â. R. Antinociceptive and antiedematogenic properties and acute toxicity of *Tabebuia avellanedae* Lor. ex Griseb. inner bark aqueous extract. *BMC Pharmacol.* **1**, 6 (2001).
283. Almeida, E. R. de. Preclinical and Clinical Studies of Lapachol and Beta-Lapachone. *Open Nat. Prod. J.* **2**, 42–47 (2009).
284. Li, C. J., Li, Y. Z., Pinto, A. V & Pardee, A. B. Potent inhibition of tumor survival in vivo by beta-lapachone plus taxol: combining drugs imposes different artificial checkpoints. *Proc. Natl. Acad. Sci. U. S. A.* **96**, 13369–74 (1999).
285. Pardee, A., Li, Y. & Li, C. Cancer Therapy with  $\beta$ -Lapachone. *Curr. Cancer Drug Targets* **2**, 227–242 (2002).
286. Lee, J. H., Cheong, J., Park, Y. M. & Choi, Y. H. Down-regulation of cyclooxygenase-2 and telomerase activity by  $\beta$ -lapachone in human prostate carcinoma cells. *Pharmacol. Res.* **51**, 553–560 (2005).
287. Lee, J. I. *et al.* Beta-lapachone induces growth inhibition and apoptosis in bladder cancer cells by modulation of Bcl-2 family and activation of caspases. *Exp. Oncol.* **28**, 30–5 (2006).
288. Moon, D.-O. *et al.*  $\beta$ -Lapachone (LAPA) Decreases Cell Viability and Telomerase Activity in Leukemia Cells: Suppression of Telomerase Activity by LAPA. *J. Med. Food* **13**, 481–488 (2010).
289. Kung, H.-N. *et al.* Involvement of NO/cGMP signaling in the apoptotic and anti-angiogenic effects of  $\beta$ -lapachone on endothelial cells in vitro. *J. Cell. Physiol.* **211**, 522–532 (2007).
290. Kalén, M. *et al.* Combination of reverse and chemical genetic screens reveals angiogenesis inhibitors and targets. *Chem. Biol.* **16**, 432–41 (2009).
291. Guiraud, P., Steiman, R., Campos-Takaki, G.-M., Seigle-Murandi, F. & de Buochberg, M. Comparison of Antibacterial and Antifungal Activities of Lapachol and  $\beta$ -Lapachone. *Planta Med.* **60**, 373–374 (1994).
292. Pereira, E. *et al.* *Tabebuia avellanedae* naphthoquinones: activity against methicillin-resistant staphylococcal strains, cytotoxic activity and in vivo dermal

- irritability analysis. *Ann. Clin. Microbiol. Antimicrob.* **5**, 5 (2006).
293. Breger, J. *et al.* Antifungal Chemical Compounds Identified Using a *C. elegans* Pathogenicity Assay. *PLoS Pathog.* **3**, e18 (2007).
294. Kung, H.-N., Yang, M.-J., Chang, C.-F., Chau, Y.-P. & Lu, K.-S. In vitro and in vivo wound healing-promoting activities of  $\beta$ -lapachone. *Am. J. Physiol. Physiol.* **295**, C931–C943 (2008).
295. Liu, S.-H., Tzeng, H.-P., Kuo, M.-L. & Lin-Shiau, S.-Y. Inhibition of inducible nitric oxide synthase by  $\beta$ -lapachone in rat alveolar macrophages and aorta. *Br. J. Pharmacol.* **126**, 746–750 (1999).
296. Moon, D.-O., Choi, Y. H., Kim, N.-D., Park, Y.-M. & Kim, G.-Y. Anti-inflammatory effects of  $\beta$ -lapachone in lipopolysaccharide-stimulated BV2 microglia. *Int. Immunopharmacol.* **7**, 506–514 (2007).
297. Ough, M. *et al.* Efficacy of beta-lapachone in pancreatic cancer treatment: Exploiting the novel, therapeutic target NQO1. *Cancer Biol. Ther.* **4**, 102–109 (2005).
298. Byun, S. J., Son, Y., Hwan Cho, B., Chung, H.-T. & Pae, H.-O.  $\beta$ -Lapachone, a substrate of NAD(P)H:quinone oxidoreductase, induces anti-inflammatory heme oxygenase-1 via AMP-activated protein kinase activation in RAW264.7 macrophages. *J. Clin. Biochem. Nutr.* **52**, 106–111 (2013).
299. Sitônio, M. M. *et al.* Anti-inflammatory and anti-arthritic activities of 3,4-dihydro-2,2-dimethyl-2H-naphthol[1,2-b]pyran-5,6-dione ( $\beta$ -lapachone). *Inflamm. Res.* **62**, 107–113 (2013).
300. Tseng, C.-H. *et al.* Synthesis and anti-inflammatory evaluations of  $\beta$ -lapachone derivatives. *Bioorg. Med. Chem.* **21**, 523–531 (2013).
301. Tzeng, H.-P. *et al.*  $\beta$ -Lapachone Reduces Endotoxin-induced Macrophage Activation and Lung Edema and Mortality. *Am. J. Respir. Crit. Care Med.* **168**, 85–91 (2003).
302. Lee, E.-J., Ko, H.-M., Jeong, Y.-H., Park, E.-M. & Kim, H.-S.  $\beta$ -Lapachone suppresses neuroinflammation by modulating the expression of cytokines and matrix metalloproteinases in activated microglia. *J. Neuroinflammation* **12**, 133 (2015).
303. da Silva Júnior, E. N. *et al.* Synthesis and potent antitumor activity of new arylamino derivatives of nor- $\beta$ -lapachone and nor- $\alpha$ -lapachone. *Bioorg. Med. Chem.* **15**, 7035–7041 (2007).
304. da Silva Júnior, E. N. *et al.* 3-Arylamino and 3-Alkoxy-nor- $\beta$ -lapachone Derivatives: Synthesis and Cytotoxicity against Cancer Cell Lines. *J. Med. Chem.* **53**, 504–508 (2010).
305. Zhang, L. *et al.* Intermolecular Interactions between Coencapsulated Drugs Inhibit Drug Crystallization and Enhance Colloidal Stability of Polymeric Micelles. *Mol. Pharm.* **14**, 3568–3576 (2017).
306. Gontijo, T. B. *et al.* Novel fluorescent lapachone-based BODIPY: synthesis, computational and electrochemical aspects, and subcellular localisation of a

- potent antitumour hybrid quinone. *Chem. Commun.* **52**, 13281–13284 (2016).
307. dos Santos, F. S. *et al.* Redox Center Modification of Lapachones towards the Synthesis of Nitrogen Heterocycles as Selective Fluorescent Mitochondrial Imaging Probes. *European J. Org. Chem.* **2017**, 3763–3773 (2017).
308. Pinho, B. R. *et al.* How mitochondrial dysfunction affects zebrafish development and cardiovascular function: an in vivo model for testing mitochondria-targeted drugs. *Br. J. Pharmacol.* **169**, 1072–90 (2013).
309. Rao, K. V., McBride, T. J. & Oleson, J. J. Recognition and Evaluation of Lapachol as an Antitumor Agent. *Cancer Res.* **28**, 1952–1954 (1968).
310. Balassiano, I. T., De Paulo, S. A., Henriques Silva, N., Cabral, M. C. & da Gloria da Costa Carvalho, M. Demonstration of the lapachol as a potential drug for reducing cancer metastasis. *Oncol. Rep.* **13**, 329–333 (2005).
311. Nagata, K., Hirai, K. I., Koyama, J., Wada, Y. & Tamura, T. Antimicrobial activity of novel furanonaphthoquinone analogs. *Antimicrob. Agents Chemother.* **42**, 700–2 (1998).
312. Eyong, K. O. *et al.* Newbouldiaquinone A: A naphthoquinone–anthraquinone ether coupled pigment, as a potential antimicrobial and antimalarial agent from *Newbouldia laevis*. *Phytochemistry* **67**, 605–609 (2006).
313. Hussain, H., Krohn, K., Ahmad, V. U., Miana, G. A. & Green, I. R. Lapachol: An overview. *Arkivoc* **2007**, 145–171 (2007).
314. de Almeida, E. R., da Silva Filho, A. A., Dos Santos, E. R. & Correia Lopes, C. A. Antiinflammatory action of lapachol. *J. Ethnopharmacol.* **29**, 239–241 (1990).
315. Guerra, M. de O., Mazoni, A. S. B., Brandão, M. A. F. & Peters, V. M. Toxicology of Lapachol in rats: embryoletality. *Rev. Bras. Biol.* **61**, 171–174 (2001).
316. Maganha, J., Rocha, E. de S., Brandão, M. A. F., Peters, V. M. & Guerra, M. de O. Embryo development alteration in rats treated with lapachol. *Brazilian Arch. Biol. Technol.* **49**, 927–934 (2006).
317. de Cássia da Silveira e Sá, R. & de Oliveira Guerra, M. Reproductive toxicity of lapachol in adult male Wistar rats submitted to short-term treatment. *Phyther. Res.* **21**, 658–662 (2007).
318. Chen, Y. *et al.* Synthesis, discovery and preliminary SAR study of benzofuran derivatives as angiogenesis inhibitors. *Bioorg. Med. Chem. Lett.* **19**, 1851–4 (2009).
319. Zhang, J. *et al.* Design, synthesis and molecular docking of a novel small-molecule inhibitor of caspase-3. *Chem. Res. Chinese Univ.* **26**, 256–258 (2010).
320. Krompiec, S., Pigulla, M., Krompiec, M., Marciniec, B. & Chadyniak, D. Highly selective isomerization of N-allyl amines catalyzed by ruthenium and rhodium complexes. *J. Mol. Catal. A Chem.* **237**, 17–25 (2005).
321. Tsang, D. S., Yang, S., Alphonse, F.-A. & Yudin, A. K. Stereoselective isomerisation of N-allyl aziridines into geometrically stable Z enamines by using rhodium hydride catalysis. *Chem. Eur. J.* **14**, 886–94 (2008).

322. List, B. Proline-catalyzed asymmetric reactions. *Tetrahedron* **58**, 5573–5590 (2002).
323. List, B. Enamine Catalysis Is a Powerful Strategy for the Catalytic Generation and Use of Carbanion Equivalents. *Acc. Chem. Res* **37**, 548–557 (2004).
324. Notz, W., Tanaka, F. & Barbas, C. F. Enamine-Based Organocatalysis with Proline and Diamines: The Development of Direct Catalytic Asymmetric Aldol, Mannich, Michael, and Diels–Alder Reactions. *Acc. Chem. Res* **37**, 580–591 (2004).
325. Geng, F., Monteleone, M. G. & Narula, A. P. S. 3-methyl-benzofuran-5-ol and its use in perfume compositions. (2015).
326. Zhang, Y., Guo, Y., Li, Z. & Xie, Z. Biomimetic Total Synthesis of Paeoveitol. *Org. Lett.* **18**, 4578–4581 (2016).
327. Domschke, G. Reaction between enamines and quinones. IV. Synthesis of substituted 5-hydroxybenzofurans. *J. fuer Prakt. Chemie* **34**, 144–157 (1966).
328. Zimmer, H., Lankin, D. C. & Horgan, S. W. Oxidations with potassium nitrosodisulfonate (Fremy's radical). The Teuber reaction. *Chem. Rev.* **71**, 229–246 (1971).
329. Smith, M. *Organic synthesis*. (Academic Press, Cambridge, 2011).
330. Schmidt, B. Ruthenium-Catalyzed Olefin Metathesis Double-Bond Isomerization Sequence. *J. Org. Chem.* **69**, 7672–7687 (2004).
331. Sanzone, J. R. & Woerpel, K. A. High Reactivity of Strained Seven-Membered-Ring trans -Alkenes. *Angew. Chem. Int. Ed.* **55**, 790–793 (2016).
332. Smith, C. R. & RajanBabu, T. V. Low pressure vinylation of aryl and vinyl halides via Heck–Mizoroki reactions using ethylene. *Tetrahedron* **66**, 1102–1110 (2010).
333. Claessens, S., Habonimana, P. & De Kimpe, N. Synthesis of naturally occurring naphthoquinone epoxides and application in the synthesis of  $\beta$ -lapachone. *Org. Biomol. Chem.* **8**, 3790–3795 (2010).
334. Salas, C. *et al.* Trypanosoma cruzi: Activities of lapachol and  $\alpha$ - and  $\beta$ -lapachone derivatives against epimastigote and trypomastigote forms. *Bioorg. Med. Chem.* **16**, 668–674 (2008).
335. Bian, J. *et al.* Lewis acid mediated highly regioselective intramolecular cyclization for the synthesis of  $\beta$ -lapachone. *Tetrahedron Lett.* **55**, 1475–1478 (2014).
336. Eyong, K. O. *et al.* A mechanistic study on the Hooker oxidation: synthesis of novel indanecarboxylic acid derivatives from lapachol. *Org. Biomol. Chem.* **11**, 459–468 (2013).
337. Hooker, S. C. The Constitution of Lapachol and its Derivatives. Part IV. Oxidation with Potassium Permanganate. *J. Am. Chem. Soc.* **58**, 1168–1173 (1936).
338. Fieser, L. F. & Fieser, M. Naphthoquinone Antimalarials. XII. The Hooker Oxidation Reaction 1. *J. Am. Chem. Soc.* **70**, 3215–3222 (1948).
339. Rideout, D. C. & Breslow, R. Hydrophobic acceleration of Diels–Alder reactions. *J. Am. Chem. Soc.* **102**, 7816–7817 (1980).

340. Reichardt, C. & Welton, T. *Solvents and Solvent Effects in Organic Chemistry*. (Wiley-VCH, Weinheim, 2010). doi:10.1002/bbpc.19890930341
341. Ruiz-Lopez, M. F., Assfeld, X., Garcia, J. I., Mayoral, J. A. & Salvatella, L. Solvent effects on the mechanism and selectivities of asymmetric Diels-Alder reactions. *J. Am. Chem. Soc.* **115**, 8780–8787 (1993).
342. Wasa, M., Engle, K. M. & Yu, J.-Q. Cross-Coupling of C(sp<sup>3</sup>)-H Bonds with Organometallic Reagents via Pd(II)/Pd(0) Catalysis. *Isr. J. Chem.* **50**, 605–616 (2010).
343. Baudoin, O. Transition metal-catalyzed arylation of unactivated C(sp<sup>3</sup>)-H bonds. *Chem. Soc. Rev.* **40**, 4902–4911 (2011).
344. Baudoin, O. Ring Construction by Palladium(0)-Catalyzed C(sp<sup>3</sup>)-H Activation. *Acc. Chem. Res.* **50**, 1114–1123 (2017).
345. Chu, J. C. K. & Rovis, T. Complementary Strategies for Directed C(sp<sup>3</sup>)-H Functionalization: A Comparison of Transition-Metal-Catalyzed Activation, Hydrogen Atom Transfer, and Carbene/Nitrene Transfer. *Angew. Chem. Int. Ed.* **57**, 62–101 (2018).
346. Wu, Y.-T. *et al.* β-Lapachone induces heart morphogenetic and functional defects by promoting the death of erythrocytes and the endocardium in zebrafish embryos. *J. Biomed. Sci.* **18**, 70 (2011).
347. Al-Awqati, Q. One hundred years of membrane permeability: does Overton still rule? *Nat. Cell Biol.* **1**, E201-2 (1999).
348. Sai, Y. & Tsuji, A. Transporter-mediated drug delivery: recent progress and experimental approaches. *Drug Discov. Today* **9**, 712–720 (2004).
349. Shitara, Y., Horie, T. & Sugiyama, Y. Transporters as a determinant of drug clearance and tissue distribution. *Eur. J. Pharm. Sci.* **27**, 425–446 (2006).
350. Dobson, P. D. & Kell, D. B. Carrier-mediated cellular uptake of pharmaceutical drugs: an exception or the rule? *Nat. Rev. Drug Discov.* **7**, 205–20 (2008).
351. Dobson, P. D., Lanthaler, K., Oliver, S. G. & Kell, D. B. Implications of the dominant role of transporters in drug uptake by cells. *Curr Top Med Chem* **9**, 163–181 (2009).
352. Giacomini, K. M. *et al.* Membrane transporters in drug development. *Nat. Rev. Drug Discov.* **9**, 215–236 (2010).
353. Kell, D. B., Dobson, P. D. & Oliver, S. G. Pharmaceutical drug transport: the issues and the implications that it is essentially carrier-mediated only. *Drug Discov. Today* **16**, 704–14 (2011).
354. Lanthaler, K. *et al.* Genome-wide assessment of the carriers involved in the cellular uptake of drugs: a model system in yeast. *BMC Biol.* **9**, 70 (2011).
355. Kell, D. B. & Oliver, S. G. How drugs get into cells: tested and testable predictions to help discriminate between transporter-mediated uptake and lipoidal bilayer diffusion. *Front. Pharmacol.* **5**, 231 (2014).

356. Kell, D. B. What would be the observable consequences if phospholipid bilayer diffusion of drugs into cells is negligible? *Trends Pharmacol. Sci.* **36**, 15–21 (2015).
357. Dobson, P. D., Patel, Y. & Kell, D. B. ‘Metabolite-likeness’ as a criterion in the design and selection of pharmaceutical drug libraries. *Drug Discov. Today* **14**, 31–40 (2009).
358. Kell, D. B. & Goodacre, R. Metabolomics and systems pharmacology: why and how to model the human metabolic network for drug discovery. *Drug Discov. Today* **19**, 171–82 (2014).
359. O’Hagan, S., Swainston, N., Handl, J. & Kell, D. B. A ‘rule of 0.5’ for the metabolite-likeness of approved pharmaceutical drugs. *Metabolomics* **11**, 323–339 (2014).
360. O’Hagan, S. & Kell, D. B. Understanding the foundations of the structural similarities between marketed drugs and endogenous human metabolites. *Front Pharmacol* **6**, 105 (2015).
361. Gray, K. A., Yates, B., Seal, R. L., Wright, M. W. & Bruford, E. A. Genenames.org: the HGNC resources in 2015. *Nucleic Acids Res.* **43**, D1079–D1085 (2015).
362. Spratlin, J. *et al.* The absence of human equilibrative nucleoside transporter 1 is associated with reduced survival in patients with gemcitabine-treated pancreas adenocarcinoma. *Clin Cancer Res* **10**, 6956–6961 (2004).
363. Kobayashi, H. *et al.* Human equilibrative nucleoside transporter 1 expression predicts survival of advanced cholangiocarcinoma patients treated with gemcitabine-based adjuvant chemotherapy after surgical resection. *Ann Surg* **256**, 288–296 (2012).
364. Lin, L., Yee, S. W., Kim, R. B. & Giacomini, K. M. SLC transporters as therapeutic targets: emerging opportunities. *Nat. Rev. Drug Discov.* **14**, 543–60 (2015).
365. Cascorbi, I. Role of pharmacogenetics of ATP-binding cassette transporters in the pharmacokinetics of drugs. *Pharmacol Ther* **112**, 457–473 (2006).
366. Colabufo, N. A., Berardi, F., Contino, M., Niso, M. & Perrone, R. ABC pumps and their role in active drug transport. *Curr. Top. Med. Chem.* **9**, 119–29 (2009).
367. Noguchi, K., Katayama, K. & Sugimoto, Y. Human ABC transporter ABCG2/BCRP expression in chemoresistance: basic and clinical perspectives for molecular cancer therapeutics. *Pharmgenomics Pers Med* **7**, 53–64 (2014).
368. Inui, K. I., Masuda, S. & Saito, H. Cellular and molecular aspects of drug transport in the kidney. *Kidney Int* **58**, 944–958 (2000).
369. Dean, M., Rzhetsky, A. & Allikmets, R. The human ATP-binding cassette (ABC) transporter superfamily. *Genome Res* **11**, 1156–1166 (2001).
370. Cunningham, F. *et al.* Ensembl 2015. *Nucleic Acids Res.* **43**, D662–D669 (2015).
371. Goujon, M. *et al.* A new bioinformatics analysis tools framework at EMBL–EBI. *Nucleic Acids Res.* **38**, W695–W699 (2010).
372. Sievers, F. *et al.* Fast, scalable generation of high-quality protein multiple sequence alignments using Clustal Omega. *Mol. Syst. Biol.* **7**, 539 (2011).

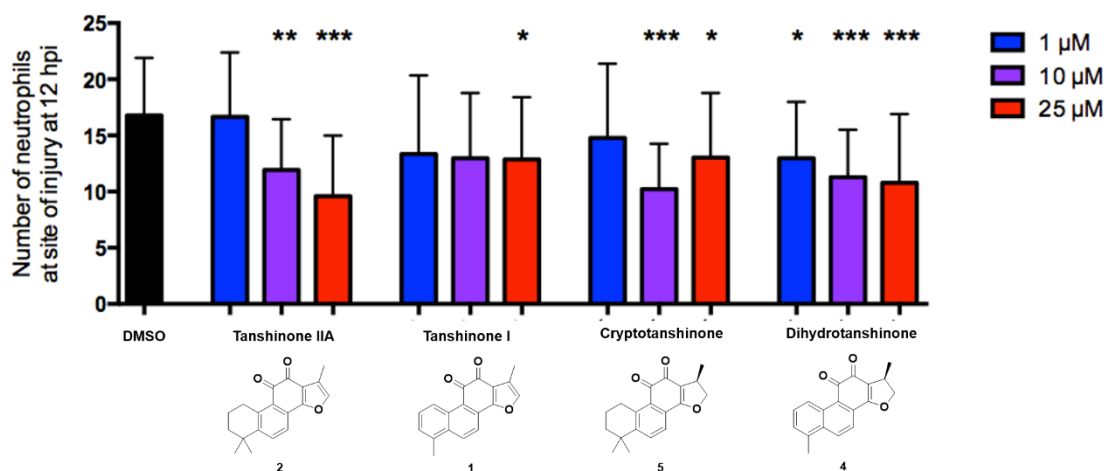
373. Dereeper, A. *et al.* Phylogeny.fr: robust phylogenetic analysis for the non-specialist. *Nucleic Acids Res.* **36**, W465–W469 (2008).
374. Letunic, I. & Bork, P. Interactive tree of life (iTOL) v3: an online tool for the display and annotation of phylogenetic and other trees. *Nucleic Acids Res.* **44**, W242–W245 (2016).
375. Wright, H. L., Thomas, H. B., Moots, R. J. & Edwards, S. W. RNA-Seq Reveals Activation of Both Common and Cytokine-Specific Pathways following Neutrophil Priming. *PLoS One* **8**, e58598 (2013).
376. Lominadze, G. *et al.* Proteomic analysis of human neutrophil granules. *Mol. Cell. Proteomics* **4**, 1503–1521 (2005).
377. de Souza Castro, M. *et al.* Proteome analysis of resting human neutrophils. *Protein Pept. Lett.* **13**, 481–487 (2006).
378. Jethwaney, D. *et al.* Proteomic analysis of plasma membrane and secretory vesicles from human neutrophils. *Proteome Sci* **5**, 12 (2007).
379. Uriarte, S. M. *et al.* Comparison of proteins expressed on secretory vesicle membranes and plasma membranes of human neutrophils. *J Immunol* **180**, 5575–5581 (2008).
380. Tomazella, G. G. *et al.* Proteomic analysis of total cellular proteins of human neutrophils. *Proteome Sci.* **7**, 32 (2009).
381. Xu, P. *et al.* Subproteome analysis of the neutrophil cytoskeleton. *Proteomics* **9**, 2037–2049 (2009).
382. Rørvig, S., Østergaard, O., Heegaard, N. H. H. & Borregaard, N. Proteome profiling of human neutrophil granule subsets, secretory vesicles, and cell membrane: correlation with transcriptome profiling of neutrophil precursors. *J. Leukoc. Biol.* **94**, 711–721 (2013).
383. Zhou, J.-Y. *et al.* Trauma-associated human neutrophil alterations revealed by comparative proteomics profiling. *Proteomics – Clin. Appl.* **7**, 571–583 (2013).
384. Chatterjee, A., Stockwell, P. A., Rodger, E. J. & Morison, I. M. Genome-scale DNA methylome and transcriptome profiling of human neutrophils. *Sci. Data* **3**, 160019 (2016).
385. Rougeot, J. *et al.* in *Host-Bacteria Interactions: Methods and Protocols* (eds. Vergunst, A. C. & O’Callaghan, D.) 261–274 (Humana Press, New York, 2014).
386. Foulkes, M. J. *et al.* Expression and regulation of drug transporters in vertebrate neutrophils. *Sci. Rep.* **7**, 4967 (2017).
387. Fuchs, B. C. & Bode, B. P. Amino acid transporters ASCT2 and LAT1 in cancer: Partners in crime? *Semin. Cancer Biol.* **15**, 254–266 (2005).
388. Liu, Y. *et al.* High expression of Solute Carrier Family 1, member 5 (SLC1A5) is associated with poor prognosis in clear-cell renal cell carcinoma. *Sci. Rep.* **5**, 16954 (2015).
389. Bhutia, Y. D., Babu, E., Ramachandran, S. & Ganapathy, V. Amino Acid

Transporters in Cancer and Their Relevance to 'Glutamine Addiction': Novel Targets for the Design of a New Class of Anticancer Drugs. *Cancer Res.* **75**, 1782–1788 (2015).

390. Rieckmann, J. C. *et al.* Social network architecture of human immune cells unveiled by quantitative proteomics. *Nat. Immunol.* **18**, 583–593 (2017).
391. Malo, N., Hanley, J. A., Cerquozzi, S., Pelletier, J. & Nadon, R. Statistical practice in high-throughput screening data analysis. *Nat Biotechnol* **24**, 167–175 (2006).
392. Larson, M. H. *et al.* CRISPR interference (CRISPRi) for sequence-specific control of gene expression. *Nat. Protoc.* **8**, 2180–2196 (2013).
393. Qi, L. S. *et al.* Repurposing CRISPR as an RNA-guided platform for sequence-specific control of gene expression. *Cell* **152**, 1173–83 (2013).
394. Wu, T.-S. *et al.* Annoquinone-A, an antimicrobial and cytotoxic principle from *Annona montana*. *Phytochemistry* **26**, 1623–1625 (1987).
395. Krohn, K. *et al.* Synthesis and electrochemistry of annoquinone-A, cypripedin methyl ether, denbinobin and related 1,4-phenanthrenequinones. *Arkivoc* **2001**, 88–130 (2001).
396. Fieser, L. F. Some derivatives of 3,4-phenanthrenequinone. *J. Am. Chem. Soc.* **51**, 940–952 (1929).
397. Elwood, T. A., Dudley, K. H., Tesarek, J. M., Rogerson, P. F. & Bursey, M. M. The mass spectra of some naphthoquinones. Lapachol, isolapachol and related compounds. *Org. Mass Spectrom.* **3**, 841–861 (1970).
398. Sacau, E. P. *et al.* Inhibitory effects of lapachol derivatives on epstein-barr virus activation. *Bioorg. Med. Chem.* **11**, 483–488 (2003).
399. Tapia, R. A., Salas, C., Morello, A., Maya, J. D. & Toro-Labbé, A. Synthesis of dihydronaphthofurandiones and dihydrofuroquinolinediones with trypanocidal activity and analysis of their stereoelectronic properties. *Bioorg. Med. Chem.* **12**, 2451–2458 (2004).

## 10. Appendix

10.1 Previous studies in the Renshaw group found that various tanshinones accelerated resolution of neutrophilic inflammation in zebrafish



Data obtained by Dr. Anne Robertson. DMSO used at 0.5% concentration, all other compounds used at concentrations of 1, 10 and 25 μM as indicated. Data shown as mean ± SD;  $n$  = approximately 40 larvae from 4 independent experiments. \*  $P < 0.05$ , \*\*  $P < 0.01$ , \*\*\*  $P < 0.001$ , all other results not significant, in comparison to the DMSO control (one-way ANOVA with Dunnett's multiple comparison post-test).

## 10.2 E3 medium

For 1 L of 10x E3 stock solution: 2.867 g NaCl (5.00 mM)  
0.127 g KCl (0.17 mM)  
0.483 g CaCl<sub>2</sub>·2H<sub>2</sub>O (0.33 mM)  
0.817 g MgSO<sub>4</sub>·7H<sub>2</sub>O (0.33 mM)  
Deionised water up to 1 L

For 1 L of 1x E3 stock solution: 100 mL 10x E3 stock solution  
Deionised water up to 1 L  
Optional: add 3 drops 1% methylene blue solution (in deionised water) as fungicide

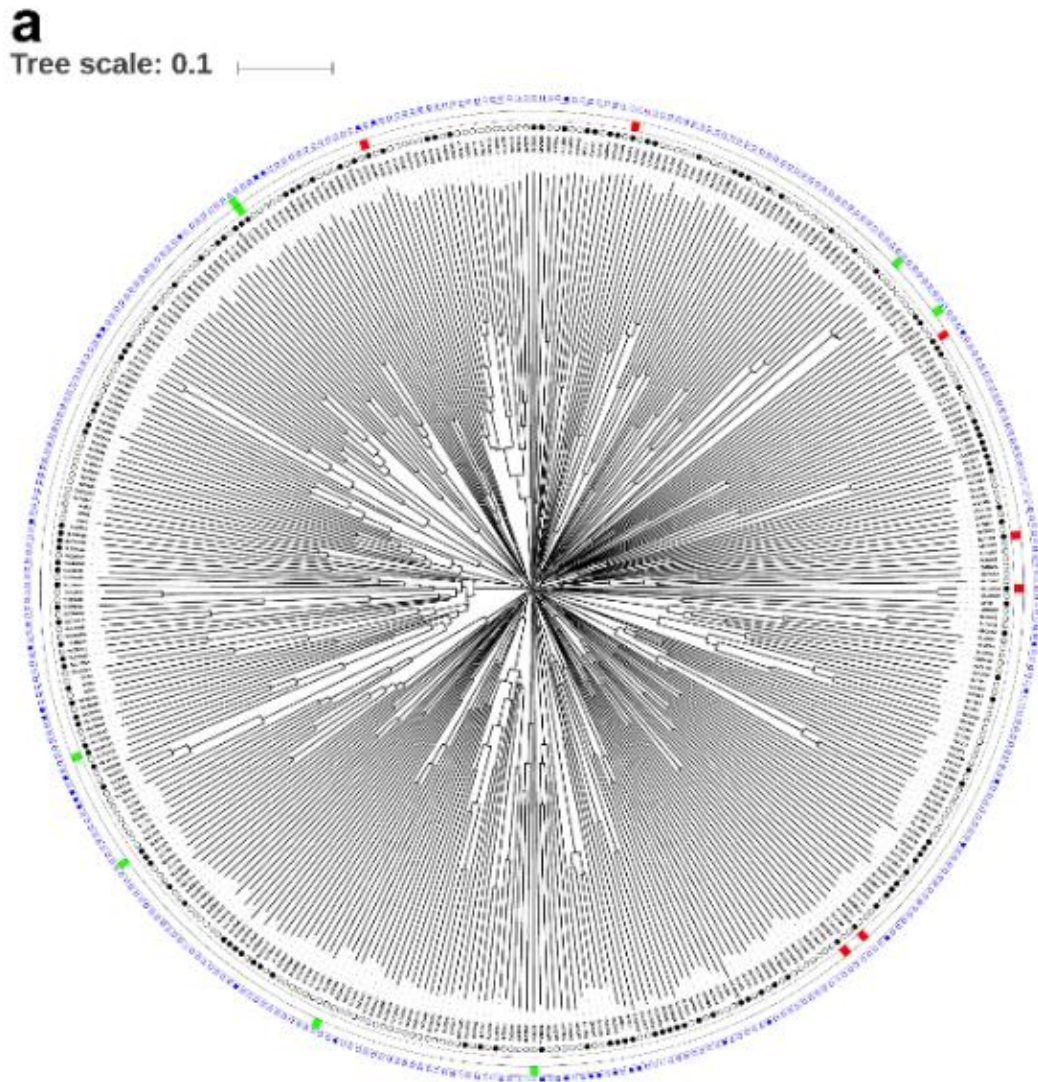
All 10x E3 stock solution was autoclaved prior to dilution and use in experiments.

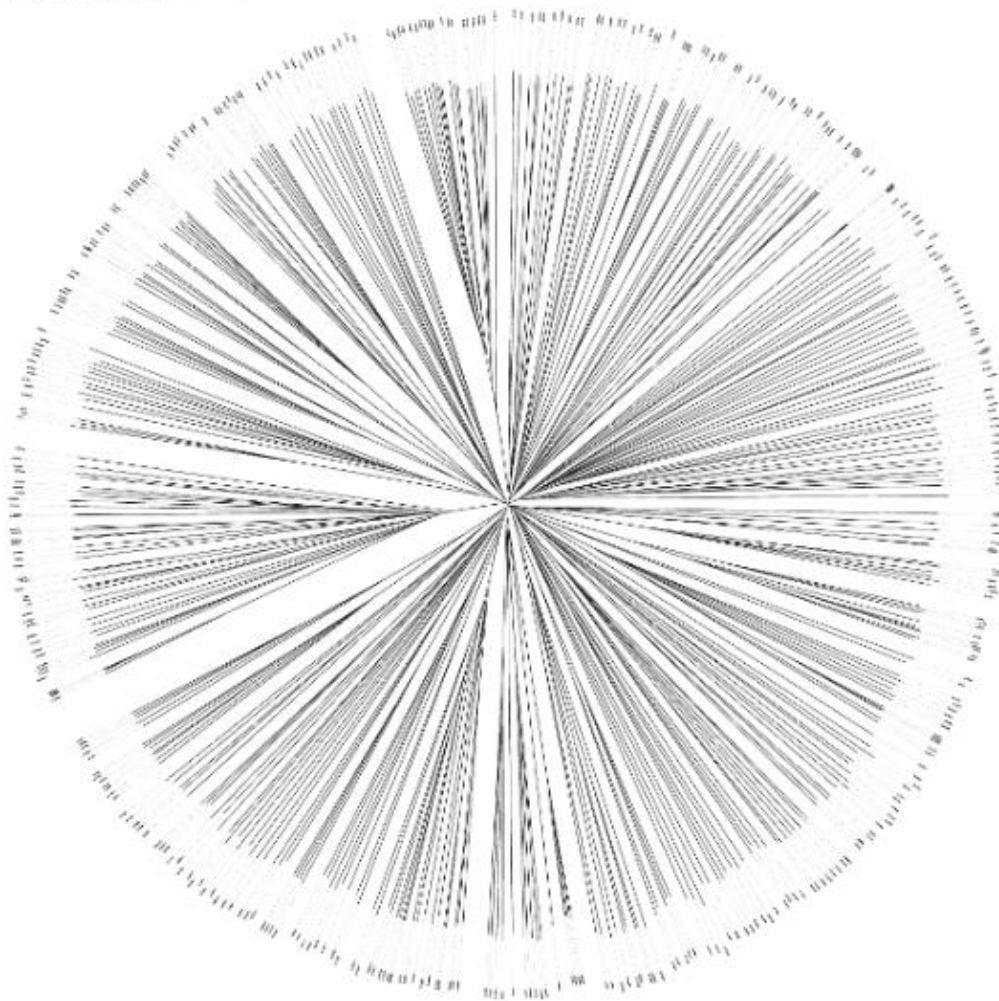
## 10.3 Tricaine solution

Tricaine solution comprises 0.017% ethyl 3-aminobenzoate methanesulfonic acid in deionised water.

## 10.4 Phylogenetic trees with proportional branch lengths

10.4.1 Subsets of SLC transporter proteins were expressed and regulated in primary human neutrophils



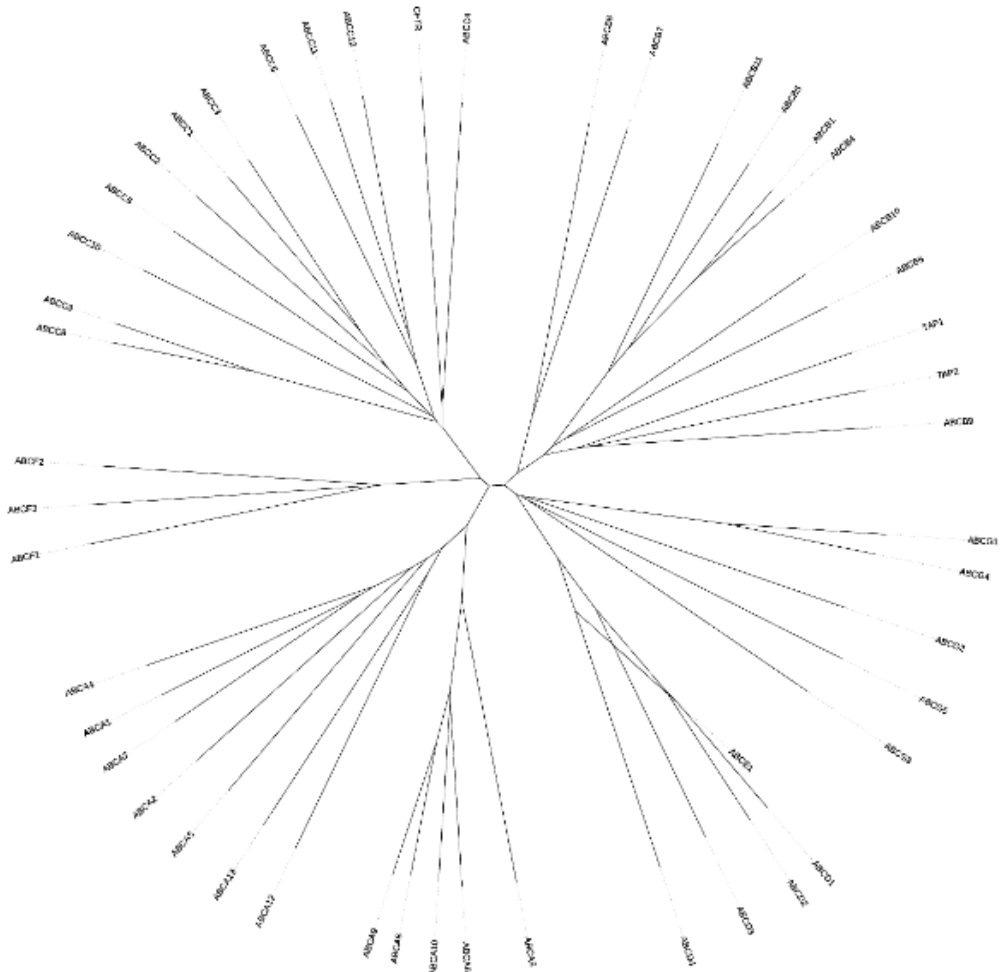
**b**Tree scale: 0.1 

Annotated phylogenetic trees in **(a)** circular and **(b)** unrooted display modes indicate evolutionary relationships between SLC transporter proteins in human neutrophils. Branch lengths are proportional to genetic distance. In **(a)**, for resting primary human neutrophil expression data (inner circle), expressed proteins were marked with a black dot, whereas proteins not expressed were denoted with a white dot. For GM-CSF (second circle from centre) and TNF $\alpha$  (third circle from centre) regulation data, significant up-regulation of a gene was denoted with a green box, significant down-regulation was denoted by a red box, and a lack of significant change in regulation unmarked. For human neutrophil proteomics data (outer circle), any proteins identified in one or more of the analyses were denoted with a blue box, and any not identified were denoted with a white box.



**b**

Tree scale: 0.1



Annotated phylogenetic trees in **(a)** circular and **(b)** unrooted display modes indicate evolutionary relationships between ABC transporter proteins in human neutrophils. Branch lengths are proportional to genetic distance. In **(a)**, for resting primary human neutrophil expression data (inner circle), expressed proteins were marked with a black dot, whereas proteins not expressed were denoted with a white dot. For human neutrophil proteomics data (outer circle), any proteins identified in one or more of the analyses were denoted with a blue box, and any not identified were denoted with a white box.

## 10.5 Comparison of human drug transporter expression between distinct RNAseq datasets

### 10.5.1 Expression of SLC transporter proteins was largely consistent across two different datasets

SLC transporter	Expression (FPKM)	
	Wright <i>et al.</i> , 2013	Chatterjee <i>et al.</i> , 2016
<i>SLC16A3</i>	416.071	206.7938
<i>SLC2A3</i>	384.863	146.301
<i>SLC25A37</i>	365.439	<b>No data</b>
<i>SLC44A2</i>	296.96	305.502
<i>SLC11A1</i>	241.006	375.1498
<i>SLC6A6</i>	174.964	308.898
<i>SLC43A2</i>	142.397	195.5783
<i>SLC15A3</i>	114.121	203.8168
<i>SLC12A6</i>	107.268	86.26105
<i>SLC15A4</i>	101.968	132.1664
<i>SLC38A2</i>	73.4412	51.29513
<i>SLC45A4</i>	62.3642	34.80962
<i>SLC25A3</i>	60.4501	74.8113
<i>SLC31A2</i>	59.4817	107.9547
<i>MTCH1</i>	58.9362	96.06843
<i>SLC19A1</i>	56.8214	50.80168
<i>SLCO3A1</i>	53.1765	134.5328
<i>SLC12A9</i>	52.23	147.5515
<i>SLC40A1</i>	37.6849	166.2416
<i>UCP2</i>	35.2824	77.73278
<i>SLC25A44</i>	33.7158	58.39863
<i>SLC20A1</i>	33.0773	16.14776
<i>SLC9A1</i>	25.9958	31.72053
<i>SLC22A4</i>	24.431	30.64313
<i>SLC25A28</i>	23.1132	26.53685
<i>DIRC2</i>	22.9076	4.079744
<i>SLC39A1</i>	21.6872	24.02363
<i>SLC22A18</i>	21.182	36.2852
<i>SLC38A10</i>	21.1819	30.27238

<i>SLC7A5</i>	20.6468	1.637648
<i>SLC9A8</i>	19.8604	18.75233
<i>SLC25A5</i>	19.6541	35.83148
<i>SLC29A1</i>	17.9369	36.96945
<i>SLC3A2</i>	17.5905	22.47888
<i>SLC25A11</i>	17.5471	25.77163
<i>SLC8B1</i>	16.841	11.64638
<i>SLC7A7</i>	16.7696	31.3496
<i>SLC16A5</i>	14.6446	30.8605
<i>SLC35A2</i>	12.2554	9.707798
<i>SLC8A1</i>	12.0016	10.08038
<i>SLC16A6</i>	11.2322	5.730955
<i>SLC35A4</i>	11.1066	13.25903
<i>SLC39A7</i>	10.6539	34.74275
<i>SLC25A51</i>	10.198	10.5348
<i>SLC35C2</i>	10.005	28.4959
<i>SLC35E1</i>	9.68586	<b>No data</b>
<i>SLC36A1</i>	9.58739	8.930435
<i>SLC10A3</i>	9.23775	11.80692
<i>SLC36A4</i>	9.22429	5.119257
<i>SLC35A5</i>	7.91078	17.37549
<i>SLC39A6</i>	7.26005	7.351105
<i>SLC25A1</i>	7.10385	10.06107
<i>SLC37A3</i>	7.06368	29.04458
<i>SLC48A1</i>	6.77426	8.336738
<i>SLC25A29</i>	6.73623	11.61707
<i>SLC23A2</i>	6.58677	6.764668
<i>SLC22A15</i>	6.44345	17.17855
<i>SLC39A9</i>	6.18562	7.195905
<i>SLC31A1</i>	5.99872	7.739965
<i>SLC2A1</i>	5.77547	3.62349
<i>SLC35B1</i>	5.4807	<b>No data</b>
<i>SLC35E2B</i>	5.37585	14.90033
<i>SLCO4C1</i>	5.25519	6.557368
<i>SLC46A3</i>	5.17528	5.261813
<i>SLC35E3</i>	4.72873	<b>No data</b>
<i>SLC35F5</i>	4.69507	12.34666

<i>SLC26A8</i>	4.56664	3.324936
<i>SLC30A5</i>	4.42129	8.462588
<i>SLC38A1</i>	4.33379	1.82469
<i>SLC19A2</i>	4.02632	0.802967
<i>SLC22A1</i>	3.91727	15.31258
<i>SLC50A1</i>	3.9015	6.878278
<i>SLC35A1</i>	3.80725	<b>No data</b>
<i>SLC18A2</i>	3.7171	1.370494
<i>SLC27A3</i>	3.67019	<b>No data</b>
<i>SLC25A46</i>	3.57248	4.63701
<i>SLC30A9</i>	3.53037	4.27509
<i>SLC17A5</i>	3.49068	3.028465
<i>SLC25A40</i>	3.45767	8.186168
<i>SLC43A3</i>	3.4212	<b>No data</b>
<i>SLC2A14</i>	3.36893	0.906642
<i>FLVCR1</i>	3.3331	11.74628
<i>SLC25A32</i>	3.31725	1.141212
<i>SLC35B3</i>	3.31298	6.968573
<i>SLC12A4</i>	3.29637	<b>No data</b>
<i>SLC35E2</i>	3.24559	14.90033
<i>SLC35B2</i>	3.1499	<b>No data</b>
<i>SLC25A20</i>	3.0388	13.83024
<i>SLC39A3</i>	3.00139	4.865003
<i>SLC25A16</i>	2.88922	2.370293
<i>SLC37A1</i>	2.87833	<b>No data</b>
<i>SLC44A1</i>	2.79355	2.664965
<i>SLC7A6</i>	2.78867	2.361488
<i>SLC39A13</i>	2.78257	4.708685
<i>SLC4A2</i>	2.70562	14.91975
<i>SLC25A45</i>	2.66672	4.06514
<i>SLC30A6</i>	2.55172	3.284525
<i>SLC25A39</i>	2.43246	2.116713
<i>SLC5A9</i>	2.41311	2.3544
<i>SLC25A14</i>	2.27557	4.54853
<i>SLC25A36</i>	2.24725	1.794893
<i>MFSD7</i>	2.17705	4.75029
<i>SLC9A6</i>	2.12071	2.086033

<i>SLC12A1</i>	1.97848	11.74522
<i>SLC6A8</i>	1.96133	2.048953
<i>SLC37A2</i>	1.94582	2.08544
<i>SLC30A7</i>	1.90897	7.608707
<i>SLC25A24</i>	1.90318	2.7849
<i>SLC52A2</i>	1.83537	6.545528
<i>SLC30A1</i>	1.65508	2.871723
<i>SLC35C1</i>	1.6161	2.864028
<i>SLC25A33</i>	1.60194	0.085965
<i>SLC35D1</i>	1.57019	0.861985
<i>SLC26A6</i>	1.53617	3.069608
<i>SLC39A8</i>	1.51151	0.808593
<i>SLC24A3</i>	1.49052	0.976179
<i>SLC6A12</i>	1.48353	3.38105
<i>SLC39A11</i>	1.44917	1.204404
<i>SLC35D2</i>	1.43724	3.107213
<i>SLC25A25</i>	1.39899	1.099743
<i>SLC1A4</i>	1.39617	0.302471
<i>SLC25A13</i>	1.38929	1.150665
<i>SLC16A14</i>	1.34748	0.57943
<i>SLC51A</i>	1.32701	<b>No data</b>
<i>SLC25A38</i>	1.32695	1.032691
<i>SLC25A30</i>	1.26993	1.05837
<i>SLC25A22</i>	1.19878	3.907003
<i>SLC5A6</i>	1.17366	1.142233
<i>SLC35A3</i>	1.16899	1.344898
<i>SLC1A5</i>	1.10623	0.933738
<i>MTCH2</i>	1.07897	3.649688
<i>SLC24A4</i>	1.07192	2.226199
<i>SLC25A34</i>	1.04847	1.105145
<i>SLC5A5</i>	1.0317	0.001373
<i>SLC33A1</i>	0.98935	1.418693
<i>SLC5A3</i>	0.967574	<b>No data</b>
<i>SLC7A8</i>	0.962858	1.744048
<i>UCP3</i>	0.927209	0.659301
<i>SLC23A1</i>	0.905577	0.376388
<i>SLC4A5</i>	0.891422	0.893974

<i>SLC2A5</i>	0.880448	0.6242
<i>SLC7A11</i>	0.839899	0.126315
<i>SLC12A7</i>	0.816008	0.604336
<i>SLC38A9</i>	0.768943	2.547703
<i>SLC36A2</i>	0.710032	0.017288
<i>SLC25A19</i>	0.679593	0.659763
<i>SLC11A2</i>	0.660908	0.767677
<i>SLC25A15</i>	0.649624	0.352065
<i>SLC27A4</i>	0.64666	1.151295
<i>SLC16A4</i>	0.646018	0.26843
<i>SLC9A7</i>	0.621709	0.838211
<i>SLC26A11</i>	0.601788	0.602508
<i>SLC4A7</i>	0.592421	0.398962
<i>SLC22A5</i>	0.586358	1.134696
<i>SLC10A1</i>	0.582003	0.089458
<i>SLC25A17</i>	0.58162	1.582018
<i>SLC26A2</i>	0.557363	0.367065
<i>SLC37A4</i>	0.545263	1.466712
<i>SLC20A2</i>	0.523111	1.663723
<i>SLC39A4</i>	0.511753	2.772043
<i>SLC15A2</i>	0.494293	<b>No data</b>
<i>SLC25A12</i>	0.491284	0.947139
<i>SLC16A13</i>	0.49106	0.266753
<i>SLC9A4</i>	0.472869	0.029917
<i>RHBG</i>	0.454494	0
<i>SLC46A2</i>	0.393315	0.506613
<i>SLC7A1</i>	0.392402	0.113242
<i>SLC41A1</i>	0.39035	0.153188
<i>SLC04A1</i>	0.386293	0.030919
<i>SLC39A10</i>	0.375107	0.280526
<i>SLC12A2</i>	0.358682	0.251158
<i>SLC10A7</i>	0.354472	0.47415
<i>SLC4A8</i>	0.346928	1.085581
<i>SLC24A1</i>	0.343325	0.556316
<i>SLC16A1</i>	0.341766	0.100955
<i>SLC41A3</i>	0.33136	1.309153
<i>SLC29A3</i>	0.3301	0.613083

<i>SLC28A2</i>	0.319969	0
<i>SLC6A16</i>	0.313818	0.702131
<i>SLC25A53</i>	0.301434	3.752335
<i>SLC25A26</i>	0.300095	0.448138
<i>SLC41A2</i>	0.293223	1.133091
<i>SLC2A6</i>	0.275303	0.812577
<i>SLC2A8</i>	0.273322	0.814157
<i>SLC45A3</i>	0.269156	0.69311
<i>SLC6A20</i>	0.25677	0.06559
<i>SLC18B1</i>	0.256123	0.353239
<i>SLC2A4</i>	0.252583	0.003538
<i>SLC3A1</i>	0.249917	0.161592
<i>SLC6A13</i>	0.235715	0.26222
<i>SLC44A4</i>	0.222833	0.025491
<i>SLC43A1</i>	0.220751	0.140674
<i>SLC25A42</i>	0.217023	0.229577
<i>SLC39A14</i>	0.215165	0.066361
<i>SLC12A8</i>	0.215099	24.8685
<i>SLC2A9</i>	0.213474	1.134367
<i>SLC9A9</i>	0.206143	0.471828
<i>SLC15A1</i>	0.205513	0
<i>SLC27A1</i>	0.190422	0.350563
<i>SLC35F1</i>	0.183551	0
<i>SLC30A4</i>	0.17871	0.043864
<i>SLC25A18</i>	0.173669	0.178288
<i>SLC23A3</i>	0.171536	<b>No data</b>
<i>SLC27A2</i>	0.165621	0.147139
<i>SLC17A9</i>	0.163025	0.220222
<i>FLVCR2</i>	0.161085	2.995074
<i>SLC25A35</i>	0.155719	0.474642
<i>SLC25A23</i>	0.152735	0.092535
<i>SLC25A27</i>	0.15039	0.499895
<i>SLC25A10</i>	0.148419	1.767058
<i>SLC2A13</i>	0.142042	0.254337
<i>SLC38A5</i>	0.140477	0.244678
<i>SLC14A2</i>	0.138358	0.023388
<i>SLC35B4</i>	0.135503	0.133596

<i>SLC16A7</i>	0.133516	0.174023
<i>SLC22A13</i>	0.132108	0.031119
<i>SLC22A14</i>	0.128302	0.112629
<i>SLC45A2</i>	0.124561	0.079131
<i>SLC47A1</i>	0.123309	0.295644
<i>SLC14A1</i>	0.120003	0.049875
<i>SLC2A11</i>	0.119388	<b>No data</b>
<i>SLC9B2</i>	0.117721	<b>No data</b>
<i>SLC25A43</i>	0.110956	0.305292
<i>SLC38A6</i>	0.106089	<b>No data</b>
<i>SLC25A2</i>	0.105079	0.012352
<i>SLC28A1</i>	0.105037	0.018301
<i>SLC35E4</i>	0.099345	0.114885
<i>SLC22A17</i>	0.096723	0.019834
<i>SLC7A10</i>	0.096162	0.056653
<i>SLC4A1</i>	0.094702	<b>No data</b>
<i>SLC52A1</i>	0.093662	0.002782
<i>SLC7A9</i>	0.091258	0.059758
<i>SLC38A7</i>	0.090202	0.139128
<i>SLC5A10</i>	0.084047	0.008357
<i>SLC16A8</i>	0.076297	0.09536
<i>SLC22A9</i>	0.075539	0
<i>SLC7A14</i>	0.071874	0
<i>SLC35F2</i>	0.07121	0.088443
<i>SLC18A1</i>	0.06938	0.193916
<i>SLC26A4</i>	0.06696	0.013925
<i>SLC35G2</i>	0.066789	0.004921
<i>SLC30A8</i>	0.064359	0.004751
<i>SLC13A4</i>	0.062869	0.292333
<i>SLC9B1</i>	0.06115	0.013052
<i>SLC28A3</i>	0.057827	0.036177
<i>SLC22A16</i>	0.056745	0.14271
<i>SLC32A1</i>	0.055365	0
<i>SLC16A10</i>	0.055337	0.013955
<i>SLC45A1</i>	0.055306	0.026179
<i>SLC24A5</i>	0.055127	0.314604
<i>SLC2A12</i>	0.053854	0.341995

<i>SLC29A2</i>	0.053376	0.038654
<i>SLC25A47</i>	0.049291	0.007801
<i>SLC16A11</i>	0.048024	0
<i>SLC22A23</i>	0.047533	0.146284
<i>SLC25A4</i>	0.047498	0.070657
<i>SLC25A52</i>	0.046697	0.01043
<i>SLC26A1</i>	0.045243	0.203451
<i>SLCO1A2</i>	0.044854	0
<i>SLC4A4</i>	0.044376	0.018906
<i>SLC4A9</i>	0.043369	0.053466
<i>SLC5A11</i>	0.042816	0.009208
<i>SLC6A14</i>	0.040641	0
<i>SLC9A3</i>	0.038749	0.010525
<i>SLC35G1</i>	0.038543	0.138574
<i>SLC1A2</i>	0.038243	0.001444
<i>SLC35G6</i>	0.036646	0
<i>SLC19A3</i>	0.035449	0
<i>SLC27A5</i>	0.03506	0.057876
<i>SLC46A1</i>	0.034287	0.0454
<i>SLC4A10</i>	0.031961	0.010504
<i>SLC29A4</i>	0.031852	0.002375
<i>SLC4A11</i>	0.030189	0.006052
<i>SLC13A1</i>	0.030136	0
<i>SLC13A5</i>	0.028342	0.014783
<i>SLC10A4</i>	0.027983	0.008142
<i>SLC1A3</i>	0.027724	0.080618
<i>SLC16A12</i>	0.027205	0
<i>SLC26A5</i>	0.026607	0
<i>SLC1A7</i>	0.026587	0.053328
<i>SLC35G5</i>	0.026139	0
<i>SLC8A2</i>	0.024413	0.011955
<i>SLC10A5</i>	0.021475	0
<i>SLCO5A1</i>	0.021423	0.01598
<i>SLC9A5</i>	0.017925	0.008151
<i>SLC4A3</i>	0.017676	0.044514
<i>SLC44A3</i>	0.017549	0.089591
<i>SLC38A11</i>	0.017394	0.057391

<i>SLC17A3</i>	0.0168	0
<i>SLC5A2</i>	0.016518	0.188793
<i>SLC34A1</i>	0.014604	0.007438
<i>RHCG</i>	0.014434	0
<i>SLC6A4</i>	0.014124	0.042066
<i>SLC34A3</i>	0.013134	0
<i>SLC6A2</i>	0.012301	0
<i>SLC7A4</i>	0.01204	0
<i>SLC44A5</i>	0.010659	0.004211
<i>SLC24A2</i>	0.009822	0
<i>SLC8A3</i>	0.009751	0.074688
<i>SLC38A3</i>	0.009671	0
<i>SLC36A3</i>	0.009293	0
<i>SLC12A3</i>	0.008825	0.008359
<i>SLC1A1</i>	0.007744	0.014113
<i>SLC12A5</i>	0.006559	0.027903
<i>SLC2A10</i>	0.006494	0.096226
<i>SLC39A5</i>	0.006383	0.008053
<i>SLC16A2</i>	0.006309	0
<i>SLC26A7</i>	0.006272	<b>No data</b>
<i>SLC6A3</i>	0.005945	0.001777
<i>SLC22A7</i>	0.005874	0
<i>SLC9A2</i>	0.004401	0.007815
<i>SLC6A9</i>	0.003785	0
<i>SLC13A3</i>	0.002597	0
<i>SLCO1B7</i>	0	0
<i>SLC22A31</i>	0	<b>No data</b>
<i>SLC26A10</i>	0	<b>No data</b>
<i>SLCO1B1</i>	0	0
<i>SLC25A6</i>	0	17.00073
<i>SLC39A2</i>	0	0.039487
<i>SLC35F3</i>	0	0.032623
<i>SLC35D3</i>	0	0.026302
<i>SLC34A2</i>	0	0.010175
<i>SLC30A2</i>	0	0.009504
<i>SLC27A6</i>	0	0.008934
<i>SLC10A6</i>	0	0.006882

<i>RHAG</i>	0	0.004514
<i>SLC17A7</i>	0	0.004465
<i>SLC22A3</i>	0	0.003755
<i>SLC26A3</i>	0	0.002922
<i>SLC16A9</i>	0	0.002449
<i>SLC52A3</i>	0	0.002154
<i>SLC17A8</i>	0	0.002021
<i>SLCO2B1</i>	0	0.001259
<i>SLC10A2</i>	0	0
<i>SLC13A2</i>	0	0
<i>SLC15A5</i>	0	0
<i>SLC17A1</i>	0	0
<i>SLC17A2</i>	0	0
<i>SLC17A4</i>	0	0
<i>SLC17A6</i>	0	0
<i>SLC18A3</i>	0	0
<i>SLC1A6</i>	0	0
<i>SLC22A10</i>	0	0
<i>SLC22A11</i>	0	0
<i>SLC22A12</i>	0	0
<i>SLC22A2</i>	0	0
<i>SLC22A24</i>	0	0
<i>SLC22A25</i>	0	0
<i>SLC22A6</i>	0	0
<i>SLC22A8</i>	0	0
<i>SLC25A21</i>	0	0
<i>SLC25A31</i>	0	0
<i>SLC25A41</i>	0	0
<i>SLC25A48</i>	0	0
<i>SLC26A9</i>	0	0
<i>SLC2A2</i>	0	0
<i>SLC2A7</i>	0	0
<i>SLC30A10</i>	0	0
<i>SLC30A3</i>	0	0
<i>SLC35F4</i>	0	0
<i>SLC35G3</i>	0	0
<i>SLC38A4</i>	0	0

<i>SLC38A8</i>	0	0
<i>SLC39A12</i>	0	0
<i>SLC47A2</i>	0	0
<i>SLC51B</i>	0	0
<i>SLC5A1</i>	0	0
<i>SLC5A12</i>	0	0
<i>SLC5A4</i>	0	0
<i>SLC5A7</i>	0	0
<i>SLC5A8</i>	0	0
<i>SLC6A1</i>	0	0
<i>SLC6A11</i>	0	0
<i>SLC6A15</i>	0	0
<i>SLC6A17</i>	0	0
<i>SLC6A18</i>	0	0
<i>SLC6A19</i>	0	0
<i>SLC6A5</i>	0	0
<i>SLC6A7</i>	0	0
<i>SLC7A13</i>	0	0
<i>SLC7A2</i>	0	0
<i>SLC7A3</i>	0	0
<i>SLC9C1</i>	0	0
<i>SLC9C2</i>	0	0
<i>SLCO1B3</i>	0	0
<i>SLCO1C1</i>	0	0
<i>SLCO2A1</i>	0	0
<i>SLCO6A1</i>	0	0
<i>UCP1</i>	0	0

The table shows all human SLC transporter genes and their expression values (given as FPKM values) as found in datasets from Wright *et al.* and Chatterjee *et al.*<sup>375,384</sup> Entries are given as the mean of replicate values, in descending order of expression according to the dataset by Wright *et al.* Any genes which could not be identified in the dataset by Chatterjee *et al.* are labelled as 'No data'.

10.5.2 Expression of ABC transporter proteins was largely consistent across two different datasets

ABC transporter	Expression (FPKM)	
	Wright <i>et al.</i> , 2013	Chatterjee <i>et al.</i> , 2016
<i>TAP1</i>	143.682	456.3108
<i>TAP2</i>	51.0473	132.7189
<i>ABCA7</i>	37.334	178.8746
<i>ABCG1</i>	25.6516	<b>No data</b>
<i>ABCA1</i>	17.5845	11.97111
<i>ABCC5</i>	12.5493	16.24293
<i>ABCD1</i>	7.27776	9.552486
<i>ABCF1</i>	7.27122	5.90886
<i>ABCA2</i>	7.15235	18.60513
<i>ABCC1</i>	6.83516	8.063192
<i>ABCF3</i>	4.72307	14.26925
<i>ABCC9</i>	2.21629	0
<i>ABCD3</i>	1.59239	1.14281
<i>ABCF2</i>	1.21202	1.350599
<i>ABCA5</i>	1.18218	1.080757
<i>ABCD4</i>	1.11062	7.700425
<i>ABCB10</i>	1.00666	1.87598
<i>ABCC6</i>	0.970651	2.83314
<i>ABCC10</i>	0.940023	4.91765
<i>ABCB7</i>	0.927628	1.25014
<i>ABCC2</i>	0.839153	17.38025
<i>ABCE1</i>	0.599287	0.6684927
<i>ABCB5</i>	0.53339	0.00458515
<i>ABCB6</i>	0.367747	20.8678
<i>ABCB1</i>	0.319107	0.2100675
<i>ABCB8</i>	0.313178	1.246972
<i>ABCA13</i>	0.291386	0.4219312
<i>ABCC4</i>	0.218874	0.505737
<i>ABCA9</i>	0.139689	0.03220053
<i>ABCB9</i>	0.0938531	0.05274925

<i>ABCB11</i>	0.0664028	0.02136092
<i>ABCC3</i>	0.0612735	2.804117
<i>ABCA3</i>	0.0505832	0.05429485
<i>ABCD2</i>	0.0494921	0.02637948
<i>ABCA10</i>	0.0291777	1.080757
<i>ABCG2</i>	0.026239	0.000778308
<i>ABCB4</i>	0.014383	0.2529438
<i>ABCC11</i>	0.0118731	0.00540443
<i>ABCA6</i>	0.0101404	0.01867935
<i>ABCA4</i>	0.00612525	0.009292483
<i>ABCA12</i>	0	0
<i>ABCA8</i>	0	0
<i>ABCC12</i>	0	0.001889568
<i>ABCC8</i>	0	0
<i>ABCG4</i>	0	0.001287225
<i>ABCG5</i>	0	0
<i>ABCG8</i>	0	0
<i>CFTR</i>	0	0

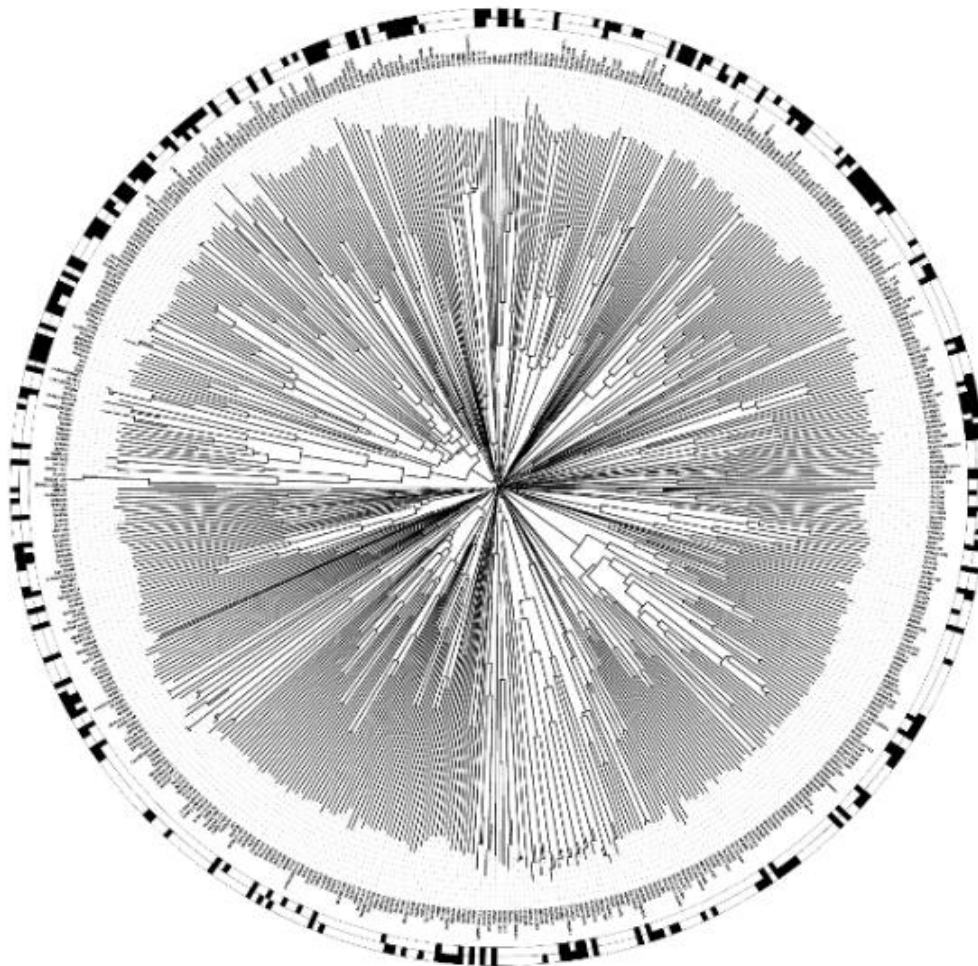
The table shows all human ABC transporter genes and their expression values (given as FPKM values) as found in datasets from Wright *et al.* and Chatterjee *et al.*<sup>375,384</sup> Entries are given as the mean of replicate values, in descending order of expression according to the dataset by Wright *et al.* Any genes which could not be identified in the dataset by Chatterjee *et al.* are labelled as 'No data'.

## 10.6 Phylogenetic trees with proportional branch lengths

### 10.6.1 Zebrafish larval neutrophils and non-neutrophil cells expressed distinct subsets of SLC transporter proteins

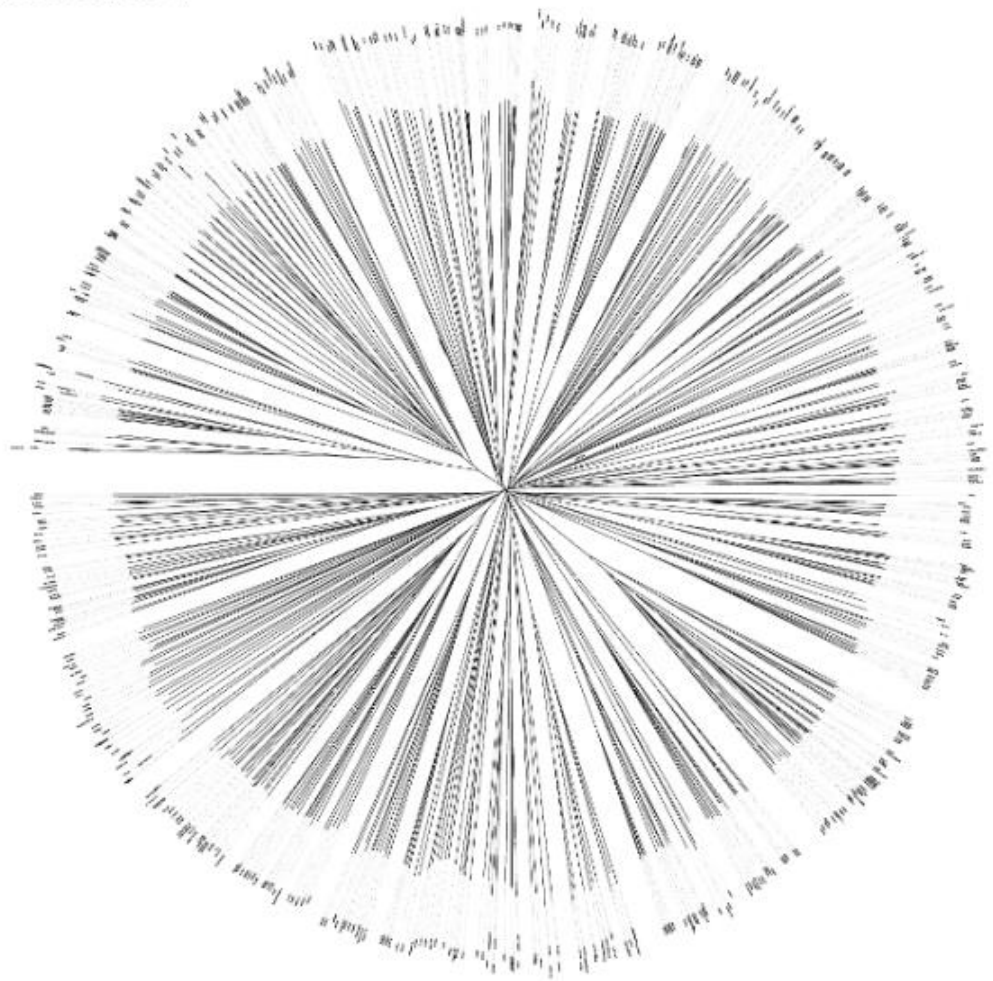
**a**

Tree scale: 0.1 



**b**

Tree scale: 0.1 —

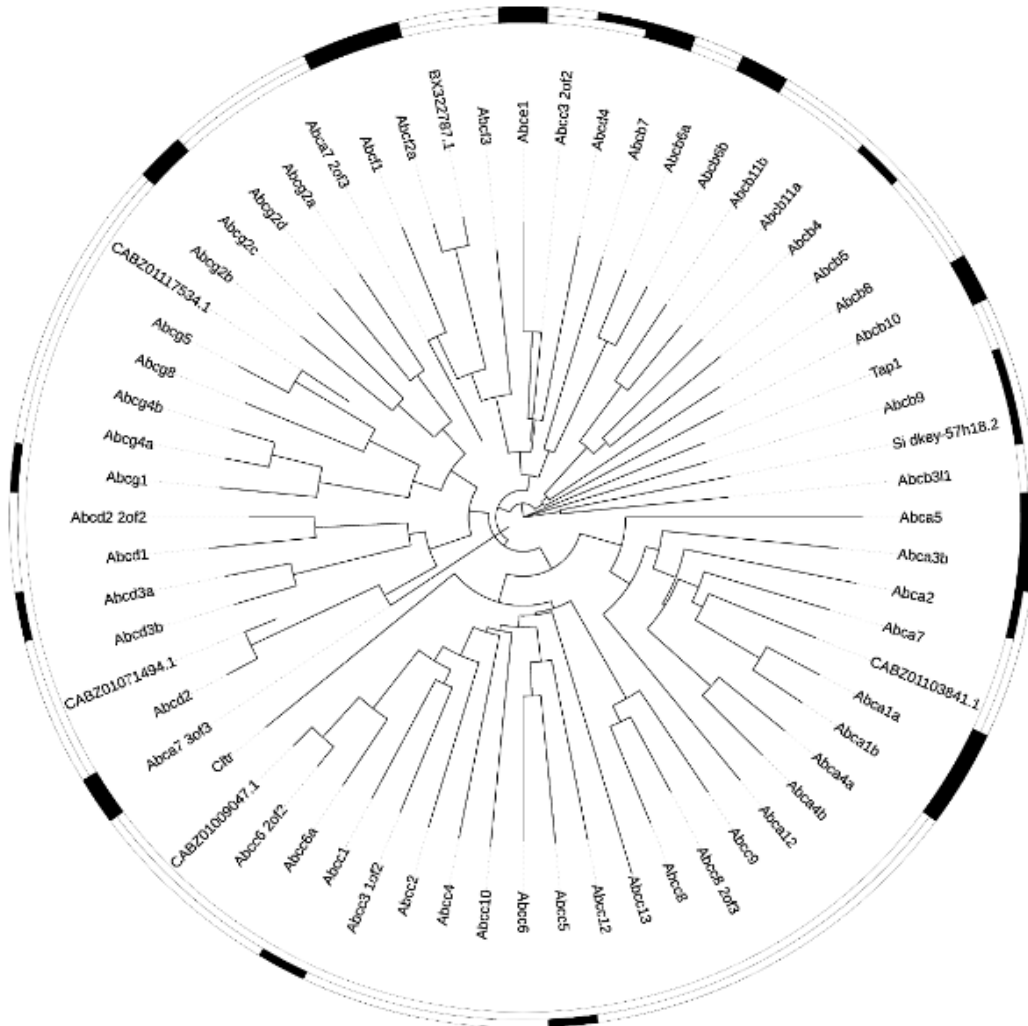


Annotated phylogenetic trees in both **(a)** circular and **(b)** unrooted display modes indicate evolutionary relationships between SLC transporter proteins in zebrafish. Branch lengths are proportional to genetic distance. In **(a)**, for both neutrophil (inner circle) and background cell (outer circle) expression data, expressed proteins were marked with a black box, whereas proteins not expressed were unmarked.

10.6.2 Zebrafish larval neutrophils and non-neutrophil cells expressed distinct subsets of ABC transporter proteins

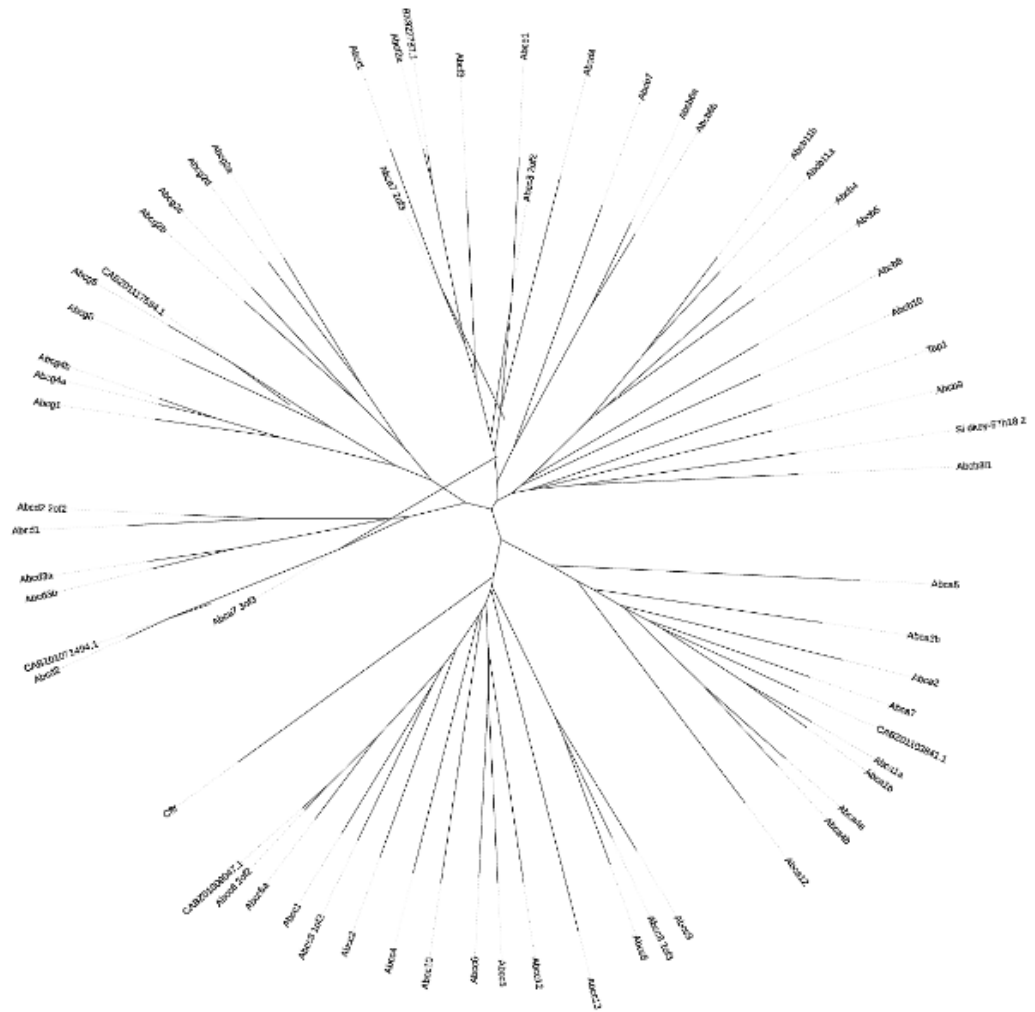
**a**

Tree scale: 0.1



**b**

Tree scale: 0.1



Annotated phylogenetic trees in both (a) circular and (b) unrooted display modes indicate evolutionary relationships between ABC transporter proteins in zebrafish. Branch lengths are proportional to genetic distance. In (a), for both neutrophil (inner circle) and background cell (outer circle) expression data, expressed proteins were marked with a black box, whereas proteins not expressed were unmarked.

## 10.7 Drug transporters expressed in both human and zebrafish neutrophils

10.7.1 A subset of SLC drug transporters was expressed in both human and zebrafish neutrophils

Human gene	Zebrafish orthologue gene(s)
<i>DIRC2</i>	<i>dirc2</i>
<i>FLVCR1</i>	<i>flvcr1</i>
<i>MTCH2</i>	<i>mtch2</i>
<i>SLC10A3</i>	<i>slc10a3</i>
<i>SLC12A9</i>	<i>slc12a9</i>
<i>SLC15A4</i>	<i>slc15a4</i>
<i>SLC16A3</i>	<i>slc16a3</i>
<i>SLC16A6</i>	<i>slc16a6b</i>
<i>SLC19A1</i>	<i>slc19a1</i>
<i>SLC1A4</i>	<i>slc1a4</i>
<i>SLC20A1</i>	<i>slc20a1b</i>
<i>SLC22A15</i>	<i>slc22a15_1of2</i>
<i>SLC22A18</i>	<i>slc22a18</i>
<i>SLC25A1</i>	<i>slc25a1a</i>
<i>SLC25A11</i>	<i>slc25a11</i>
<i>SLC25A14</i>	<i>slc25a14</i>
<i>SLC25A20</i>	<i>slc25a20</i>
<i>SLC25A22</i>	<i>slc25a22</i>
<i>SLC25A24</i>	<i>slc25a24</i>
<i>SLC25A25</i>	<i>slc25a25a</i>
<i>SLC25A28</i>	<i>slc25a28_first</i>
<i>SLC25A3</i>	<i>slc25a3b</i>
<i>SLC25A32</i>	<i>slc25a32a</i>
<i>SLC25A33</i>	<i>slc25a33</i>
<i>SLC25A36</i>	<i>slc25a36a; slc25a36b</i>
<i>SLC25A39</i>	<i>slc25a39</i>
<i>SLC25A40</i>	<i>slc25a40</i>

<i>SLC25A44</i>	<i>slc25a44b</i>
<i>SLC25A46</i>	<i>slc25a46</i>
<i>SLC25A5</i>	<i>slc25a5</i>
<i>SLC27A3</i>	<i>slc27a3</i>
<i>SLC2A1</i>	<i>slc2a1b</i>
<i>SLC2A3</i>	<i>slc2a3b</i>
<i>SLC30A1</i>	<i>slc30a1a</i>
<i>SLC30A5</i>	<i>slc30a5</i>
<i>SLC30A7</i>	<i>slc30a7</i>
<i>SLC30A9</i>	<i>slc30a9</i>
<i>SLC31A1</i>	<i>slc31a1</i>
<i>SLC31A2</i>	<i>slc31a2</i>
<i>SLC35A2</i>	<i>slc35a2</i>
<i>SLC35C1</i>	<i>slc35c1</i>
<i>SLC35D1</i>	<i>slc35d1a</i>
<i>SLC35D2</i>	<i>slc35d2</i>
<i>SLC35E1</i>	<i>slc35e1</i>
<i>SLC35E3</i>	<i>slc35e3</i>
<i>SLC36A1</i>	<i>slc36a1</i>
<i>SLC37A2</i>	<i>slc37a2</i>
<i>SLC38A2</i>	<i>slc38a2</i>
<i>SLC39A6</i>	<i>slc39a6</i>
<i>SLC39A7</i>	<i>slc39a7</i>
<i>SLC3A2</i>	<i>slc3a2a; slc3a2b; slc3a2_3of3; slc3a2_4of4</i>
<i>SLC40A1</i>	<i>slc40a1</i>
<i>SLC43A2</i>	<i>slc43a2a; slc43a2b</i>
<i>SLC43A3</i>	<i>slc43a3b</i>
<i>SLC44A2</i>	<i>slc44a2</i>
<i>SLC48A1</i>	<i>slc48a1a; slc48a1b</i>
<i>SLC4A2</i>	<i>slc4a2b</i>

<i>SLC51A</i>	<i>slc51a</i>
<i>SLC6A6</i>	<i>slc6a6a</i>
<i>SLC7A5</i>	<i>slc7a5</i>
<i>SLC7A7</i>	<i>slc7a7</i>
<i>SLC8B1</i>	<i>FP103011.3</i>
<i>SLC9A8</i>	<i>slc9a8</i>
<i>SLCO3A1</i>	<i>slco3a1</i>
<i>UCP2</i>	<i>ucp2</i>

The list shows all SLC drug transporter genes which were expressed in primary human neutrophils, and which also had at least one corresponding zebrafish orthologue (shown here alongside the relevant human gene) expressed in zebrafish neutrophils.

10.7.2 A subset of ABC drug transporters was expressed in both human and zebrafish neutrophils

<b>Human gene</b>	<b>Zebrafish orthologue gene(s)</b>
<i>ABCA1</i>	<i>abca1a; abca1b</i>
<i>ABCA2</i>	<i>abca2</i>
<i>ABCA5</i>	<i>abca5</i>
<i>ABCA7</i>	<i>abca7_3of3</i>
<i>ABCB10</i>	<i>abcb10</i>
<i>ABCF1</i>	<i>abcf1</i>
<i>ABCF2</i>	<i>abcf2a</i>
<i>TAP2</i>	<i>si:dkey-57h18.2</i>

The list shows all ABC drug transporter genes which were expressed in primary human neutrophils, and which also had at least one corresponding zebrafish orthologue (shown here alongside the relevant human gene) expressed in zebrafish neutrophils.